*Molecular Compounds between Heterocyclic Compounds Containing Nitrogen**

By Tadashi MASAMUNE and Masato KOSHI

(Received August 30, 1956)

Although extensive researches[1-3] have been made on molecular compounds, little information[4] is found in the literature concerning those formed from heterocyclic compounds. In the present note the writers show that molecular compounds of a similar type are formed by heterocyclic compounds containing nitrogen atoms; further, interacting forces between the partner molecules are not essentially different from those acting in other molecular compounds.

Experimental

The following compounds (I—IX, group A) and their hydrogenated compounds (group B) were prepared for the examination.

Group A; benzo-[f]-quinoline (I), 5,6-dihydrobenzo-[f]-quinoline (II), benzo-[h]-quinoline (III), acridine (IV), 1,2,3,4-tetrahydroacridine (V), 7,8,9,10-tetrahydrophenanthridine (VI), 2,3-trimethylenequinoline (VII), quinoline (VIII), and 1,2,3,4-tetrahydrocarbazole (IX).

Preparation of Compounds.—The following compounds were prepared by the procedure described in the literature as cited. Solid compounds were recrystallized to constant melting point from the solvents indicated and, on the other hand, oily compounds were regenerated from their solid derivatives of constant melting point and redistilled before use: (I)[5], m. p. 93-93.5°C (benzine); 1,2,3,4,7,8,9,10-octahydrobenzo-[f]-quinoline[6], m. p. 65-66°C (petroleum-ether), 1,2,3,4,5,6,4a,4b-octahydrobenzo-[f]-quinoline[6], m. p. 90-91°C (petroleum-ether), (III)[7], m. p. 51-52.5°C (petroleum-ether); 1,2,3,4-tetrahydrobenzo-[h]-quinoline[7] m. p. 46-47°C (petroleum-ether); (IV), m. p. 109-110° (benzene); (V)[8], m. p. 54-55°C (benzene); *cis*-1,2,3,4,9,10,4a,4b-octahydroacridine[9], m. p. 71-73°C (petroleum-ether); *trans*-1,2,3,4,9,10,4a,4b-octahydroacridine[10], m. p. 81-83°C (petroleum-ether); (VI)[11], m. p. 63-64°C (benzine); 5,6,7,8,9,10,6a,10a-octahydrophenanthridine[12], m. p. 70-72°C (aqueous alcohol); (VII)[13], m. p. 60-61°C (benzine); *cis*-1,2,3,4-tetrahydro-2,3-trimethylenequinoline[14], oil, benzoyl derivative[14], m. p. 159-160°C (acetone), *trans*-1,2,3,4-tetrahydro-2,3-trimethylenequinoline[14], m. p. 68-68.5°C (petroleum-ether), (VIII), m. p. about −15°C, picrate, m. p. 228-230°C (ethanol); 1,2,3,4-tetrahydroquinoline[15], m. p. about 20°C, benzoyl derivative, m. p. 73-74°C (alcohol); (IX)[16], m. p. 117-118°C (methanol); *cis*-1,2,3,4,10,11-hexahydrocarbazole[17], m.p. 98-99°C (ethanol); *trans*-1,2,3,4,10,11-hexahydrocarbazole[17], m. p. 124-126°C (ethanol).

1,2,3,4-Tetrahydrobenzo-[f]-quinoline.—A mixture of 20 g. of benzo-[f]-quinoline and 20 g. of granulated tin was refluxed in 150 cc. of conc. hydrochloric acid for three hours until the tin was entirely consumed. The reaction mixture was made strongly alkaline with 6 N sodium hydroxide solution after cooling, and it was distilled with steam. The distillate was extracted with ether and recrystallized from ligroin after removal of ether, yielding 10 g. of pale yellow crystals[18], m. p. 93-93.5°C.

Anal. Found: C, 86.12, H, 6.00. Calcd. for $C_{13}H_{11}N$: C, 86.16, H, 6.12%.

This base was dissolved in 50 cc. of ether and treated with a small excess of equivalent benzoyl chloride and N sodium hydroxide solution. After the odor of benzoyl chloride had entirely disappeared, the ethereal layer was separated from

* Partly presented at the Annual Meeting of the Chemical Society of Japan, April 3, 1956. The 8th Part on "The Condensed Polynuclear Perhydro-Compounds Containing Nitrogen." The 7th Part, T. Masamune and G. Homma, *J. Chem. Soc. Japan (Pure Chem. Sect.)*, **77**, 1766 (1956).

1) C. W. Wheland, "Advanced Organic Chemistry" John Wiley and Son's, 2nd ed., New York 1949 p. 54.

2) Ch. Shinomiya, This Bulletin, **15**, 92, 137, 259, 281, 309 (1940).

3) S. Seki and K. Suzuki, ibid., **26**, 63, 209, 372 (1953).

4) It was found by Masamune and Kubota in this laboratory that a molecular compound is formed between tetrahydro-and octahydrophenanthridine. Ref., *J. Chem. Soc. Japan. (Pure Chem. Sect.)*, **77**, 1467 (1956).

5) H. C. A. Knueppel, *Ber*, **29**, 708 (1896).

6) E. Bamberger, ibid., **24**, 2648 (1891).

7) E. Bamberger and L. Stettenheimer, ibid., **24**, 2473 (1891).

8) W. Borsche, ibid., **41**, 2203 (1908).

9) W. H. Perkin and S. G. P. Plant, *J. Chem. Soc.*, **1928**, 2583.

10) W. H. Perkin and W. G. Sedgwick, ibid., **1926**, 438.

11) B. L. Hollingsworth and L. Petrow, ibid., **1948**, 1537.

12) See Ref. (4).

13) W. Borsche, *Ann.*, **377**, 120 (1910).

14) W. H. Perkin and S. G. P. Plant, *J. Chem. Soc.*, **1928**, 638.

15) H. Rupe, M. Seiberth and W. Kussmaul, *Helv. Chim. Acta*, **3**, 75 (1920).

16) C. V. Rogers and B. B. Corson, *J. Am. Chem. Soc.*, **69**, 2910 (1947).

17) J. Gurney, W. H. Perkin and S. G. P. Plant, *J. Chem. Soc.*, **1927**, 2676.

18) This substance was shown to correspond to dihydro-derivative of benzo-[f]-quinoline from analytical value, and was proved to be a molecular compound between (I) and its pure tetrahydro-derivative in the present paper. Bamberger's "1,2,3,4-tetrahydrobenzo-[f]-quinoline" would probably be the same substance as this. See Ref. (5).

CHEMISTRY HALL LIBRARY

the aqueous solution and was washed with 2 N hydrochloric acid to remove unreacted benzo-[f]-quinoline. A benzoylated compound obtained from the ethereal solution by removal of the solvent, had m. p. 153–4°C on recrystallization from alcohol. It was refluxed with 12 g. of potassium hydroxide in 300 cc. aqueous alcoholic solution for four hours. The product was again extracted with ether, after distillation of alcohol under reduced pressure and addition of water. The ethereal solution was treated with 2 N hydrochloric acid. After separation from the ethereal layer, the acidic solution gave 7 g. of oily tetrahydrobenzo-[f]-quinoline, b. p. 200–202°C (14mm.), on alkalification, separation from aqueous solution and distillation under diminished pressure. The hydrochloride was prepared by passing hydrogen chloride into the ethereal solution of the base.

Anal. Found: C, 70.95; H, 6.39. Calcd. for $C_{13}H_{13}NHCl$: C, 71.03; H, 6.42%.

Its picrate had m. p. 167–168°C, when the base was added into saturated alcoholic solution of picric acid and was recrystallized from the same solvent.

5,6-Dihydrobenzo-[f]-quinoline [II].—Benzo-[f]-quinoline (10 g.) was hydrogenated with 1 g. of Raney-nickel[19] at 100°C in an autoclave, starting at 70 atmospheric pressures and the reaction was stopped when one and a half mole of hydrogen were absorbed. The products were extracted with 200 cc. of ether. When the ethereal solution was concentrated up to 50 cc. and cooled, about 4 g. of pale yellow crystals were separated. The crystals thus isolated by filtration gave m. p. 88–90°C, on recrystallization from aqueous alcohol. On the other hand, when the solvent of the filtrate was entirely removed, the residue consisting of some oil and a small amount of solid was again filtered. The filtrate thus separated was proved to be tetrahydrobenzo-[f]-quinoline as above mentioned, by derivation of the benzoyl compound and by the mixed melting point determination. The yield of the base was 6 g.

The crystals of m. p. 88–90°C were dissolved in 100 cc. of ether and subjected to benzoylation with 3.3 g. of benzoylchloride and alkaline solution. After seven hours, the ethereal solution (a) was separated from the aqueous solution and treated with 100 cc. of 2 N-hydrochloric acid. As the acidic solution was made alkaline and extracted with ether, the ethereal solution gave 1.7 g. of an oily dihydrobenzo-[f]-quinoline. Its picrate and hydrochloride had m. p. 205–206°C and m. p. 255–257°C respectively.

Anal. Found: C, 71.72; H, 5.73. Calcd. for

System of (I) and 1,2,3,4-tetrahydrobenzo-[f]-quinoline (Fig. 1).													
Mol % of (I)	100	90	80	70	60	50	40	30	20	10			
Melting points	92	66	80	88	92	93	92	87	80	63			
Thawing points	90	64	64	79	87	91.5	88	78	—	—			
System of (II) and 1,2,3,4-tetrahydrobenzo-[f]-quinoline.													
Mol % of (II)	70		60		50		40		30		20		
Melting points	73		87		90		89		83		70		
Thawing points	—		80		88		84		75		—		
System of (V) and *cis*-1,2,3,4,9,10,4a,9a-octahydroacridine (Fig. 2).													
Mol % of (V)	100	90	85	80	70	60	50	40	30	20	10	0	
Melting points	55	47	42	45	52	56	58	51	54	63	69	73	
Thawing points	54	39	38	38	38	51	57	48	48	49	58	71	
System of (VI) and 5,6,7,8,9,10,6a,10a-octahydrophenanthridine.													
Mol % of (VI)	100	90	85	80	70	60	50	40	33	30	20	10	0
Melting points	64	60	54	60	63	69	73	75	76	75	73	66	72
Thawing points	63	52	52	52	52	53	66	73	75	74	66	64	70
System of (V) and *trans*-1,2,3,4,9,10,4a,9a-octahydroacridine.													
Mol % of (V)	100	90	80	70	60	50	40	30	20	10	0		
Melting points	55	51	47	43	51.5	57	63	68	75	80	83		
Thawing points	54	43	42	42	43	43	44	45	51	64	81		
System of (IV) and *cis*-1,2,3,4,9,10,4a,9a-octahydroacridine.													
Mol % of (IV)	100	90	80	70	60	50	40	30	20	10	0		
Melting points	110	105	102	98	95	90	80	55	65	71	73		
Thawing points	109	99	94	89	83	73	—	—	—	53	71		
System of (I) and 1,2,3,4,7,8,9,10-octahydrobenzo-[f]-quinoline.													
Mol % of (I)	100	90	80	70	60	50	40	30	20	10	0		
Melting points	93	91	85	78	69	55	42	40	50	61	66		
Thawing points	92	80	66	47	36	34	33	33	35	43	65		
System of (IX) and *cis*-1,2,3,4,10,11-hexahydrocarbazole.													
Mol % of (IX)	100	90	80	70	60	50	40	30	20	10	0		
Melting points	118	114	106	99	92	84	72	83	88	94	99		
Thawing points	116	85	74	71	70	70	70	71	73	78	98		

19) R. Mozingo, "Org. Syntheses" Vol. 21 (1941), p. 15.

$C_{13}H_{11}NHCl$: C, 71.72; H, 5.55%.

On the other hand, the benzoylated compound of tetrahydrobenzo-[f]-quinoline was isolated from the ethereal solution (a).

Melting Point-Composition Diagram. — A sample each of group (A) and group (B) was weighed (about 5 mg.) and dissolved in ether respectively. These ethereal solutions were mixed in a proper ratio, heated for a short time to remove the solvent and then poured into a capillary with a diameter 3–4 mm. The mixture was furthermore dried in a desiccator after complete removal of ether. The phase diagram was obtained by recording both the thawing and melting points of these mixtures, using the common procedures of melting point determination and sometimes using the method of Shinomiya[2].

Thawing and melting points of four combinations resulted in formation of a peak in the diagram (see below and Figs. 1 and 2). For the sake of comparison the same points of several representative cases not forming a molecular compound are also recorded in the following.

Ultraviolet Absorption Measurements. — The measurements were made by the use of a Beckmann quartz spectrophotometer, Model DU. Alcohol or iso-octane (dried over phosphorous pentoxide) was used as solvent. The spectrum was examined at 0.5 mμ intervals near maximum and at 3 mμ intervals at the region from 215 to 360 mμ.

Results and Discussion

The results of thermal analysis for mixtures of one of group (A) and one of group (B) were summarized in Table I and the diagrams of two representative pairs forming molecular compounds were shown in Figs. 1 and 2. Four combinations yielded a peak in the melting point diagram, viz., (I: 1,2,3,4-tetrahydrobenzo-[f]-quinoline), (II: 1,2,3,4-tetrahydrobenzo-[f]-quinoline), (V: *cis*-1,2,3,4,9,10,4a,9a-octahydroacridine) and (VI: 5,6,7,8,9,10,6a,10a-octahydrophenanthridine); but there was no peak in the others. It is to be noted that these molecular compounds are

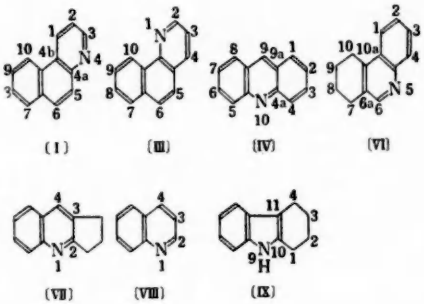

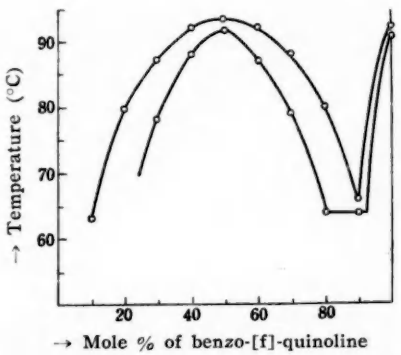

Fig. 1. Molecular compound between benzo-[f]-quinoline and 1,2,3,4-tetrahydrobenzo-[f]-quinoline.

TABLE I

ON THE FORMATION OF CRYSTALLINE MOLECULAR COMPOUNDS

Group A	Group B	Molecular compound	
		Molar ratio	Melting point (°C)
(I)	1,2,3,4-Tetrahydrobenzo-[f]-quinoline	1 : 1	93—93.5
(I)	1,2,3,4,7,8,9,10-Octahydrobenzo-[f]-quinoline	None	
(I)	1,2,3,4,5,6,4a,4b-Octahydrobenzo-[f]-quinoline	None	
(II)	1,2,3,4-Tetrahydrobenzo-[f]-quinoline	1 : 1	88—90
(III)	1,2,3,4-Tetrahydrobenzo-[h]-quinoline	None	
(IV)	*cis*-1,2,3,4,9,10,4a,9a-Octahydroacridine	None	
(V)	〃	1 : 1	56—58
(V)	*trans*-1,2,3,4,9,10,4a,9a-Octahydroacridine	None	
(VI)	5,6,7,8,9,10,6a,10a-Octahydrophenanthridine	1 : 2	75—76
(VII)	*cis*-1,2,3,4-Tetrahydro-2,3-trimethylenequinoline	None	
(VIII)	1,2,3,4-Tetrahydroquinoline	None	
(IX)	*cis*-1,2,3,4,10,11-Hexahydrocarbazole	None	
(IX)	*trans*-1,2,3,4,10,11-Hexahydrocarbazole	None	

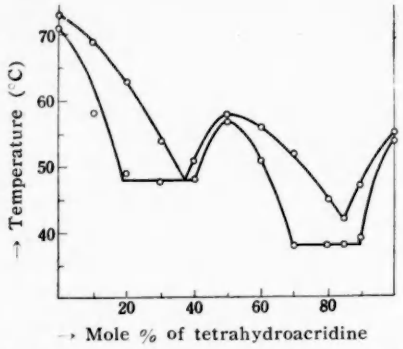

Fig. 2. Molecular compound between 1,2,3,4-tetrahydroacridine and *cis*-1,2,3,4,9,10,4a,9a-octahydroacridine.

formed between the compounds containing nitrogen of anilino-type and those of pyridino-type, but their mixture does not always result in the formation of a molecular compound.

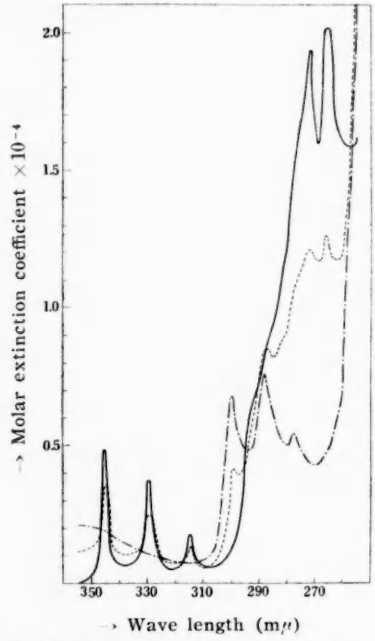

Fig. 3. Ultraviolet absorption spectrum of molecular compound between benzo-[f]-quinoline and its 1,2,3,4-tetrahydro-derivative.
Solvent: isoöctane; conc.: $M \times 10^{-4}$
—— Benzo-[f]-quinoline
—·— 1,2,3,4-Tetrahydrobenzo-[f]-quinoline
----- Molecular compound

The ultraviolet absorption spectra of one of the molecular compounds examined are shown in Fig. 3 together with those of component molecules concerned. They refer to the measurements of the same concentration. Examination of Fig. 3 shows that the intensity of a molecular compound is half of the sum of intensity of partner molecules, indicating that the molecular compound concerned is in a state of complete dissociation. In the other three molecular compounds, a similar phenomenon is found.

There are several papers available which deal with the nature of intermolecular forces in molecular compounds[20-23]. However, no satisfactory explanation has been given even for the most familiar type of molecular compound, viz., quinhydrone formed from quinone and hydroquinone. According to Suzuki and Seki[22], the hydrogen bond is important in the same quinhydrone: they ascribed 4.6 to 1.6 kcal. of the total heat of formation (5.386 kcal.) to this cause. As the molecules of the substance in group A which form molecular compounds have one N atom and those of B have an N—H bond, a hydrogen bond of the N—H···N type may possibly be formed between the interacting molecules in the present case. But this is not the most important cause of the formation of such a molecular compound. For instance, it is to be noted that no molecular compound is formed between benzo-[f]-quinoline and 1,2,3,4,7,8,9,10-octahydrobenzo-[f]- quinoline (see Table 1).

Contrary to Suzuki and Seki, Tsubomura[23] holds a view that the effect of charge transfer is most important in quinhydrone. However, no definite support was obtained for that theory of charge transfer from the present authors' measurement of ultraviolet absorption spectra. Therefore, further measurement under different conditions is desirable.* It may, however, suffice to point out here that all the molecules concerned have π-electrons and that the formation of molecular compounds seems to be affected by such a factor as the number of unsaturated rings.

Lastly it is of interest to note that the *cis*-isomer of hydrogenated acridine is

20) K. Higasi and K. Hirota, "Riron Yuki-Kagaku." Asakura-Shoten, Tokyo (1951), p. 40.
21) H. Murakami, This Bulletin, **26**, 441 (1953).
22) S. Seki and K. Suzuki, ibid., **26**, 372 (1953).
23) H. Tsubomura, ibid., **26**, 304 (1953).
* The writers propose to study this problem in the future.

capable of participating in molecular compound formation, while the *trans*-isomer has no such capacity. Therefore, the spatial configuration seems to be one of the factors, suggesting the importance of van der Waal's force in the molecular compound formation.

The present research was conducted under the supervision of President H. Suginome of the University and the authors are especially indebted to Professor K. Higasi for his kind guidance and criticism.

Chemistry Department, Faculty of Science
Hokkaido University, Sapporo

Effect of Emulsifier upon the Compositions of Emulsion Copolymers of Acrylonitrile and Water-soluble Monomers

By Moriya UCHIDA and Hideo NAGAO

(Received October 3, 1956)

Introduction

In a previous paper[1] we reported that the compositions of emulsion copolymers of acrylonitrile and water-insoluble monomers such as vinylidene chloride or styrene depend upon the concentrations of emulsifier in aqueous solutions. In this paper, first, the relations between the compositions of emulsion copolymers of acrylonitrile and the other water-soluble monomers such as methyl methacrylate vinylacetate and methyl acrylate and the amounts of emulsifier used are given and then the deviations of monomer polymer composition curves of emulsion copolymerizations from those of bulk copolymerizations are discussed.

Experimental

Acrylonitrile (AN).—Redistilled American Cyanamide Co. material was used for all experiments.

Methyl Methacrylate (MMA).—Redistilled Mitsubishi Rayon Co, material was used.

Vinyl Acetate (VAc).—Redistilled commercial material was used.

Methyl Acrylate (MA).—Redistilled Toa Gosei Chemical Co. material was used.

Emulsifier (Sodium Dodecyl Sulfate).—Recrystallized Kao soap Co. material was used.

Emulsion polymerization procedure was the same as that used in the previous report[2].

The amount of water used was 8 times as much as that of the monomer, and 0.8% by weight of the potassium persulfate as the catalyst, and 0.8% by weight of sodium bisulfate as reductant (both based on the total monomers) were employed. The polymerization temperature was 45°C. The combined acrylonitrile in copolymer was determined by the Kjeldahl method. The composition of monomer oil phase was determined by the refractive indices method as we previously reported[1].

Results and Discussion

(1) Effect of Emulsifier upon the Compositions of Copolymers.—In the copolymerization 0, 0.1, 0.2, 0.4, 0.6, 1.0 and 1.5%

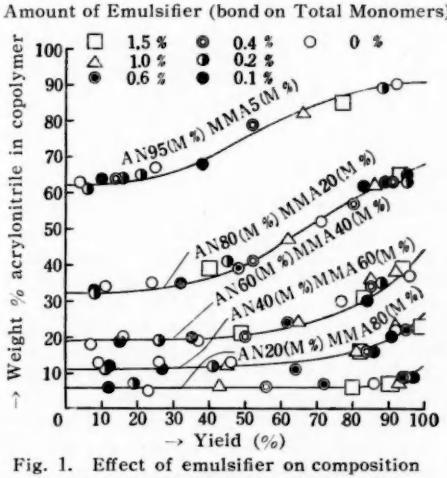

Fig. 1. Effect of emulsifier on composition of acrylonitrile methyl methacrylate copolymers.

1) M. Uchida and H. Nagao, This Bulletin, **30**, 314 (1957).
2) M. Uchida and H. Nagao This Bulletin, **29**, 928 (1956).

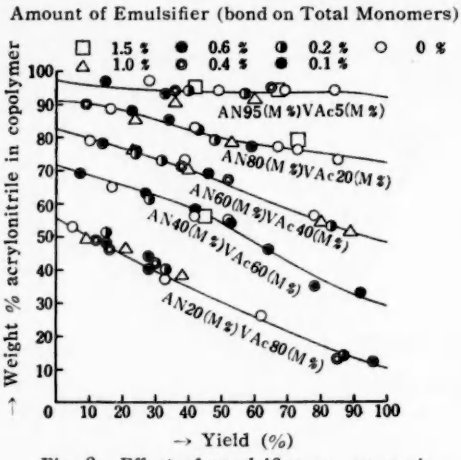

Fig. 2. Effect of emulsifier on composition of acrylonitrile vinyl acetate copolymers.

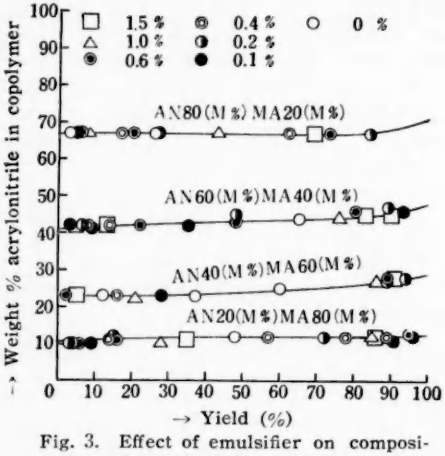

Fig. 3. Effect of emulsifier on composition of acrylonitrile methyl acrylate copolymers.

by weight of emulsifier based on total monomers were used. The compositions of copolymers thus formed in various degrees of conversion for the copolymerization of acrylonitrile and methyl methacrylate are given in Fig. 1, Fig. 2 and Fig. 3 show the corresponding results for the copolymerization of acrylonitrile and vinyl acetate and that of acrylonitrile and methyl acrylate respectively. In these copolymerizations, the compositions of copolymers are independent of the concentrations of emulsifier.

(2) Monomer-polymer Composition Curves.—The monomer-polymer composition curves obtained from the compositions of copolymers extrapolated to 0 conversion are given in Figs. 4, 5 and 6. As to the relative reactivities between acrylonitrile and the other monomers for the bulk copolymerization, the data hitherto known are cited as follows.

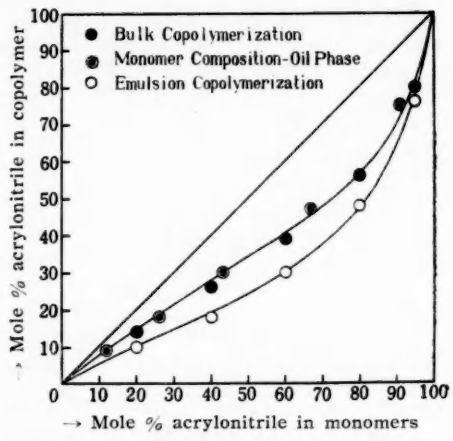

Fig. 4. Monomer-polymer composition curves for acrylonitrile methyl methacrylate copolymerization.

Monomer		Relative Reactivity	
M_1	M_2	r_1	r_2
Methyl methacrylate	Acrylonitrile	1.35±0.1	0.18 ±0.1[3]
Acrylonitrile	Vinyl acetate	4.05±0.3	0.061±0.013[4]
Acrylonitrile	Methyl acrylate	0.67±0.1	1.26 ±0.1[5]

From the monomer-polymer composition curves given in Figs. 4, 5 and 6, it will be seen that while the curve of acrylonitrile methyl methacrylate emulsion copolymerization is not superposed on that of the bulk copolymerization, those of the other copolymerizations fall on the latter. For the purpose of determining monomer oil phase compositions, the refractive indices of monomer mixture of known compositions saturated with water and monomer oil phases were measured. The results are given in Table I, II and III.

3) F. M. Lewis, F. R. Mayo, and W. F. Hulse, *J. Am Chem. Soc.*, **67**, 1701 (1945).
4) F. R. Mayo, C. Walling, F. M. Lewis and W. F. Hulse, ibid., **70**, 1523 (1948).
5) S. Okamura, "Outlook of High Polymer" Vol. 5, Association of High polymer Chemistry, Kyoto, Japan (1952), p. 42.

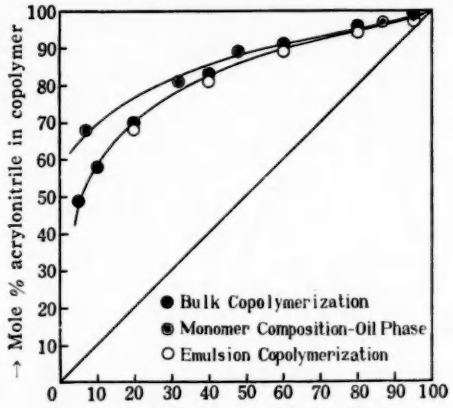
→ Mole % acrylonitrile in copolymer
→ Mole % acrylonitrile in monomers
● Bulk Copolymerization
◉ Monomer Composition-Oil Phase
○ Emulsion Copolymerization

Fig. 5. Monomer-polymer composition curves for acrylonitrile vinyl acetate copolymerization.

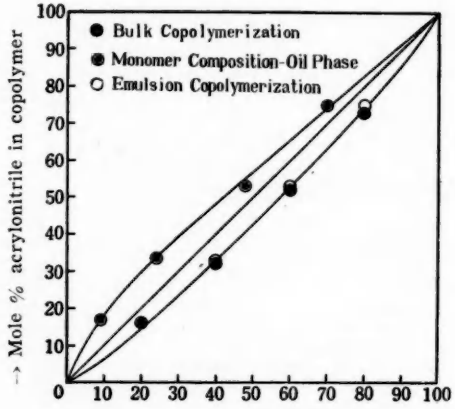
→ Mole % acrylonitrile in copolymer
→ Mole % acrylonitrile in monomers
● Bulk Copolymerization
◉ Monomer Composition-Oil Phase
○ Emulsion Copolymerization

Fig. 6. Monomer-polymer composition curves for acrylonitrile methyl acrylate copolymerization.

TABLE I

REFRACTIVE INDICES OF ACRYLONITRILE-METHYL METHACRYLATE SOLUTIONS

Composition of solution		Monomer saturated with water	Oil phase
AN (M%)	MMA (M%)	n_D^{45}	n_D^{45}
95	5	1.3780	1.3795
80	20	1.3830	1.3860
60	40	1.3882	1.3919
40	60	1.3930	1.3965
20	80	1.3975	1.3991
0	100	1.4009	1.4009

TABLE II

REFRACTIVE INDICES OF ACRYLONITRILE-VINYL ACETATE SOLUTIONS

Composition of solution		Monomer saturated with water	Oil phase
AN (M%)	VAc (M%)	n_D^{45}	n_D^{45}
100	0	1.9769	—
95	5	1.3777	1.3779
80	20	1.3780	1.3787
60	40	1.3800	1.3804
40	60	1.3807	1.3808
20	80	1.3813	1.3814
0	100	1.3820	1.3820

TABLE III

REFRACTIVE INDICES OF ACRYLONITRILE-METHYL ACRYLATE SOLUTIONS

Composition of solution		Monomer saturated with water	Oil phase
AN (M%)	MA (M%)	n_D^{45}	n_D^{45}
95	5	1.3776	1.3779
80	20	1.3799	1.3816
60	40	1.3830	1.3846
40	60	1.3852	1.3867
20	80	1.3872	1.3882
0	100	1.3885	1.3885

If polymerization occurs in oil phase as Fordyce, Chapin[6] and Smith[7] asserted, the monomer-polymer composition curves will be dependent upon the composition of oil phase.

The amounts of acrylonitrile in oil phase were estimated from their refractive indices. The composition of oil phase was used in place of the monomer compositions. The monomer-polymer composition curves thus represented are shown in Figs. 4, 5 and 6.

It is seen that this correction of the compositions of emulsion oil phases makes the emulsion and bulk copolymerzation composition curves identical only in the case of acrylonitrile-methyl methacrylate copolymerization. Consequently, it seems that the water solubility of the monomer affects the compositions of copolymers formed in emulsion copolymerization. The water solubility of this monomer is as follows.

6) R. G. Fordyce and E. D. Chapin, *J. Am. Chem. Soc.*, **69**, 581 (1947).
7) W. V. Smith, ibid., **70**, 2177 (1948).

TABLE IV
WATER SOLUBILITY OF THE MONOMER

Monomer	Solubility (%)	Temperature (°C)
Styrene	0.28	25[8]
Methyl methacrylate	1.5	30[8]
Vinyl acetate	2.5	20[9]
Methyl acrylate	5.2	[9]
Acrylonitrile	7.4	25[10]

In the emulsion copolymerizations of monomers having good water solubility, the composition curves are identical with those of the bulk copolymerizations, that is to say, such emulsion copolymerizations behave just like a solution copolymerization, even if the monomer oil phase exists.

8) F. A. Bovey, I. M. Kolthoff, A. I. Medalia and E. J. Beehan, "Emulsion polymerization," (1955) p. 157.
9) E. R. Blout, W. P. Hohenstein and H. Mark, "Monomer," Inerscience Inc. New York (1949). p. 23 in chapter on "Vinyl Acetate," p. 23 in chapter on "Esters of Acrylic Acid."
10) H. S. Davis, and O. F. Wiedeman, *Ind. Eng. Chem.* **37**, 482 (1945).

Summary

The following facts are found from emulsion copolymerizations of acrylonitrile and water soluble monomers such as methyl methacrylate, vinyl acetate and methyl acrylate.

(1) The compositions of copolymer are independent of the concentration of the emulsifiers used.

(2) The monomer-polymer composition curve of emulsion copolymerization of acrylonitrile and methyl methacrylate is made consistent with that of bulk copolymerization, when the composition of emulsion oil phace is used in place of that of the monomer.

(3) The monomer-polymer composition curves of emulsion copolymerization of acrylonitrile and vinyl acetate or methyl acrylate fall on that of bulk copolymerization.

Research Institute of Teikoku Rayon Co. Ltd., Iwakuni

Action of Emulsifier upon Compositions of Emulsion Copolymers of Acrylonitrile and Water-insoluble Monomers

By Moriya UCHIDA and Hideo NAGAO

(Received August 1, 1956)

Introduction

It has been reported by several investigators[1-5] that the composition of copolymer forming in a copolymerization depends upon the monomer composition at that instant. Moreover, Alfrey and Goldfinger[6], Mayo and Lewis[7], and Walling and Briggs[8] derived independently the general equation describing monomer-polymer composition relationship, with which the experimental data determined for bulk copolymerization showed agreement. However, the water solubility of a monomer can not be neglected in the copolymerization system, in case water is used as the medium.

Fordyce and Chapin[9] compared the composition of the copolymer of styrene and acrylonitrile obtained in emulsion polymerization with that of the copolymer obtained in bulk polymerization, and found that the emulsion copolymer is consistently richer in styrene, though by a small amount, than the bulk copolymer produced from the same initial monomer composition.

They have suggested that this difference may be due solely to the decrease in the content of acrylonitrile of the oil phase, which resulted from the water solubility of acrylonitrile. Smith[10] determined the

1) F. T. Wall, *J. Am. Chem. Soc.*, **66**, 2050 (1944).
2) F. M. Lewis, F. R. Mayo and W. F. Hulse, ibid. **67**, 1701 (1945).
3) T. Alfrey, Jr., and E. Lavin., ibid., **67**, 2044 (1945).
4) T. Alfrey, Jr., E. Merz and H. Mark, *J. Polymer. Sci.*, **1**, 37 (1946).
5) T. Alfrey, Jr., and G. Goldfinger, *J. Chem. Phys.*, **14**, 115 (1946).
6) T. Alfrey, Jr., and G. Goldfinger, ibid., **12**, 202, 322 (1944).
7) F. R. May and F. M. Lewis, *J. Am. Chem. Soc.*, **66**, 1594 (1944).
8) C. Walling and E. R. Briggs, ibid., **67**, 1774 (1945).
9) R. G. Fordyce and E. C. Chapin, ibid., **69**, 581 (1947).
10) W. V. Smith, ibid., **70**, 2177 (1948).

compositions of styrene-acrylonitrile solutions in equilibrium with water-acrylonitrile solutions and showed that Fordyce and Chapins' emulsion polymerization data were indentical with their bulk polymerization data in regard to composition of copolymer produced from a given oil phase, when the equilibrium composition was used to calculate the acrylonitrile contents of the oil phases presented in their emulsion copolymerization experiments.

However, in the system of copolymerization of water soluble monomer as acrylonitrile and water-insoluble monomer such as styrene, the copolymer compositions are not always dependent upon the monomer composition in oil phase as shown by Fordyce and Smith.

As we reported, in the copolymerization of acrylonitrile-vinylidene chloride[11] and acrylonitrile-styrene[12], the compositions of emulsion copolymers depend upon the amount of emulsifier used. This paper deals with the variation of the monomer-polymer composition curve arising from the variation of the amount of emulsifier used.

Experimental

The emulsion polymerization procedure was the same as that of previous reports[2,3]. The emulsifier is Sodium Dodecyl Sulfate.

In the case of benzoyl peroxide as a catalyst, the amount of benzoyl peroxide used was 1 weight % against total monomers and the copolymerizations were done at the temperature of 75°C. The polymerizations were allowed to proceed to low conversions (mostly <5%) and the initial polymer was isolated and purified. The amount of combined acrylonitrile in the initial copolymer was determined by the Kjeldahl analysis.

The acrylonitrile-vinylidene chloride solutions were thoroughly shaken with the given amounts of water, in a water bath maintained at 25°C and thus the solutions were separated into two phases. Then the concentrations of acrylonitrile in the partition phases were determined by the following methods.

A. Method by Acrylonitrile Analysis.—The acrylonitrile in a sample with-drawn from oil phase was analysed by n-dodecyl-mercaptan method[14] and the amount of acrylonitrile in oil phase was determined. In this case, vinylidene chloride did not injure the acrylonitrile analysis as shown in Fig. 1.

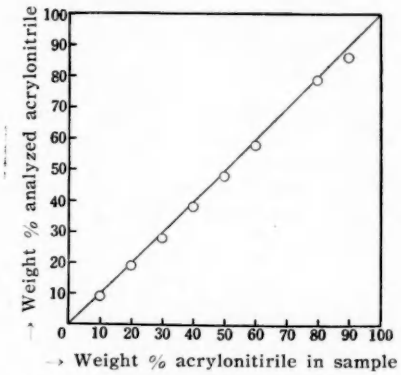

Fig. 1. Analyses of acrylonitrile in vinylidene chloride.

Then the amount of acrylonitrile in water phase was determined by the procedure.

B. Method by Specific Gravity Measurement.—The relationship between specific gravity and composition was established by preparing acrylonitrile-vinylidene chloride solutions of known compositions and measuring the specific gravity with pycnometer.

The results used to establish the relationship are given in Table I. All compositions were determined by linear interpolation of the data in Table I.

TABLE I

SPECIFIC GRAVITIES AND REFRACTIVE INDICES OF ACRYLONITRILE VINYLIDENE CHLORIDE SOLUTIONS

Composition of solution		Specific gravity	Refractive index
Acrylonitrile (weight %)	Vinylidene chloride (weight %)	25°C	n_D^{25}
100.00	0.00	0.8002	1.3888
90.00	10.00	0.8264	1.3908
80.00	20.00	0.8554	1.3918
70.00	30.00	0.8855	1.3945
60.00	40.00	0.9199	1.3976
50.00	50.00	0.9542	1.3999
40.00	60.00	0·9905	1.4018
30.00	70.00	1.0410	1.4077
20.00	80.00	1.0879	1.4113
10.00	90.00	1.1438	1.4163
0.00	100.00	1.2074	1.4215

The relationship between specific gravity and acrylo-nitrile concentration in its aqueous solution was established by the same procedure as above. The results thereof are given in Table II.

11) H. Nagao, M. Uchida and T. Yamaguchi, *J. Chem. Soc. Japan*, in press "Emulsion Copolymerization of Acrylonitrile and Vinylidene chloride."

12) H. Nagao, M. Uchida and T. Yamaguchi, ibid., in press "Heat Stability of Emulsion Copolymer of Acrylonitrile and Vinylidene chloride."

13) M. Uchida and H. Nagao, This Bulletin, **29**, 928 (1956).

14) D. W. Beesing, W. P. Tyler, D. M. Kurtz and S. A. Harrison, *Anal. Chem.*, **21**, 1073 (1949).

TABLE II
SPECIFIC GRAVITIES AND REFRACTIVE INDICES OF ACRYLONITRILE AQUEOUS SOLUTION

Composition of solution		Specific gravity	Refractive index
H_2O (weight %)	Acrylonitrile (weight %)	25°C	n_D^{25}
100.00	0.00	0.9971	1.3325
99.00	1.00	0.9965	1.3329
98.00	2.00	0.9950	1.3337
97.00	3.00	0.9941	1.3341
96.00	4.00	0.9931	1.3348
95.00	5.00	0.9915	1.3363
94.00	6.00	0.9911	1.3375
93.00	7.00	0.9898	1.3376

Then the compositions of partition phases were determined by measuring their specific gravities, respectively.

C. Method by Refractive Index Measurement.—The relationship between refractive index and composition was established by preparing monomer solution and acrylonitrile aqueous solutions of known compositions and measuring the refractive index with Pulfrich refractometer. The results are given in Table I, II and III.

TABLE III
REFRACTIVE INDICES OF ACRYLONITRILE-STYRENE SOLUTIONS

Composition of solution		Refractive index	Refractive index of solution saturated with water
Acrylonitrile (mol. %)	Styrene (mol. %)	n_D^{25}	n_D^{25}
100.00	0.00	1.3888	1.3881
95.00	5.00	1.4027	1.3996
80.00	20.00	1.4385	1.4356
60.00	40.00	1.4750	1.4726
40.00	60.00	1.5019	1.5028
20.00	80.00	1.5276	1.5252
0.00	100.00	1.5464	1.5460

Then the compositions of oil and water phases were determined by measuring their refractive indices.

The composition of Acrylonitrile in styrene phase was determined by refractive index measurement and by calculating from analytical value of acrylonitrile in water phase.

Results and Discussion

(1) Acrylonitrile-Vinylidene chloride Copolymerization.—The various equilibrium compositions of oil and water phases were measured. The results are given in Figs. 2 and 3.

In the emulsion copolymerization of acrylonitrile-vinylidene chloride, the composition of copolymer was dependent upon

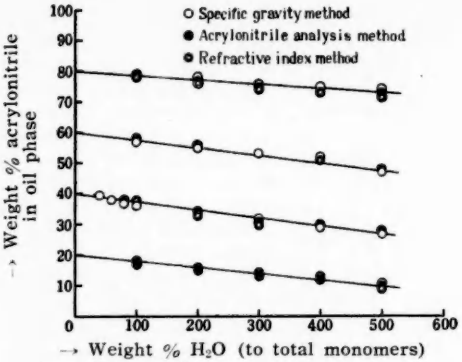
Specific gravity method
Acrylonitrile analysis method
Refractive index method
→ Weight % acrylonitrile in oil phase
→ Weight % H_2O (to total monomers)

Fig. 2. Partition of acryronitrile in vinylidene chloride.

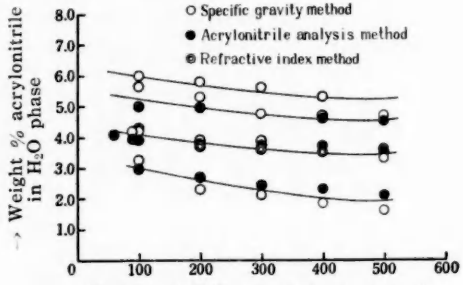
Specific gravity method
Acrylonitrile analysis method
Refractive index method
→ Weight % acrylonitrile in H_2O phase
→ Weight % H_2O (to total monomers)

Fig. 3. Partition of acrylonitrile in water.

the amount of emulsifier used; the composition of the compolymer forming either no emulsifier or very dilute emulsifier solutions, containing much acrylonitrile. The monomer-polymer composition curves are shown in Fig. 4.

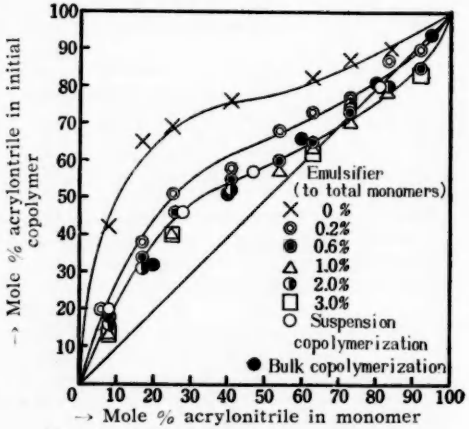

Fig. 4. Monomer-polymer composition curves for acrylonitrile-vinylidene chloride (I).

The compositions of copolymers became richer in styrene along with the increase in the amount of emulsifier used.

The relative reactivity between acrylonitrile and vinylidene chloride has been found in bulk polymerization[2].

r_1 (Acrylonitrile)	r_2 (Vinylidene chloride)	Temperature.
0.91±0.10	0.37±0.10	60°C

When the monomer-polymer composition curve is drawn in Fig. 4 from above r_1, r_2 values, it will be seen that this curve comes between that of emulsifier-free copolymerization and that of emulsion copolymerizations. If polymerization occurs in oil phase as was asserted by Fordyce, Chapin[9] and Smith[10], the monomer-polymer composition curves will be dependent upon the composition of oil phase. The amounts of acrylonitrile in oil phase are shown in Fig. 5. As we substituted the compositions of oil phase in aqueous polymerization instead of the charged compositions, the monomer-polymer composition curves thereof are shown in Fig. 6.

It is seen that these corrections of the compositions of the emulsion oil phases make the emulsion and bulk copolymerization composition curves identical only in case of the emulsion polymerization using the emulsifier of the critical micell concentration[11]. Moreover, the monomer-polymer composition curve in aqueous suspension copolymerization using benzoyl peroxide as an oil soluble catalyst is shown in Fig. 7.

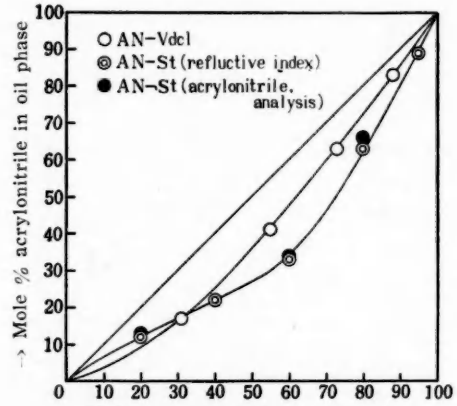
○ AN-Vdcl
◎ AN-St (refluctive index)
● AN-St (acrylonitrile, analysis)
→ Mole % acrylonitrile in oil phase
→ Mole % acrylonitrile in monomers

Fig. 5. Relation between composition of monomer and that of oil phase.

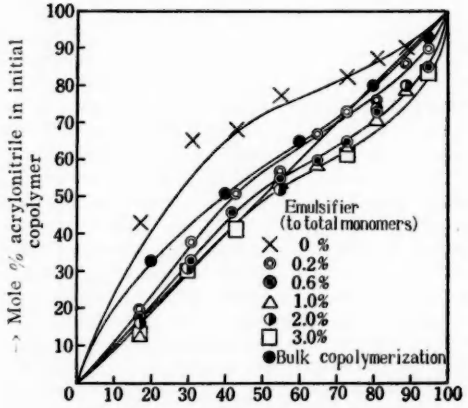

Fig. 6. Monomer-polymer composition curves for acrylonitrile vinylidene chloride (2).

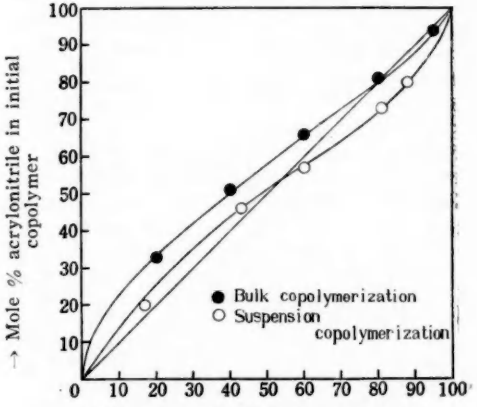
● Bulk copolymerization
○ Suspension copolymerization
→ Mole % acrylonitrile in initial copolymer
→ Mole % acrylonitrite in monomers

Fig. 7. Monomer-polymer composition curves for acrylonitrile-styrene (1).

It will be observed that the aqueous suspension copolymers consistently contain less combined acrylonitrile than the corresponding bulk copolymers. The copolymer composition values for suspension copolymerization were plotted on the basis of monomer concentrations charged to the reaction system, the most of the reacted monomers exist in the oil droplets of the dispersed phase.

With the oil phase compositions, the composition curve of the aqueous suspension copolymerization is identical with that of the bulk copolymerization and also with that of emulsion copolymerization using thicker emulsifier solution. Although

these identities coinside with Smith's theory of oil phase mechanism of emulsion polymerization as Fordyce and Chapin[9] reported about acrylonitrile-styrene emulsion copolymerization, it does not seem to be reasonable that the composition of emulsion copolymers is dependent only upon the oil phase composition, for the copolymer composition varies by emulsifier concentrations as showed in Fig. 6.

(2) Acrylonitrile -Styrene Copolymerization.—As in the case of acrylonitrile-vinylidene chloride emulsion copolymerization, the monomer-polymer composition curve in acrylonitrile-styrene emulsion copolymerization depended upon the amount of the used emulsifier. The results are shown in Fig. 8.

The relative reactivity in bulk copolymerization is shown as follows.

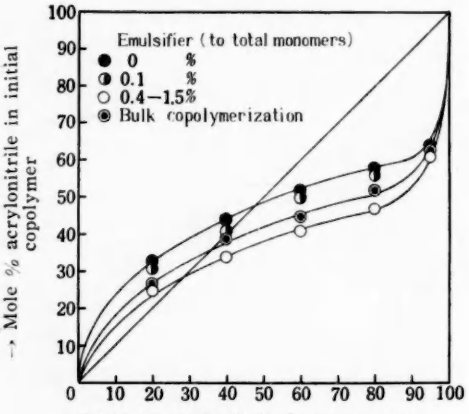
Emulsifier (to total monomers)
● 0 %
◑ 0.1 %
○ 0.4−1.5%
◉ Bulk copolymerization
→ Mole % acrylonitrile in initial copolymer
→ Mole % acrylonitrile in monomers

Fig. 8. Monomer-polymer composition curves for acrylonitrile-styrene. (2).

author	r_1 (styrene)	r_2 (acrylonitrile)	Temperature °C
Lewis, Mayo and Hulse[4]	0.41±0.08	0.04±0.04	60
Fordyce and Chapin[9]	0.41±0.08	0.03±0.03	75
Simha and Wall[15]	0.37±0.02	0.05±0.02	50
Fordyce[16]	0.52±0.04	0.03±0.03	67-80
Goldfinger and Steidlitz[17]	0.38±0.03	0.05±0.02	41.5
〃	0.45±0.03	0.02±0.02	65
〃	0.47±0.03	0.02±0.02	86.5

15) R. Simha and L. A. Wall., *J. Research Natl. Bur. Standards*, **41**, 521 (1948).
16) R. G. Fordyce, *J. Am. Chem. Soc.*, **69**, 1903 (1947).
17) G. Goldfinger and G. I. Carothers, *J. Polymer Sci.*, **4**, 97, (1949).

The values of r_1 and r_2 are mostly independent of the temperature of polymerization with the inrange of 40-80°C. Although our copolymerization temperature was 45°C, the monomer-polymer composition curve in bulk copolymerization was drawn from the data of Lewis, Mayo and Hulse in Fig. 8. This curve comes between the curve of emulsifier-free copolymerization and that of emulsion copolymerization. In this case, the above described emulsion oil phases make the composition curves of emulsion copolymerization using thick concentrations of emulsifier and that of bulk copolymerization identical, but emulsifier-free copolymers contain less combined styrene than the corresponding bulk copolymer.

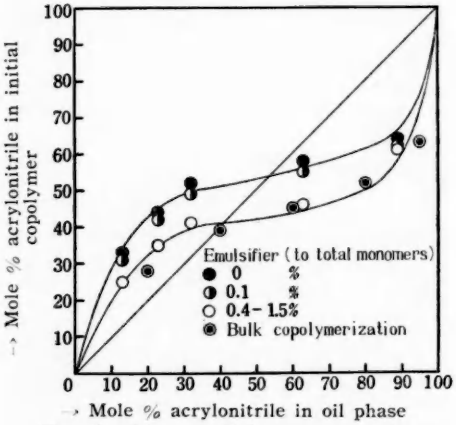
Emulsifier (to total monomers)
● 0 %
◑ 0.1 %
○ 0.4− 1.5%
◉ Bulk copolymerization
→ Mole % acrylonitrile in initial copolymer
→ Mole % acrylonitrile in oil phase

Fig. 9. Monomer-Polymer composition curves for acrylonitrile-styrene (3).

It seems that the water solubility of monomer affects the compositions of forming copolymers in aqueous copolymerizations of water soluble monomer as acrylonitrile and water insoluble monomer as styrene and vinylidene chloride using water soluble catalyst. The initiation of polymerization occurs by reaction between catalyst and monomer in water phase, since in the case of emulsifier-free copolymerization the water phase contains acrylonitrile, so the initial copolymer seems to contain much acrylonitrile. The water phase will contain more water insoluble monomer solubilized in micell, and the initial copolymer seems to contain less acrylonitrile, as the amount of emulsifier.

Summary

The following are the facts found from the monomer-polymer composition curves of aqueous copolymerization of the water soluble monomer as acrylonitrile and the water insoluble monomers as vinylidene chloride and styrene using the water soluble catalyst.

(1) The emulsifier-free aqueous copolymers contained consistently much more combined acrylonitrile than the corresponding bulk and emulsion copolymer.

(2) The emulsion copolymer contained less acrylonitrile as the amount of used emulsifier increased.

(3) The monomer-polymer composition curves of emulsion copolymerizations were identical with that of bulk copolymerization, only when critical micell concentration of emulsifier was in use.

Research Institute of Teikoku Rayon Co, Ltd., Iwakuni

Structure of Reineckate Complex Ion

By Yoshio TAKÉUCHI and Yoshihiko SAITO

(Received November 30, 1956)

Introduction

In the study of the crystal structure of Reinecke's salt, $NH_4[Cr(NCS)_4(NH_3)_2]\cdot 2/3H_2O$, it was found that the reineckate complex ion $[Cr(NCS)_4(NH_3)_2]^-$ contains linear NCS groups. The bond character of the NCS group is expressed by the structure $N\equiv C-S^-$. The reineckate complex ion with the same bond character was also found in pyridine reineckate, $C_5H_5N[Cr(NCS)_4(NH_3)_2]$. The shape and the size of the complex ion in both crystals are identical within the errors of experiment. However, a modified configuration of the complex ion has been found by the study of Patterson projections of choline reineckate, $(CH_3)_3N\cdot CH_2\cdot CH_2\cdot OH[Cr(NCS)_4(NH_3)_2]$, which was prepared from choline chloride and Reinecke's salt solution. In the case of choline reineckate, the bond distances of the complex ion are considerably different from those found in the other two cases and the bond character is no more expressed by the structure $N\equiv C-S^-$ but very close to the structure $N^-=C=S$. Although brief accounts on the crystal structures of these reineckates already appeared separately, because of the importance of understanding the nature of complex ions, a detailed description of the structure of reineckate complex ion will be given in the present paper.

1. The Structure of Reinecke's Salt[1]

(i) Unit Cell and Space Group.— The crystals of Reinecke's salt whose chemical formula had been known as $NH_4[Cr(SCN)_4(NH)_3)_2]H_2O$ crystallize from ethyl alcohol and water in well formed garnet-red rhombic dodecahedra combined with a cube (Fig. 1).

Oscillation and Weissenberg photographs taken with copper radiation ($\lambda=1.5418$ Å) gave lattice constant:

$$a=13.25\pm0.02 \text{ Å},$$

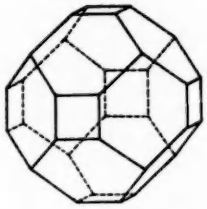

Fig. 1. The crystal habit of Reinecke's salt.

and unit cell contains six formula units. The calculated density 1.496 g./cc. was in good agreement with the observed value 1.503 g./cc. measured by the pycnometer method. The Laue symmetry is O_h-m3m and h,k,l reflexions are systematically absent when $h+k+l$ is odd. Hence, the possible space groups are $O_h^9-I_{m3m}$, $T_d^3-I_{\bar{4}3m}$

1) Y. Saito, Y. Takéuchi and R. Pepinsky, *Z. Krist.* **106**, 476, (1955).

or O^5-I_{43}. Taking account of all possibilities of these space groups, the structure analysis was started. However, by the study of Patterson projection, it became obvious that O_h^9 was a distinct possibility.

(ii) Analysis.—The multiple film technique was employed and intensities were recorded for all three dimensional reciprocal spaces which are covered by copper radiation. These intensities were measured visually using an intensity scale prepared with the same specimen as that used for intensity recording.

The following characteristics of reflexions were observed: hkl is strong when $h=4n_1$, $k=4n_2$, $l=4n_3$ or $h=4n_4+2$, $k=4n_5+2$, $l=4n_6+2$, where n_i are integers. These conditions immediately fixed the positions of heavy atoms as follows: 6Cr in the six-fold positions (b) $0\frac{1}{2}\frac{1}{2}$, and 24S in the twenty four-fold positions (h) $0xx$ with $x\simeq0.25$. This arrangement of heavy atoms was in good accord with conclusions drawn from the Patterson projection P(xy). Distribution of peaks in P(xy) also indicated that 24C and 24N atoms from the thiocyanate groups are on 12(e) $x00$. The first Fourier synthesis was calculated using the signs based on chromium and sulphur atoms. In the electron density projection $\rho(xy)$ thus obtained, two peaks were observed between chromium and sulphur. These peaks must be due to nitrogen and carbon atoms. The distances between these peaks approximately corresponded to the usual bond lengths of Cr—N, N—C and C—S. Since it seems reasonable that the majority of the signs of $F(hk0)$ reflexions are determined by the contribution of the complex ion $[Cr(NCS)_4(NH_3)_2]^-$, the further steps of refinement were made by computing $\rho(xy)$ and generalized projection $\rho(xyl)$ using the signs based on the complex ion. The atomic positions found from these refinements are:

	x	y	z
Cr	0	0.5	0.5
N	0.40	0.40	0
C	0.33	0.33	0
S	0.24	0.24	0
NH_3	0.34	0.34	0

If the empirical formula of the Reinecke's salt is correct, there should be six ammonium and six water molecules in the unit cell. However, in the space group I_{m3m} and any of its subgroups, no six-fold positions are available for these atoms. Then, to find out possible positions of these atoms, the contribution of the complex ion F_r was subtracted from observed structure factor F_{hk0} and trial of computing $\sum\sum(F_{hk0}-F_r)\cos 2\pi(hx+ky)$ was made on X-RAC. The result showed well-defined peaks on sets of special positions 2(a)000 and 8(c)$\frac{1}{4}\frac{1}{4}\frac{1}{4}$ (Fig. 2.).

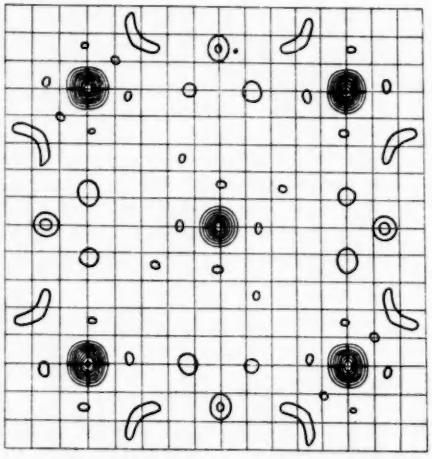

Fig. 2. Residual Fourier projection showing the positions of NH_4 and H_2O groups. Origine is taken at the center of this projection.

In order to obtain the best agreement between observed and calculated structure factors, it was necessary to distribute $6NH_4$ and $4H_2O$ atoms random among these positions. The final refinement of the structure was made by three dimensional Fourier synthesis. The final atomic parameters are:

6Cr:	6(b)	0
24N:	24(h)	$0xx$ with $x=0.395$
24C:	24(h)	$0xx$ with $x=0.334$
24S:	24(h)	$0xx$ with $x=0.238$
$12(NH_3)$:	12(e)	$x00$ with $x=0.338$
$6(NH_4)$ and $2H_2O$:		
	8(c)	$\frac{1}{4}\frac{1}{4}\frac{1}{4}$
$2H_2O$:	2(a)	000

With these coordinates, structure factors were calculated using the temperature factor of the form $\exp-B(\sin^2\theta/\lambda^2)$, where $B=2.0$ Å^2. The R-factor is 11.6% for $F(hk0)$ and 19.0% for $F(hkl)$ reflexions.

(iii) Description of the Structure.—Fig. 3 shows the structure of Reinecke's salt. Chromium atoms are at six corners of the one-eighth of the unit cell. The rest of the corners and the body-centered

position of the cube are occupied by ammonium ions and water molecules randomly. The ammonium ion (and water molecule) at the body-centered position is surrounded by six sulphur atoms octahedrally with the distance of 3.35 Å. The water molecules at the corners of the cube are surrounded by twelve sulphur atoms with the distance of 4.44 Å. Since the bond between ammonium ion and sulphur atoms is ionic from the stand point of atomic distances, it seems reasonable to conclude that the eight-fold position $\left[\frac{1}{4}\frac{1}{4}\frac{1}{4}\right]$ is occupied by six ammonium ions and two water molecules randomly and the two-fold position [000] is occupied by two water molecules. The correct formula of Reinecke's salt is thus $NH_4[Cr(NCS)_4(NH_3)_2]\,\frac{2}{3}\,H_2O$. A similar random distribution of atoms has also been found in the mineral analcite[2].

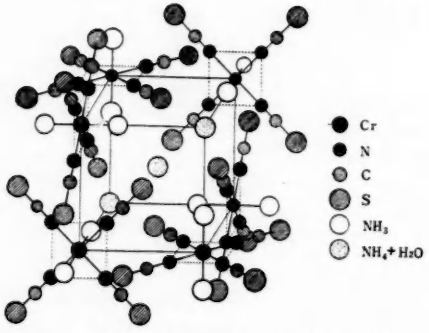

Fig. 3. 1/8 unit cell of Reinecke's salt. $NH_4[Cr(NCS)_4(NH_3)_2]\cdot 2/3\,H_2O$

The square coordination of NCS groups to chromium atoms is shown in Fig. 4 which was obtained from the zero section of the three dimensional Fourier synthesis. The supposed SCN group is actually an iso-thiocyanato group NCS, with N atoms coordinated to chromium. This iso-thiocyanato group is in contrast to $[Hg(SCN)_4][Cu(en)_2]$[3] where the thiocyanato group SCN was found. Four linear NCS groups are arranged along the diagonals of a square around the chromium atom, and NH_3 groups are in the remaining octahedral positions. The symmetry of the complex ion is thus $4/mmm$. Bond lengths of the complex ions are:

Cr—NH_3	2.15±0.03 Å
Cr—N	1.97±0.03
N—C	1.14±0.03
C—S	1.80±0.03

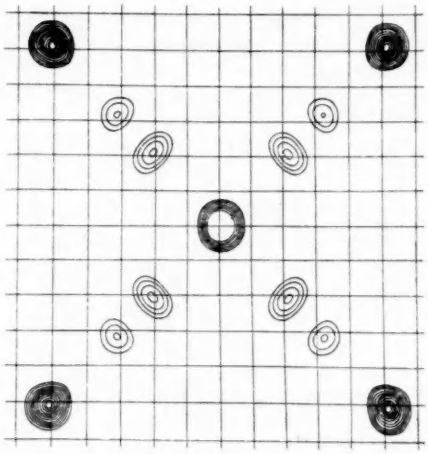

Fig. 4. Three dimensional Fourier section $\rho(xy0)$ of Reinecke's salt with origine at the center.

2. The Structure of Pyridine- and Choline-reineckate

Prior to the discussion on the structure of the complex ion, the crystal structures of pyridine- and choline-reineckate are described. The lattice constants and space groups of these reineckates are given in Table I.

TABLE I
THE LATTICE CONSTANTS AND SPACE GROUPS OF SOME REINECKATES

	Lattice constants				Space group
	a	b	c	β	
Reinecke's salt	13.25 Å				$O_h^9-I_{m3m}$
Pyridine reineckate	15.52	7.64	14.64	102°24′	$C_{2h}^5-A_{2/a}$
Choline reineckate	12.69	22.80	6.75		$D_{2h}^{26}-I_{bma}$

(i) Pyridine Reineckate[4].—The crystals of pyridine reineckate were prepared by Christensen's method[5] and recrystallized in hot alchoholic solution. The measured density of the crystals 1.560 g./cc. is in agreement with the calculated

2) W. H. Taylor, *Z. Krist.*, **74**, 1 (1930); **99**, 283(1938).
3) H. Scouloudi, *Acta Cryst.*, **6**, 651 (1953).
4) Y. Takéuchi and R. Pepinsky, Presented to the Thirteenth Annual Pittsburgh Diffraction Conference, 1955.
5) O. T. Christensen, *J. Prak. Chem.*, **45**, 364 (1891).

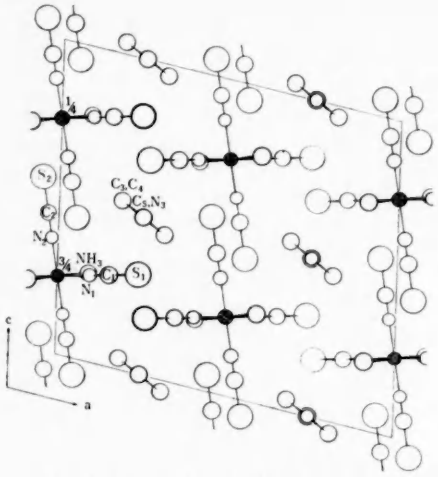

Fig. 5. Projection of the structure of pyridine reineckate aiong *b*-axis.

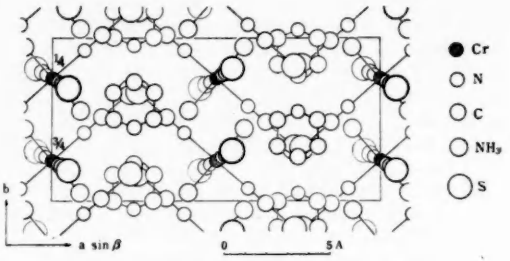

Fig. 6. Projection of the structure of pyridine reineckate along *c*-axis.

density 1.56 g./cc. The crystals obtained were found to be twinned about (101). However, it was possible to separate single crystals and they were used for X-ray work.

The structure was determined by the use of two dimensional Fourier synthesis which resulted in a final agreement factor, $R=\Sigma(|F_o|-|F_c|)/\Sigma|F_o|$, of 0.107 for the (010) projection and of 0.112 for the (001) projection. Fig. 5 and Fig. 6 show the projections of the crystal structure of pyridine reineckate on (010) and (001) respectively. Reineckate groups are arranged around a two-fold screw axis, making a frame-like structure and leaving a big hole around the two-fold axis. The pyridine molecule on the twofold axis is located in a region surrounded by twelve sulphur atoms. Four of these sulphur atoms coordinate to the nitrogen atom of the pyridine molecule with two distances of 3.36 Å and two of 3.60 Å. The configuration of sulphur atoms about a pyridine molecule is shown in Fig. 7. The mean values of the bond lengths determined for the reineckate complex ion are Cr—N= 1.95 Å, N—C=1.15 Å and C—S=1.76 Å. These values agree with those found in Reinecke's salt (p. 321). The bond lengths of pyridine molecules and non-bonded distances of atoms are given in Table III.

The estimation of the accuracy of atomic parameters was carried out especially to the atoms of pyridine molecules. Because of the special position, errors of atomic coordinates in a pyridine molecule mainly

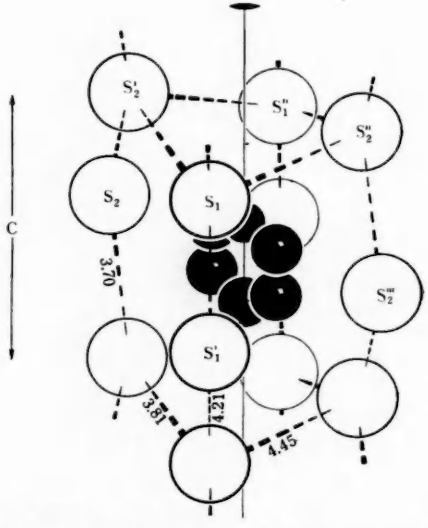

Fig. 7. Configuration of sulphur atoms about a pyridine molecule. Numbers indicate the distances between sulphur atoms in Å.

TABLE II

COORDINATES OF ATOMS IN PYRIDINE REINECKATE

Atom	x/a	y/b	z/c	No. of atoms per cell
Cr	0	3/4	1/4	4
S_1	0.237	0.117	0.306	8
S_2	−0.050	0.831	0.563	8
C_1	0.152	0.021	0.287	8
C_2	−0.035	0.802	0.439	8
N_1	0.095	0.922	0.273	8
N_2	−0.025	0.783	0.365	8
NH_3	0.080	0.536	0.292	8
C_3	0.184	0.489	0.535	8
C_4	0.182	0.671	0.536	8
C_5	1/4	0.746	1/2	4
N_3	1/4	0.420	1/2	4

TABLE III
ATOMIC DISTANCES IN PYRIDINE REINECKATE

Bond lengths of pyridine molecule

$C_3-C_4=1.39$ Å	$C_4-C_5=1.40$ Å
$C_3-N_3=1.35$ Å	

Nonbond distances

$S_1-S_1'=4.21$ Å	$S_1-S_2'=3.80$ Å
$S_2'-S_2=3.70$	$S_1'-S_2''=4.45$
$NH_3-N_3=3.60$	$NH_3-C_3=3.78$
$NH_3-C_3'=3.99$	$NH_3-C_4'=4.11$
$NH_3-C_4=3.90$	$NH_3-C_5=3.84$
$N_3-S_1=3.36$	$N_3-S_2'=3.60$
$C_3'-S_1=3.38$	$C_3'-S_2''=3.47$
$C_4-S_2=3.82$	$C_4-S_1'=4.34$
$C_5-S_1=4.33$	

distribute in their y-parameter. The standard deviations $\sigma(y)$ for the positions of carbon and nitrogen atoms were calculated, using Cruickshank's method[6] were found to be 1.9×10^{-2} Å and 1.7×1.0^{-2} Å respectively. Standard deviations $\sigma(x)$ and $\sigma(z)$ for carbon atoms of pyridine molecule were 1.2×1.0^{-2} Å.

(ii) Choline Reineckate[7].—Choline reineckate was prepared using a diffusion method with choline chloride and Reinecke's salt solution in silica gel. The colour of the crystal is magenta as are other reineckates. A study of morphology and optical properties showed the crystal to be orthorhombic with holohedral symmetry. The crystal is tabular parallel to (010) and shows (110), (101) forms. There are four formula units of $[C_5H_{13}N(OH)][Cr(NCS)_4(NH_3)_2]$ in the cell giving a calculated specific gravity of 1.48 g./cc. which compares well with the measured value of 1.475 g./cc.

From cell dimension and space group symmetry, it is obvious that the chromium atom is located on a centre of symmetry whose point symmetry is $2/m$. On a Patterson projection $P(uv)$, a fairly well-resolved peak is observed at the point $u=0.175$, $v=0.118$. It has been known that Cr—N—C—S bond is straight and Cr—S distance is 4.9 Å, accordingly the Cr—S vector should appear on the line $y=4.9\times1/\sqrt{2}$ Å (0.153 as decimal fraction of the b-axis). From the packing view point, the estimated Cr—S vector position will be $u_0\simeq0.180$, $v_0\simeq0.153$. (Fig. 8) The relative peak height at (u_0, v_0) seems to be unreasonable as Cr—S vector, while the peak at (u, v) could not be explained from Cr—N—C—S straight configuration. However, it was found that the position (u, v) is better for sulphur location to obtain better agreement between calculated and observed structure factors of several strong reflexions. Then the first Fourier based on signs of $F(hk0)$ calculated from Cr and S at (u, v) position was computed on X—RAC. The result revealed that the Cr—N—C angle is not 180° as has been found in other reineckates but has a value of 158° on the (001) projection.

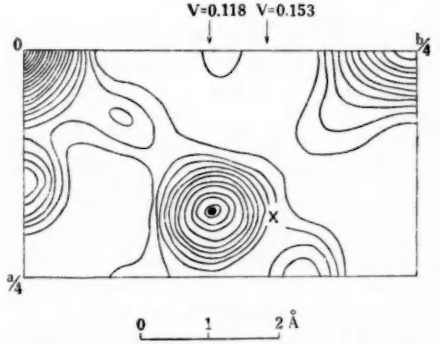

Fig. 8. Patterson projection $P(xy)$ of choline reineckate.
● Cr—S vector position in choline reineckate.
× Cr—S vector position expected from Cr—N—C—S straight configuration.

The structure was refined on the projections (100) and (001). The final refinement was made by computing a three-dimensional Fourier synthesis. The atomic parameters derived from the three-dimensional Fourier are given in Table 4. The R-factor is 11.2% for $F(hk0)$, 13.5% for $F(0kl)$ and 17.0% for $F(hkl)$.

TABLE IV
ATOMIC PARAMETERS FOUND IN CHOLINE REINECKATE

Atom	x/a	y/b	z/c	
Cr	0	0	0	
N	0.058	0.057	0.182	
C	0.107	0.084	0.317	
S	0.173	0.115	0.493	
NH_3	0.139	0	−0.175	
N	0	0.25	0.03	
C_1	0.07	0.28_3	0.16	Choline molecule *
C_2	−0.07	0.28_3	−0.13	
C_3	−0.08	0.25_9	-0.29_1	
OH	0.01_8	0.27	-0.29_3	

6) D. W. J. Cruickshank, *Acta Cryst.*, **2**, 151 (1949).
7) Y. Takéuchi and R. Pepinsky, Presented to the ACA annual meeting (1956).

* This set of coordinates corresponds to the orientation given in Fig. 10.

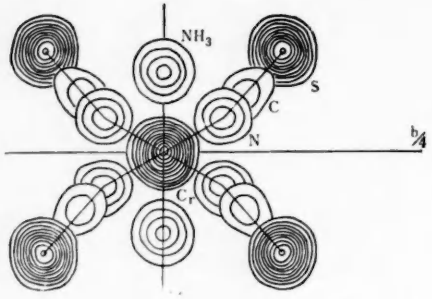

Fig. 9. Composite electron density map of the reineckate group in choline reineckate; view along c-axis. Even-contours only drawn for chromium.

Fig. 9 shows the composite electron density map of the complex ion found in choline reineckate. The structure projections on (001) and (100) are given in Fig. 10. The chromium atoms of the complex ions are on the mirror plane and form a layer-like structure parallel to (010). Between these layers, choline molecules are located on the two-fold axis in a region surrounded by four sulphur atoms tetrahedrally. The choline molecule is randomly oriented in four possible positions so that the two fold axis at $\left(0, \frac{1}{4}, z\right)$ has only statistical meaning. The configuration of the choline molecule was found to be close to a "gauche" configuration. Possibly, the weak interaction between the choline and the complex ion results in a significant interaction between the positive nitrogen atom and the hydroxyl group in the same molecule.

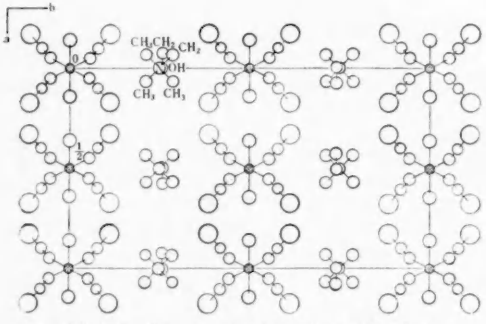

Fig. 10 (a). Structure of choline reineckate, projected on (001).

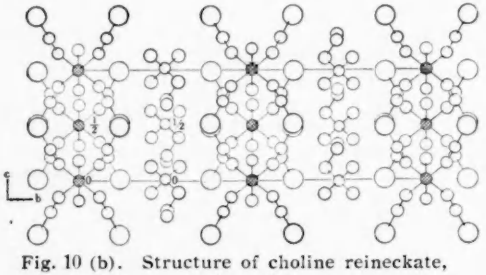

Fig. 10 (b). Structure of choline reineckate, projected on (100). Only one possible orientation is shown for choline molecule.

3. Structure of Reineckate Complex Ion

Fig. 11 shows two different configurations of the reineckate complex ion which we have found by the study of these three reineckates. Bond lengths and bond angles are compared in Table V.

These results suggest that in choline reineckate the contribution of the structure

$$N^{-}=C=S \qquad (1)$$

is dominant, while in ammonium and pyridine reineckates the contribution of the structure

$$N\equiv C-S^{-} \qquad (2)$$

is dominant. These two different cases may be explained as follows.

TABLE V

	Cr-S	N-C	C-S	Cr-NH_3	Cr-N-C
Reinecke's salt	1.97	1.14	1.80	2.15	180°
Pyridine reineckate	1.95	1.15	1.76	2.11	180°
Choline reineckate	1.94	1.27	1.64	2.12	155.5°

In the case of ammonium and pyridine reineckates, positively charged nitrogen atoms can approach the sulphur atoms of the reineckate groups closely. The electrons are, accordingly, more shifted towards the sulphur atoms in the NCS groups due to the polarization by the nitrogen atoms. In this case, structure (2) will be more stable than structure (1). On the other hand, in the case of the choline molecule, the nitrogen atom with positive charge is surrounded by carbon atoms tetrahedrally and does not approach the sulphur atoms as closely, and the polarization effect on the NCS groups due to the nitrogen of the choline molecule will be smaller. This would result in the dominant contribution of the structure (1). Actually, the NH_4—S and NH—S distances in ammonium and pyridine reineckates are

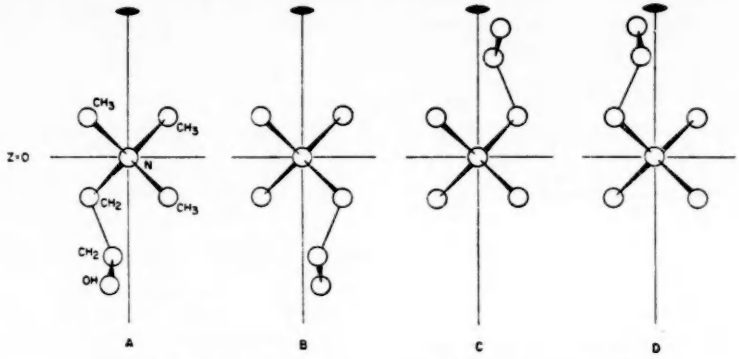

Random orientation of choline molecule in choline reineckate. Four possible orientations are shown.

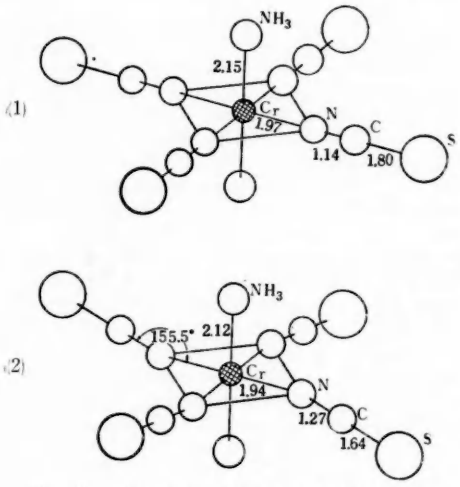

Fig. 11. Configuration of reineckate complex ion found in Reinecke's salt (1) and in choline reineckate (2). Bond distances and bond angle are shown.

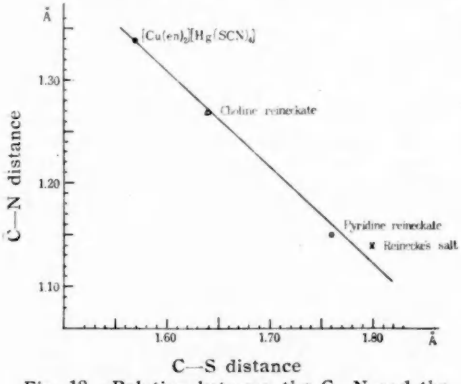

Fig. 12. Relation between the C—N and the C—S distances in various reineckates.

respectively 3.35 Å and 3.36 Å, while in choline reineckate the N—S distance is 4.9 Å. Also, it is interesting to note that in comparison with the other reineckates, the nitrogen atoms of the choline molecule are closer to the nitrogen atoms of the reineckate groups with the distance of about 4.6 Å.

An interesting relation has been found between the C—N and the C—S distances in NCS groups found in various reineckates. If C—N distances are plotted against the C—S distances, a straight line is obtained as illustrated in Fig. 12.

Summary

The crystal structure analyses of Reinecke's salt, pyridine reineckate and choline reineckate established the configuration and bond characters of the reineckate complex ion, $[Cr(NCS)_4(NH_3)_2]^-$.

The bond character of the complex ion in Reinecke's salt and pyridine reineckate corresponds to the structure $N\equiv C-S^-$, while in choline reineckate the bond character is acounted for by the structure $N^-=C=S$. This mutation of the bond character is discussed together with crystal structures of these reineckates.

This work was done at the Pennsylvania State University in the laboratory of Prof. Ray Pepinsky, to whom we are greatly indebted for the facilities made available to us. We are also grateful to Mr. H. Yamatera of Osaka City University for helpful discussions.

Mineralogical Institute
Department of Science
The University of Tokyo, Hongo Tokyo

Institute of Polytechnics
Osaka City University, Kita-ku, Osaka

Studies on Micelles. III. A Check of the New Conclusion from the Spectral Experiments with the Well-known Experimental Facts of Other Authors

By Hiroji SASAKI

(Received September 8, 1956)

Introduction

From his absorption spectral experiment, the author has discovered[1] that in a certain wide concentration range of surfactants in aq. solutions the micellar concentration C_m is independent of the surfactant concentration C_s and that in this surfactant concentration range only the association number of micelle N_m increases with increasing surfactant concentration.

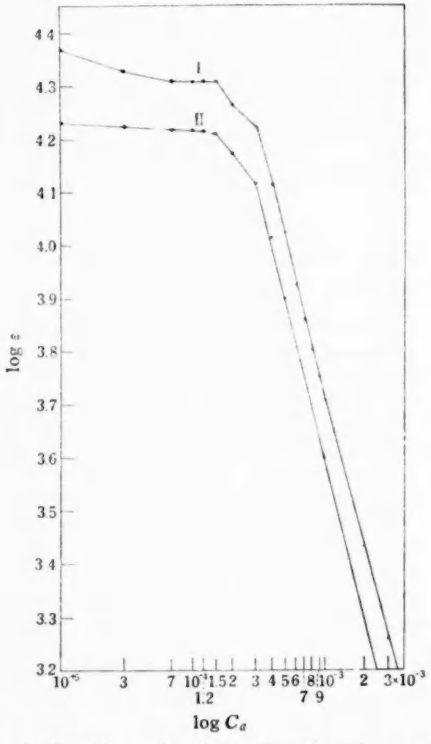

Fig. 1. Absorption intensity of azobenzene at 320 mμ. C_a is the molar concentration of azobenzene. Solvents: I C_2H_5OH, II 10% SDS.

1) H. Sasaki, S. Saito and H. Okuyama, This Bulletin, **30**, 186 (1957).

The facts which have led the author to this conclusion will be discussed briefly.

(a) The curve I in Fig. 1 is the absorption intensity of azobenzene at 320 mμ in ethanol. The curve bends remarkably at about azobenzene concentration C_a being 1.2×10^{-4} M. This lowering of absorption intensity is caused by the association of azobenzene. The curve II in Fig. 1 is the absorption intensity of azobenzene in aq. 10% SDS (sodium dodecyl sulfate) solution. The curve is almost parallel to the abscissa until C_a reaches about 1.2×10^{-4} M, which means that azobenzene molecules are mainly in the unassociated state, i. e., until C_a reaches about 1.2×10^{-4} M there are few micelles which contain more than two azobenzene molecules. The curve bends remarkably at about C_a being 1.2×10^{-4} M, which means that the micelles containing more than two azobenzene molecules appear largely at about this concentration. Therefore the micellar concentration C_m can be

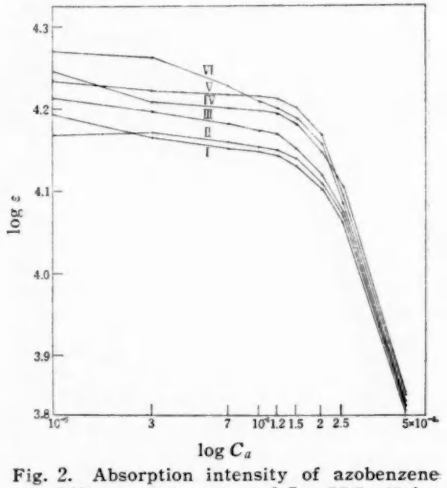

Fig. 2. Absorption intensity of azobenzene at 320 mμ. Solvents: I 0.5% SDS, II 1% SDS, III 2.5% SDS, IV 5% SDS, V 10% SDS, VI 20% SDS.

estimated safely as about 1.2×10^{-4} M in aqueous 10% SDS solution.

(b) Fig. 2 shows absorption intensity of azobenzene at 320 mμ in aqueous SDS solutions of various concentrations. The bending part of every curve is almost at the same azobenzene concentration, from which it is concluded that the micellar concentration of SDS is almost constant irrespec tive of SDS concentration in the range above 0.5% and below 20%.

(c) The reasonable conclusion deduced from the discussion (a) and (b) is that in a certain wide range of SDS concentration, the association number of SDS-molecules in one micelle increases with increasing SDS concentration.

The author has stated, in his previous report, how a micelle will grow*). The conclusions mentioned there and the natural inference deduced from these conclusions are as follows: (1) above the CMC, micellar concentration C_m increases with increasing surfactant concentration C_s but this range is very limited, meanwhile the range of C_s, where C_m is constant, is very wide: (2) the range of surfactant concentration, where C_m is constant, is dependent upon the size of surfactant molecules, especially upon whether surfactant molecules have unsaturated linkage in them or not. The author thinks that it is necessary to check the above mentioned conclusions from the absorption spectra of aqueous surfactant solutions solubilizing absorber molecules with the known experimental facts of other authors.

The Check of the Conclusions from the Spectral Experiments with the Well-known Experimental Facts

(1) Solubilization. — A curve of solubilization of water-insoluble dye in aqueous surfactant solution, i. e., (the amount of dye solubilized)/(the amount of surfactant C_s) vs. C_s curve bends suddenly after the steep rise above CMC and becomes almost parallel to the abscissa. The curve will begin to rise again when C_s becomes considerably high. Taking the conclusion of constant micellar concentration into consideration, the first rise of the curve must be due to the increase in C_m with increasing C_s. If only C_m continues to increase but N_m is constant with increasing C_s, as are concluded by other authors, the solubilization curve would not show such a sudden bending in a very narrow surfactant concentration range; in this case there is no reason for solubilizing efficiency of micelles to change suddenly with changing surfactant concentration, so the gradient of the curve would be almost constant independent of C_s. An example is shown in Fig, 3, which is the result of Hartley[2] and recalculated in the form of {(the amount of dye solubilized) − (solubility of dye in aq. phase)}/(C_s-CMC) vs. C_s. This curve shows that from CMC to 0.0354% of CPC (cetyl pyridinium chloride) C_m increases and above 0.0354% N_m increases mainly, as at this concentration of CPC the solubilization curve bends remarkably.

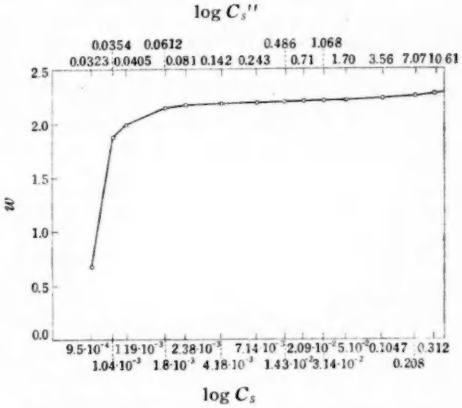

Fig. 3. Solubilization of AB (azobenzene) in aq. CPC (cetyl pyridinium chloride) solution from G. S. Hartley[2] $w=\log\{C_a'/C_s')\times10^3\}$, $C_a'=C_a-2.4\times10^{-5}$, C_a is the molar concentration of AB solubilized, 2.4×10^{-5} M is the solubility of AB in water. $C_s'=C_s-7.2\times10^{-4}$, C_s is the molar concentration of CPC, 7.2×10^{-4} M is the CMC of CPC, C_s'' is the weight percent. of CPC.

That the curve continues to rise slightly in the range of 0.081-3.56% shows the packing density of micelles increasing and the amount of water molecules contained in the inside of micelles[3] decreasing with increasing C_s. Above 3.5% the gradient of the curve begins to increase again, which shows the appearance of larger micelles with several double layers. From the solubilization curves of Green's[4] the concentrations at which the first rising finishes and the second rising begins respectively is as follows;

Surfactant	The concentration at which the first rising finishes	The concentration at which the second rising begins
Na-C_{12}	0.1 M (2.3%)	
Na-Oleate	5×10^{-3} M (0.15%)	0.3 M (9.12%)
$C_{12}NH_3Cl$	0.05 M (1.15%)	
Dodecyl sulfonic acid	0.05 M (1.23%)	0.727 M (16.4%)
Triton X-100	0.1%	10%

*) H. Sasaki et al., op. cit.

2) G. S. Hartley, *J. Chem. Soc.*, **1938**, 1968.
3) H. Sasaki, H. Okuyama and S. Saito, This Bulletin, **29**, 752 (1956).
4) S. A. A. Green, *J. Phys. Chem.*, **51**, 286 (1947).

These concentrations of various kinds of surfactant must have definite physical meaning, and the conclusion obtained by the spectral method agrees well with the behavior of these solubilization curves, as discussed above.

(2) Diffusion. — Hartley et. al.[5] have taken the notion that the micellar volume is independent of C_s, from their experimental results of diffusion of surfactants in aqueous salt or alkaline solutions. From the results of diffusion of surfactants in aqueous phase Lamm et. al.[6a] have also reached the same conclusion. M. E. L. McBain recognized that the diffusion coefficients of surfactants in aq. phase decrease with their increasing concentration, and she attributed this to the interaction among the increasing number of micelles[6b]. Stigter et. al.[6c] also accepted the interaction theory, but Abbott et. al.[6d] concluded

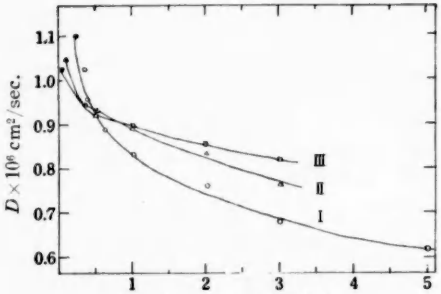

Fig. 4a. Micellar self-diffusion coefficient of SDS at 25°C from D. Stigter et. al.[6c]
Solvents; I. H_2O, II. 0.03 M NaCl, III. 0.1M NaCl.

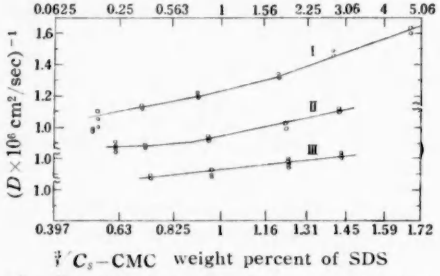

Fig. 4b. Micellar self-diffusion coefficient of SDS at 25°C.
Solvents; I. H_2O, II. 0.03 M NaCl, III. 0.1 M NaCl.

that the micellar radius increases with increasing concentration of the simple salt.

When simple salt is added to aqueous surfactant solution, it is thought that simple salt depresses the dissociation constant of paraffin chain salt[7] and these undissociated molecules are solubilized in the palisade of micelles; accordingly the volume of micelles increases. If so, it is natural to think that when C_s is increased, the surfactant molecules newly added are solubilized in the palisade of the existing micelles, and increase their volume, also depressing their diffusion coefficient. Fig. 4a is the result of Stigter et. al.[6c]. At about 1%, the curve I bends remarkably, which shows that until C_s reaches about 1%, C_m increases and above 1% of SDS, N_m increases mainly with increasing C_s. The curve D^{-1} vs. $(C_s\text{-CMC})^{1/3}$ {D, the diffusion coefficient, is proportional to r, the micellar radius, and also r is proportional to $(C_s\text{-CMC})^{1/3}$} must be linear in the range of $C_s \geq 1\%$, if the conclusion that above 1% of SDS, C_m is constant irrespective of C_s is correct. This is the case as is observed in Fig. 4b {the original paper shows that the curve D^{-1} vs. $(C_s\text{-CMC})^{1/2}$ is straight, but no explanation for this was given}. It must be strictly noted that these discussions mentioned above should be applicable only to the self diffusion coefficient. In usual diffusion experiments, two aqueous surfactant solutions of different concentration, which is above CMC, are used. The diffusion coefficients obtained by such a procedure depend not only on micellar diffusion velocity but also on micellar reconstructing velocity.

(3) Electrical Conductivity. — Hartley et. al.[8] pointed out that the association number of micelles can not be determined by the equivalent conductivity, Λ, alone. McBain asserted that when micelles are formed from free ions, Λ should increase[9]. But Hartley et. al. suspected McBain's theory from the consideration that after the lowering of Λ due to the secondary effect (the inclusive and the atmospheric effects) outweighing the primary effect (McBain's effect), the equivalent conductivity Λ should again increase owing to the occurence of the reverse case of both the effects with increasing C_s[8], and they presented the desorption theory[10]. McBain et. al.[11] explained the behavior of Λ vs. $C_s^{1/2}$ curves by the hypothesis of ionic micelle and neutral colloid, but Schmid et. al.[12] were doubtful about this hypothesis from their experimental results of high frequency effect. On the other hand, in the author's opinion, when n unassociated paraffin chain ions form one aggregate, Λ would decrease owing to the secondary effect overcoming the primary effect. But if we compare a smaller micelle with a larger micelle, i. e., if we

5) G. S. Hartley and D. F. Runnicles, *Proc. Roy. Soc.*, **A168**, 420 (1938); O. Lamm, *Kolloid-Z.*, **98**, 45 (1942); G. Jander and K. F. Weitendorf, *Angew. Chem.*, **47**, 197 (1934).

6) (a) O. Lamm and H. Högberg. *Kolloid-Z.*, **91**, 10 (1940); (b) M. E. L. McBain, *J. Am. Chem. Soc.*, **55**, 545 (1933); (c) D. Stigter, R. J. Williams and K. J. Mysels, *J. Phys. Chem.*, **59**, 330 (1955); (d) A. D. Abbott and H. V. Tartar, ibid., **59**, 1193 (1955).

7) H. V. Tartar, *J. Phys. Chem.*, **59**, 1195 (1955).

8) J. L. Moilliet, B. Collie, C. Robinson and G. S. Hartley, *Trans. Faraday Soc.*, **31**, 120 (1935).

9) J. W. McBain, ibid., **9**, 99 (1913).

10) G. S. Hartley, B. Corrie and C. S. Samis ibid., **32**, 795 (1936).

11) J. W. McBain and C. S. Salmon, *J. Am. Chem. Soc.*, **42**, 426 (1920).

12) G. Schmid and E. C. Larsen, *Z. Electrochem.*, **44**, 651 (1938).

compare an aq. paraffin chain salt solution at different concentrations, the secondary effect would be almost constant for the both surfactant concentrations but the primary effect should increase with increasing micelle size. So that it is the strong evidence of constant C_m irrespective of C_s for Λ to increase with C_s. Stigter[13] mentioned that the curve $\kappa - C_s$ (κ is the specific conductivity) consists of, in a typical case, two straight lines in an unassociated and an associated region. But taking the conclusion of constant micellar concentration into account, the curve $\kappa - C_s$ must have, at least, three knicks, that is, at CMC, at the point where the increase of C_m finishes and at the point where the larger micelle appears. Fig. 5 is the results of Ward[14] recalculated to the form $\log \kappa$ vs. $\log C_s$. At 0.25%, 0.75% and 17.5% there are definite changes in the curve. These three concentrations can be made to correspond to those points mentioned above respectively. The gradient of the curve, κ', decreases rapidly when the curve proceeds across the CMC, which is caused by the secondary effect, but gradually recovers with increasing C_s, which is caused by the primary effect, and at 3.9% κ' is 1, and still continues to increase with increasing C_s. In these regions κ' is higher than even that in the unassociated region. In concordance with these changes of κ' there appears the minimum in the curve Λ vs. $C_s^{1/2}$ ($\Lambda = 1000\kappa/C_s$) as observed in Fig. 6. The importance is not the minimum itself but the increase of κ' in the range from 0.75% to 17.5%. In the range of 3.9-17.5% κ' is greater than the unit, and above 21.5% κ' is less than the unit, therefore there appears maximum in the vs. $C_s^{1/2}$ curve, and this maximum (17.5-21.5%) is the concentration at which the larger micelle consisting of several double layers appears as mentioned above. It is easily understandable that when the larger micelle appears Λ, begins to decrease again owing to the higher viscosity. In conclusion the fact that the vs. $C_s^{1/2}$ curve has the minimum and the maximum is the proof that C_m is constant and N_m increases with increasing C_s.

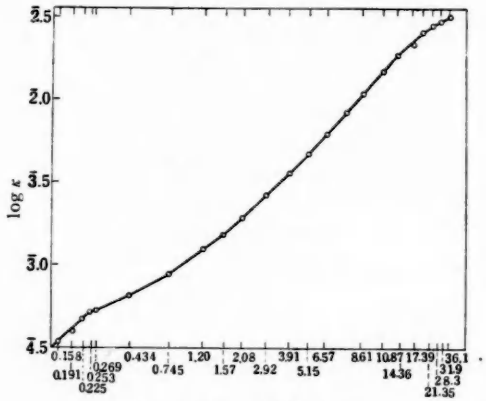

Fig. 5. Specific conductivity κ of SDS in aq. phase from A. F. H. Ward[14].

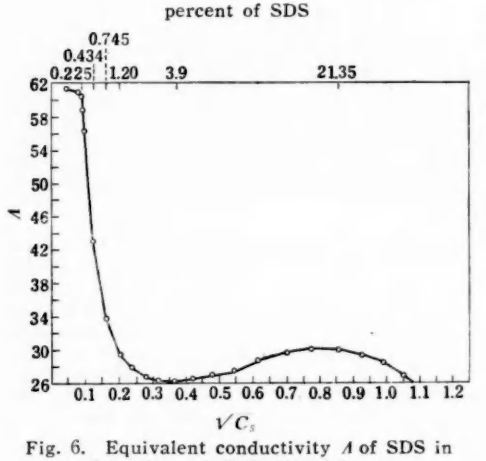

Fig. 6. Equivalent conductivity Λ of SDS in aq. phase from A. F. H. Ward[14].
C_s is the molar concentration of SDS.

(4) Light Scattering. — The most direct method to determine the micellar volume is light scattering, but the micellar molecular weight obtained by this method is generally at CMC[15] and there are few systematic investigations about the relation between the micellar volume and C_s. On the other hand, there are many studies about the charge effect[16] and different views are presented[15a,b,c]. It is desirable that some attentions are paid to nonionic surfactants (which have no charge) and also to the relation between the micellar volume and the surfactant concentration.

(5) X-Ray. — Corrin[17] pointed out that the micellar shape can not be determined decisively by X-Ray diffraction alone. Therefore very different micellar models have been presented by many X-Ray investigators, e. g., some authors have the idea of a larger micelle consisting of several double layers[15]. Others hold a small spherical model; especially Brady[19] has reported that the micelle of SDS is spherical even in such a high concentration as 14.71% and 29.42%, and some have explained the relation between the

13) D. Stigter, *Rec.trav. chim. Poy-Bas*, **73**, 611 (1954).
14) A. F. H. Ward, *Proc. Roy. Soc*, **A176**, 412 (1940).

15) (a) P. Debye, *Ann. N. Y. Acad. Sci.*, **51**, 575 (1949); *J. Phys. Chem.*, **53**, 1 (1949); (b) H. V. Tartar, ibid., **59**, 1185 (1955); J. N. Phillips and K. J. Mysels, ibid., **59**, 325 (1955); (c) E. Hutchinson, *Z. physik. Chem.*, neue Folge **2**, 363 (1954).
16) J. J. Hermans, *Rec. trav. chim. Poy-Bas*, **68**, 859 (1948); T. M. Doscher and K. J. Mysels, *J. Chem. Phys.*, **19**, 254 (1951); E. Hutchinson, *J. Colloid Sci.*, **9**, 191 (1954). K. J. Mysels, *J. Phys. Chem.*, **58**, 303 (1954).
17) H. L. Corrin, *J. Chem. Phys.*, **16**, 844 (1948).
18) E. W. Hughes, W. M. Swayer and J. R. Vinograd, *J. Chem. Phys.*, **13**, 131 (1945); J. Stauff, *Kolloid-Z.*, **96**, 244 (1941); H. K. Kiessig, ibid., **96**, 252 (1941).
19) G. W. Brady, *J. Chem. Phys.*, **19**, 1547 (1951).

smaller micelle and the larger micelle[20] but as yet have not ascertained it experimentally. Many authors, e. g. Philippoff[21], have discussed the X-Ray CMC. Although the values of X-Ray CMC given by these authors are not always in agreement with each other, generally X-Ray CMC is detectable in 10-20% of surfactant concentration range[21]. The concentration at which the solubilization curve for dye begins to rise again is 9.12% for sodium oleate and 16.4% for dodecyl sulfonic acid; the conductivity curve reaches its maximum at 17.5-21.5% for SDS. It is an interesting problem whether these concentrations at which larger micelles appear have any relation with the X-Ray CMC.

(6) Density, Viscosity and Osmotic Coefficient.—Fig. 7 is the curve of density-concentration and Fig. 8 is that of viscosity-concentration in aq. SDS solution derived from Wright et. al.[22].

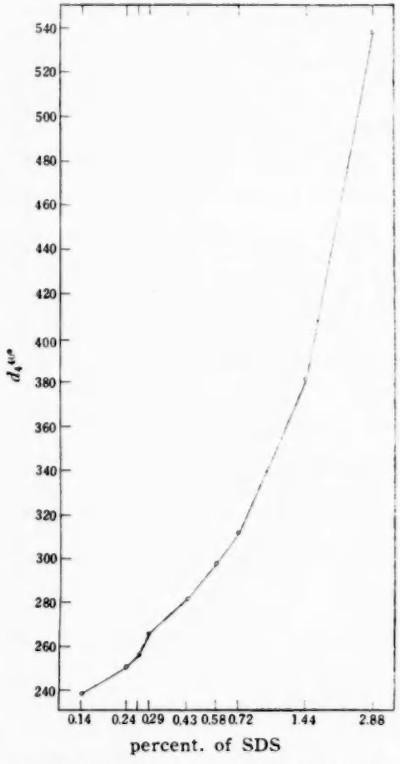

Fig. 7. Density d_4^{40} of aq. SDS solution from K. A. Wright et. al.[22].

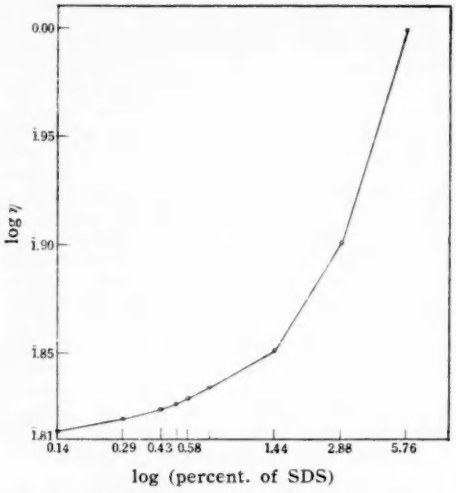

Fig. 8. Viscosity η of aq. SDS solution from K. A. Wright et. al.[22].

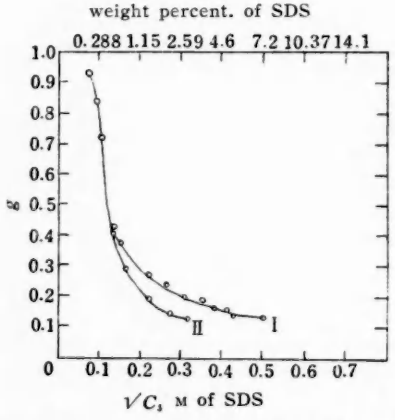

Fig. 9. Osmotic coefficient of aq. SDS solution from H. Huff et. al.[23].
Temperature; I. 30°C, II. 50°C.

At about 1.44%, the gradients of both curves increase remarkably. Huff et. al.[23] have shown that the osmotic coefficient of aqueous SDS solution vs. $C_s^{1/2}$ curve bends remarkably at about 0.023 M (0.66%) as is shown in Fig. 9. These concentrations must be those at which the increase of C_m finishes. But such properties of aqueous surfactant solutions as density[24], viscosity[25], osmotic coefficient or vapor pressure depression and

20) R. W. Mattoon, R. S. Stearns and W. D. Harkins, ibid., **15**, 209 (1947); W. D. Harkins, ibid., **16**, 156 (1948); J. Stauff, *Naturwiss.*, **27**, 213 (1939); *Kolloid-Z.*, **89**, 224 (1939); J. W. McBain, *Nature*, **145**, 702 (1940).
21) W. Philippoff, *Disc. Faraday Soc.*, NO. **11**, 96 (1951).
22) K. A. Wright and H. V. Tartar, *J. Am. Chem. Soc.*, **61**, 544 (1939).
23) H. Huff, J. W. McBain and A. P. Brady, *J. Phys. Chem.*, **55**, 311 (1951).
24) R. G. Paquette, E. C. Lingafelter and H. V. Tartar, *J. Am. Chem. Soc.*, **65**, 686 (1943); A. B. Scott and H. V. Tartar, ibid., **65**, 692 (1943); C. R. Bury and G. A. Parry, *J. Chem. Soc.*, **1935**, 626.
25) W. Philippoff and K. Hess, *Ber.*, **70**, 1808 (1937).

cryoscopic behavior[26] can not sensitively reveal the relation among C_s, C_m and N_m.

Conclusion

By no experimental method other than spectral, can we obtain any intimate relationship among the surfactant concentration, the micellar concentration and association number of molecules forming every micelle; there therefore exists some space of alternative explanations for these experimental results. In the author's present paper, it is proved that the conclusion from the spectral experiments coincides well with many results obtained by various other experimental methods. Contrariwise the assumptions on the relation between micellar volume and surfactant concentration, having been presented by many authors, fail to prove any explanation of the various experimental results uniformly, especially they fail to explain the behavior of absorption intensity and solubilization curves in wide range of surfactant concentrations. For example, in aqueous SDS solution, the solute concentration, at which the micellar concentration becomes constant first, exists in the range from 0.5% to 1.5%, which is obtained by the spectral method and is not contradicted with solubilization, diffusion, conductivity, viscocity and osmotic coefficient data (here it is assumed that solubilization curve of sodium dodecyl sulfate for dye does not so much differ from that of dodecyl sulfonic acid). If we took an alternative explanation, e. g., of micellar interaction to elucidate the behavior at the minimum in the curve of equivalent conductivity or to elucidate the decrease in self diffusion coefficient at about 1% in aqueous SDS solution, there would remain some inexplicable points, e. g., why the solubilization curve bends so rapidly at about this concentration. Also the author has determined the SDS concentration at which the larger micelle appears first to be 17.5–21.5%. If we took the desorption theory of Hartley's, some doubts would remain, e. g., why the solubilization curve of SDS for dyes begins to rise again at about this concentration, where the equivalent conductivity curve reaches its maximum.

26) J. W. McBin and M. M. Barker, *Trans. Faraday Soc.*, **31**, 149 (1935); J. W. McBain and M. D. Bety, *J. Am. Chem. Soc.*, **57**, 1909 (1935); E. Gonick and J. W. McBain, ibid., **69**, 334 (1947); M. H. Norris *J. Chem. Soc.*, **121**, 2161 (1922); M. N. Fineman and J. W. McBain, *J. Phys. Chem.*, **52**, 881 (1948); A. Smits, *Z. Physik. Chem.*, **45**, 608 (1903); H. Okuyama and k. Tyuzyo, *Bull. Chem. Soc. Japan*, **27**, 259 (1954); J. W. McBain, "Colloid Science," D. C. Heath and Co., San Francisco (1950), p. 243.

Summary

The conclusion, which is obtained by the spectral experiments on aqueous surfactant solutions, that the micellar concentration in aqueous surfactant solution is constant irrespective of surfactant concentration in the range which is from a little above the CMC to a considerably high surfactant concentration, coincides well with many other experimental results such as solubilization of dye, conductivity, self diffusion, X-Ray diffraction, density, viscosity and osmotic coefficient or cryoscopic behavior.

The author wishes to express his sincere thanks to Prof. N. Sata, Mr. H. Okuyama and Mr. S. Saito for their kind discussion and encouragement.

Department of Chemistry,
Faculty of Science
Osaka University, Kita-ku, Osaka

The Adsorption of Non-polar Gases on Alkali Halide Crystals. IV[1] *Calculations of the Adsorption Behaviour of Non-polar Gases on Cubic Potassium Chloride and Cubic Potassium Bromide**

By Teruo HAYAKAWA

(Received November 22, 1956)

Introduction

In the previous communication[2], the author carried out a theoretical calculations of the adsorption energy of an isolated atom or molecule (argon, nitrogen and carbon dioxide) on the (100) plane of cubic sodium chloride. In that work, the total repulsive potential between an isolated atom or molecule and the lattice ions was calculated using the repulsive constants of the modified Buckingham-Corner (6-exp) potential for these non-polar gases. The quadrupole interaction of an isolated nitrogen or carbon dioxide molecule with the lattice ions was theoretically calculated and the correction due to the potential barrier hindering the turning over of the molecular axis was made.

It was therefore of interest in the present work to extend a similar calculations to the (100) plane of cubic potassium chloride and cubic potassium bromide crystals and to compare the theoretical values with the experimental ones obtained by the present author.

Outline of Calculation

The calculation of the adsorption potential was divided into four sections,

(A) the Van der Waals' (dispersion) potential, (B) the electrostatic potential, (C) the repulsive potential, (D) the quadrupole potential and the correction due to the potential barrier hindering the turning over of the molecular axis.

Calculations were made of these quantities for following four representative positions on the (100) plane of an alkali halide crystal; (i) above the center of a lattice cell (sites type A), (ii) above the

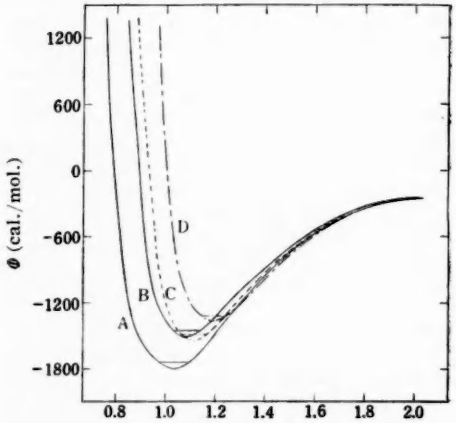

Fig. 1. Potential energy curves of argon on cubic (100) KCl. The symbols denote the type of sites.

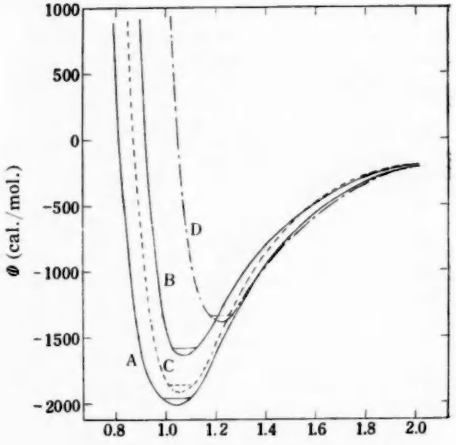

Fig. 2. Potential energy curves of nitrogen on cubic (100) KCl. The symbols denote the type of sites.

1) Part III of this series, T. Hayakawa, This Bulletin, **30**, 243 (1957).

* Part of this paper was read before the 9th Annual Meeting of the Chemical Society of Japan held in Kyoto, April, 1956. Another part of this paper was also read before the symposium on the surface heterogeneity of catalysis held in Kyoto, March, 1956.

2) Part II of this series, T. Hayakawa, This Bulletin, **30**, 236 (1957).

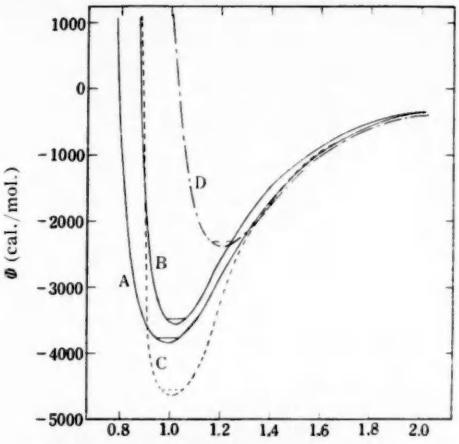

Fig. 3. Potential energy curves of carbon dioxide on cubic (100) KCl. The symbols denote the type of sites.

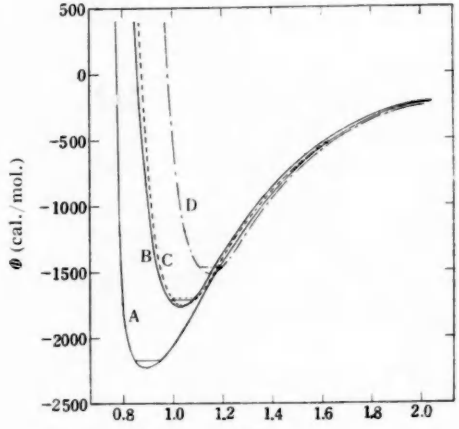

Fig. 4. Potential energy curves of argon on cubic (100) KBr. The symbols denote the type of sites.

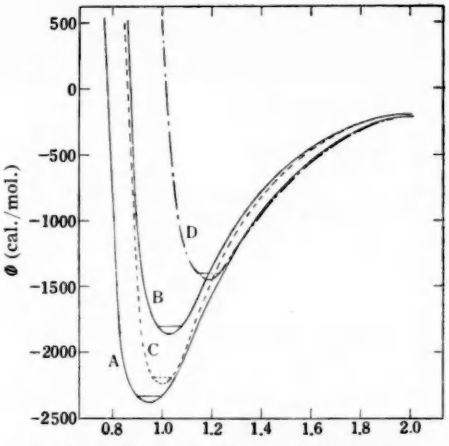

Fig. 5. Potential energy curves of nitrogen on cubic (100) KBr. The symbols denote the type of sites.

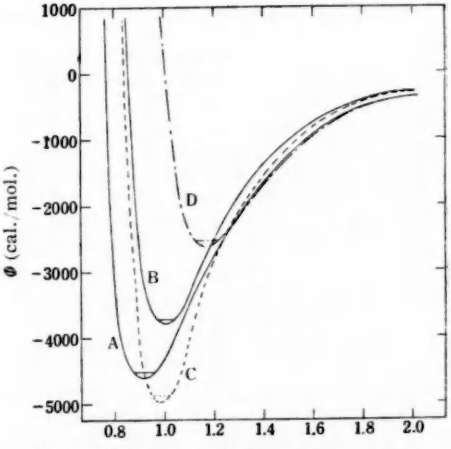

Fig. 6. Potential energy curves of carbon dioxide on cubic (100) KBr. The symbols denote the type of sites.

mid-point of a lattice edge (sites type B), (iii) above an alkali ion (sites type C) and (iv) above a halogen ion (sites type D).

The method of calculation of each interaction potential was already described in a previous communication[2]. The calculated potential energy curves for the four types of sites considered are shown in Figs. 1, 2, 3, 4, 5 and 6. From these curves the values collected in the following tables were calculated. The position of the minimum gives the equilibrium distance Z_e from the surface; the depth of the trough at Z_e is $-\Phi_m$. For each curve, the region around the minimum was fitted to a parabola and the vibrational frequency normal to the surface ν_z and the zero-point energy ε_0 were calculated. The values of the quadrupole potential Φ_Q are also listed in these tables, from which the considerably large contribution of the quadrupole inter-

TABLE I

RESULTS OBTAINED FROM THE POTENTIAL ENERGY CURVE, ARGON ON CUBIC (100) KCl

Sites type	Z_e (Å)	$r_{eff.}$ (Å)	$-\Phi_m$ (cal./mol.)	$\nu_z \times 10^{-12}$ (sec.$^{-1}$)	ε_0 (cal./mol.)	$-\Delta H_0$ (at 76°K) (cal./mol.)
A, Above the center of a lattice cell	3.22	2.10	1792	0.98	46.3	1898
B, Above the mid-point of a lattice edge	3.44	1.98	1506	0.90	42.7	1615
C, Above a K^+	3.52	2.19	1532	0.99	46.7	1637
D, Above a Cl^-	3.75	1.94	1365	0.94	44.2	1473

TABLE II

RESULTS OBTAINED FROM THE POTENTIAL ENERGY CURVE, NITROGEN ON CUBIC (100) KCl

Sites type	Z_e (Å)	$-\Phi_m$ (cal./mol.)	$-\Phi_Q$ at Z_e (cal./mol.)	$\nu_z \times 10^{-12}$ (sec.$^{-1}$)	ε_0 (cal./mol.)	$-\Delta H_0$ (at 76°K) (cal./mol.)
A, Above the center of a lattice cell	3.25	2021	815	1.19	56.0	2117
B, Above the mid-point of a lattice edge	3.34	1635	1016	1.06	50.1	1737
C, Above a K^+	3.31	1915	1522	1.20	56.7	2010
D, Above a Cl^-	3.85	1384	352	1.12	53.1	1483

TABLE III

RESULTS OBTAINED FROM THE POTENTIAL ENERGY CURVE, CARBON DIOXIDE ON CUBIC (100) KCl

Sites type	Z_e (Å)	$-\Phi_m$ (cal./mol.)	$-\Phi_Q$ at Z_e (cal./mol.)	$\nu_z \times 10^{-12}$ (sec.$^{-1}$)	ε_0 (cal./mol.)	$-\Delta H_0$ (at 190°K) (cal./mol.)
A, Above the center of a lattice cell	3.09	3826	2432	1.22	57.6	4148
B, Above the mid-point of a lattice edge	3.22	3548	2887	1.21	57.1	3871
C, Above a K^+	3.18	4656	4390	1.40	66.0	4970
D, Above a Cl^-	3.75	2483	968	1.21	57.1	2806

TABLE IV

RESULTS OBTAINED FROM THE POTENTIAL ENERGY CURVE, ARGON ON CUBIC (100) KBr

Sites type	Z_e (Å)	$r_{eff.}$ (Å)	$-\Phi_m$ (cal./mol.)	$\nu_z \times 10^{-12}$ (sec.$^{-1}$)	ε_0 (cal./mol.)	$-\Delta H_0$ (at 76°K) (cal./mol.)
A, Above the center of a lattice cell	2.95	1.79	2228	1.17	55.2	2325
B, Above the mid-point of a lattice edge	3.39	1.81	1762	0.99	46.7	1867
C, Above a K^+	3.42	2.09	1750	1.02	48.1	1854
D, Above a Br^-	3.77	1.81	1507	0.95	44.8	1614

TABLE V

RESULTS OBTAINED FROM THE POTENTIAL ENERGY CURVE, NITROGEN ON CUBIC (100) KBr

Sites type	Z_e (Å)	$-\Phi_m$ (cal./mol.)	$-\Phi_Q$ at Z_e (cal./mol.)	$\nu_z \times 10^{-12}$ (sec.$^{-1}$)	ε_0 (cal./mol.)	$-\Delta H_0$ (at 76°K) (cal./mol.)
A, Above the center of a lattice cell	3.05	2389	1130	1.25	59.0	2482
B, Above the mid-point of a lattice edge	3.35	1855	1071	1.12	52.9	1954
C, Above a K^+	3.29	2256	1664	1.26	59.5	2348
D, Above a Br^-	3.92	1458	358	1.17	55.2	1555

TABLE VI

RESULTS OBTAINED FROM THE POTENTIAL ENERGY CURVE, CARBON DIOXIDE ON CUBIC (100) KBr

Sites type	Z_e (Å)	$-\Phi_m$ (cal./mol.)	$-\Phi_Q$ at Z_e (cal./mol.)	$\nu_z \times 10^{-12}$ (sec.$^{-1}$)	ε_0 (cal./mol.)	$-\Delta H_0$ (at 190°K) (cal./mol.)
A, Above the center of a lattice cell	2.99	4610	2915	1.33	62.8	4927
B, Above the mid-point of a lattice edge	3.32	3810	2667	1.25	59.0	4131
C, Above a K^+	3.27	4982	3924	1.35	63.7	5298
D, Above a Br^-	3.85	2601	952	1.23	58.1	2923

TABLE VII

INITIAL HEATS OF ADSORPTION ON CUBIC (100) KCl

Adsorbate	$(-\Delta H_0)$expt. (cal./mol.)	$(-\Delta H_0)$calc. (cal./mol.)	(ΔH_0)expt. $-(-\Delta H_0)$calc. (cal./mol.)
Argon	2080 (2140[9])	1900 (1780[10])	180 (360[9,10])
Nitrogen	3010 (3200[9])	2120	890
Carbon dioxide	6400	4970	1430

TABLE VIII

INITIAL HEATS OF ADSORPTION ON CUBIC (100) KBr

Adsorbate	$(-\Delta H_0)$expt. (cal./mol.)	$(-\Delta H_0)$calc. (cal./mol.)	$(-\Delta H_0)$expt. $-(-\Delta H_0)$calc. (cal./mol.)
Argon	2440	2330	110
Nitrogen	3280	2480	800
Carbon dioxide	6780	5300	1480

action energy will be at once apparent*. The initial heat of adsorption (i.e. the isosteric heat of adsorption at zero coverage) in these tables was calculated from the relation

$$-\Delta H_0 = (-\Phi_m - \varepsilon_0) + RT.$$

The values of the effective radius of argon $r_{eff.}$ were calculated from the equilibrium distances, assuming Goldschmidt's values[3] for the radii of the ions. The results are given in column 3 of Tables I and IV.

Discussion

The Initial Heat of Adsorption.—As seen in Tables I, II, IV and V, the most energetic positions for argon and nitrogen on the (100) plane of cubic potassium chloride and cubic potassium bromide are sites type A (i.e. above the center of a lattice cell), and these results are dissimilar from those obtained for the (100) plane of cubic sodium chloride. On the other hand, Tables III and VI indicate that the most energetic positions for carbon dioxide on the (100) plane of cubic potassium chloride and cubic potassium bromide are sites type C (i.e. above a K^+ in the lattice plane). These results may be attributed to the following causes:

(1) Although, in general, sites type C gives the greatest value of the quadrupole interaction potential for the same value of the equilibrium distance (Z_e) from the surface, the value of the quadrupole interaction potential at each sites type is inversely proportional to the third powers of the lattice parameter of the crystal[4].

(2) The repulsive constant of a K^+ is considerably greater than that of an Na^+ [5].

(3) The permanent quadrupole moment of the carbon dioxide molecule is considerably greater than that of the nitrogen molecule[6,7].

The values of the initial heats of adsorption obtained from the present theoretical calculations are listed in Tables VII and VIII, together with the experimental values by the present author[1,8]. For the sake of comparison, Orr's results[9,10] are also listed in Table VII.

* In the case of argon, the quadrupole potential is surely zero.

3) V. M. Goldschmidt, *Trans. Faraday Soc.*, **25**, 253 (1929).

4) L. E. Drain, *Trans. Faraday Soc.*, **49**, 650 (1953).

5) M. L. Huggins and J. E Mayer, *J. Chem. Phys.*, **1**, 643 (1933).

6) W. V. Smith and R. Howard, *Phys. Rev.*, **79**, 132 (1950).

7) R. M. Hill and W. V. Smith, ibid., **82**, 451 (1951).

8) Part V of this series, T. Hayakawa, This Bulletin, **30**, 337 (1957).

9) W. J. C. Orr, *Proc. Roy. Soc.* (*London*), **A173**, 349 (1939).

10) W. J. C. Orr, *Trans. Faraday Soc.*, **35**, 1247 (1939).

As seen in Tables VII and VIII, the present theoretical values of the initial heat of adsorption for argon on the (100) plane of cubic potassium chloride and cubic potassium bromide are in considerably good agreement with the experimental values, while the discordance between the experimental and theoretical values for nitrogen or carbon dioxide is somewhat remarkable. However, since the order of magnitude of the theoretical values for these gases agrees with that of the experimental values, it seems reasonable to consider that the high initial heat of adsorption experimentally found for nitrogen or carbon dioxide is mainly attributed to the quadrupole interaction of each molecule with the surface of the crystal.

The Non-Uniformity of the Surface.—Tables I, II and III indicate that the differences between the highest and the weighted mean values of the initial heats of adsorption for argon, nitrogen and carbon dioxide on the (100) plane of cubic potassium chloride amount to about 230, 280 and 1030 cal./mol. respectively. In the case of cubic (100) potassium bromide, as seen in Tables IV, V and VI, the corresponding values for argon, nitrogen and carbon dioxide amount to about 380, 400 and 970 cal./mol. respectively. Since the mutual interaction between the adsorbed atoms or molecules in the low coverage region gives no marked influence upon the heats of adsorption, the surface heterogeneity of this type may be maintained especially in the non-localized adsorption.

On the other hand, the difference between the experimental and theoretical values of the initial heat of adsorption gives a crude measure of the surface heterogeneity of the other type due to the lattice imperfection or the defects of the crystals. As seen in Tables VII and VIII, the differences between the experimental and theoretical values for nitrogen or carbon dioxide are considerably greater than the values anticipated from the results for argon. Although these results are not satisfactorily explained from the difference in the intermolecular potential energy between these non-polar molecules, it may be pointed out that the accuracy of the theoretical calculations for nitrogen or carbon dioxide is somewhat inferior to that for argon. This incorrectness is mainly attributed to the facts that the values of the permanent quadrupole moment of nitrogen and carbon dioxide are somewhat uncertain and that the estimation of the potential energy barrier hindering the turning over of the molecular axis is insufficiently accurate.

Surface Migration of the Adsorbed Atoms and Molecules.—As already discussed in a previous communication[2], the height of the potential energy barrier separating two sites which belonged to the same type in the low coverage region is roughly equal to the difference in the initial heat of adsorption between one of them and the adjacent site separating them. In the case of the (100) plane of cubic potassium chloride, as seen in Tables I, II and III, the values of these potential energy barriers for argon, nitrogen (excepting the difference between the sites type A and D) and carbon dioxide amount to about 0.9–3.0 RT, 0.7–2.5 RT and 0.7–3.5 RT respectively. Tables IV, V and VI also indicate that the values of the potential energy barriers (excepting the difference between the sites type A and D) for argon, nitrogen and carbon dioxide on the (100) plane of cubic potassium bromide amount to about 1.5–3.0 RT, 0.9–3.5 RT and 1.0–3.0 RT, respectively. Since the mean kinetic energy of thermal movement of the adsorbed atoms or molecules is RT per mole, it seems reasonable to consider that the adsorbed atoms or molecules easily pick up the energy corresponding to each potential energy barrier from the thermal energy fluctutaions. The present results on the surface migration of the adsorbed atoms or molecules in the low coverage region are qualitatively in good agreement with the nature of the experimental entropy curves for these non-polar gases[1,8].

Summary

The potential energy of each isolated atom or molecule (argon, nitrogen, or carbon dioxide) adsorbed on the (100) plane of cubic potassium chloride and cubic potassium bromide has been theoretically calculated at four representative positions on the surface.

According to the present theoretical calculations, it seems reasonable to consider that the high initial heat of adsorption experimentally found for nitrogen or carbon dioxide is mainly attributed to the quadrupole interaction of each molecule with the surface of the crystals. The present results suggest that the surface may be influenced by the different types of the surface heterogeneity due to the

defects of the crystals and the distribution of sites grouped in patches. The present theoretical calculations also suggest that the adsorbed atoms or molecules of these non-polar gases easily migrate two-dimensionally along the surface in the low coverage region. These results on the surface migration are qualitatively in good agreement with the experimental entropy curves.

The author wishes to express his grateful thanks to Dr. S. Horiba and Professor O. Toyama of Osaka Prefectural University for their kind encouragement and discussion. The author's sincere thanks are also due to Professor R. Kiyama of Kyoto University for his kind discussion.

Department of Chemistry, Faculty of Education, Osaka Prefectural University, Sakai

*The Adsorption of Non-polar Gases on Alkali Halide Crystals. V. The Low-temperature Adsorption of Non-polar Gases on Cubic Potassium Bromide**

By Teruo HAYAKAWA

(Received December 4, 1956)

Introduction

In the former papers of this series[1,2,3,4], the author has described the measurements and the theoretical calculations of the low-temperature adsorption of non-polar gases (argon, oxygen, nitrogen and carbon dioxide) on cubic sodium chloride and cubic potassium chloride. The high initial heat of adsorption experimentally found for nitrogen or carbon dioxide has been considered to be mainly attributed to the quadrupole interaction of each molecule with the surface. It has also been indicated from these works that the adsorbed atoms or molecules (argon, oxygen and nitrogen) have the nature of the two-dimensional gas at least in the range of $\theta=0.3\sim0.9$ and the surface is influenced by the different types of the non-uniformity due to the defects of the crystals and the distribution of sites grouped in patches.

The present paper reports similar investigations on cubic potassium bromide and discusses these problems mentioned above on the basis of the experiments and the theoretical calculations given in the preceding paper[4].

Experimental

Materials.—*Potassium bromide* was recrystallized by rapidly cooling an aqueous solution of potassium bromide (Wako Chemical Co., extra pure grade) saturated at 90°C. The crystals were collected on a sintered glass filter funnel, washed with successive portions of 70 and 99.9% ethyl alcohol, and stored in a vacuum desiccator over phosphorus pentoxide for about two weeks. Microscopic examination of this sample revealed a large number of small cubes, and in some crystals the defects in the corners or edges were somewhat perceptible. The examination of this sample by an electron diffraction apparatus also showed that the (100) was the predominant surface plane. 42.3 g. of this sample which passed through a 45-mesh sieve was used in the subsequent experiments.

Helium was supplied by the Teikoku Oxygen Co. as spectroscopically pure and was not further purified. The method of preparation of other gases has already been given[4].

Apparatus and Procedure. — The apparatus and the procedure have also been described in a previous communication[4]. The salt was outgassed by heating in vacuo at 280–300°C for a minimum period of 6 hr. prior to each experiment.

Results

The isotherms obtained for the four gases on cubic potassium bromide crystals are summarized in Figs. 1, 2, 3 and 4. The adsorption was found

* Part of this paper was read before the 9th Annual Meeting of the Chemical Society of Japan held in Kyoto, April, 1956. Another part of this paper was also read before the symposium on the surface heterogeneity of catalysis held in Kyoto, March, 1956.

1) Part I of this series, T. Hayakawa, This Bulletin, **30**, 124 (1957).

2) Part II of this series, T. Hayakawa, This Bulletin, **30**, 236 (1957).

3) Part III of this series, T. Hayakawa, This Bulletin, **30**, 243 (1957).

4) Part IV of this series, T. Hayakawa, This Bulletin, **30**, 332 (1957).

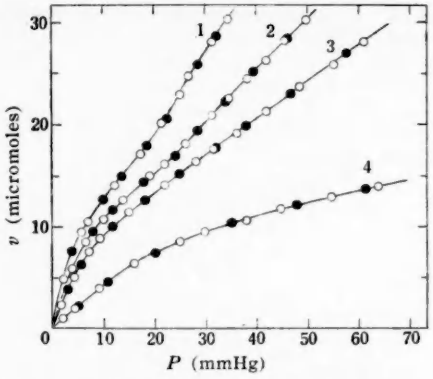

Fig. 1. Adsorption isotherms of argon on cubic potassium bromide.
curve 1·····73.70°K, curve 2·····75.67°K,
curve 3·····77.32°K, curve 4·····85.01°K.
-o-o- adsorption, -•-•- desorption.

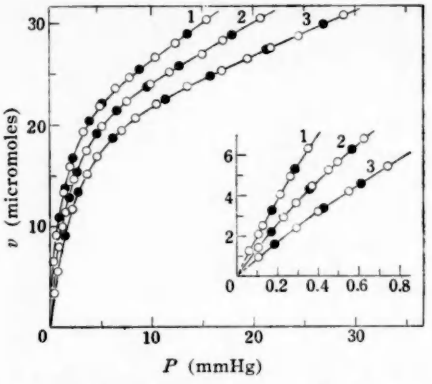

Fig. 3. Adsorption isotherms of nitrogen on cubic potassium bromide.
curve 1·····73.75°K, curve 2·····75.44°K,
curve 3·····77.32°K.
-o-o- adsorption, -•-•- desorption.

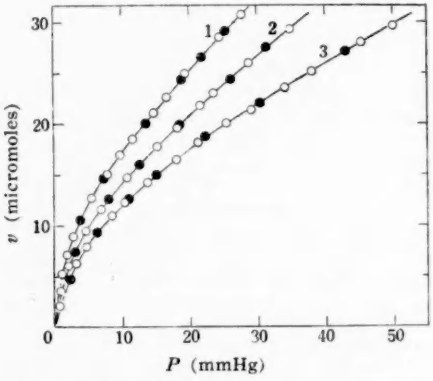

Fig. 2. Adsorption isotherms of oxygen on cubic potassium bromide.
curve 1·····73.70°K, curve 2·····75.44°K,
curve 3·····77.32°K.
-o-o- adsorption, -•-•- desorption.

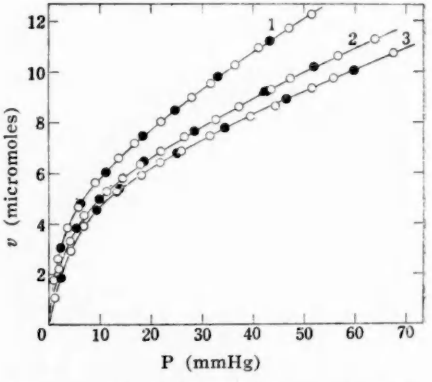

Fig. 4. Adsorption isotherms of carbon dioxide on cubic potassium bromide.
curve 1·····187.66°K, curve 2·····192.63°K,
curve 3·····194.64°K.
-o-o- adsorption, -•-•- desorption.

to be reversible in this temperature range. The isosteric heats of adsorption were calculated from these isotherms using the Clausius-Clapeyron equation and showed no definite trend with temperature within the experimental error. In the calculations of the entropy decreases due to the adsorption, the gas phase under the pressure of 760 mmHg and the temperature which coincided with that of each isotherm was chosen as the standard state.

The present results on the isosteric heats of adsorption and the entropy decreases caused by the adsorption are shown in Figs. 5, 6, 7 and 8. Since the adsorbed amount of carbon dioxide was considerably small in this temperature range, the measurements were not extended to the region of high coverage.

Discussion

Isosteric Heats of Adsorption. — The heat curves shown in Figs. 5, 6 and 7 indicate that the initial decrease due to the nonuniformity of the surface and the increase in the succeeding region for these three non-polar gases are considerably predominant. The present results on cubic potassium bromide indicate, however, that the increase in the heats of adsorption for each adsorbate, which gives a measure of the mutual interaction between the adsorbed atoms or molecules, is somewhat less than that obtained for cubic sodium chloride and cubic potassium chloride[1,3].

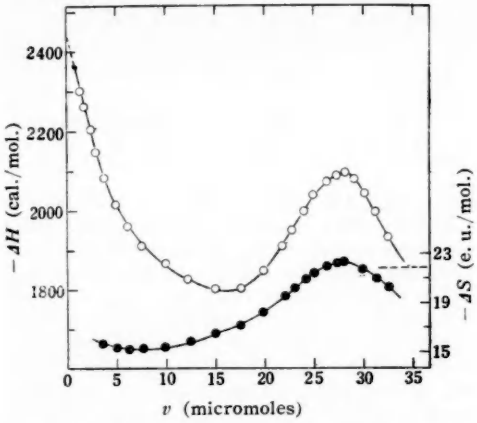

Fig. 5. Isosteric heats and entropies of adsorption for argon on cubic potassium bromide.
-○-○-, isosteric heats of adsorption ($-\Delta H$);
-●-●-, entropies of adsorption ($-\Delta S$);
-----, heat of sublimation.

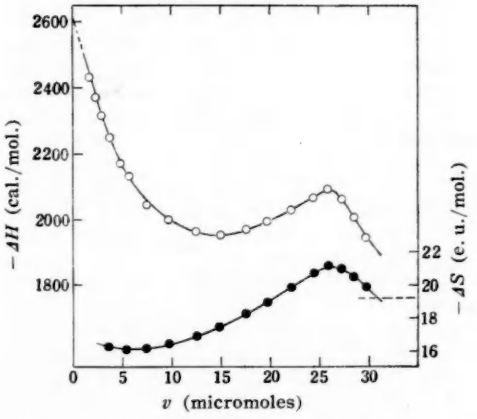

Fig. 6. Isosteric heats and entropies of adsorption for oxygen on cubic potassium bromide.
-○-○-, isosteric heats of adsorption ($-\Delta H$);
-●-●-, entropies of adsorption ($-\Delta S$);
-----, heat of evaporation.

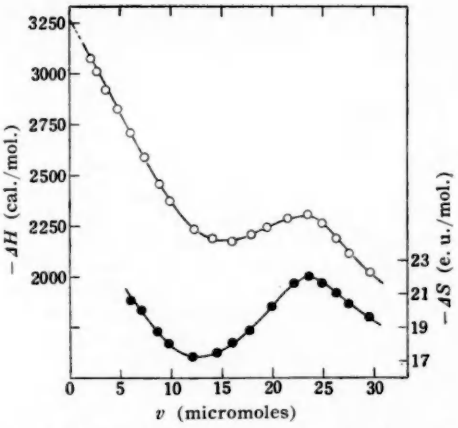

Fig. 7. Isosteric heats and entropies of adsorption for nitrogen on cubic potassium bromide.
-○-○-, isosteric heats of adsorption ($-\Delta H$);
-●-●-, entropies of adsorption.

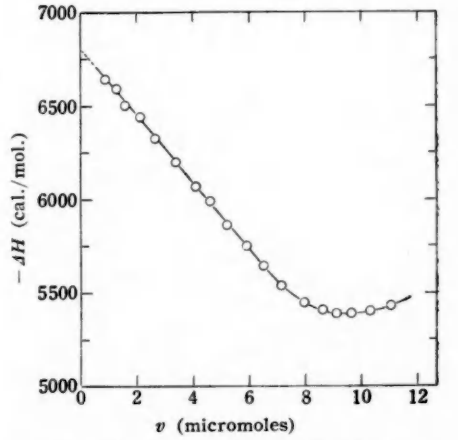

Fig. 8. Isosteric heats of adsorption for carbon dioxide on cubic potassium bromide.

TABLE I

INITIAL HEAT OF ADSORPTION, $-\Delta H_0$, ON CUBIC POTASSIUM BROMIDE

Adsorbate	$(-\Delta H_0)_{\text{expt.}}$ (cal./mol.)	$(-\Delta H_0)_{\text{calcd.}}$ (cal./mol.)	$(-\Delta H_0)_{\text{expt.}} - (-\Delta H_0)_{\text{calcd.}}$ (cal./mol.)
Argon	2440	2330	110
Oxygen	2610	—	—
Nitrogen	3280	2480	800
Carbon dioxide	6780	5300	1480

TABLE II

MONOLAYER CAPACITIES (V_m) AND SURFACE AREAS (A), CUBIC POTASSIUM BROMIDE (42.3 g.)

Adsorbate	Cross-sectional area, (Å^2)	V_m (micromoles) from heat curve	(B. E. T.)	A (m^2) from heat curve	(B. E. T.)
Argon	12.8	27.8	(25.7)	2.14	(1.98)
Oxygen	14.1	26.2	(24.1)	2.22	(2.05)
Nitrogen	13.8	24.1	(28.3)	2.00	(2.35)

The values of the initial heat of adsorption (i. e. the isosteric heat of adsorption extrapolated to zero coverage) obtained for the four gases are summarized in Table I, together with the theoretical values obtained by the present author[4].

As already reported in the previous paper[4], the high initial heat of adsorption theoretically obtained for nitrogen or carbon dioxide is mainly attributed to the quadrupole interaction of each molecule with the surface. Although the discordance between the experimental and theoretical values for nitrogen or carbon dioxide is somewhat remarkable (see Table I), the order of magnitude of the experimental values is similar to that of the theoretical values. Moreover, the experimental values of the initial heat of adsorption inevitably contain some uncertainty due to the extrapolation, and the theoretical values for nitrogen and carbon dioxide also contain some incorrectness due to the uncertainty of the observed values of the permanent quadrupole moment. Considering the question from these facts, it seems reasonable to consider that the high initial heat of adsorption experimentally found for nitrogen or carbon dioxide is mainly attributed to the quadrupole interaction of each molecule with the surface of cubic potassium bromide.

Since the theoretical calculations were carried out on the assumption of an ideal lattice, the difference between the experimental and theoretical values of the initial heat of adsorption gives a crude measure of the surface heterogeneity due to the lattice imperfection and the defects of the crystals. As seen in Table I, the values of this difference for argon, nitrogen and carbon dioxide amount to 110, 800 and 1480 cal./mol. respectively. On the other hand, the heat curves shown in Figs. 5, 7 and 8 indicate that the initial decreases due to the non-uniformity of the surface for argon, nitrogen and carbon dioxide roughly amount to 640, 1100 and 1400 cal./mol. respectively. Since the mutual interaction between the adsorbed atoms or molecules is included in these values of the initial decreases and the theoretical values for nitrogen and carbon dioxide are also somewhat uncertain, it is reasonable to consider that the surface is influenced not only by the non-uniformity due to the lattice imperfection and the defects of the crystals but by another type of the non-uniformity. As already discussed in the preceding paper[4], this latter type of the surface heterogeneity may be attributed to the distribution of sites on the surface.

Monolayer Capacities.—Since the heat curves indicate that the surface heterogeneity in the low coverage region and the mutual interaction in the succeeding region are both predominant, it is quite unreasonable to apply the B. E. T. theory to the present systems. As seen in Figs. 5, 6 and 7, there are fairly sharp maxima in the isosteric heat and entropy decrease curves for all three non-polar gases, and the gradual decrease beyond each maximum may be attributed to the formation of multilayers. Considering this fact, it is reasonable to assign the amount adsorbed corresponding to this maximum in the heat or entropy decrease curve as a monolayer capacity.

The present results on the monolayer capacities and on the surface areas which are thus obtained are summarized in Table II. The values of the cross-sectional area in this table were calculated from the results on the entropies of the adsorbed atoms and molecules using the assumption of a hexagonally close-packed layer.

Entropies of the Adsorbed Phase.—As seen in Figs. 5, 6 and 7, the magnitudes of the entropies of adsorption and the variation of these with the amount adsorbed for argon and oxygen are similar to each other, while nitrogen shows somewhat different features from other gases. In order to obtain more information about the freedom of the adsorbed atoms or molecules, the entropies of the adsorbed phase derived from the present results were compared with those statistically calculated. The methods of the statistical calculations of the entropies of the gas phase under the standard states and of

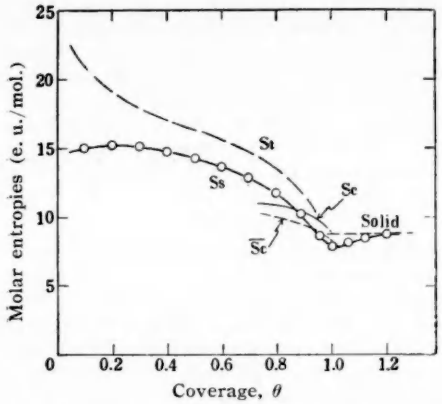

Fig. 9. Molar entropies of argon adsorbed on cubic potassium bromide at 76.5°K.
S_s, experimental values; S_t, calculated values of the two-dimensional gas; S_c, integral configurational entropies; $\bar{S}_c$, differential configurational entropies.

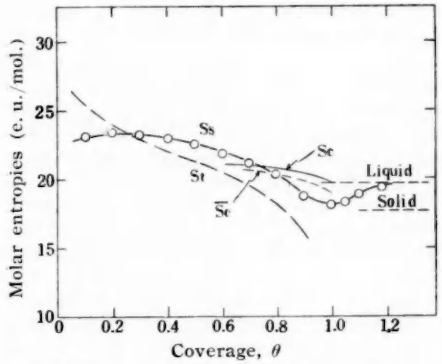

Fig. 10. Molar entropies of oxygen adsorbed on cubic potassium bromide at 76.4°K.
S_s, experimental values; S_t, calculated values of the two-dimensional gas; S_c, integral configurational entropies; $\bar{S}_c$, differential configurational entropies.

the entropies of the adsorbed phase were already given in a previous communication[1].

The entropy curves of the adsorbed phase obtained from the present experiments are summarized in Figs. 9, 10 and 11, together with the calculated curves. The experimental values in these figures are the partial molar total entropies and hence contain the entropy changes of the adsorbent[5], while the calculated values are all the integral entropies and are

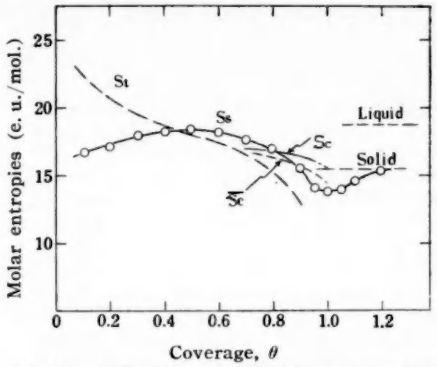

Fig. 11. Molar entropies of nitrogen adsorbed on cubic potassium bromide at 76.4°K.
S_s, experimental values; S_t, calculated values of the two-dimensional gas; S_c, integral configurational entropies; $\bar{S}_c$, differential configurational entropies.

usually somewhat greater than those of the partial molar total entropies. Considering this fact, the experimental curves (S_s) for adsorbed argon and nitrogen are comparatively in good agreement with the calculated curves (S_t) of the two-dimensional gas in the ranges of θ=0.3–0.9 and θ=0.3–0.8 respectively. In the case of oxygen, since the entropy associated with the vibrational motion normal to the surface was calculated on assuming that the vibrational frequency of the adsorbed oxygen molecule was identical with that of the adsorbed argon atom, the present calculations of the two-dimensional gas for oxygen (S_t in Fig. 10) probably resulted in somewhat smaller values. Consequently, it seems reasonable to consider that the agreement of the experimental curve for oxygen with the calculated curve of the two-dimensional gas is considerably satisfied in the range of θ=0.2–0.8.

The discrepancy between the experimental and calculated curves at lower coverage (θ<0.2) in these figures would imply the entropy changes of the adsorbent. When θ approaches to unity, as seen in Fig. 9, the restriction on the freedom of adsorbed argon is further increased and the experimental curve (S_s) falls below the calculated curve (S_t) of the two-dimensional gas. At higher coverage (θ>1), the entropy of adsorbed argon remains close to the entropy of solid argon*, while the entropy of adsorbed oxygen approaches

5) T. L. Hill, *J. Chem. Phys.*, **17**, 520 (1949).

* The entropy of solid argon was calculated from the heat of sublimation and the value of the saturation pressure at 76.5°K.

to the entropy of liquid oxygen**. These results obtained for cubic potassium bromide are similar to those obtained for cubic potassium chloride[5]. In the case of nitrogen, the entropy of the adsorbed phase at higher coverage approaches to the entropy of solid nitrogen***.

Kemball[6] suggested that the phase change of argon on cubic potassium chloride occurred at about $\theta=0.8$, since the experimental values shifted from the entropy curve of the two-dimensional gas to the entropy curve of the localized adsorption obtained by adding the configurational entropy on the Langmuir model to the entropy of solid argon. This explanation involves, however, considerable uncertainty, since it is quite unreasonable to apply the Langmuir model to the adsorption system in which the surface heterogeneity at lower coverage and the mutual interaction in the succeeding region are both predominant. In the present work, therefore, the configurational entropy (S_c) and the differential configurational entropy ($\bar{S}$) for the localized adsorption were calculated from the experimental results using the expressions derived by Drain and Morrison[7]. In these expressions, however, the non-uniformity of the surface was taken into consideration, while the mutual interaction between the adsorbed atoms or molecules was almost entirely ignored.

The present results on the configurational and differential configurational entropies for these three gases (argon, oxygen and nitrogen) are also summarized in Figs. 9, 10 and 11. As seen in Fig. 9, the present results suggest that the phase change of argon from a gaseous film to a condensed film has occurred at about $\theta=0.9$. On the other hand, Figs. 10 and 11 suggest that the phase changes of oxygen and nitrogen on cubic potassium bromide have occurred at about $\theta=0.8$. However, since the mutual interaction between the adsorbed atoms or molecules was almost entirely ignored in these calculations of the configurational and differential configurational entropies, the present results on the phase change of the adsorbed phase inevitably contain some uncertainty.

** The entropies of solid and liquid oxygen were calculated from the work of Giauque and Johnston (*J. Am. Chem. Soc.*, **51**, 2300 (1929)).

*** The entropies of solid and liquid nitrogen were calculated from the work of Kingston et al. (*J. Am. Chem. Soc.*, **72**, 1780 (1950)).

6) C. Kemball, "Advances in Catalysis," Vol. II, Academic Press Inc., New York (1950), p. 233.

7) J. M. Drain and J. O. Morrison, *Trans. Faraday Soc.*, **48**, 316 (1952).

Summary

The low-temperature adsorption of non-polar gases (argon, oxygen, nitrogen and carbon dioxide) on cubic potassium bromide was investigated. According to the results of the present experiments and the theoretical calculations given in the preceding paper, the high initial heat of adsorption experimentally found for nitrogen or carbon dioxide is mainly attributed to the quadrupole interaction of each molecule with the surface of the crystal. The present results also indicate that the non-uniformity of the surface is considerably predominant at lower coverage and this is partly attributed to the lattice imperfection and the defects of the crystals.

According to the present results on the entropies of the adsorbed atoms or molecules, the adsorbed phase of argon has the nature of the two-dimensional gas at least in the range of $\theta=0.3$–0.9, while the adsorbed phase of oxygen or nitrogen shows a similar nature in the range of $\theta=0.3$–0.8. The present results suggest that the phase change of argon from a gaseous film to a condensed film has occurred at about $\theta=0.9$. In the case of oxygen or nitrogen, it is also suggested that the phase change of each adsorbed phase from a gaseous film to a condensed film has occurred at about $\theta=0.8$.

The author wishes to express his grateful thanks to Dr. S. Horiba and Professor O. Toyama of Osaka Prefectural University for their kind encouragement and discussions. The author's sincere thanks are also due to Professor R. Kiyama of Kyoto University for his kind discussions.

Department of Chemistry
Faculty of Education
Osaka Prefectural University, Sakai

The Adsorption of Non-polar Gases on Alkali Halide Crystals. VI[1]. *The Low-temperature Adsorption of Non-polar Gases on Octahedral Potassium Chloride**

By Teruo HAYAKAWA

(Received December 15, 1956)

Introduction

In recent years comparatively few experiments have been carried out to determine the influence of crystal face on low-temperature adsorption. Measurable differences between the heats of adsorption of nitrogen on the (100), (110) and (111) faces of copper were found by Rhodin[2]. The alkali halides lend themselves admirably to such a study, since they have certain habits in which the crystal is solely bound by one type of face. Moreover, the crystal habit of potassium chloride can easily be completely modified by both inorganic ions and by very small amounts of dyestuffs[3,4]. The low-temperature adsorption of argon on the lead-modified and dye-modified samples of octahedral potassium chloride has recently been measured by Young[5], who has found measurable difference in the heats of adsorption between the (111) and (100) faces of potassium chloride.

In the former papers of this series[1,6-9], the author has described the measurements and the theoretical calculations of the low-temperature adsorption of non-polar gases on cubic alkali halide crystals. It was therefore of interest in the present work to study the low-temperature adsorption on octahedral potassium chloride, since this permits a comparison of the adsorptive properties of the (100) and (111) faces of potassium chloride crystals.

Experimental

Materials. — Lead-modified octahedral potassium chloride was prepared by rapidly cooling an aqueous solution of potassium chloride (A.R., Merck) containing enough lead chloride to provide $[Pb^{++}]/[K^+]=9/1000$. The crystals were collected on a sintered glass filter funnel, washed with successive portions of 70% ethyl alcohol, absolute alcohol and dry ether, and stored in a vacuum desiccator over phosphorous pentoxide for about two weeks. The lead content of this sample was estimated gravimetrically as lead chromate; the analysis gave $[Pb^{++}]/[K^+]=5/100$. Microscopic examination of this sample revealed a large number of very small octahedrals plus a few large cubes in which the defects in the corners or edges were somewhat perceptible; hence it was concluded that the (111) was the predominant surface plane. 25.9 g. of this sample which passed through a 48-mesh sieve was used in the subsequent experiments.

Helium was supplied by the Teikoku Oxygen Co. as spectroscopically pure and was not further purified. The method of preparation of other gases has already been given[6].

Apparatus and Procedure.—The apparatus and the procedure were already described in a previous communication[6]. The lead-modified salt was outgassed by heating in vacuo at 280–300°C for a minimum period of 6 hr. prior to each experiment.

Results

The isotherms obtained for the four gases on lead-modified octahedral potassium chloride are summarized in Figs. 1, 2, 3 and 4. The adsorption was found to be reversible and practically instantaneous. The isosteric heats of adsorption were calculated from these isotherms using the Clausius-Clapeyron equation and showed no definite trend with temperature within the experimental error. In the calculations of the entropies of adsorption, the gas phase under the pressure of 760 mmHg and the temperature which coincides with that of each isotherm was chosen as the standard state.

1) Part V of this series, T. Hayakawa, This Bulletin, **30**, 337 (1957).

* Part of this paper was read before the 7th Annual Meeting of the Chemical Society of Japan held in Tokyo, April, 1954. Another part of this paper was also read before the symposium on the surface hetercgeneity of catalysis held in Kyoto, March, 1956.

2) T. N. Rhodin, Jr., *J. Am. Chem. Soc.*, **72**, 5691 (1950).

3) C. Frondel, *Am. Mineral.*, **25**, 91 (1940).

4) H. E. Buckley, "Crystal Growth," Chapman and Hall Ltd., London (1951), p. 461.

5) D. M. Young, *Trans. Faraday Soc.*, **48**, 548 (1952).

6) Part I of this series, T. Hayakawa, This Bulletin, **30**, 124 (1957).

7) Part II of this series, T. Hayakawa, This Bulletin, **30** 236 (1957).

8) Part III of this series, T. Hayakawa, This Bulletin, **30** 243 (1957).

9) Part IV of this series, T. Hayakawa, This Bulletin, **30**, 332 (1957).

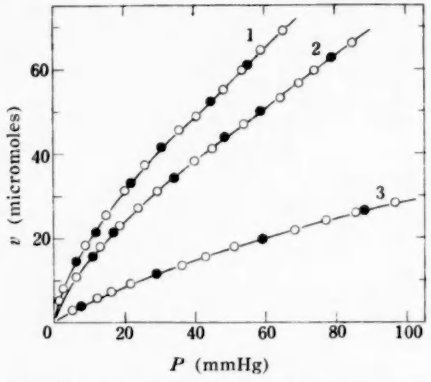

Fig. 1. Adsorption isotherms of argon on octahedral potassium chloride.
curve 1, 75.29°K; curve 2, 77.32°K; curve 3, 85.42°K.

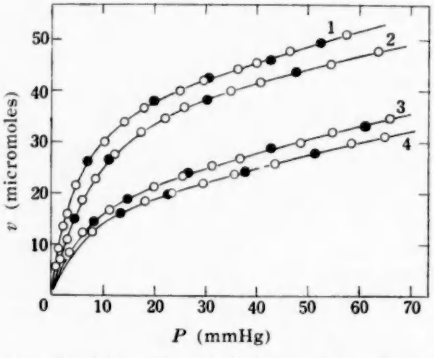

Fig. 2. Adsorption isotherms of oxygen on octahedral potassium chloride.
curve 1, 75.29°K; curve 2, 77.32°K; curve 3, 88.41°K; curve 4, 90.20°K.

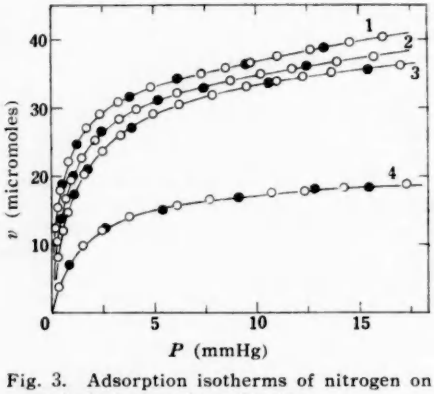

Fig. 3. Adsorption isotherms of nitrogen on octahedral potassium chloride.
curve 1, 73.69°K; curve 2, 75.79°K; curve 3, 77.32°K; curve 4, 88.36°K.

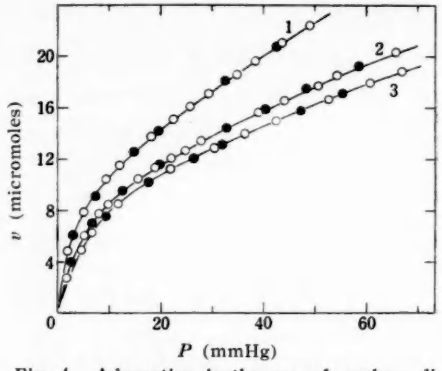

Fig. 4. Adsorption isotherms of carbon dioxide on octahedral potassium chloride.
curve 1, 187.66°K; curve 2, 192.63°K; curve 3, 194.64°K.

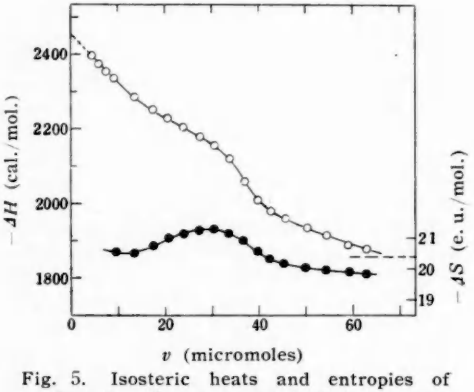

Fig. 5. Isosteric heats and entropies of adsorption of argon on octahedral potassium chloride.
-○-○-, isosteric heats of adsorption ($-\Delta H$);
-●-●-, entropies of adsorption ($-\Delta S$).

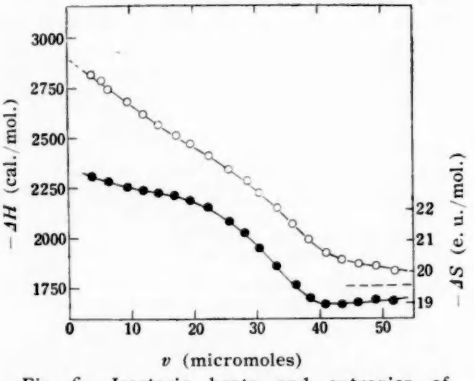

Fig. 6. Isosteric heats and entropies of adsorption of oxygen on octahedral potassium chloride.
-○-○-, isosteric heats of adsorption ($-\Delta H$);
-●-●-, entropies of adsorption ($-\Delta S$).

The present results on the isosteric heats and entropies of adsorption are summarized in Figs. 5, 6, 7 and 8. In the case of carbon dioxide, the measurements were not extended to the region of high coverage, since the amount adsorbed was considerably small in this temperature range.

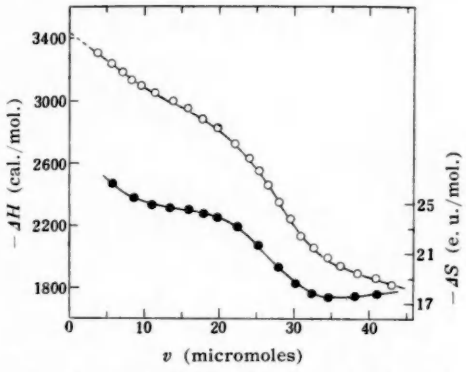

Fig. 7. Isosteric heats and entropies of adsorption of nitrogen on octahedral potassium chloride.
-o-o-, isosteric heats of adsorption ($-\Delta H$);
-•-•-, entropies of adsorption ($-\Delta S$).

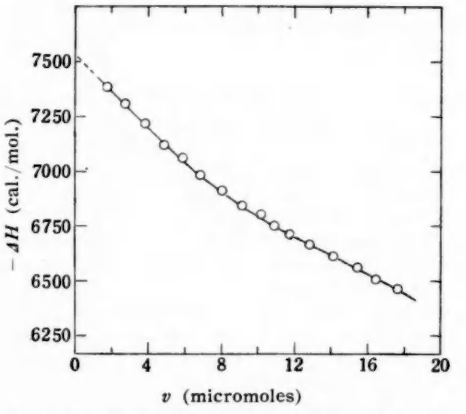

Fig. 8. Isosteric heats of adsorption of carbon dioxide on octahedral potassium chloride.

Discussion

Isosteric Heats of Adsorption.—As seen in Figs. 5, 6 and 7, the isosteric heats of adsorption obtained for the three gases (argon, oxygen and nitrogen) linearly fall at low coverage, reveal a considerably well-defined loop in the succeeding region, and then fall gradually to the value of latent heat of sublimation or evaporation at higher coverage. These results are markedly distinguishable from those already obtained for cubic potassium chloride[8].

Although the technique of habit-modification is open to the criticism that the impurities incorporated into the lattice during growth may alter the properties of the crystal surface, it has been indicated from Young's results[5] that the influence of the impurities is not clearly observable in the region where the surface is sparsely covered. The situation seems, however, somewhat different in the region of moderate coverage, since octahedral potassium chloride is bound by two types of (111) plane, one composed entirely of chlorine ions and the other of potassium ions. Now the present lead-modified adsorbent contains 5 lead ions for every 100 potassium ions, so that the heats of adsorption of these non-polar gases on the potassium faces are much more likely to be somewhat increased by the presence of this impurity. In order to obtain more informations on the isosteric heats of adsorption, the theoretical calculations of the initial heat of adsorption (i. e. the isosteric heat of adsorption at zero coverage) and the approximate calculation of the heat curve for each adsorption system were

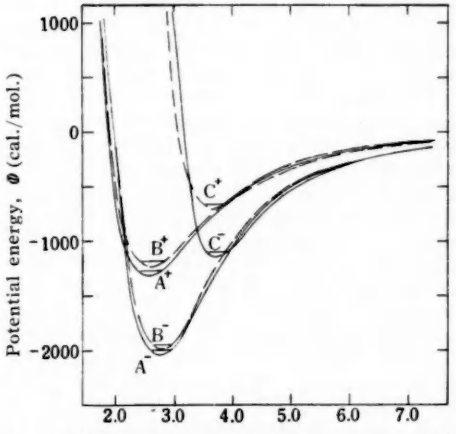

Fig. 9. Potential energy curves of argon on the (111) plane of potassium chloride. The symbols denote the type of sites and the surface layer.
A, above the center of a lattice triangle (directly above an underlying ion); B, above the centre of a lattice triangle (directly above the centre of an underlying lattice triangle); C, above a lattice point.

undertaken. In the case of nitrogen or carbon dioxide, however, owing to the low symmetry of the (111) plane and the poor covergence of the values of the quadrupole interaction potential, no satisfactory results have yet been obtained. The theoretical calculation of the adsorption potential of an isolated argon atom on the (111) plane of potassium chloride was carried out similarly following the method used by Young[10] except that the repulsive constant[7] of the modified Buckingham-Corner repulsive potential for argon was used. The calculated potential energy curves of argon for the six types of sites considered are shown in Fig. 9. From these curves the values of the equilibrium distance from the surface (Z_e), the minimum potential ($-\Phi_m$), the vibrational frequency normal to the surface (ν_z), the zero-point energy (ε_0) and the initial heat of adsorption ($-\Delta H_0$) were calculated. The results are summarized in Table I, together with the theoretical values of the initial heat of adsorption by Young.

As seen in Table I, the initial heat of adsorption of argon has been evaluated theoretically as 2140 cal./mol. for the Cl^- faces (sites type A) and 1420 cal./mol. for the K^+ faces (sites type A). Thus it may be anticipated that adsorption at low coverage proceeds exclusively on the Cl^- faces and when these faces become almost covered ($\theta > 0.5$) the proportion of argon atoms being adsorbed on the K^+ faces greatly increases. Similar tendencies may be expected for the adsorption of other non-polar gases on octahedral potassium chloride. Since the K^+ faces, on which adsorption takes place predominantly between $\theta = 0.5$ and 1.0, are somewhat activated by the presence of lead ions, the loop in each experimental heat curve (see Figs. 5, 6 and 7) may be mainly attributed to this activation by lead ions. Table I also indicates that the non-localized mobile adsorption is improbable* on account of the low adsorption heat of an argon atom adsorbed above a lattice point (sites type C). The approximate calculation of the heat curve of argon was also carried out similarly following the method used by Young[10], in which a localized hexagonal arrangement and an uniform surface were assumed. In the present calculation of the heat curve in a primary monolayer, the energy of a pair of argon atoms (distance 4.44 Å) was calculated using the modified Buckingham-Corner (6-exp) intermolecular potential[11]. The calculated heat curve for argon is shown in Fig. 10, together with the corresponding experimental values. For the sake of comparison, the

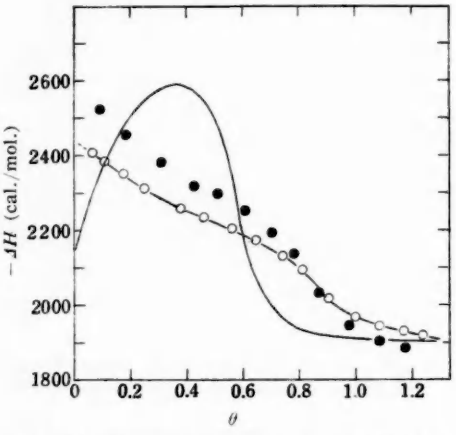

Fig. 10. Heat curves of argon on octahedral potassium chloride.
——, calculated heat curve; -o-o-, present experimental curve; •, values obtained by Young.

experimental curve obtained by Young is also shown in this figure. The values of coverage θ correlated to the present experimental values were derived from the monolayer capacity given in the subsequent discussion.

The agreement between the present experimental and calculated heat curves for argon is considerably satisfied at higher coverage, and this is probably attributed to the fact that the localized configuration has been adopted. While the discrepancy between the experimental and calculated heat curves at low coverage indicates that the surface heterogeneity is considerably predominant. Since it is of interest to compare the values of the initial heat of adsorption for the two crystal planes of potassium chloride, the experimental and theoretical values obtained in the present and preceding works[7,8] are given in Tables II and III. Since the difference between the experimental and theoretical values of the initial heat of adsorption gives a crude measure of the surface heterogeneity due to the imperfection of the crystal,

10) D. M. Young, *Trans. Faraday Soc.*, **47**, 1228 (1951).
* A partially localized arrangement seems, however, somewhat feasible on account of the similar properties of sites type A and B.
11) E. A. Mason and W. E. Rice, *J. Chem. Phys.*, **22**, 522 (1954).

TABLE I

RESULTS OBTAINED FROM THE POTENTIAL ENERGY CURVE, ARGON ON OCTAHEDRAL (111) KCl

Sites type	Surface layer	Z_e (Å)	$-\Phi_m$ (cal./mol.)	$\nu_z \times 10^{-12}$ (sec.$^{-1}$)	ε_0 (cal./mol.)	$-\Delta H_0$ (at 76°K) (cal./mol.)
Above the center of a lattice triangle (type A)	K^+	2.65	1307	0.86	40.7	1420(1610*)
	Cl^-	2.86	2030	0.94	44.6	2140(2220*)
Above the center of a lattice triangle (type B)	K^+	2.69	1232	0.82	38.9	1350(1500*)
	Cl^-	2.90	1988	0.96	45.5	2100(2370*)
Above a lattice ion (type C)	K^+	3.72	698	0.90	42.5	810(840*)
	Cl^-	3.74	1145	0.90	42.5	1250(1210*)

* values obtained by Young[10].

TABLE II

INITIAL HEAT OF ADSORPTION, $(-\Delta H_0)$, OF ARGON ON CUBIC (100) AND OCTAHEDRAL (111) KCl (in cal./mol.)

	(111) plane	(100) plane	$(-\Delta H_0)_{(111)} - (-\Delta H_0)_{(100)}$
$(-\Delta H_0)_{\text{expt.}}$	2460	2080	380
$(-\Delta H_0)_{\text{calcd.}}$	2140	1900	240
$(-\Delta H_0)_{\text{expt.}} - (-\Delta H_0)_{\text{calc.}}$	320	180	

TABLE III

INITIAL HEAT OF ADSORPTION, $(-\Delta H_0)_{\text{expt.}}$, OF NON-POLAR GASES ON CUBIC (100) AND OCTAHEDRAL (111) KCl (in cal./mol.)

Adsorbate	$(-\Delta H_0)_{(111)}$	$(-\Delta H_0)_{(100)}$	$(-\Delta H_0)_{(111)} - (-\Delta H_0)_{(100)}$
Oxygen	2870	2410	460
Nitrogen	3440	3010	430
Carbon dioxide	7540	6400	1140

TABLE IV

MONOLAYER CAPACITIES (V_m) AND SURFACE AREAS (A), OCTAHEDRAL POTASSIUM CHLORIDE (25.9 g.)

Adsorbate	Cross-sectional area, a (Å^2)	V_m (micromoles) from $(-\Delta S)$	V_m (micromoles) (B. E. T.)	A (m^2) from $(-\Delta S)$	A (m^2) (B. E. T.)
Argon	14.4	41.4	(40.9)	3.59	(3.55)
Oxygen	14.1	40.2	(36.6)	3.41	(3.11)
Nitrogen	17.0	34.4	(37.2)	3.52	(3.81)

TABLE V

NON-CONFIGURATIONAL ENTROPIES (S_{NC}) ON OCTAHEDRAL POTASSIUM CHLORIDE AT $\theta = 0.4$

Adsorbate	$(S_{NC})_{\text{calcd.}}$, (e. u./mol.)	$(S_{NC})_{\text{expt}}$, (e. u./mol.) $(S_s - S_c)$	$(S_{NC})_{\text{expt}}$, (e. u./mol.) $(S_s - \overline{S_c})$
Argon	9.6(a)	5.7	6.7
Oxygen	13.9(b)	12.9	13.4
Nitrogen	10.9(c)	7.8	8.9

(a) $\nu_x = \nu_y = 8.2 \times 10^{11}$ sec.$^{-1}$ ν_z (mean value) $= 0.93 \times 10^{12}$ sec.$^{-1}$

(b) Following values were assumed: $\nu_x = \nu_y = 8 \times 10^{11}$ sec.$^{-1}$ $\nu_z = 1.0 \times 10^{12}$ sec.$^{-1}$

(c) Following values were assumed: $\nu_x = \nu_y = 8.5 \times 10^{11}$ sec.$^{-1}$ $\nu_z = 1.1 \times 10^{12}$ sec.$^{-1}$

Table II indicates that the surface heterogeneity of this type for octahedral potassium chloride is more predominant than that for cubic crystals. As seen in Tables II and III, the experimental values of the initial heat of adsorption for these non-polar gases on the (111) plane of potassium chloride are all considerably greater than the corresponding values on the (100) plane. As it has already been pointed out by Young[5], this is mainly attributed to the facts that the (111) plane contains fewer ions per unit area than the (100) plane and that initial adsorption on the (111) plane occurs predominantly on the Cl^- faces.

Monolayer Capacities. — As discussed above, it is reasonable to consider that adsorption in the range between $\theta=0.5$ and 1.0 takes place predominantly on the K^+ faces. In this range, since the increase in the heats due to the mutual interaction may be overcome by the decrease in the heats due to the increased proportion of adsorption on the K^+ faces, the isosteric heats steadily decrease with the increased amounts adsorbed. At higher coverage ($\theta>1$), since the formation of multilayers proceeds on a large scale, the isosteric heats of adsorption in this range slowly decrease and approach the latent heat of sublimation or evaporation. Consequently, in the region where θ approaches unity, there will be a bend point in each heat or entropy curve (see Figs. 5, 6 and 7). Considering this fact, it seems reasonable to assign this value of the amount adsorbed as a monolayer capacity.

The present results on the monolayer capacities and thus calculated surface areas are summarized in Table IV. Each value of the cross-sectional area in this table was determined from referring to the results on the entropies of the adsorbed phase.

Entropies of the Adsorbed Phase. — The present results on the entropies of adsorption shown in Figs. 5, 6 and 7 are obviously distinguishable from those already obtained for cubic potassium chloride[8]. In order to obtain more information about the freedom of the adsorbed atoms or molecules, the entropies of the adsorbed phase were calculated from the experimental data and compared with those already obtained for cubic potassium chloride. The method of the statistical calculations of the entropies of the gas phase under the standard states was already given in a previous communication[6]. The integral (S_c) and differential ($\bar{S}_c$) configurational entropies were calculated from the present experimental data using the expressions derived by Drain and Morrison[12]. The experimental entropy curves of the adsorbed phase on octahedral potassium chloride are summarized in Figs. 11, 12 and 13, together with the experimental curves on cubic potassium chloride. As seen in these

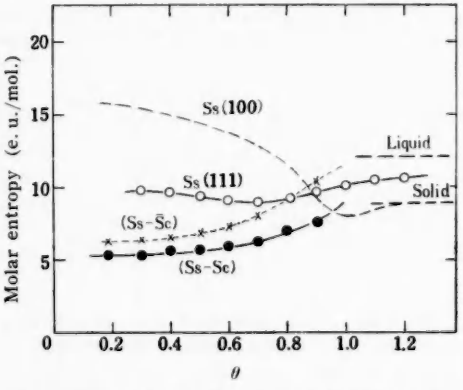

Fig. 11. Molar entropies of adsorbed argon on potassium chloride.
-o-o-, entropies on the (111) plane;
-----, entropies on the (100) plane.

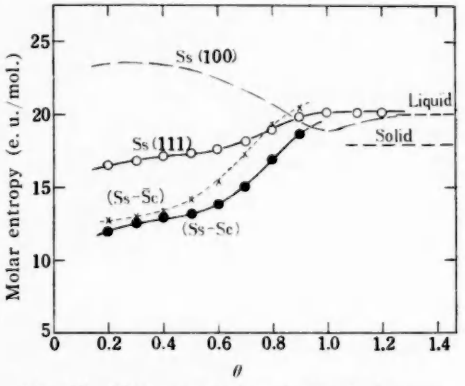

Fig. 12. Molar entropies of adsorbed oxygen on potassium chloride.
-o-o-, entropies on the (111) plane;
-----, entropies on the (100) plane.

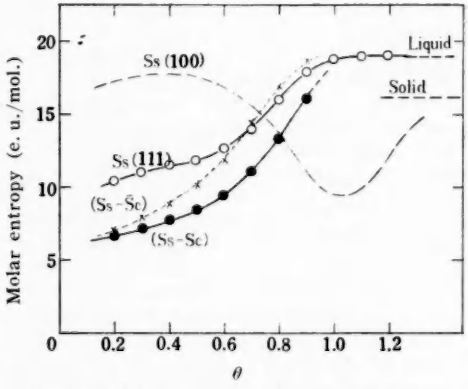

Fig. 13. Molar entropies of adsorbed nitrogen on potassium chloride.
-o-o-, entropies on the (111) plane;
-----, entropies on the (100) plane.

12) J. M. Drain and J. O. Morrison, *Trans. Faraday Soc.*, **48**, 316 (1952).

figures, the experimental curves (S_s) of these non-polar gases on octahedral potassium chloride show quite different features from those on cubic potassium chloride. Since the experimental curves for the (100) plane of potassium chloride well agree with the calculated curves of the two-dimensional gas at least in the range of $\theta<0.8$[13], it is reasonable to consider that the low-temperature adsorption of these non-polar gases on the (111) plane of potassium chloride is localized (or at least partially localized) in this same range. These figures also indicate that at higher coverage ($\theta>1$) the entropies of each adsorbed phase all remain close to the entropies of the liquid state.

Since the experimentally determined values (S_s) in these figures are the partial molar total entropies[13], the non-configurational entropies of the adsorbed phase on octahedral potassium chloride may be indicated approximately by ($S_s-\bar{S}_c$) or (S_s-S_c) curves shown in these figures. Now the non-configurational entropies of the adsorbed atoms or molecules are approximately calculated and compared with the experimental values at $\theta=0.4$. The reason of choosing the experimental values at $\theta=0.4$ is mainly that at this coverage adsorption proceeds exclusively on the Cl^- faces and these surfaces are almost covered by the adsorbed atoms or molecules.

In the present work, the entropy associated with the vibrational motion parallel to the surface (two degree of freedom, x and y directions) was approximately calculated following the method used by Hill[14], in which the vibrational motion was assumed to be isotropic. In the case of oxygen or nitrogen, the entropy associated with the planar rotation in the plane parallel to the surface was calculated using an expression derived by Halford[15]. Since the surface essentially introduces a high potential barrier restricting the turning over of the molecular axis, another rotational motion may be replaced by the rocking vibration of the molecular axis[14]. In the present calculations, however, the entropy associated with this rocking vibration was assumed to be negligible. The calculations of the entropy associated with the intramolecular vibration resulted in the values of nearly zero. Further, the electronic entropy of the oxygen molecule was taken into consideration. The calculated results are summarized in Table V, together with the experimental values.

As seen in Table V, the agreement between the experimental and approximately calculated values of the non-configurational entropy for oxygen is considerably satisfied, while the experimental values of argon and nitrogen are somewhat smaller than the calculated values. However, in view of the facts that the present calculations contain considerable approximations and that the experimentally determined values (S_s) are all the partial molar total entropies, the agreement may be regarded as rather satisfactory.

Summary

1. The low-temperature adsorption of non-polar gases on octahedral potassium chloride was studied. The present results were compared with those already obtained for cubic potassium chloride.

2. The initial heats of adsorption of non-polar gases on the (111) plane of potassium chloride are all considerably greater than the corresponding values on the (100) plane.

3. The surface heterogeneity due to the imperfection of the crystal for octahedral potassium chloride is more predominant than that for cubic crystals.

4. The present results on the isosteric heat of adsorption and the entropies of the adsorbed phase indicate that the low-temperature adsorption of non-polar gases on the (111) plane of potassium chloride is practically localized.

The author wishes to express his grateful thanks to Dr. S. Horiba and Professor O. Toyama of Osaka Perfectural University for their kind encouragement and discussion. The author's sincere thanks are also due to Professor R. Kiyama of Kyoto University for his kind discussion.

Department of Chemistry
Faculty of Education
Osaka Prefectural University, Sakai

13) T. L. Hill, *J. Chem. Phys.*, **17**, 520 (1949).
14) T. L. Hill, ibid., **16**, 181 (1948).
15) J. O. Halford, ibid., **2**, 694 (1934).

Photo-dichroism of Printed-out Silver. IV. An Explanation of the Relation between Dichroism Curve and Absorption Difference Curve and the Effect of After-, and Pre-illumination in Terms of the Theory of Anisotropic Herschel Effect

By Isao KAMIYA

(Received December 4, 1956)

In the previous paper[1], the author has reported that the absorption difference curve of printed-out silver between before and after exposure to natural red (or orange) light is very analogous to spectral dispersion curve of photo-dichroism of printed-out silver which is produced after being exposed to polarized red (or orange) light, and that, if it is assumed that the absorption difference curve would be taken approximately as the dichroism curve, the author has been able to explain the mechanism of "Color adaptation" and "Inversion effect"[2], as well as of the peculiar behavior of dichroism being observed with the light of which the wave lengths are in the region between 580 and 550 mμ.

However, the question why the difference curve is analogous to the dichroism curve has not been answered.

In the present paper, the author has first given a theoretical expression of this relation from the point of view that the phenomenon of photo-dichroism would be anisotropic Herschel effect.

It has been known that the values of photo-dichroism produced after being exposed to polarized red light are to be decreased by subsequent illumination with natural red light, which is called "the effect of after-illumination", and it is also known that the value of dichroism of the film which was previously illuminated with natural red light is smaller than that of non-pre-illuminated film[3].

The author has also considered the mechanism of these effects and given a quantitative explanation, which is in good agreement with experimental results, using the theory of anisotropic Herschel effect[4].

1) I. Kamiya, This Bulletin **30**, 298 (1957).
2) F. Weigert, *Z. phys. Chem.*, **B3**, 377 (1929).
3) E. Elvegård, "Über den Weigert-Effect," Univ. Leipzig (1929), p. 32.
4) I. Kamiya, This Bulletin, **30**, 294 (1957).

Explanation of the Relation between Dichroism Curve and Absorption Difference Curve

In the previous paper, it has been shown that, if $J_{\parallel}$ and $J_{\perp}$ are the numbers of inner-photo-electrons raised from the surfaces of colloidal particles of metallic silver to conduction band of the crystals of silver chloride when exposed to polarized red light of which the electric vectors are in the plane of incidence ($L_{\parallel}$), and perpendicular to the plane ($L_{\perp}$), the plane of incidence is formed with the line of exposing ray and the normal to the surface of colloidal particle of metallic silver, and n_0 is the number of the colloidal particles before exposure, the number of remaining particles which have not been destroyed after t minutes' exposure are given as,

$$n_{\parallel}=n_0[1-\{1-K(1-\exp(-J_{\parallel}t))\}] \text{ for } L_{\parallel} \tag{1}$$

$$n_{\perp}=n_0[1-\{1-K(1-\exp(-J_{\perp}t))\}] \text{ for } L_{\perp} \tag{2}$$

where K is constant if the temperature is constant.

Then, the value of photo-dichroism (D) produced after t minutes' exposure is given,

$$D=(n_{\perp}-n_{\parallel})(\lambda_{\parallel}-\lambda_{\perp}) \tag{3}$$

where $\lambda_{\parallel}$ and $\lambda_{\perp}$ are the absorption coefficients of observed light of which the electric vectors are in the plane of incidence and perpendicular to the plane.

In eq. (3), it may be assumed that $\lambda_{\parallel}$ is much greater than $\lambda_{\perp}$, as is probable, (3) is approximately taken as,

$$D=\lambda_{\parallel}n_{\perp}-\lambda_{\parallel}n_{\parallel} \tag{4}$$

When the above consideration is permissible, the first term in (4), $\lambda_{\parallel}n_{\perp}$, will approximately show the absorption curve analogous to that before exposure, because the value of $J_{\perp}$ might, in fact, be very small, and the second term, $\lambda_{\parallel}n_{\parallel}$, will be

shown as the absorption curve after exposure, which is shown as curve-a and curve-*c* in Fig. 1. This is the reason why the dichroism curve is analogous to absorption difference curve between, before and after exposure to natural red (or orange) light.

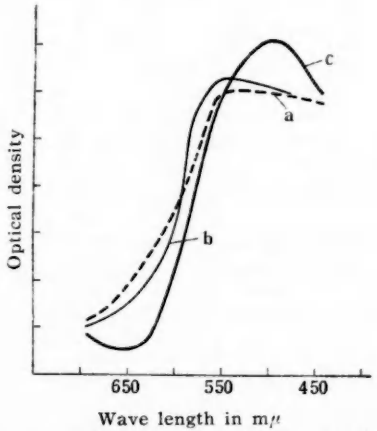

Fig. 1. Schematic representation of the absorption spectra of printed-out Valenta's film. curve-*a*: before exposure, curve-*b*: after a short exposure, curve-*c*: after a long exposure to natural red light.

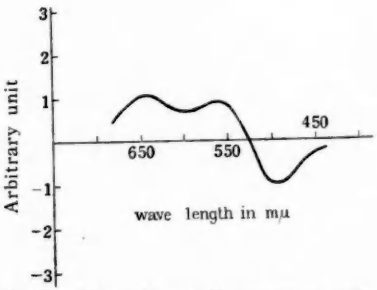

Fig. 2. Absorption difference curve between curve-*b* and curve-*c* in Fig. 1.

For long-exposure, $n_{\perp}$ will be no longer n_0, and hence the curve of $\lambda_{\parallel} n_{\perp}$ will not be shown as curve-*a* but will be shown as curve-*b* in Fig. 1, since $n_{\perp}$ is decreased a little for a long-time exposure, so that the curve is to be taken as that analogous to the absorption curve after short-time exposure having been shown as curve-*b* in the previous paper[1]. Thus, the values of photo-dichroism being taken as *c*—*b*, it may be found that the spectral dispersion curve of D might have two maxima in certain special cases as illustrated in Fig. 2.

In reality, these two maximum points have been observed for long-time exposure by several authors[5] (Fig. 3).

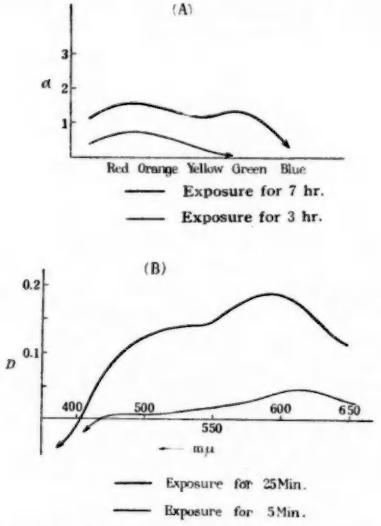

Fig. 3. Spectral dispersion curves of photo-dichroism observed by Horiba, Kondo (A), and Narath, Wasserroth (B).

The Effect of After-illumination

It has been known that the values of photo-dichroism produced after exposure to polarized red light is to be decreased by subsequent illumination with natural red light. This is called, "The effect of after-illumination".

The author has carried out the experiments on the effect using the films of Valenta's emulsion by the way as follows.

The values of dichroism of the films which had been exposed to polarized red light for various periods were measured with red light after being illuminated for 10, 20, 30, 40 and 50 minutes with strong natural red light. The source of illuminating light was the same as described in the previous paper[6]. These results are shown in Table I.

From these, it is seen that; (i). the rate of decreasing during this after-illumination is fast in the initial stages and then becomes slower and slower, (ii). if D and D' are the values of dichroism before and after illumination, the values of $(D-D')/D$,

5) S. Horiba, and T. Kondo, *The Sexagint* (Osaka Fest.) Kyoto Univ., **1927**, p. 68.
A. Narath and K. Wasserroth, *Sc. et Industr. phot.*, **23A**, 39 (1952).
6) I. Kamiya, This Bulletin, **30**, 6 (1957).

TABLE I
VALUES OF DICHROISM FOR VARIOUS PERIODS OF AFTER-ILLUMINATION WITH NATURAL RED LIGHT (D')

Film No.	Time of after illumination with natural red light, (Min.)	0	10	20	30	40	60
I	$D'(2\alpha)$	2.31 (=D)	1.61	1.46	1.30	1.16	1.12
	$(D-D')/D$	—	0.30	0.37	0.43	0.50	0.50
II	$D'(2\alpha)$	3.30 (=D)	2.26	2.06	1.86	1.67	1.64
	$(D-D')/D$	—	0.31	0.37	0.43	0.49	0.50

D: Values of dichroism before illuminations.

that is the percentages of decreasing values, seem to be independent of D. These values are also illustrated in Table I.

The author has considered the mechanism of this effect and proposed a theory, which enables him to understand why these characters described above are found, from the point of view that the phenomenon of photo-dichroism would be an anisotropic Herschel effect.

As has been shown by the author, the values of dichroism D is given as,

$$D=(n_\perp-n_\parallel)(\lambda_\parallel-\lambda_\perp)$$

It is reasonable to assume that the remaining numbers of $n_\perp$ and $n_\parallel$ are destroyed by after-illumination with natural red light having the same mechanism as Herschel effect. The light of illumination being divided into two components: one is the most effective to destroy $n_\perp$ and the other $n_\parallel$ since the destruction of these colloidal particles are the most effective to be destroyed when the electric vector of illuminating light is in the plane of incidence, the numbers of destroyed particles, $\Delta n_\perp$, and $\Delta n_\parallel$ in each case are calculated from the same point of view as in the previous treatments[4].

$$\begin{aligned}\Delta n_\perp &= n_\perp[1-\exp(-J_\parallel t)]ke^{-\frac{U}{RT}}\\ \Delta n_\parallel &= n_\parallel[1-\exp(-J_\parallel t)]ke^{-\frac{U}{RT}}\end{aligned} \quad (5)$$

where $J_\parallel t$ is the number of inner-photoelectrons after t minutes' exposure, k is constant and U/RT is constant at a constant temperature. Hence, the value of dichroism after t minute's illumination can be obtained,

$$D'=\{(n_\perp-\Delta n_\perp)-(n_\parallel-\Delta n_\parallel)\}(\lambda_\parallel-\lambda_\perp) \quad (6)$$

From (5), (6) becomes,

$$\begin{aligned}D' &= (n_\perp-n_\parallel)(\lambda_\parallel-\lambda_\perp)-(n_\perp-n_\parallel)\\ &\quad\times[1-\exp(-J_\parallel t)]ke^{-\frac{U}{RT}}(\lambda_\parallel-\lambda_\perp)\\ &= D-k\cdot D\cdot e^{-\frac{U}{RT}}[1-\exp(-J_\parallel t)] \quad (7a)\end{aligned}$$

where D' is the value of dichroism after t minutes' illumination and D that before illumination.

(6) is also written as,

$$(D-D')/D=ke^{-\frac{U}{RT}}[1-\exp(-J_\parallel t)] \quad (7b)$$

In order to be in agreement with experimental results, the constants $ke^{-\frac{U}{RT}}$ and $J_\parallel$ in (7) are put to 0.5 and 0.08 respectively.

The curve of $(D-D')/D$ against t using the formula of $0.5\ (1-e^{-0.08t})$ and the experimental values are illustrated in Fig. 4. These are in good agreement with each other.

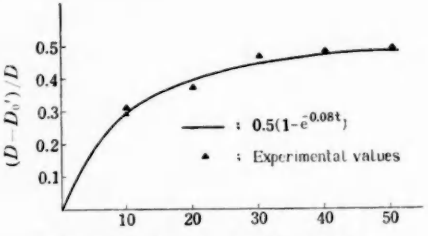

Fig. 4. Theoretical curve and experimental values of the percentages of decreasing dichroism against the time of after-illumination with natural red light.

The value of $J_\parallel$ (=0.08) used here is somewhat larger than that before (=0.026). This deviation will be probably due to the fact that the later is the value when the illuminating light was passed through a Nikol's prism whereas the former is that which was not passed through.

The Effect of Pre-illumination

It is also known that the values of photo-dichroism of printed-out silver which had been pre-illuminated with natural red light is less than that of non-pre-illuminated silver, when exposed to polarized

TABLE II

VALUES OF DICHROISM FOR VARIOUS PERIODS OF PRE-ILLUMINATION WITH NATURAL RED LIGHT (D') (Observed by Elvegård)

Time of exposure to polarized red light (Min.)	Time of pre-illumination with natural red light (Min.)	0	4	16	64
2	D'	12 ($=D$)	8.6	5.6	5.3
	$(D-D')/D$	—	0.28	0.52	0.55
8	D'	29 ($=D$)	21	15	11
	$(D-D')/D$	—	0.28	0.48	0.62
16	D'	35 ($=D$)	29	22	16
	$(D-D')/D$	—	0.26	0.37	0.54

red light. This is called, "The effect of pre-illumination with natural red light" or "die Wirkung einer Vorbelichtung mit naturlichem lichte"[3].

Elvegard has investigated the effect. His results are shown in Table II.

The author has considered the mechanism in regard to the same points as before.

If the number of colloidal particles before being illuminated with natural red light is n_0, and that after t minutes' pre-illumination is n', n' is obtained as before; that is,

$$n'=n_0[1-k'\{1-\exp(-Jt)\}e^{-\frac{U}{RT}}] \quad (8)$$

where J is the number of inner-photo-electrons per minute when illuminated with natural red light.

Next, if the film is exposed to polarized red light for t minutes, the number of colloidal particles of metallic silver which remained undestroyed on exposure to the light of which the electric vector is in the plane of incidence, $n_\parallel'$ is

$$n_\parallel'=n'[1-k'\{1-\exp(-J_\parallel t)\}e^{-\frac{U}{RT}}] \quad (9a)$$

and that to the light of which the electric vector is perpendicular to the plane, $n_\perp'$ is

$$n_\perp'=n'[1-k'\{1-\exp(-J_\perp t)\}e^{-\frac{U}{RT}}] \quad (9b)$$

Thus, the value of dichroism is to be taken as,

$$D'=(n_\perp'-n_\parallel')(\lambda_\parallel-\lambda_\perp) \quad (10)$$

From (8) and (9), (10) becomes

$$D'=(n_\perp-n_\parallel)(\lambda_\parallel-\lambda_\perp)\times[1-k'\{1-\exp(-Jt)\}e^{-\frac{U}{RT}}]$$
$$=D[1-k'\{1-\exp(-Jt)\}e^{-\frac{U}{RT}}]$$

so that

$$(D-D')/D=k'e^{-\frac{U}{RT}}\{1-\exp(-Jt)\} \quad (11)$$

where D' and D are the values of dichroism to be taken when the film is pre-illuminated for t minutes and if the same film was not illuminated.

In reality, D being unable to be determined by experiment, the following approximation is made.

D obtained with a film is the same as that with another film, though these values are actually slight by different from another.

From this approximation, the author has calculated the values of $(D-D')/D$ using the values of D and D' obrerved by Elvegård. These results are also shown in Table II.

In order to explain the experimental results with (11), the constants $k'e^{-\frac{U}{RT}}$ and J are to be taken as 0.55 and 0.16 respectively. In Fig. 5, the curve of $(D-D')/D$ against t and the experimental values observed by Elvegård are illustrated. It is seen that the theoretical is in fairly good agreement with the experimental for such approximation.

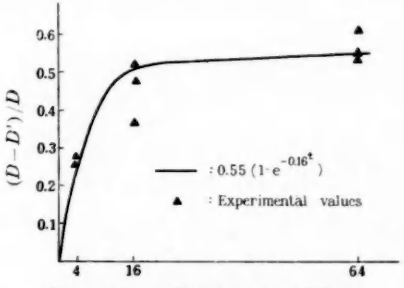

Fig. 5. Theoretical curve and experimental values of the percentages of decreasing dichroism against the time of pre-illumination with natural red light.

From these evidences described in this paper, it is also emphasized that the

phenomenon of photo-dichroism would be an anisotropic Herschel effect.

The author gives thanks to the late Prof. J. Shidei and Dr. D. Yamamoto for their kind advice.

Department of General Education
Nagoya University, Nagoya

Non-Newtonian Viscosity of Dilute High Polymer Solutions. III. On the Method of Measuring Zero Shear Viscosity

By Toshiaki KUROIWA

(Received December, 4, 1956)

Introduction

It is now recognized that, when molecular weight of a polymer is high enough, the effect of the rate of shear on the solution viscosity is by no means negligible even when working with extremely dilute solutions[1-3]. As the result, various investigators have sought to obtain a method of extrapolating the viscosity data at the finite rate of shear to zero shear rate[2-4,10,11].

Some have proposed the linear extrapolation of logarithm of viscosity vs. rate of shear plot for such a method[2,12]. E. Wada[7] and the present writer[8], however, have found that the viscosity vs. shear rate curve shows an antisigmoidal form having a horizontal tangent at the origin rather than an exponential form. This behavior is in accordance with the theories of Kuhn and Kuhn[13] and Saito[14] according to which the viscosity of a dilute polymer solution should be given by an equation of the form:

$$\eta_{sp}=\eta_{sp0}(1-aq^2+bq^4-\cdots\cdots), \qquad (1)$$

where η_{sp0} is η_{sp} at zero shear rate, q denotes rate of shear and a, b, etc. are non-Newtonian parameters. This means that the linearity of such a semi-log plot can not be satisfied at least in low shear rate region. Fig. 1 shows log η_{sp}/c vs. q plots for several polystyrene fractions of different molecular weights in toluene by

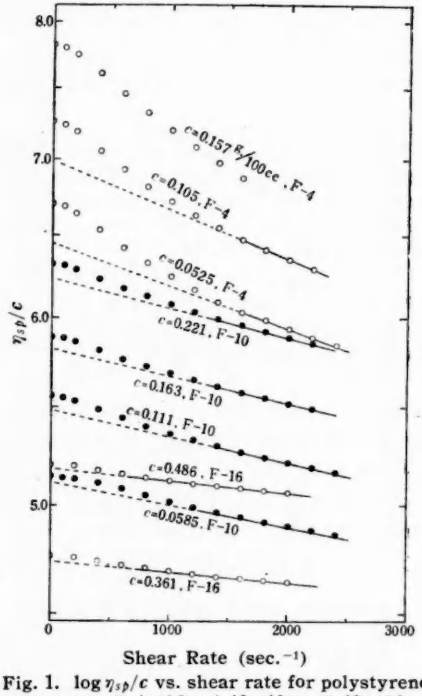

Fig. 1. log η_{sp}/c vs. shear rate for polystyrene fractions F-4 ($M_w=4.10\times10^6$), F-10 ($M_w=3.08\times10^6$) and F-16 ($M_w=1.98\times10^6$) in toluene at 25°C.

1) C. M. Conrad, V. W. Tripp and T. Mares, *J. Phys. Colloid Chem.*, **55**, 1474 (1951).
2) T. G. Fox Jr., J. C. Fox, and P. J Flory, *J. Am. Chem. Soc.*, **73**, 1901 (1951).
3) H. T. Hall and R. M. Fuoss, ibid., **73**, 265 (1951).
4) G. De Wind and J. J. Hermans, *Rec. trav. chim.* Bay-Bas, **70**, 521, 615 (1951).
5) F. Akkerman, D. T. F. Pals and J. J. Hermans, ibid., **71**, 56 (1952).
6) L. S. Sharman, R. H. Sones and L. H. Cragg, *J. Appl. Phys.*, **24**, 703 (1953).
7) E. Wada, *J. Sci. Research Inst.*, **47**, 149, 159, 168 (1953); *J. Polymer Sci.*, **14**, 305, 307 (1954).
8) T. Kuroiwa, This Bulletin, **29**, 164, 962 (1956).
9) M. A. Golub, *J. Polymer Sci.*, **18**, 27, 156 (1955); *J. Phys. Chem.*, **60**, 431 (1956).
10) J. Schurz and E. H. Immergut, *J. Polymer Sci.*, **9**, 279 (1952).
11) J. Schurz, ibid., **10**, 123 (1953).
12) W. R. Krigbaum and P. J. Flory, *J. Polymer Sci.*, **11**, 37 (1953).
13) W. Kuhn and H. Kuhn, *Helv. Chim. Acta*, **28**, 1533 (1945); ibid., **29**, 609 (1946).
14) N. Saito, *J. Phys. Soc. Japan*, **6**, 302 (1951).

the experimental data reported in the previous paper[8]*. Evidently, it is not possible to give a fully linear representation to each of these plots over the entire range of shear rate. The plots for the lower molecular weight fractions, however, may be regarded to be linear in the region of higher shear rates and the approximately linear portions of these curves appear to extend towards a low rate of shear as molecular weight of the polymer decreases. Therefore the linear extrapolation of log η_{sp}/c in these shear ranges to zero shear will yield a fairly good approximation to the zero shear viscosity when molecular weight of the polymer is not so much high as those of the fractions shown in Fig. 1. Moreover, it seems that the tangent of the linear portion is independent of concentration for a given fraction as pointed out by Fox, Fox and Flory.[2] An upward deviation from linearity of $\ln \eta_r$ vs. q curves at lower shear rates has been observed also by Cragg et al.[6] for polystyrene solutions, although the shear rate at which the deviation commences appears to be higher than in the present case.

Recently, Katchalsky[15] has suggested the method of obtaining the zero shear viscosity making use of the relationship he derived:

$$\frac{t_s}{t}=\frac{\eta_s}{\eta_0}\left(1+\frac{aP^2R^2}{3\eta_0^2L^2}\right), \qquad (2)$$

where t and t_s are the flow times of the solution and solvent, respectively, at pressure P, η_s is the viscosity of the solvent and η_0 the viscosity of the solution at zero shear, a is a non-Newtonian parameter appeared in Eq. (1), R and L the radius and length of the capillary, respectively. According to Eq.(2), if a series of measurements are made in viscometers of different capillary radii at the same pressure, or alternatively, at different pressures in the same viscometer, then the resulting t_s/t vs. P^2R^2 plot should be a straight line, and the zero shear viscosity, η_0, can be determined as the reciprocal of the intercept of this line at the origin multiplied by η_s. Katchalsky derived Eq. (2) on the basis of the theoretical equation (1). For small shear rate, Eq. (1) reduces to the simpler form:

$$\eta_{sp}=\eta_{sp0}(1-aq^2), \qquad (3)$$

and this equation was used in deriving Eq. (2).

For most polymer solutions, however, the shear rate range in which Eq. (3) can adequately describe the shear dependence of solution viscosity appears to be confined to very low shear rates which the ordinary viscosity method by a capillary viscometer can deal with only with difficulty. This opinion may be borne out by the fact that such a quadratic dependence of viscosity has been observed only by a few recent investigators[7,8,16,17] who have extended the measurements down to very low shear rates by the use of a specially designed viscometer. For example, the quadratic range was found to lie below the gradients of about 200–300 sec.$^{-1}$ for those polystyrene fractions in toluene though it depends on concentration and molecular weight of the polymer to some extent (see Fig. 2). Therefore Katchalsky's equation (2) may be expected to hold when measurements are made only at small gradients to which the routine method of viscometry by a capillary viscometer is not easily accessible.

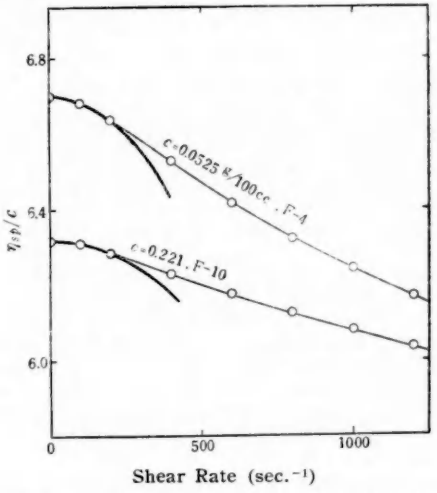

Fig. 2. η_{sp}/c vs. shear rate. The heavier line shows the curve according to Eq. (3).

The present writer has examined these previous results on polystyrene in various ways, seeking after an available method for obtaining zero shear viscosity involving nothing more than a straight-line extrapo-

* The shear rate dealt with in the routine method of viscometry of dilute polymer solutions will usually fall in the shear rate range of 500-3000 sec^{-1}.

15) A. Katchalsky and N. Sternberg, *J. Polymer Sci.*, **10**, 253 (1953).

16) H. Fujita and T. Homma, *J. Polymer Sci.*, **15**, 277 (1955).

17) P. Alexander and K. A. Stacey, *Trans. Faraday Soc.*, **51**, 299 (1955).

lation, which should hold over a sufficiently wide range of shear rates. But the mathematical relationship between viscosity and shear rate was too complex to warrant generalization and none of these attempts was successful.

Another method of measuring the zero shear viscosity has been proposed by E. Wada[7] in which the use of a tilting viscometer is recommended. Taking advantage of a horizontal tangent at very small shear rates in the viscosity vs. shear curve, the apparent relative viscosities are measured at successively low pressures by tilting the viscometer until they begin to assume a constant value, which is substantially the relative viscosity at zero shear.

The present writer has measured the zero shear viscosities of polystyrene fractions in toluene according to the same principle using a multi-bulb viscometer instead of the tilting type and found that the results thus obtained are in good agreement with the zero shear viscosities previously measured by a horizontal viscometer[8]. In the following, the viscometer is briefly described and the results are compared with the previous results.

Viscometer

A sketch of the viscometer used is shown in Fig. 3. In order to carry out measurements at sufficiently low rates of shear, the capillary was made small in radius ($R=0.0131$ cm.) and long ($L=30.0$ cm.). The upper part of each tube of the viscometer was bent as shown in Fig. 3 so as to allow the viscometer to be inclined at nearly horizontal positions without shedding the charged liquid, which procedure is necessary to fill the liquid in the capillary portions without allowing air to remain in the bent portion between the two capillaries.

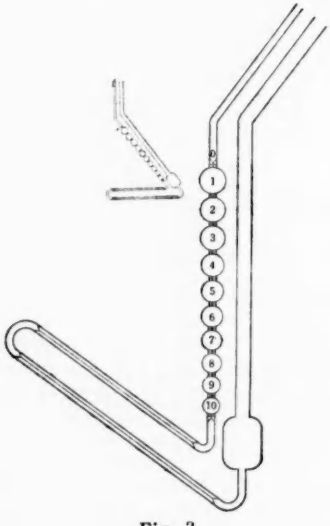

Fig. 3.

Since fairly rapid fall of the liquid in the strait portions at the etched lines (0, 1, 2, 3, etc. in Fig. 3) is desirable for the facility of flow time measurements, and since the flow velocity in this viscometer is very small owing to the long fine capillary, the straits in lower part of the viscometer were made fairly narrow (0.03 cm. in diameter for the lowest at the line 10). These narrow straits not only play a roll of capillary to some extent but also cause the surface tension error when the difference in surface tension between the solution and solvent is appreciable. But for the present case, at least, this error is considered negligible if it exists at all since the results obtained by this viscometer are in good agreement with those by a horizontal viscometer, in which the surface tension effect is almost completely absent. The measurement using the lowest efflux bulb (9–10) was found to be impossible for polystyrene solutions in toluene due to the capillary rise of the solvent in the strait at the line 10, which was absent in measurements of polymethylmethacrylate solutions in chloroform.

The viscometer was fixed on a brass frame, which in turn can be mounted on a frame in a thermostat so as to ensure the reproducibility of the viscometer position, which is very essential to the reliable measurements.

The kinetic energy correction for this viscometer was found to be negligible being consistent with the very small flow velocity in the viscometer. The drainage error was assumed to be also negligible.

Results

The ratios of the flow times of the solution and solvent, t/t_0, for two polystyrene fractions in toluene, measured at 25°C are shown graphically in Figs. 4 and 5 plotted against the mean pressure head, h, and shearing stress, τ. Here τ was calculated according to the equation:

$$\tau = \rho g h R / 2L \qquad (4)$$

which is the expression for the maximum shearing stress at the capillary wall, where ρ is the density of the solution. The shear rate ranges covered by these measurements are 54–201 sec.$^{-1}$ for the solution of $c=0.196$ g./100 cc. of F-4, 109–405 sec.$^{-1}$ for $c=0.0568$ of F-10.

As seen in Figs. 4 and 5, t/t_0 appears to attain a constant value at lower pressures and this value may be regarded as the t/t_0 at zero pressure. In this range of pressures, the linearity of the Katchalsky plot, t_0/t vs. h^2, was found to be satisfied very well by these data as may be expected. Though these plots are not shown here, t/t_0 at zero shear rate determined from the intercept of the straight line in these plots was substantially coincident with the one provided by

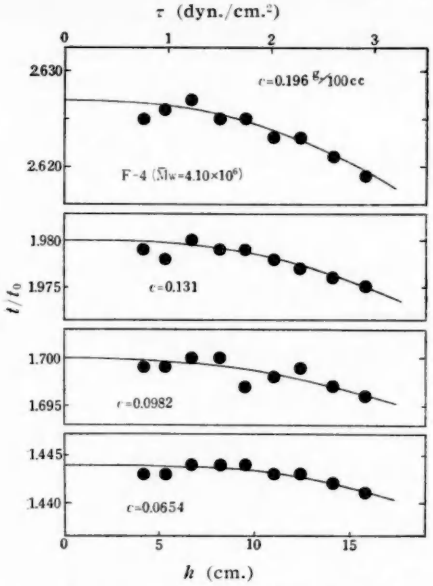

Fig. 4. The ratio of the flow times of the solution and the solvent vs. the mean pressure head, h, and shearing stress, τ. See Eq. (4) for τ.

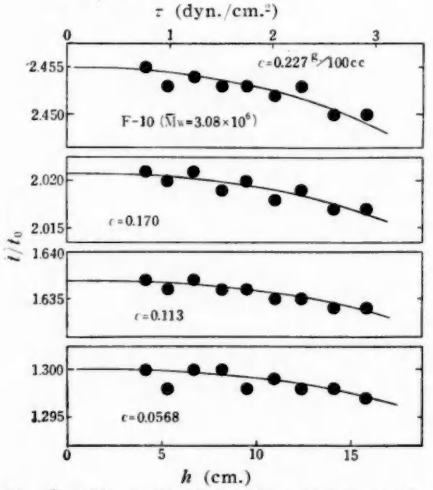

Fig. 5. The ratio of the flow times of the solution and the solvent vs. the mean pressure head, h, and shearing stress, τ. See Eq. (4) for τ.

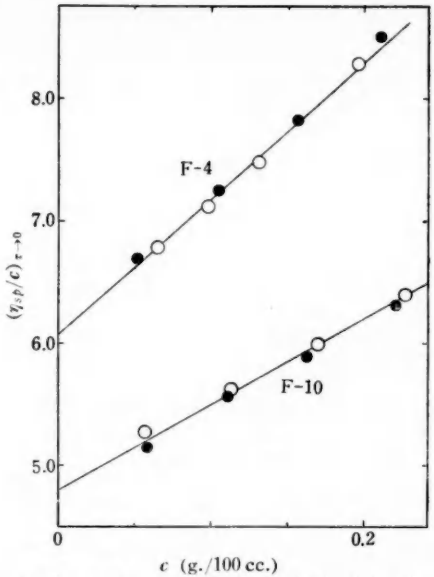

Fig. 6. η_{sp}/c vs. c relations obtained by the multi-bulb viscometer (○) and by the horizontal viscometer (●).

the conventional extrapolation such as shown in Figs. 4 and 5.

η_{sp}/c at zero pressures, calculated from $(t/t_0)_{P\to 0}$ as $((t/t_0)_{P\to 1}-1)/c$ for each fraction is shown in Fig. 6 as a function of c. η_{sp}/c vs. c plots at zero pressure for these fractions obtained by a horizontal viscometer and reported previously[3], are inserted in the same figure for comparison's sake. The general agreement is not perfect but may be considered satisfactory taking account of the independence of the two methods employed.

This author would like to express his hearty thanks to Prof. S. Murahashi and Prof. S. Akabori of this university and to Mr. E. Wada of the Scientific Research Institute for their kind encouragement throughout the course of this study. The financial asistance of Tekkósha Company is also gratefully acknowledged.

Department of Chemistry
Faculty of Science
Osaka University, Kita-ku, Osaka

Amino Acid Synthesis from Nitromalonic Ester. II[1]. *Synthesis of Proline and Glutamic-γ-semialdehyde*

By Tôru OKUDA

(Received December 7, 1956)

Akabori, Izumi and Okuda[1] have recently reported the synthetic preparations of DL-ornithine, starting from acrylonitrile and readily available diethyl nitromalonate (I) which has a reactive methine group. A new synthesis of DL-proline and the dimethyl acetal of glutamic-γ-semialdehyde (VI) which is biochemically interesting, but has been tedious for synthetic approach, from the same nitroester (I) and acrolein is described in this communication.

Since Albertson and Fillman[2] accomplished an excellent and practical work for the preparation of DL-proline, an amino acid that had been very difficult to synthesize, several similar or different methods[3-6] have appeared. Although inferior to their method in the yield, a simpler procedure to obtain this amino acid has been found. The addition reaction of diethyl nitromalonate (I) to acrolein proceeded very smoothly in the presence of basic catalyst such as triethylamine at lower temperature. The resulting γ,γ-dicarbethoxy-γ-nitrobutyraldehyde (II), of which the 2,4-dinitrophenylhydrazone had already been prepared by Yamada et al[7] from the crude product for the characterization, was distilled without any decomposition in an yield of 94%. γ-Aminobutyraldehyde and the related compounds are reported to react in the cyclized form under the usual conditions[8,9]. The possibility that in the γ-aminaldehydes ring formation may be substantially complete, was proved by Vogel and Davis[10] by the fact that crude glutamic-γ-semialdehyde or Δ^1-pyrroline-5-carboxylic acid prepared from γ,γ-dicarbethoxy-γ-acetamidobutyraldehyde was hydrogenated catalytically to proline.

Therefore, cyclization would be expected if γ-nitrobutyraldehyde (II) were reduced to the corresponding γ-amino compound. Accordingly, the catalytic hydrogenation of γ,γ-dicarbethoxy-γ-nitrobutyraldehyde (II) has been undertaken in glacial acetic acid containing an equimolecular amount of fused sodium acetate as condensing agent[11]. The possible intermediates, 5,5-dicarbethoxy-Δ^1-pyrroline and the ethyl ester of α-carbethoxyproline were not able to be isolated. On refluxing the hydrogenated product with hydrochloric acid and on the subsequent treatment with ammonium rhodanilate, DL-proline was obtained in an yield of 12–21%.

It is well-known that glutamic-γ-semialdehyde is a common intermediate in the enzymatic interconversions of glutamic acid, proline and ornithine. Several biochemical studies are currently underway on this compound in various laboratories, but the inaccessibility in a practical amount appears to restrict the use in experiments. The Vogel's method[10] to prepare the semialdehyde itself was re-investigated in laboratory scale, but appeared inadequate from the standpoint of preparation. Good and Mitchell[12] prepared the diethyl acetal of the glutamic-γ-semialdehyde with very poor yield by alkaliere hydrolisis of the diethyl acetal of γ,γ-dicarbethoxy-γ-acetamidobutyraldehyde and paper-chromatographic separation.

The method reported here affords a simple and practical synthesis of the dimethyl acetal of the semialdehyde (VI) through the following reaction diagram:

1) Paper I in this series, S. Akabori, Y. Izumi and T. Okuda, *J. Chem. Soc. Japan*, **77**, 490 (1956).
2) N. F. Albertson and J. L. Fillman, *J. Am. Chem. Soc.*, **71**, 2818 (1949).
3) P. E. Gagnon, J. L. Boivin and P. A. Boivin, *Can. J. Research*, **28B**, 207 (1950).
4) H. Plieninger, *Chem. Ber.*, **83**, 2710 (1950).
5) J. Caprová-Jirků, J. V. Koštir and M. Vondráček, *Chem. Listy*, **44**, 19 (1950).
6) R. Gaudry and L. Berlinquet, *Can. J. Research*, **28B**, 245 (1950).
7) S. Yamada, I. Chibata and T. Tsurui, *J. Pharm. Soc. Japan*, **73**, 123 (1953).
8) C. Schöpf and F. Oechler, *Ann.*, **523**, 1 (1936).
9) C. Schöpf and H. Steuer, ibid., **558**, 124 (1947).
10) H. J. Vogel and B. D. Davis, *J. Am. Chem. Soc.*, **74**, 109 (1952).
11) "Organic Reactions", Vol. IV, John Wiley & Sons, Inc. New York, N. Y. 1948, p. 201.
12) N. Good and H. K. Mitchell, *J. Am. Chem. Soc.*, **74**, 4953 (1952).
13) Ulpiani, *Gazz. chim. ital.*, **34**, 174 (1904).
14) D. I. Weisblat and D. A. Lyttle, *J. Am. Chem. Soc.*, **71**, 3078 (1949).

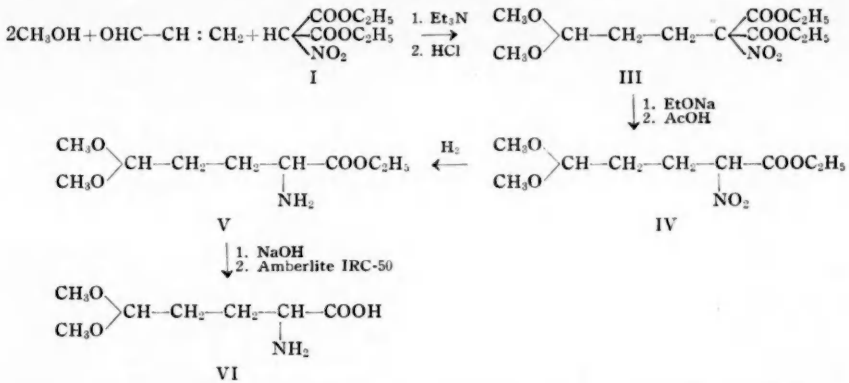

When the above-described addition of diethyl nitromalonate (I) to acrolein was carried out in methanolic solution and the reaction mixture was then directly treated with a small amount of dry hydrogen chloride, the acetal diester (III) was readily obtained in one step in fairly good yield. After the decarbethoxylation of III by the Ulpiani's method[13,14,15], the resulting acetal monoester (IV) was hydrogenated catalytically under pressure in methanol. The ester of the acetal amino acid (V) was readily purified by vacuum distillation with an yield of about 80%. On treatment of the amino acid ester (V) with aqueous sodium hydroxide and then with Amberlite IRC-50 exchange resin to remove sodium ions, the dimethyl acetal of glutamic-γ-semialdehyde (VI) was obtained as white crystals. Although the diethyl acetal of the semialdehyde was reported to be very soluble in ethanol[12], the dimethyl acetal was found to be less soluble like other common amino acids.

Experimental

γ,γ-Dicarbethoxy-γ-nitrobutyraldehyde (II).—In a three-necked flask fitted with a drying tube, a thermometer, a dropping funnel and a stirrer was placed a solution of 102.5 g. (0.50 mole) of diethyl nitromalonate (I) in 450 ml. of ethanol containing 0.2 ml. of triethylamine. A mixture of 29 g. (0.52 mole) of acrolein and 30 ml. of ethanol was added dropwise to this with vigorous stirring over the course of about one hour at such a rate that the temperature remained below 40°C. After additional stirring for two hours the solvent was removed in vacuo and the residual oil was distilled. One hundred twenty-three grams of γ, γ-dicarbethoxy-γ-nitro-butyraldehyde was obtained as yellowish oil, b. p. 134–137°C/1 mm.

Anal. Found: N, 5.31. Calcd. for $C_{10}H_{15}O_7N$: N, 5.36%.

2,4-Dinitrophenylhydrazone of the aldehyde (II) prepared by usual method melted at 74–76°C after recrystallization from methanol-water. (*lit.* 74–76°C[12])

Anal. Found: N, 15.75. Calcd. for $C_{16}H_{19}O_{10}N_5$: N, 15.87%.

DL-Proline.—In the pressure bottle of an apparatus for catalytic reduction were placed 26.1 g. (0.10 mole) of freshly distilled γ,γ-dicarbethoxy-γ-nitrobutyraldehyde (II), 9 g. of fused sodium acetate, 130 ml. of glacial acetic acid and 10 g. of Raney nickel. An initial pressure of 90 atm. of hydrogen was applied. When, after about twenty-four hours, 0.4 mole of hydrogen had been absorbed, the reaction was stopped and the catalyst was removed by filtration. After removing the acetic acid in vacuo, 50 ml. of concentrated hydrochloric acid was added to the syrupy residue and the mixture was cooled overnight in an ice box. Precipitated Sodium chloride was filtered off and the filtrate was refluxed for five hours. The dark solution was concentrated to a syrup under reduced pressure, then taken up in water and charcoaled. Then the pH of the solution was adjusted to 2.6–3.0 by adding aqueous sodium hydroxide and the solution was treated with methanolic solution of 25 g. of ammonium rhodanilate by the usual method. Recrystallization of the crude product from isopropyl alcohol-ether gave 2.5 g. of white crystals of DL-proline, m. p. 206° (dec.). Yield, 21%.

Anal. Found: N, 11.84. Calcd. for $C_5H_9O_2N$: N, 12.17%.

Ethyl δ,δ-Dimethoxy-α-carbethoxy-α-nitrovalerate (III, Dimethyl Acetal of γ,γ-Dicarbethoxy-γ-nitrobutyraldehyde).—102.5 g. (0.50 mole) of diethyl nitromalonate (I), 29 g. (0.52 mole) of acrolein and 360 ml. of methanol instead of ethanol were treated in the same manner as described above. About 3 g. of dry hydrogen chloride was dissolved in the mixture and then 70 g. of anhydrous sodium sulfate was added. After standing at room temperature for forty-eight hours, the reaction mixture was neutralized with aqueous sodium bicarbonate and concentrated under reduced pressure. The residue was then poured into about 1 l. of ice water, the aqeous phase was extracted three times with ether or isopropyl ether and the extracts were combined

with the oil. The combined ether solution was washed twice with water and dried over sodium sulfate in an ice box. After removal of the ether, the residue was distilled at 0.5 mm. and the fraction boiling between 145–150°C was collected as the product. The dimethyl acetal of γ,γ-dicarbethoxy-γ-nitrobutyraldehyde (III) thus obtained was yellowish and weighed 130 g. Yield, 84.6%.

Anal. Found: N, 4.62. Calcd. for $C_{12}H_{21}O_8N$: N, 4.56%.

Ethyl δ,δ-Dimethoxy-α-nitrovalerate (IV, Dimethyl Acetal of γ-Carbethoxy-γ-nitrobutyraldehyde).—Ethyl δ,δ-dimethoxy-α-carbethoxy-α-nitrovalerate (III), 42 g. (0.136 mole), in 400 ml. of anhydrous isopropyl ether was cooled in an ice-bath. A solution of 3.25 g. (0.141 mole) of sodium in 150 ml. of absolute alcohol was added slowly, with vigorous stirring, over a period of two hours. Precipitation of the sodium salt of IV and probably some sodium ethylate occured to form a very thick slurry. This was stirred further for five hours and allowed to stand overnight in an ice-box and then filtered. The salt was washed twice with 50 ml. portions of ether, transferred to a separatory funnel, together with the salt obtained from the mother liquor, covered with 200 ml. of isopropyl ether and acidified with 45ml. of 20% aqueous acetic acid. Vigorous shaking was continued until all the solid had disappeared. The ether layer was separated and the aqueous phase extracted with ether. The ether solutions were combined and washed with two 50 ml. of water. Drying, concentration and vacuum-distillation gave 30 g. (94%) of oily IV, which boiled at 118–123°C/2 mm.

Anal. Found: C, 45.94; H, 6.91; N, 5.86. Calcd. for $C_9H_{17}O_6N$: C, 45.95; H, 7.29; N, 5.96%.

Hydrolysis of the acetal group of IV and the subsequent treatment with 2,4-dinitrophenyl hydrazine gave yellow crystals that melt at 106–108°C. (*lit.* 110–111°C[15]).

Anal. Found: C, 41.93; H, 4.26; N, 18.91. Calcd. for $C_{13}H_{15}O_8N_5$: C, 42.28; H, 4.07; N, 18.97%.

Ethyl δ,δ-Dimethoxy-α-aminovalerate (V).—The reduction of 47 g. (0.2 mole) of IV was carried out in a stainless steel autoclave using 200 ml. of methanol and 4 g. of Raney nickel catalyst at 50–70°C for three hours. The autoclave was heated as rapidly as possible to avoid the formation of undesirable by-products. The catalyst was removed by filtration and the methanol was distilled off in vacuo. Thirty-three grams of V was obtained as colorless liquid by distillation; b. p. 105–107°C at 2 mm. Yield, 80.5%.

Anal. Found: C, 51.87; H, 9.23; N, 6.66. Calcd. for $C_9H_{19}O_4N$: C, 52.68; H, 9.27; N, 6.34%.

Dimethyl Acetal of Glutamic-γ-semialdehyde (VI).—Five grams of ethyl δ,δ-dimethoxy-α-aminovalerate (V) was dissolved in 10 ml. of 10% aq. sodium hydroxide solution and the mixture was heated at 60°C for about one hour. The aqueous solution of the sodium salt of the dimethyl acetal of glutamic-γ-semialdehyde was treated with Amberlite IRC-50 and then evaporated to dryness in vacuo. The crude product which melts at 206–209°C was dissolved in a small volume of warm water, and then charcoaled. Addition of ethanol and ether and cooling gave 2.5 g. of white crystals of VI melting at 215–217°C (dec.). This amino acid is very soluble in water, less soluble in ethanol and insoluble in ether and benzene.

Anal. Found: C, 47.08; H, 8.14; N, 7.78. Calcd. for $C_7H_{13}O_4N$: C, 47.46; H, 8.47; N, 7.91%.

15) O. A. Moe and D. T. Warner, *U. S. Patent.*, 2. 599, 653 (June 10, 1952).

Summary

1. A synthesis of DL-proline from diethyl nitromalonate and acrolein by intramolecular reductive alkylation is described.

2. A new method for preparation of the dimethyl acetal of glutamic-γ-semialdehyde from the same starting materials in an over-all yield of 38% (based on diethyl nitromalonate) is also presented.

The author wishes to thank Professor S. Akabori for his kind guidance and also to thank Messrs. Y. Izumi and S. Sakurai for their helpful advice.

Laboratory of Organic Chemistry
Faculty of Science
Osaka University, Kita-ku, Osaka

Polymorphism of Bis-β-hydroxyethyl Terephthalate

By Akihisa MIYAKE

(Received December 21, 1956)

In the course of a study of the infrared spectra of various derivatives of terephthalic acid, it was found that bis-β-hydroxyethyl terephthalate has several modifications. The crystal of bis-β-hydroxyethyl terephthalate prepared by the usual method, recrystallization from water or slow cooling of the melt, is obtained in the most stable form, which is called α-form in this paper. Besides this α-form, at least three other forms can be obtained by rapid cooling of the melt. These three modifications are tentatively called β-, γ- and δ-forms. The infrared spectra of these modifications are shown in Fig. 1, and the x-ray diffraction patterns in Fig. 2. There are some remarkable differences between the infrared spectra of these modifications; it seems that these differences offer some valuable information for the interpretation of the infrared spectrum of polyethylene terephthalate.

Method of Preparation

α-Form.—This form is the common one. Recrystallization from water generally gives this form. It is the most stable form and cannot be changed to any other form unless remelted.

β-Form.—Molten mixture of bis-β-hydroxyethyl terephthalate and ethylene glycol (ca. 1:1) kept at a temperature of ca. 100°C, is quenched dropwise on the surface of an ice-cooled metal plate. Removing ethylene glycol from the solidified drops at a temperature below ca. 20°C by means of filter papers or a porous plate, β-form is obtained. It is essentially important to maintain this at a low temperature; otherwise, the δ-form is obtained. This form changes to the α-form when washed with water or alcohol. It converts to in the δ-form at ca. 40°C, and to the α-form above ca. 45°C. These transition temperatures become lower as the atmospheric humidity becomes higher.

γ-Form.—This form is obtained by rapid cooling of the melt. Washing with water, it changes to the α-form. It also changes gradually above ca. 60°C, to the α-form.

δ-Form.—Molten mixture of bis-β-hydroxyethyl terephthalate and ethylene glycol is quenched dropwise. Ethylene glycol is removed from the solidified drops by filter papers, as in the case of β-form, at a temperature of 30°C to 40°C. Once formed, this form is rather stable; it does not change when washed with water, nor when kept at 100°C for an hour.

It was ascertained that all these modifications are chemically the same. The analytical values of C and H conform to the formula $C_6H_4(CO_2CH_2CH_2OH)_2$, and determination of the ethylene glycol content by periodic acid after saponification of each modification, also agrees with the above formula.

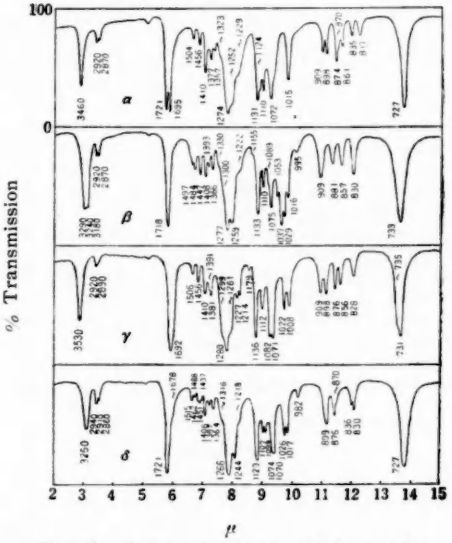

Fig. 1. Infrared spectra of four polymorphic forms.

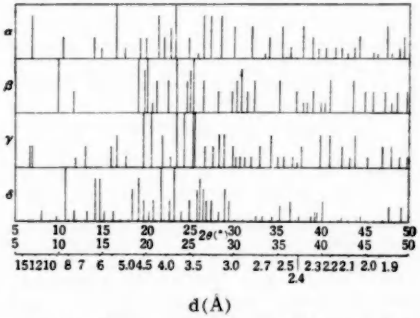

Fig. 2. X-ray diffraction patterns of four polymorphic forms.

Infrared and X-ray Measurements

The infrared spectra were obtained with a Perkin-Elmer Model 21 Spectrometer using NaCl prism. Samples were measured as nujol mulls except in the C—H frequency region. For this region, hexachlorobutadiene or low molecular weight polytrifluorochloroethylene oil was used as the mulling agent.

X-ray diffraction patterns were obtained with a Norelco Geiger counter x-ray diffractometer. Nickel filtered radiation from a copper target was used. In the case of the β-form which is easily transformed into the δ-form under the influence of atmospheric moisture, the specimen shield assembly was covered with cellophane and desiccated with phosphorous pentoxide.

Some Remarks on the Infrared Spectra

From the differences in the infrared spectra, it might be possible to obtain some information about the molecular form or the crystal structure of the four modifications. In this respect, there are at least three characteristic points. The first of these is the absorption band at 3500–3200 cm^{-1}. The position of this band shows that the O—H terminal groups are all hydrogen bonded in these modifications; however the type of hydrogen bond is different between each modification. The next point is the C=O band at 1720 cm^{-1} and 1695 cm^{-1}. The former shows the existence of free ester carbonyl groups, the latter hydrogen bonded carbonyl groups. Accordingly, β- and δ-form have only free ester groups, while γ-form has hydrogen bonded carbonyls, α-form has both of them in equal amount. The third point is concerned with the four absorption bands which appear at 910 to 850 cm^{-1}. The vibrations expected to appear in this region are the CH_2 rocking vibrations and certain vibrations of the benzene ring. For the determination of the latter, the comparison with the spectra of other terephthalic acid esters is useful. In Fig. 3, three such esters are given; comparing these spectra with that of bis-β-hydroxyethyl terephthalate, it becomes apparent that there exists only one band 875 cm^{-1} which seems to be a benzene ring vibration, so long as it is assumed that the benzene ring vibrations have almost constant frequencies in such series. Thus the absorption bands chosen in Table I can be assigned to the CH_2 rocking vibrations.

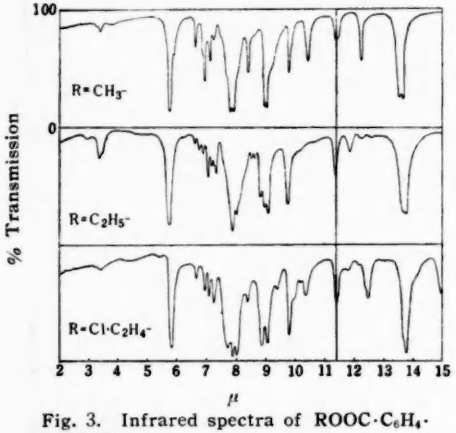

Fig. 3. Infrared spectra of ROOC·C_6H_4·COOR.

TABLE I

FREQUENCIES OF THE CH_2 ROCKING VIBRATION (cm^{-1})

α	909	898	~870	861
β	909			857
γ	909	898	876	856
δ		899	~870	

The absorption band 876 cm^{-1} of the γ-form is assumed to be composed of two components, benzene ring vibration and CH_2 rocking vibration. The frequencies given in Table I consist of two pairs, (909, ~857) and (899, ~870). β-Form has only the former pair, δ-form only the latter, while α-and γ-form have both.

Nakagawa[1] has shown that CH_2 rocking frequencies in a molecule of the type X—CH_2—CH_2—X depends profoundly on the angle of internal rotation, and their values decrease in the following order: B_g (*trans*) > A (*gauche*) > B (*gauche*) > A_u (*trans*). In the light of this conception, the former pair (909, ~857) can be considered as the CH_2 rocking frequencies arising from *trans* configuration of the O—CH_2CH_2—O group. The latter pair (899, ~870) represents the existence of *gauche* configuration. Thus, the configuration of the O—CH_2CH_2—O group in β-form is *trans*, in δ-form *gauche*, in α- and γ-form both *trans* and *gauche*.

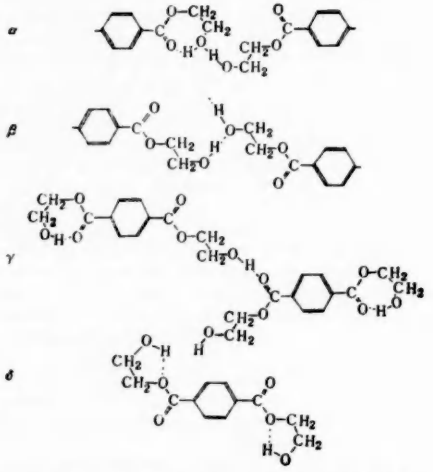

Fig. 4. Structures of four polymorphic forms.

1) I. Nakagawa, *J. Chem. Soc. Japan* (*Pure Chem. Sect.*), **76**, 813 (1955).

It might be too speculative to derive structural conceptions from only the arguments made above; the four modifications may be considered to have the structures something like those shown in Fig. 4 at the present time.

Summary

It is found that bis-β-hydroxyethyl terephthalate shows polymorphism, and there exist at least four different modifications. From the infrared spectra of these modifications, differences between the molecular forms are elucidated to some extent. These differences occur mainly from the difference in configuration of the side chain attached to the benzene ring.

The author wishes to express his sincere thanks to Dr. K. Hoshino and Mr. Y. Numata for their encouragement and support which made the present work possible. Thanks are also due to Mr. Y. Kinoshita for the measurement of the x-ray diffraction pattern and for many discussions. The author also wishes to thank Mr. S. Tanaka for his assistance with the infrared measurements.

Research Department, Toyo Rayon Co. Ltd., Otsu, Shiga

Sorption of Monobasic Dye-acid by Nylon-6 Fibre

By Minoru NISHIO

(Received December 27, 1956)

Introduction

Much quantitative information has been published in regard to the mechanism accounting for the uptake of acid dyes by the polyamide fibres (wool, nylon-66). It is generally agreed that the dye molecule is held by means of a salt-type linkage between the sulphonic acid groups of the dye and the basic amine ends of the fibre in stoichiometric amounts, and that the process of formation of these linkages constitutes much of the driving force for the penetration of dyes into the fibre[1-5].

The pH isotherms obtained by dyeing nylon-6(polycapramide) fibre from baths of varying pH containing a large amount of dye salt have been described in the previous paper[6] and it was found that at moderate pH levels, adsorption was in close agreement with available end groupings. Moreover, additional evidence has been presented for this conclusion by determining the saturation adsorption of the typical monobasic acid dye onto hydrolysed nylon-6 samples which had various amounts of free amino-groups.

The objectives of the present investigation were to elucidate the mechanism of the combination of monobasic dye-acid with nylon-6 fibre under normal dyeing conditions and to calculate the magnitude of the forces involved.

Experimental

Materials.—The nylon-6 sample employed for dyeing was 3 denier semidull staple fibre which had an end amino-group analysis of 0.043 milli-equivalent per g. of fibre by DNFB method*[6-9]. Before use, the fibres were scoured at 60°C for 20 min. in a bath containing 5 g. soap per l. and then thoroughly rinsed and dried. Distilled water was used throughout.

Dye Purification.—The dyes used were the free acids of Orange II (β-naphthol-azo-p-benzene sulphonic acid, sodium salt, Colour Index No. 151) and Metanil Yellow YK (diphenyl-azo-m-benzene sulphonic acid, sodium salt, Colour Index No. 138).

Two dyes were first isolated as sodium salts free from inorganic electrolytes by the method

1) E. Elöd and T. Schachowsky, *Melliand Textilber.*, **23**, 437 (1942), ibid., **25**, 237 (1914).
2) R. H. Peters, *J. Soc. Dyers and Colourists*, **61**, 95 (1945).
3) P. W. Carlene, A. S. Fern and T. Vickerstaff, ibid., **63**, 388 (1947).
4) F. C. McGrew and A. K. Schneider, *J. Am. Chem. Soc.*, **72**, 2547 (1950).
5) W. R. Remington and E. K. Gladding, ibid., **72**, 2553 (1950).
6) M. Yoshida, and M. Nishio, Scientific Reports of Toyo Rayon Co. **9**, 85 (1954) (in Japanese).

* This is a simple method which is carried out chemically with the aid of dinitrofluorobenzene for the precise determination of the primary amine content of the polyamide.

7) F. Sanger, *Biochem. J.*, **39**, 507 (1945).
8) J. H. Bows and J. A. Moss, ibid., **55**, 735 (1953).
9) H. Zahn and P. Rathgeber, *Melliand Textilber.*, **34**, 239 (1953).

of Robinson and Mills[10] which involved three or fourfold salting out with sodium acetate followed by repeated extraction with ethyl alcohol until an aqueous solution containing a known amount of dye salt gave a constant optical density as shown in Fig. 1 (Orange II).

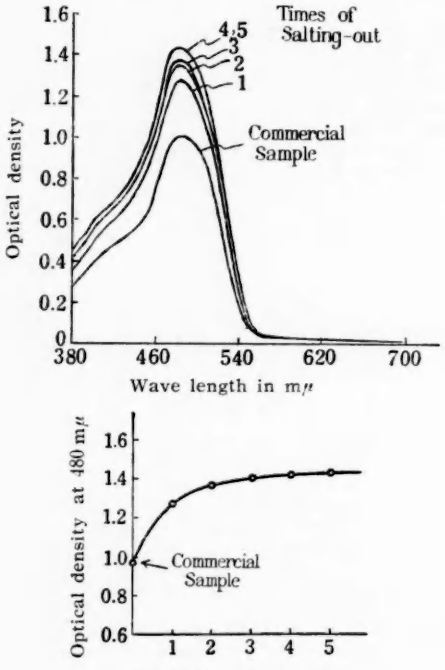

Fig. 1. Variation of absorption spectrum and optical density at 480 mμ of dye solution with time of salting-out. (Orange II, 50 mg./l.).

The free acid of Orange II was then precipitated from the concentrated solution of sodium salt of dye obtained above by means of concentrated hydrochloric acid, filtered off, washed with dilute hydrochloric acid, and finally dried in vacuo over caustic soda flakes until free from chloride ions.

In the case of Metanil Yellow YK, ion exchange resin was employed to obtain electrolyte-free dye-acid. Two % aqueous solution of the above-obtained dye-salt was allowed to run through a column of Amberlite IR-120 (strongly acidic ion exchange resin of Rohm & Hass Co.) previously washed with water and methanol and then activated by treatment with 10% hydrochloric acid.

The pure dye-acid, isolated from the effluent on evaporation and washed with water to remove any inorganic acid, was obtained as bright black sparingly soluble needles.

The ash content of both samples were almost nil and analytical values according to titanous chloride method indicated high purity of at least 98 %. They were dried to constant weight at 105°C before use.

Procedure.—One gram samples of nylon-6 fibre were dyed in a 200 : 1 liquor ratio at 60° (±0.1°)C for a period of 3 to 6 days (i. e. to equilibrium) in the absence of any acids. The acidity was adjusted by varying concentrations of the dye-acid and the pH values reported were those at the end of the dyeing, at room temperature. Glass electrode pH meter was used for pH determination. After dyeing the dyed sample was removed from the dye liquor, rinsed rapidly with a minimum quantity of distilled water and then air-dried.

TABLE I
ADSORPTION OF FREE DYE-ACIDS BY NYLON-6 FIBRE AT 60°C

Dye in Solution (m.eq./l.)	Final pH of Dye-bath	Dye in Fibre (m.eq./g.)	θ_D	$-\Delta\mu°_{HD}$ (kcal./mole)
Orange II				
4.16	2.85	0.083	—	—
1.17	3.15	0.068	—	—
0.77	3.38	0.060	—	—
0.49	3.65	0.055	—	—
0.22	5.53	0.048	0.89	16.9
0.12	5.72	0.037	0.69	15.8
0.060	5.83	0.029	0.54	16.0
0.031	5.72	0.024	0.45	15.4
0.024	5.69	0.014	0.26	14.6
0.002	5.69	0.007	0.13	15.2
	$[S]_F=0.054$		Average:	15.7
Metanil Yellow YK				
0.782	2.05	0.117	—	—
0.597	3.02	0.104	—	—
0.597	3.08	0.104	—	—
0.441	3.12	0.102	—	—
0.229	3.30	0.101	—	—
0.229	3.31	0.097	—	—
0.444	3.34	0.093	—	—
0.229	3.56	0.092	—	—
0.441	3.10	0.091	—	—
0.229	3.59	0.090	—	—
0.229	3.28	0.088	—	—
0.206	3.20	0.087	—	—
0.449	3.87	0.083	—	—
0.096	3.20	0.072	—	—
0.081	3.58	0.071	—	—
0.115	4.93	0.062	—	—
0.022	5.97	0.059	—	—
0.049	4.75	0.049	0.94	17.6
0.048	6.07	0.049	0.94	17.5
0.017	6.07	0.043	0.83	18.8
0.011	6.07	0.038	0.73	18.3
0.003	5.90	0.028	0.54	17.8
0.002	5.65	0.020	0.38	16.4
~0	6.07	0.015	—	—
~0	6.50	0.010	—	—
	$[S]_F=0.052$		Average:	17.8

10) C. Robinson and H. A. T. Mills. *Proc. Roy. Soc. (London)*, **A131**, 576, 596 (1931).

Measurements of dye adsorbed on nylon-6 were made by dissolving the dyed fibre in 80% formic acid and determining the quantity of dye in solution by means of the photoelectric spectrophotometer (Beckman type) on the basis of the application of Beer's law.

Concentrations of dye-acid in aqueous bath were likewise measured spectrophotometrically.

Results and Discussion

Isotherms were determined for varying concentration of the free dye-acids.

The results obtained are given in Table I, illustrated by Fig. 2.

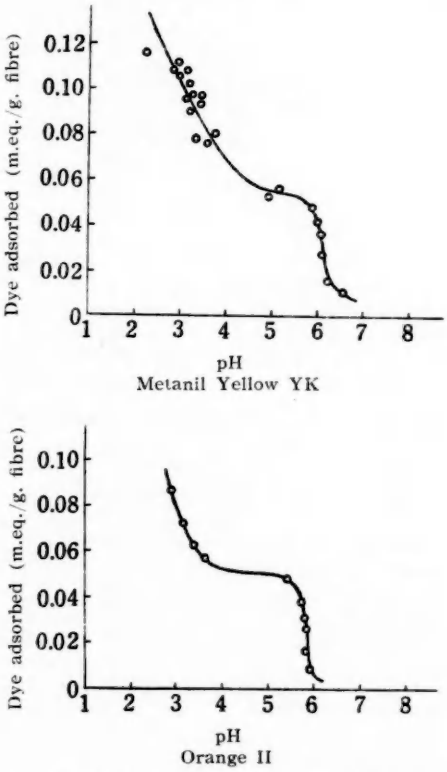

Fig. 2. Adsorption of monobasic free dye-acids on nylon-6 fibre at 60°C.

The amount of dye adsorbed at equilibrium has been plotted against the final pH of the dyebath. The curves are similar to those in the case of sodium salt of dye which was reported in the previous paper[6], being sigmoid in shape and reaching a fairly constant value (about 0.05 milliequivalent of dye-acid per g. of fibre) corresponding to saturation of the end amino-groups. Such correspondence has been found to exist generally for acid dyes[1-6].

As the pH is further decreased, there is another sharp increase in the uptake which corresponds to adsorption of the dye onto weakly basic amide-groups of the polymer chain (amide-dyeing) and new primary amine groups liberated by the occurrence of dye-catalysed hydrolysis. Such a phenomenon has been observed in the case of acid dyes and referred to as "overdyeing"[11,12].

The uptake of monobasic dye-acid by nylon may be represented schematically as

$$-OOC-N_y - NH_3^+ + H^+ + D^- \longrightarrow HOOC-N_y-NH_3^+ \cdot D^-$$

where Ny is the polyamide chain separating the end amino and carboxyl groups and D^- is a dye anion. On immersion of the fibre in a dyebath containing free dye-acid, hydrogen ions are first adsorbed onto carboxyl groups and the more slowly diffusing dye anion is then able to attach itself to the positively charged amino-groups. This mechanism is now accepted as accounting for the adsorption of acid dyes by nylon.

Gilbert and Rideal[13,14] first proposed a method of analysis of the adsorption forces of acids and acid dyes on wool, which has been extended to the case with free dye-acids by Lemin and Vickerstaff[15] and later applied to nylon-66 by American workers[1,5], by the use of the equation

$$-\frac{0.434}{RT}(\Delta\mu^\circ_H+\Delta\mu^\circ_D) = 2\log\left(\frac{\theta_D}{1-\theta_D}\right)-\log[D]s+pH \qquad (1)$$

in which [D]s represents the molar concentration of the free dye-acid in solution and θ_D the fraction of the available basic sites of the fibre which are occupied by dye anion. The notations $\Delta\mu^\circ_H$ and $\Delta\mu^\circ_D$ represent the standard changes in chemical potential (partial molal free energy) for the hydrogen ion and for the monobasic dye anion involved in the sorption of the ions from the solution by the fibre, and the negative of their sum represents the

11) C. D. O'Briain and R. H. Peters, *J. Soc. Dyers and Colourists*, **69**, 435, (1950).
12) E. Atherton, D. A. Downey and R. H. Peters, *Text. Res. J.*, **25**, 977 (1955).
13) G. A. Gilbert and E. K. Rideal, *Proc. Roy. Soc.*, **A182**, 335 (1944).
14) G. A. Gilbert, ibid., **A183**, 167 (1944).
15) D. R. Lemin and T. Vickerstaff, *J. Soc. Dyers and Colourists*, **63**, 405 (1947).

standard affinity of the acid form of the dye for the fibre ($\Delta\mu^\circ_{HD}$).

This quantity gives a measure of the tendency of the dye acid to move from its standard state in solution to its standard state on the fibre. On this basis calculations were carried out by use of equation (1) and the affinity values obtained are given in the last column of Table I.

In order to evaluate θ_D, the fractional saturation of the fibre sites, it is necessary to determine the saturation value $[S]_F$ which is the concentration of dye in the fibre when all the available sites, end amino-groups, are occupied.

Equation (1) may be converted into the form—

$$-\frac{0.434}{RT}\Delta\mu^\circ_{HD} = \log\left(\frac{\theta_D}{1-\theta_D}\right)^2 \cdot \frac{1}{[H]_S \cdot [D]_S} \qquad (2)$$

where, $pH = \log 1/[H]_S$

$\theta_D = [D]_F/[S]_F$

Removing logarithms,

$$\left[\frac{\theta_D}{1-\theta_D}\right]^2 = \left(\frac{[D]_F}{[S]_F - [D]_F}\right)^2 = K[H]_S \cdot [D]_S \qquad (3)$$

Where K is a constant, $[D]_F$ and $[H]_S$ refer to the concentrations of dye in the fibre and hydrogen ions in solution respectively. Inverting both sides of the equation, and dividing by $[S]_F$,

$$\frac{1}{[D]_F} - \frac{1}{[S]_F} = \frac{1}{\sqrt{K}} \cdot \frac{1}{[S]_F} \cdot \frac{1}{[H]_S \cdot [D]_S} \qquad (4)$$

A plot of the reciprocal of $[D]_F$ against the reciprocal of the mean molarity of the dye-acid in solution, $\sqrt{[H]_S \cdot [D]_S}$, should yield a straight line as is shown in Fig. 3, the intercept of which on "$1/[D]_F$" axis gives the reciprocal of the saturation value $[S]_F$. The values obtained by extrapolation in this way are 0.054 milliequivalent per g. of nylon-6 fibre for Orange II free acid and 0.052 for Metanil Yellow YK free acid, which were used for calculation of dye affinity.

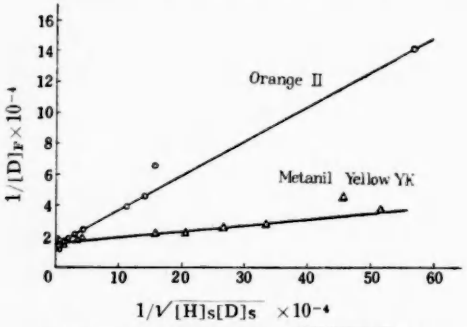

Fig. 3. $1/[D]_F$ against $1/\sqrt{[H]_S[D]_S}$ plot for adsorption of monobasic dye-acid by nylon-6 fibre at 60°C.

Assuming the affinity of hydrogen ion for nylon at 80°C to be −11.9 kg. cal.[16] and the heat of reaction to be negligible as temperature appears to have little effect on adsorption of hydrochloric acid by wool[15] anion affinities have been calculated for two monobasic dyes, with the results shown in the last column of Table II.

TABLE II

AFFINITY OF MONOBASIC DYE ANIONS FOR NYLON-6 FIBRE AT 60°C

Dye-Acid	(Affinity kcal./mole)		
	$\Delta\mu^\circ_{HD}$	$\Delta\mu^\circ_H$	$\Delta\mu^\circ_D$
Orange II	−15.7	−11.9	−3.8
Metanil Yellow YK	−17.8		−5.9

The value for Metanil Yellow YK anion is in good agreement with values for nylon-66 obtained by McGrew and Schneider of −6.1 and −5.9[4], by Remington and Gladding of −6.1 kcal./mole[5,16], being somewhat higher than the affinity value of this dye anion for wool of −5.0 ~ −5.3 kcal./mole[15]. The affinity of acid dye is generally known to be higher for nylon than for wool.

With Orange II, McGrew and Schneider also determined the affinity for nylon-66 of −3.3~−3.9 kcal./mole by adsorption of the sodium salt of the dye from neutral solution in presence of salt at 98°C.

Judging from these results it seems to be possible to conclude that the affinities of two monobasic dye anions are approximately the same on two fibres, nylon-66 and nylon 6.

Thus, the fundamental energetics of dyeing process and the mode of dye attachment are the same on these two fibres and some slight differences in dyeing behavior—for instance, the rate of dyeing and levelness etc. as is often said—must be accounted for by purely physical differences due to the production process of the fibre. Under practical dyeing conditions, however, it is evident that the amine content is of course the controlling factor for building acid dyes upon nylon.

16) T. Vickerstaff, "The Physical Chemistry of Dyeing", 2nd edition, Oliver and Boyd, London (1954), p. 471.

Finally, the adsorption isotherms already determined give straight lines, when $[D]_S/[D]_F$ is plotted against $[D]_S$ according to the Langmuir's equation:

$$[D]_F = \frac{a[D]_S}{1+b[D]_S} \quad (5)$$

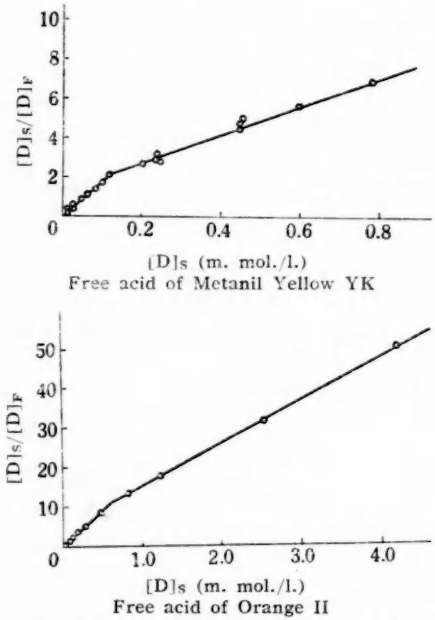

Fig. 4. $[D]_S/[D]_F$ against $[D]_S$ plot for adsorption of monobasic dye-acid by nylon-6 fibre at 60°C.

The curves of Fig. 4 consist really of two straight lines with an abrupt change of slope. It therefore appears that the type of site on which dye is adsorbed is different between these two portions. The line at higher concentration has already been discussed and can mainly be attributed to the adsorption of dye on weakly basic amide-groups of the polymer chain. The line of different slope at lower concentration must refer to the primary adsorption of dye on terminal amino-groupings which should also obey the Langmuir adsorption isotherms.

The point at which this change takes place corresponds to $[D]_F$ value of 0.054 m. eq. dye per g. of fibre for Orange II and 0.052 for Metanil Yellow YK which are in good agreement with the values obtained by extrapolation illustrated in Fig. 3 and also close to the number of free amino end groupings (0.043 m. eq./g. fibre) determined by DNFB method. The difference might be due to the substantivity of these dye-acids for nylon or attributed to the fact that overdyeing occurs to a slight extent even at moderate pH levels.

Summary

The equilibrium uptake of two typical monobasic dye-acids by nylon-6 (polycapramide) fibre has been measured for varying concentrations and additional evidence was given to confirm the mechanism of dye attachment to nylon as consisting of (1) combination with basic amine ends at normal dye bath pH and (2) combination mainly with the weakly basic nonterminal amide groups of the polymer chain at lower pH values. The Langmuir equation can well be applied to both regions of adsorption.

It is well known that the thermodynamic affinity of a dye for the fibre represents a fundamental characteristics of the dyeing process. The anion affinities of dye-acids for nylon-6, calculated from data on the equilibrium distribution of dye-acid between bath and fibre in terms of the change in standard chemical potential of the dye sorption process using the equation for wool developed by Gilbert and Rideal, were in good agreement with values for nylon-66 obtained by other workers.

Thus, the fundamental energetics of dyeing process and the mode of dye attachment are the same on these two fibres and some slight differences in dyeing behaviour must arise solely from differences in their physical structure due to the production process.

The author wishes to express his sincere thanks to Dr. K. Hoshino and Mr. M. Yoshida for their kind encouragement and for permission to publish this paper.

Research Department
Toyo Rayon Co. Ltd.
Otsu, Shiga

Hydrogen Bonding Effect on the Fluorescence of Some Nitrogen Heterocycles. I

By Noboru MATAGA and Shizuyo TSUNO

(Received December 19, 1956)

1. Introduction

It is well known that whereas the aromatic hydrocarbons such as benzene, naphthalene and anthracene fluoresce fairy well or strongly in the near ultraviolet or visible spectral region, the corresponding aza-derivatives such as pyridine, quinoline and acridine are completely non-fluorescent or emit very weakly in spite of their comparable or stronger absorption intensity compared with aromatic hydrocarbons. Some interpretations have been made for these behaviors of nitrogen heterocycles; for example according to Bowen[1], this effect has been ascribed to the increase in spin-orbital interaction by a nitrogen atom, while Förster[2], has interpreted this phenomenon in the case of pyridine as due to the predissociation of CN bond, though he has made no interpretation on the very weak fluorescence of acridine or quinoline. We will propose another interpretation, perhaps more plausible, for the phenomenon in question, on the basis of the solvent effects upon the absorption spectra and fluorescence yields of these nitrogen heterocycles. One of the present authors has previously reported[3] that, although quinoline and acridine are almost non-fluorescent in non-polar solvent such as hexane and benzene, they fluoresce fairy well in alcohols which are capable of making hydrogen bond with nitrogen atoms of these heterocycles. Moreover, the fluorescence yield has been found greatly enhanced in quinolinium and acridinium ion in the aqueous solution. He has suggested, from these facts, that the non-bonding electron pair on a nitrogen atom may play an important role in the inner quenching of fluorescence in these molecules. To elucidate the problem further, we have measured the absorption spectra and relative fluorescence yields of these molecules hydrogen bonded with various proton donors in non-polar solvent. The results obtained clearly show the parallel relation between relative fluorescence yield and proton donating power, i. e., the greater the proton donating power, the larger the increase in relative fluorescence yield. Moreover, we have found an interesting fact that the difference in the emitting π-electronic state leads to the different behavior of these nitrogen heterocycles in fluorescence quenching by a halogen atom.

The object of the present paper is to report these facts with some discussions on the role of the interaction between n- and π-electrons, and also the character of emitting π-electronic state in the fluorescence of these molecules.

2. Experimental

Apparatus: Absorption spectra were measured with a Beckman spectrophotometer model DU. The fluorometer was the same as described previously[4]. The fluorescence spectra were photographed with a Hilger E_2 type quartz spectrograph or a small type glass prism spectrograph, using a high-pressure mercury lamp with appropriate filters[3] as an exciting light source.

Reagents: Quinoline and acridine were the same samples as reported previously[3]. Chemical pure grade *n*-hexane was shaken with fuming sulfuric acid diluted with conc. sulfuric acid and distilled carefully. Extra pure grade benzene was dried over metallic sodium and distilled before use. Carbon tetrachloride and chloroform were shaken with conc. solfuric acid, washed with water, and after being dried over phosphorus pentoxide, distilled carefully. Ethanol was refluxed with silver nitrate to remove aldehyde, and after refluxing with calcium oxide, distilled carefully. Commercial β-phenylethylalcohol was fractionally distilled. Benzylalcohol was dried over potassium carbonate, and distilled under an atmosphere of dry nitrogen. Chemical pure grade mono- and trichloracetic acid were recrystallized several times from benzene, then stored over concentrated sulfuric acid in a vacuum

1) E. J. Bowen and F. Wokes, "Fluorescence of Solutions", Longmans (1953), p. 26.
2) Th. Förster, "Fluoreszenz Organischer Verbindungen", Vandenhoech and Ruprecht (1951), p. 118.
3) N. Mataga, Y. Kaifu and M. Koizumi, This Bulletin, **29**, 373 (1956).
4) N. Mataga, Y. Kaifu and M. Koizumi, ibid., **29**, 115 (1956).

desiccator. Dichloracetic acid was fractionally distilled under a pressure of 17 mm.

3. Experimental Results

A. Remarks on the Electronic Spectra of Nitrogen Heterocycles. — The π-electronic spectra of nitrogen heterocycles such as pyridine, quinoline and acridine are very similar to those of isoelectronic aromatic hydrocarbons such as benzene, naphthalene and anthracene, and their excitation energies are almost the same. A systematization of this correspondence between nitrogen heterocycles and aromatic hydrocarbons was made by Zanker[5] using Platt's perimeter model[6]. According to Platt's notation, the lowest excited singlet state ($\pi \rightarrow \pi^*$) is ^1L_b in pyridine and quinoline, and ^1L_a in acridine, and these are regarded as the emitting state of fluorescence, respectively. The second excited singlet state is ^1L_a in pyridine and quinoline, and ^1L_b in acridine.

B. Change in Absorption Spectrum by Hydrogen Bonding. — When various proton donors are added to the solutions of quinoline and acridine in non-polar solvent, the absorption spectra show characteristic changes due to the hydrogen bonding equilibrium. In both quinoline and acridine, hydrogen bonding strengthens the ^1L_b band somewhat, its wave length being not altered, but induces the red shift of ^1L_a band. The stronger the donating power, the larger the degree of the increase of absorption intensity of ^1L_b band and the red shift of ^1L_a band. In the case of the acid-base interaction in which trichloracetic acid was used as proton donor, the degree of the change of absorption spectrum is very close to the case of quinolinium or acridinium ion in the aqueous solution, but slightly less prominent.

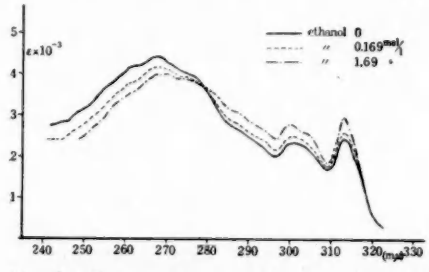

Fig. 1. Change in absorption spectrum of quinoline in *n*-hexane with addition of ethanol.
Concentration of quinoline $\sim 10^{-4}$ mol./l.

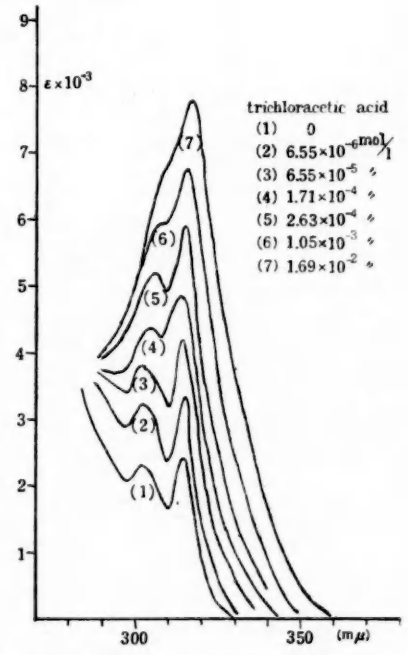

Fig. 2. Change in absorption spectrum of quinoline in benzene with addition of trichloracetic acid.
Concentration of quinoline $\sim 10^{-4}$ mol./l.

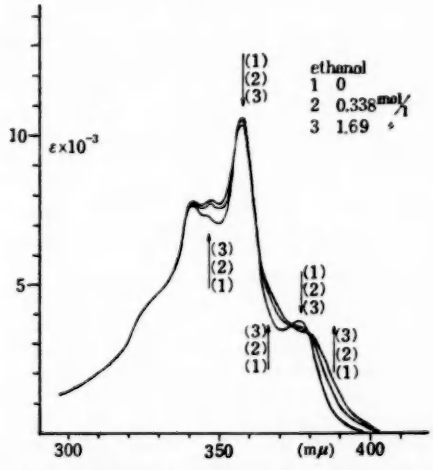

Fig. 3. Change in absorption spectrum of acridine in benzene with addition of ethanol.
Concentration of acridine: 5×10^{-5} mol./l.

5) V. Zanker, *Z. Physikal. Chem.*, N. F., **2**, 52 (1954). see also Ref. 3).
6) J. R. Platt, *J. Chem. Phys.*, **17**, 484 (1949). H. B. Klevens and J. R. Platt, ibid., **17**, 470 (1949).

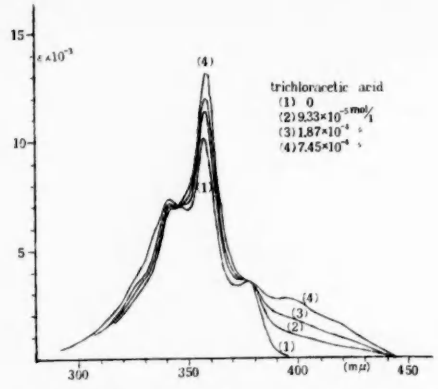

Fig. 4. Change in absorption spectrum of acridine in benzene with addition of trichloracetic acid.
Concentration of acridine: 5×10^{-5} mol./l.

Some examples of these spectral changes caused by hydrogen bonding are shown in Figs. 1—4.

These spectral changes caused by the perturbation of π-electronic states by hydrogen bonding, seem to correspond definitely to the above-mentioned Zanker's assignment. The same correspondence seems to hold also in pyridine[5,7]. From these spectral changes we can obtain the equilibrium constant of hydrogen bond formation in the ground state.

C. Method of Evaluation of Equilibrium Constant from Absorption Spectra. —The optical density at a definite wave length, d, is expressed as follows, using molar extinction coefficients of a free molecule A and a hydrogen bonded one AD, ε_a and ε_c:

$$d=\varepsilon_a[A]+\varepsilon_c[AD]=\varepsilon_a[A]+\varepsilon K[A][D]$$

The optical density of the solution without donor is:

$$d_0=\varepsilon_a[A]_0=\varepsilon_a[A](1+K[D]),$$

where $[A]_0$ is the analytical concentration of A.

From these equations we obtain:

$$\frac{1-(d_0/d)}{[D]}=-K+\left(\frac{\varepsilon_c}{\varepsilon_a}\right)K\left(\frac{d_0}{d}\right) \qquad (1)$$

For moderately weak donors, we can approximately replace [D] by $[D]_0$, the analytical concentration of D.

For a strong donor such as trichloracetic acid, however, we cannot use such an approximate method.

Instead, we put as follows:

$$K=\frac{[AD]}{([D]_0-[AD])([A]_0-[AD])},$$

$$[A]_0(\varepsilon-\varepsilon_a)=[AD](\varepsilon_c-\varepsilon_a),$$

$$[AD]=\frac{[A]_0(\varepsilon-\varepsilon_a)}{(\varepsilon_c-\varepsilon_a)}$$

where ε is the apparent molar extinction coefficient. Hence,

$$K=\frac{(\varepsilon-\varepsilon_a)(\varepsilon_c-\varepsilon_a)}{[D]_0(\varepsilon_c-\varepsilon_a)(\varepsilon_c-\varepsilon)-[A]_0(\varepsilon-\varepsilon_a)(\varepsilon_c-\varepsilon)}.$$

When $\varepsilon_a=0$ at the wave length used for the calculation,

$$[D]_0\left(\frac{\varepsilon_c}{\varepsilon}-1\right)=\frac{1}{K}+[A]_0\left(1-\frac{\varepsilon}{\varepsilon_c}\right) \qquad (2)$$

By means of Tsubomura's method[8], we can obtain [AD], and from $[A]_0\varepsilon=[AD]\varepsilon_c$,

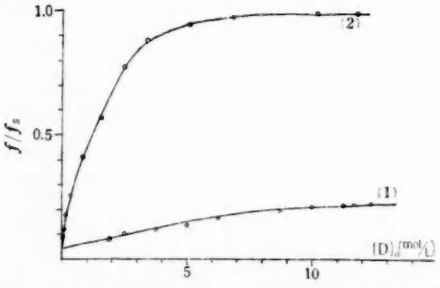

Fig. 5. Change in fluorescence intensity of acridine in benzene with addition of chloroform and ethanol.
Concentration of acridine: 5×10^{-5} mol./l.
(1) chloroform, (2) ethanol.
f_s: fluorescence intensity of ethanol solution used as standard.

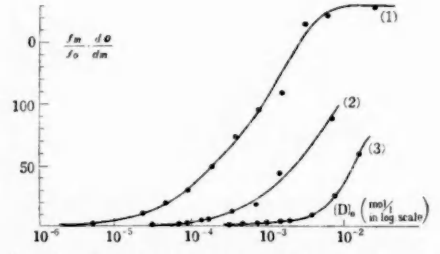

Fig. 6. Change in fluorescence intensity of acridine in benzene with addition of chloracetic acids.
Concentration of acridine: 5×10^{-5} mol./l.
(1) trichloracetic acid
(2) dichloracetic acid
(3) monochloracetic acid

7) L. W. Pickett, et al., *J. Am. Chem. Soc.*, **75**, 1618 (1953).

8) H. Tsubomura, *J. Chem. Phys.*, **23**, 2130 (1955).

ε_c is evaluated. Then, K can be evaluated from (2).

D. Change in Fluorescence Intensity and Its Interpretation on the Basis of Hydrogen Bonding Equilibrium. — In all the cases of hydrogen bonding, the fluorescence intensity is increased. Moreover, the stronger the donating power, the greater the increase in fluorescence intensity. Some examples of those changes in fluorescence intensities are shown in Figs. 5 and 6.

Now it is almost certain that the observed changes in fluorescence intensity may be attributed to the fact that the free and hydrogen bonded heterocycles have different efficiency of fluorescence and that the concentration of these molecular species are determined by the association equilibrium. Hence the experimental results will be analyzed as follows.

(i) When the equilibrium of the ground state is maintained during the course of fluorescence, the fluorescence intensity f_m with addition of D is:

$$f_m = \frac{(\varepsilon_a \Phi_a + \varepsilon_c \Phi_c K[\mathrm{D}])}{1+K[\mathrm{D}]} [\mathrm{A}]_0 I_0 \qquad (3)$$

where ε_a and ε_c are the molar extinction coefficient of A and AD at the wave length of the exciting light, respectively. I_0 is the intensity of the exciting light, and, Φ_a and Φ_c are the quantum yields of fluorescence of A and AD, respectively. It is to be noted that (3) is derived on the condition that the absorption of each molecular species is proportional to its concentration, which approximately holds in the present experiment.

From (3) we derive,

$$\frac{1-(f_0/f_m)}{[D]} = -K + \alpha\left(\frac{\varepsilon_c}{\varepsilon_a}\right)K\left(\frac{f_0}{f_m}\right) \qquad (4)$$

where f_0 is the fluorescence intensity of the solution without D, and $\alpha = \Phi_c/\Phi_a$.

When $\Phi_a \simeq 0$,

$$\frac{1}{f_m} = \mathrm{Const.}\left(1+\frac{1}{K}\frac{1}{[\mathrm{D}]}\right) \qquad (5)$$

(ii) In contradistinction to (i), when an equilibrium in the excited state is different from that of the ground state and the state of association approaches a new equilibrium state during the lifetime of the excited molecule, until a new equilibrium state is almost completely reached prior to the emission, we should use euqation (6) instead of (3):

$$f_m = \frac{(\Phi_a + K'\Phi_c[\mathrm{D}])}{1+K'[\mathrm{D}]} d_m I_0 \qquad (6)$$

$$d_m = \frac{(\varepsilon_a + \varepsilon_c K[\mathrm{D}])[\mathrm{A}]_0}{1+K[\mathrm{D}]}$$

where K' is the equilibrium constant in the excited state. From equation (6) we can easily derive (7) and (8), which correspond to (4) and (5), respectively.

$$\frac{1-(f_0/f_m)(d_m/d_0)}{[\mathrm{D}]} = -K' + \alpha(d_m/d_0)K'(f_0/f_m) \qquad (7)$$

$$d_0 = \varepsilon_a[\mathrm{A}]_0, \quad d_m/f_m = \mathrm{Const.}\left(1+\frac{1}{K'}\frac{1}{[\mathrm{D}]}\right) \qquad (8)$$

For moderately weak donors such as chloroform and ethanol, we can approximate [D] with $[\mathrm{D}]_0$. Since the increase in fluorescence intensity by hydrogen bonding with those donors is not so much remarkable, we cannot neglect the fluorescence of A compared with that of AD, and we should use for these cases equations (4) or (7).

The ranges of fluorescence spectra of A and AD for these cases are practically the same.

Owing to a very small difference in extinction coefficients of A and AD at the wave length of the exciting light, (4) and (7) practically coincide in their forms and it has been established that the experimental results can be reproduced by either equations (4) or (7) satisfactorily, the equilibrium constants evaluated by (4) and (7) being practically the same.

Further, the equilibrium constant obtained in this way from fluorescence intensity measurement agrees with that evaluated from the change in the absorption spectrum.

Therefore, we can conclude that, in these cases, the association equilibrium in the excited state is practically the same as that in the ground state, in contrast to the case of naphthols[4,9].

For strong donors such as trichloracetic acid, we cannot approximate [D] with $[\mathrm{D}]_0$ and [D] should be evaluated using an equilibrium constant obtained from an absorption spectrum.

For acridine-trichloracetic acid system, the spectral range of fluorescence of AD is considerably different from that of A, but the increase of fluorescence intensity by hydrogen bonding is so remarkable, that we can neglect Φ_a compared with Φ_c.

9) N. Mataga, Y. Kaifu and M. Koizumi, *Nature*, **175**, 731 (1955).

TABLE I

Acceptor	Donor	Solvent	T[a]	K_T	$\delta\tilde{\nu}$[b] (cm^{-1})	Φ_r
Acridine	Chloroform	Benzene	286	0.1	*	0.6
	Ethanol	Benzene	290	1.0	*	1.0
		Hexane	290	1.6	*	1.0
		CCl_4	291	1.8	*	1.0
	Benzylalcohol	Benzene	287	2.0	*	1.0
	β-phenylethylalcohol	Benzene	287	1.0	*	1.6
	$CH_2ClCOOH$	Benzene	293	1.4×10^2	~600	
	$CHCl_2COOH$	Benzene	293	8×10^2	~800	9.5
	CCl_3COOH	Benzene	293	1.3×10^4	~900	11
Quinoline	$CH_2ClCOOH$	Benzene	295	~10^2	*	
	CCl_3COOH	Benzene	297	5×10^3	*	

a) Temperature at which measurement was made.
b) Wave number shift of ^1L_a band due to hydrogen bonding.
* Uncertain.

Hence it is suitable to employ equation (5) or (8) and the experimental results are really well reproduced by these equations.

In contradistinction to acridine-trichloracetic acid system, the increase in fluorescence intensity is very slight in the quinoline-trichloracetic acid system. In quinolinium ion in aqueous solution, the emitting state is ^1L_a in contrast to ^1L_b of quinoline base, and the range of fluorescence spectrum is considerably different from each other. In the quinoline-trichloracetic acid system, however, it was confirmed that the emitting state is ^1L_b, the spectral range of fluorescence being the same as in non-polar solvent (310–360 mμ).

Some examples of the analysis of fluorescence intensities are shown in Figs. 7, 8.

The concentration ranges of ethanol, benzylalcohol and β-phenylethylalcohol used for the evaluation of equilibrium constants from the results of absorption and fluorescence measurements were approximately 0.03–0.5 mol./l.

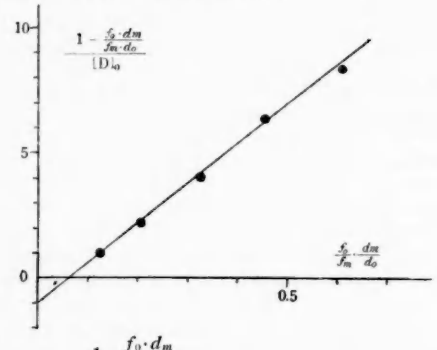

Fig. 7. $\dfrac{1-\dfrac{f_0\cdot d_m}{f_m\cdot d_0}}{[D]_0}\sim\dfrac{f_0\cdot d_m}{f_m\cdot d_0}$ relation for acridine-benzene-ethanol system.
Concentration of acridine: 5×10^{-5} mol./l.

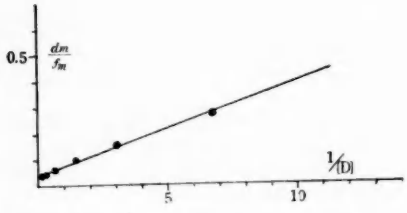

Fig. 8. $\dfrac{d_m}{f_m}\sim\dfrac{1}{[D]}$ relation for acridine-benzene-trichloracetic acid system.
Concentration of acridine: 5×10^{-5} mol./l.

The results of infrared measurements[10] on the dimerization of chloracetic acids were used for the estimation of concentration ranges where the fraction of monomer is at least 80%, and the calculation of equilibrium constants was made in this concentration range.

E. The Relative Fluorescence Yields of Hydrogen Bonded Nitrogen Heterocycles.—It is clear from the above mentioned results, that the change in fluorescence intensity is well interpreted on the basis of hydrogen bonding equilibrium. Further, it is possible to deduce some information on the interelation between the fluorescence yields of hydrogen bonded nitrogen heterocycles and the donating powers of various proton donors.

Ethanol solution was used as a standard. The fluorescence intensity of this standard solution is expressed as follows:

$$f_s=\Phi_s\cdot d_s\cdot I_0 \qquad (10)$$

where d_s is the optical density at the wave length of exciting light and Φ_s is the quantum yields of fluorescence. Then,

10) J. T. Harris, Jr. and M. E. Hobbs, *J. Am. Chem. Soc.*, **76**, 1419 (1954). H. A. Pohl, M. E. Hobbs and P. M. Gross, *J. Chem. Phys.*, **9**, 408 (1941).

from equations (10), (3) and (6), the following equations are derived.

$$f_m/f_s = \frac{\varepsilon_a(\Phi_a/\Phi_s)+\varepsilon_c(\Phi_c/\Phi_s)K[\mathrm{D}]}{1+K[\mathrm{D}]}\frac{[\mathrm{A}]_0}{d_s} \quad (11)$$

$$f_m/f_s = \frac{(\Phi_a/\Phi_s)+(\Phi_c/\Phi_s)K'[\mathrm{D}]}{1+K'[\mathrm{D}]}\frac{d_m}{d_s} \quad (12)$$

From these equations, (Φ_c/Φ_s) can be evaluated, and the ratios of (Φ_c/Φ_s) for various proton donors give the ratio of Φ_c. The results obtained for acridine by (11) and (12) are practically the same. As shown in Table I, Φ_c's of acridine hydrogen bonded with ethanol, benzylalcohol and β-phenylethylalcohol are almost the same, and it is somewhat smaller when acridine is hydrogen bonded with chloroform.

Moreover, Φ_c for ethanol does not change irrespective of whether benzene, hexane, or carbon tetrachloride, is used as solvent. For chloracetic acids, the value of Φ_c is far greater than that for ethanol, and owing to the red shift of fluorescence spectrum, the "true value" of Φ_c may be larger than the value given in the table*.

For quinoline, since the weakness of its fluorescence intensity did not allow precise measurement, we did not attempt extensive study, and measurements were made only for monochlor- and trichloracetic acid. From the increases in fluorescence intensity, we can see, for these cases that Φ_c may be only several times of Φ_B in its order of magnitude, whereas $\Phi_s/\Phi_B \sim 30$[3], therefore, Φ_c may be probably much smaller than Φ_s, for these cases.

Now, $\Phi = \dfrac{k_f}{k_f+k_i}$, where k_f and k_i are the rate constant of fluorescent transition and that of the radiationless process. k_f can be estimated using Ladenburg's formula[11],

$$k_f \simeq 2.88\times10^{-9}\, n^2 \tilde{\nu}^2_{\max} \int_0^\infty \varepsilon(\tilde{\nu})d\tilde{\nu}\ \mathrm{sec}^{-1}$$

Both in acridine and quinoline, the overlapping of ^1L_b and ^1L_a bands is fairy large; nevertheless, in the case of acridine, we can estimate $\int_0^\infty \varepsilon(\tilde{\nu})d\tilde{\nu}$ in its order of magnitude.

For acridine-trichloracetic acid-benzene system,

$$k_f' \sim 5.5\times10^7\ \mathrm{sec}^{-1},$$

and for acridine-ethanol-benzene system,

$$k_f \sim 2.5\times10^7\ \mathrm{sec}^{-1}.$$

Putting these k_f' and k_f value into the equation,

$$\Phi'/\Phi = \frac{k_f'}{k_f}\frac{(k_f+k_i)}{(k_f'+k_i')} \sim 11,$$

the following relations are derived.

$$k_i' < \frac{1}{5}k_i, \quad \tau' \simeq 5\tau$$

For quinoline, the estimation of $\int_0^\infty \varepsilon(\tilde{\nu})d\tilde{\nu}$ is more difficult. It is certain, however, that the integrated absorption is far larger in quinoline-trichloracetic acid-benzene system compared with those in benzene or ethanol solution. Therefore, it is clear that k_i of quinoline hydrogen bonded with trichloracetic acid is far greater than k_i in ethanol solution.

4. Discussion

(a) Role of n-Electron in the Inner Quenching of Fluorescence. — From all the facts described above, it is clear that the hydrogen bonding or proton addition plays an important role in the fluorescence of these nitrogen heterocycles. This circumstance is well comprehended by assuming that the n-electrons (non-bonding electrons) on a nitrogen atom is intimately related with the mechanism of fluorescence; the interaction between n- and π-electrons in the excited state may perhaps induce the radiationless transition to the ground state**, directly or indirectly. Such n–π interaction may be weakened more or less owing to the acquisition of bonding character by the n-electron due to hydrogen bonding or proton addition, making the fluorescence transition possible.

In contradistinction to the case of naphthols, the equilibrium constant obtained from the fluorescence intensity is almost the same as that calculated from absorption spectrum, for these nitrogen heterocycles. This fact may be correlated with the proposed mechanism of the inner quenching by n-electron.

The possible interpretations may be as follows.

(i) Although the equilibrium in the excited state is shifted toward hydrogen bonding, the excited free molecule has such a short lifetime, due to high probability of inner quenching, that it has no time to be bonded with neighboring OH

* The phototube used is an ultraviolet sensitive one.

11) See for example, Th. Förster, loc. cit., p. 158.

** An analogous discussion was made recently by Sangster and Irvine in relation to their study of the efficiencies of organic scintillators. R. C. Sangster and J. W. Irvine, Jr., *J. Chem. Phys.*, **24**, 670 (1956).

groups during its life. Thus only the molecules which are hydrogen bonded in the ground state may be able to fluoresce.

(ii) Owing to the n–π interaction the non-bonding character of n-electron may be lost more or less in the excited state, decreasing the proton accepting power, but the π-electron density on the nitrogen atom plausibly be increased in the excited state[***], thus compensating the decrease in proton accepting power by n-electron, and the accepting power may be the same in the ground and in the excited state. In this case, even when the equilibrium state is reached during the lifetime of an excited free molecule, the equilibrium constant obtained from fluorescence intensity ought to be equal to that evaluated from absorption spectrum. In the present stage it cannot be decided definitely which of (i) and (ii) is the dominant mechanism for the phenomenon question.

(b) Effect of π-Electronic State on the Fluorescence Quenching. — Although the increase in fluorescence yields of quinoline and acridine by hydrogen bonding with ethanol or by proton addition in aqueous solution is almost the same, we see a distinct difference between these molecules in the effect of halogen atom on the fluorescence yields. The fluorescence yield of acridine is greatly enhanced by hydrogen bonding with trichloracetic acid, but the fluorescence yield of quinoline hydrogen bonded with trichloracetic acid is rather small compared with the fluorescence yield in ethanol solution. This distinction in these two molecules may be ascribed to the difference of emitting π-electronic state. In aromatic hydrocarbons, such as benzene, naphthalene and anthracene, there exists an ^3L_b state which has the same energy as ^1L_b[12,13].

If the lowest singlet excited state is ^1L_b, the phosphorescence transition occurs with relative ease probably by the processes, $^1L_b \rightarrow {}^3L_b \rightarrow {}^3L_a \rightarrow$ ground state. However, when the lowest singlet excited state is ^1L_a, phosphorescence transition may be very difficult. The difference between naphthalene and anthracene in the experimental results of T→T absorption[14] may be interpreted by these mechanisms. Now, as the electronic spectra of nitrogen heterocycles are very similar to those of isoelectronic aromatic hydrocarbons, we may be allowed to assume that the analogous situation probably prevails also in these heterocyclic molecules. Thus, in the case of quinoline, the near-by existence of a halogen atom may easily accelerate $^1L_b \rightarrow {}^3L_b$ process owing to the spin-orbital perturbation, but it may be difficult to realize such a situation in acridine.

After all, the results reported in this paper, are well comprehended by assuming that the n–π interaction is a chief cause of inner quenching and also by considering the effect of emitting π-electronic state on the quenching phenomenon. From the present results, the interpretations of the inner quenching in these molecules as due to the spin-orbital perturbation by the existence of nitrogen atom or predissociation of CN bond may not be appropriate.

*** A theoretical study using the molecular orbital method is now in progress.

12) R. Pariser, *J. Chem. Phys.*, **24**, 250 (1956).
13) J. A. Pople, *Proc. Phys. Soc.*, **68A**, 81 (1955).
14) D. P. Craig and I. G. Ross, *J. Chem. Soc.*, **1954**, 1589.

Summary

1. The hydrogen bonding effect on the fluorescence of quinoline and acridine was studied in non-polar solvent mixed with various proton donors.

2. The equilibrium constants of hydrogen bonding calculated from the absorption and fluorescence data were the same for these molecules, in contradistinction to the case of naphthols. Possible mechanisms for this experimental fact were proposed.

3. The larger the relative fluorescence yields of hydrogen bonded nitrogen heterocycles become, the stronger the donating powers of proton donors are, and from this fact, discussions were given on the role of non-bonding electrons in the inner-quenching of these molecules.

4. The difference between quinoline and acridine in their fluorescence quenching caused by the existence of a halogen atom was ascribed to the different emitting π-electronic states in these molecules (^1L_b in quinoline, ^1L_a in acridine), and some considerations by means of analogy to the π-electronic structures of aromatic hydrocarbons were given.

The authors express their cordial thanks to Dr. H. Baba of Hokkaido University for his discussion. Their thanks are especially due to Prof. M. Koizumi for his encouragement and discussion throughout this investigation.

Institute of Polytechnics
Osaka City University
Kita-ku, Osaka

Note on the Polymerization of Dyes in Solution

By Noboru MATAGA

(Received December 24, 1956)

1. Introduction

Many investigations have been made on the aggregation of dye molecules or ions in aqueous solution, and it seems clear that some dyes form dimers and polymers in suitable conditions. For example, thionine, methylene blue, toluidine blue[1-3], rhodamine 6G[4], pyronine G[5] form dimers while acridine orange[6] forms dimer and higher polymers. Even in organic solvents dye molecules can often exist in a certain aggregated state. For example, Lewis et al.[7] reported that methylene blue in EPA at low temperature (liquid nitrogen) shows dimerization and polymerization of higher degree. Further, according to Zanker[8,9], acridine orange forms a definite polymer at low temperature in a mixed solvent of alcohol and ether.

Some qualitative discussions on the factors determining the association and also on the mechanism of spectral shift caused by association, have been made heretofore. For example, Rabinowitch and Epstein[1] have ascribed the cause of association to a large dispersion force between dye ions which have strong absorption bands in the visible spectral region.

Förster[10] has proposed a classical model for the interpretation of spectral shift caused by association. According to his theory, the dye ions in dimerized state take the plane parallel configuration, in which the dispersion force between pair of each dye ion is the largest. In this configuration, the electron oscillators of dye ions couple with each other, and there result symmetric and antisymmetric combinations, of which the former with a larger frequency than that of the original one can appear as absorption.

It is questioned, however, whether the complicated nature of the dimerization or polymerization of dyes in solution can well be comprehended by such a simplified interpretation.

As to a delicate aspect of dimerization or polymerization, some remarks were made previously by the present author in relation to the mechanism of metachromasy phenomenon[11].

Recently, Levshin has studied the effect of concentration on the optical properties of solution of acridine derivatives such as monoamino- and diamino-acridine[12-14]. He insists that the concentration effect is due to the dimerization of these molecules.

The present author has also investigated the concentration effect on the absorption spectra of 2,8-diaminoacridine (DAA) and 2,8-bisdimethylaminoacridine (BDAA) in various organic solvents. By the analysis of absorption spectrum according to the method of Zanker[8], it has been established that, contrary to Levshin's opinion, these molecules form higher polymers very easily in some organic solvents. It has also been confirmed that, the influence of solvent and of a slight difference in molecular structure between DAA and BDAA is very prominent in the phenomenon.

Levshin did not make any remarks about these points.

The object of the present paper is to report about these points with some discussions on the mechanism of dimerization or polymerization.

1) E. Rabinowitch, and L. F. Epstein, *J. Am. Chem. Soc.*, **63**, 69 (1941).
2) S. E. Sheppard, *Rev. Mod. Phys.*, **14**, 303 (1942).
3) S. E. Sheppard and A. L. Geddes, *J. Am. Chem. Soc.*, **66**, 1995, 2003 (1944).
4) V L. Levshin, *Acta Physicochim. USSR.*, **1**, 685 (1935); **4**, 221, (1936).
5) N. Mataga and M. Koizumi, *J. Inst. Polytech. Osaka City Univ.*, **4C**, 167 (1953); M. Koizumi and N. Mataga, This Bulletin, **27**, 194 (1954).
6) V. Zanker, *Z. Physikal. Chem.* **199**, 225 (1952).
7) G. N. Lewis et al., *J. Am. Chem. Soc.*, **65**, 1150 (1943).
8) V. Zanker. *Z. Physikal. Chem.*, **200**, 250 (1952).
9) G. Scheibe and V. Zanker, *Z. Physik*, **133**, 244 (1952).
10) Th. Förster, "Fluoreszenz organischer Verbindungen", Gottingen, Vandenhoech and Ruprecht (1951), p. 254.
11) N. Mataga, *J. Inst. Polytech. Osaka City Univ.*, **4C**, 189 (1953).
12) V. L. Levshin, *Doklad. Akad. Nauk SSSR*, **96**, 173 (1954).
13) V. L. Levshin, *Zhur. Eksptl. i. Teoret. Fiz.*, **28**, 201 (1954).
14) V. L. Levshin, ibid., **28**, 213 (1955).

2. Experimental

Apparatus. — Absorption spectra were measured with Beckman spectrophotometer model D. U. and the lengths of cells used were 10, 1, 0.1 and 0.007 cm. Using these cells, measurement in the concentration range from 10^{-6} to 10^{-2} mol./l. was possible.

Reagent.—DAA was the same sample as described elsewhere[15]. BDAA was purified by the method of Moudgill[16] and Biehringer[17]. Excess of sodium hydroxide was added to the aqueous solution of acridine orange (Zinc Salt of BDAA) which was kindly supplied by Sumitomo Chemical Co. Ltd.; BDAA was extracted with ethanol, and purified by repeated recrystallization from ethanol-water mixture.

Methanol was refluxed with calcium oxide and distilled. Ethanol was also refluxed with calcium oxide and distilled fractionally. Extra pure-grade butanol was used without further purification. Purified acrylonitrile was kindly supplied by Mr. K. Nakatsuka of this Institute.

Acetone was refluxed with potassium permanganate and, after being dried over potassium carbonate, distilled fractionally. Extra pure grade pyridine was dried over sodium hydroxide and distilled before use.

3. Experimental Results

Zanker[18] has systematized the electronic spectra of nitrogen heterocycles in analogy to those of aromatic hydrocarbons, using Platt's perimeter model[19]. According to his classification, the longest wave length bands of these molecules are due to the transition to ^1L_a. Because of the light absorption by solvent, the observation of shorter wave length bands is not possible. Therefore only the effect of concentration on the ^1L_a band was studied. Some examples of the concentration dependence of absorption spectra are shown in Figs. 1–5.

It is clear from these spectral changes that there are only two molecular species

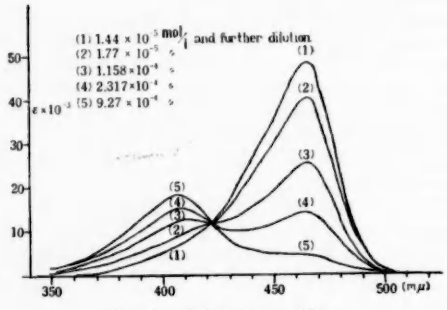

Fig. 1. DAA in pyridine

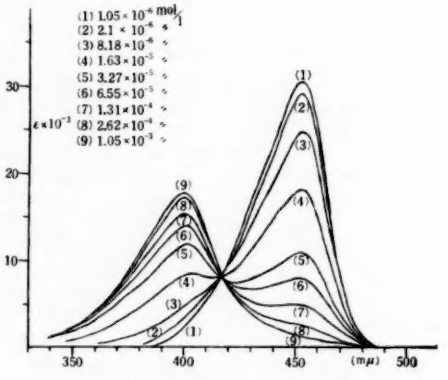

Fig. 2. DAA in acrylonitrile

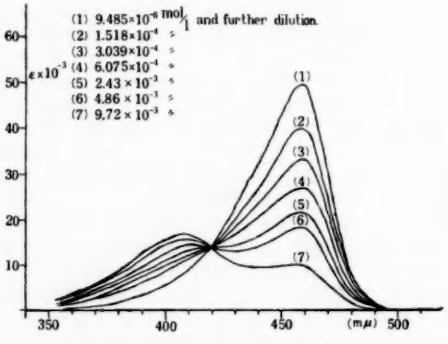

Fig. 3. DAA in ethanol

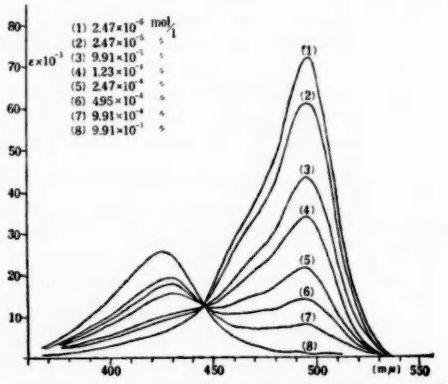

Fig. 4. BDAA in acrylonitrile

15) N. Mataga, Y. Kaifu and M. Koizumi, This Bulletin, **29**, 373 (1956).
16) K. L. Moudgill, *J. Chem. Soc.*, **1922**, 1508.
17) J. Biehringer, *J. Praktisch. Chem.*, **57**, 217 (1896).
18) V. Zanker, *Z. Physikal. Chem., N. F.*, **2**, 52 (1954).
19) J. R. Platt, *J. Chem. Phys.*, **17**, 484 (1949); H. B Klevens and J. R. Platt, ibid., **17**, 470 (1949).

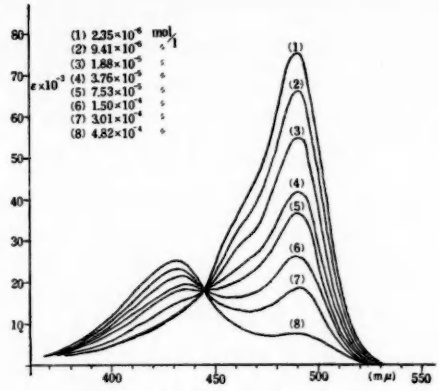

Fig. 5. BDAA in ethanol

in equilibrium, i.e., monomer and polymer. For the equilibrium between monomer and polymer of nth degree, the equilibrium constant of association is expressed as:

$$K=\frac{x}{nc_0^{n-1}(1-x)^n} \tag{1}$$

where, $(1-x)$ is the fraction of monomer against the total quantity as monomer and c_0 is the analytical concentration of dye.

The apparent extinction coefficient ε at a definite wave length can be expressed by means of ε^n and ε^m which are the extinction coefficients of polymer and monomer, respectively, at the same wave length.

$$\varepsilon=\frac{1}{n}x\varepsilon^n+(1-x)\varepsilon^m \tag{2}$$

From (1) and (2), we obtain the following equations.

$$\log c_0\left(1-\frac{\varepsilon}{\varepsilon^m}\right)=\log(C\cdot K)+n\log c_0\left(\frac{\varepsilon}{\varepsilon^m}-\frac{\varepsilon^n}{n\varepsilon^m}\right) \tag{3}$$

$$C=\frac{1}{n^n\left(n-\frac{\varepsilon^n}{\varepsilon^m}\right)^{n-1}}$$

In the first approximation, we can neglect $\frac{\varepsilon^n}{n\varepsilon^m}$ as compared with $\frac{\varepsilon}{\varepsilon^m}$

$$\log c_0\left(1-\frac{\varepsilon}{\varepsilon^m}\right)=\log(C\cdot K)+n\log c_0\left(\frac{\varepsilon}{\varepsilon^m}\right) \tag{4}$$

By means of (4), we can determine n, then using (3) we can evaluate K.

Some examples of $\log c_0\left(1-\frac{\varepsilon}{\varepsilon^m}\right)\sim\log c_0\left(\frac{\varepsilon}{\varepsilon^m}-\frac{\varepsilon^n}{n\varepsilon^m}\right)$ plots are shown in Fig. 6. It is clear from these plots, that there is only monomer-polymer equilibrium, in contradistinction to the case of acridine orange in aqueous solution[6] where polymerization proceeds stepwise, i.e., monomer-dimer equilibrium exists in relatively dilute solution, and dimer-tetramer equilibrium is established in a highly concentrated solution.

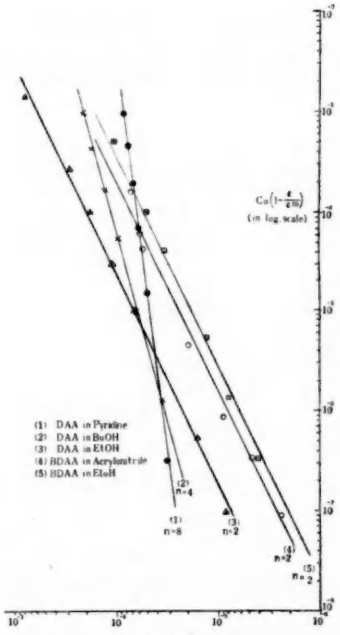

$C_0\left(\frac{\varepsilon}{\varepsilon^m}-\frac{\varepsilon^n}{n\varepsilon^m}\right)$ (in log scale)

Fig. 6. $\log C_0\left(1-\frac{\varepsilon}{\varepsilon^m}\right)\sim\log C_0\left(\frac{\varepsilon}{\varepsilon^m}-\frac{\varepsilon}{n\varepsilon^m}\right)$ relations for DAA and BDAA.

4. Discussion

The results obtained are collected in Tables I and II for DAA and BDAA, respectively.

As Levshin has pointed out[13], the dimerization or polymerization tendency has no correlation with refractive index, dielectric constant, or dipole moment of the solvent used.

TABLE I
COLLECTED DATA FOR DAA

Solvent	Pyridine	Acrylonitrile	Acetone	BuOH	EtOH	H_2O
Equilibrium constant	1.2×10^{4}	1.6×10^{10}	3.0×10^{20}	9.2×10^{15}	1.7×10^{4}	2.7×10^{3}
K_n^T	K_8^{283}	K_4^{283}	K_4^{283}	K_4^{283}	K_2^{283}	K_2^{283}
$\delta\tilde{\nu}$ (kcal.)	8.7	8.4	8.1	8.2	7.8	1.9
$\bar{f}_{\text{monomer}}$ a)	0.74	0.37	0.44	0.66	0.66	0.33
$f^{v.}_{\text{monomer}}$ a)	0.36	0.21	0.27	0.38	0.40	0.21

a) $\bar{f}_{\text{monomer}} = \dfrac{n}{N}\dfrac{c^2m}{\pi e^2}10^3\int_0^\infty \varepsilon(\tilde{\nu})d\tilde{\nu} = 4.32\times10^{-9}\, n\int_0^\infty \varepsilon(\tilde{\nu})d\tilde{\nu}$

n: Refractive index of solvent

$\int_0^\infty \varepsilon(\tilde{\nu})d\tilde{\nu}$: Integrated absorption for monomeric band

$f^{v.}_{\text{monomer}} = \left(\dfrac{3}{n^2+2}\right)^2 f_{\text{monomer}}$

$\bar{f}$ and $f^{v.}$ are the oscillator strengths in solution and in vapor state, respectively. N. Q. Chako, *J. Chem. Phys.*, **2**, 644 (1934).

TABLE II
COLLECTED DATA FOR BDAA

Solvent	Acrylonitrile	Acetone	BuOH	EtOH	MeOH
Equilibrium constant	$1.2+10^{5}$	3.2×10^{6}	1.3×10^{5}	1.9×10^{5}	4.1×10^{4}
K_n^T	K_2^{293}	K_2^{295}	K_2^{294}	K_2^{294}	K_2^{301}
$\delta\tilde{\nu}$ (kcal.)	9.4	8.4	8.1	8.1	7.6
$\bar{f}_{\text{monomer}}$	0.93	0.68	0.83	1.01	0.84
$f^{v.}_{\text{monomer}}$	0.54	0.42	0.47	0.61	0.53

TABLE III

Dye ions	Thionine a)	Methylene blue a)	Rhodamine 6G b)	Pyronine G c)	Acridine orange d)	Trypaflavine e)	DAA
$\delta\tilde{\nu}$ (kcal.)	3.4	4.1	3.4	3.3	3.4	2.0	1.9
$\bar{f}_{\text{monomer}}$	0.77	0.60	0.72	0.13	0.82	0.73	0.33
$f^{v.}_{\text{monomer}}$	0.48	0.38	0.45	0.08	0.52	0.46	0.21

a) Ref. 1), b) Ref. 4), c) Ref. 5), d) Ref. 6),
e) Measured by the present writer.

An analogous idea to that of Förster[10], but in wave mechanical form was developed by Mori[20] for the case of dimerization, assuming a simplified model of dipole-dipole interaction similar to that used in the calculation of dispersion force, and the treatment was extended to the case of polymer[21].

This has its analogy in the theory of Davydov splitting or exciton migration.

According to it, the blue shift due to dimerization is expressed as follows:

$$hc\Delta\sigma = \frac{1}{R^3}(\vec{\mu}^1_{eg} \mid \vec{\mu}^2_{eg}) \qquad (5)$$

where $\Delta\sigma$ is the wave number shift, R is the distance between dye molecules which are in plane-parallel configuration, and $\vec{\mu}_{eg}$ is the transition dipole of monomeric dye molecule, and in this configuration, $(\vec{\mu}^1_{eg} \mid \vec{\mu}^2_{eg}) > 0$. If the association is due to the dispersion force between monomers and the spectral shift is determined by equation (5), then the association tendency and the magnitude of spectral shift should depend on the oscillator strength of monomeric band.

As seen from Table III, however, the spectral shifts of various dye ions in aqueous solution have no correlation with their oscillator strengths of monomeric bands.

20) Y. Mori, Symposium on π-electronic state, *Chem. Soc. Japan*, 1955.
21) N. Mataga, Unpublished.

Moreover, it is clear from Tables I and II, that the polymerization tendencies of DAA and BDAA in organic solvents have no dependence on their oscillator strengths of monomeric bands. For the association to occur it might be necessary that the oscillator strength of monomeric band be fairy large, because, for example, the integrated absorption $\int_0^\infty \varepsilon(\tilde{\nu})d\tilde{\nu}$ of ^1L_a band of acridine is nearly 10^7 in its order of magnitude, whereas it is approximately 10^8 for DAA and BDAA, and we could not observe any concentration dependence of spectra of acridine in various solvents such as used for DAA and BDAA, in the concentration range from 10^{-5} to 10^{-3} mol./l.

It seems clear, however, that the association is very sensitive to the solvent used, and also it depends remarkably on the slight difference of molecular structures of dye molecules.

By inspection of Tables I and II, we see that the association tendency of DAA is greater than that of BDAA. Further, it is remarkable, that in pyridine, DAA forms octamer, whereas BDAA shows no associating tendency. Hydrogen bonding of solvent molecules with amino groups of DAA, might play some important role in the association.

Summary

The effect of concentration on the absorption spectra of DAA and BDAA in various organic solvents was studied in the concentration range from 10^{-6} to 10^{-2} mol./l. Contrary to Levshin's opinion, DAA forms polymers higher than dimer very easily in some organic solvents, and the association tendency of DAA is greater than that of BDAA.

Further, the association of these molecules is very sensitive to the solvents used. The association tendency and the spectral shift due to dimerization or polymerization have no correlation with the oscillator strengths of monomeric bands of these molecules, and this is true also for the various dye ions in aqueous solution.

The author expresses his thanks to Sumitomo Chemical Co. Ltd. for the gift of acridine orange. He is grateful to Prof. M. Koizumi for his fruitful discussion and encouragement throughout the investigation.

Institute of Polytechnics
Osaka City University
Kita-ku, Osaka

---

*Separation of α-Glycerophosphate from Its β-Isomer by Column Chromatography**

By Chieko URAKAMI, Hiroko MURAHASHI and Yoshiko KAKUTANI

(Received January 8, 1957)

It has been reported previously from our laboratory that sodium glycerophosphates can be resolved completely into the α and β-isomers on the alumina impregnated paper with methanol-ammonia (60 : 5) as a developing solvent and that no hydrolysis or migration of the phosphoryl group seems to occur, as far as the sensitivity of the test employed is concerned[1]. The purpose of application of this method to column chromatography is twofold: firstly, to obtain pure samples of both isomers on a milligram level for biochemical interest and secondly, to give an absolute experimental evidence to support our previous results on hydrolysis and migration of the phosphoryl group. For the latter, the samples obtained by chromatography were analyzed according to Burmaster's method[2], which affords the determination of the inorganic phosphate, α and β-glycerophosphates in a mixture of the three by spectrophotometrical means on the color developed by the reduction of the phosphomolybdate with stannous chloride.

* Presented at the 10th Annual Meeting of the Chem. Soc., Japan, April, 1956.

1) C. Urakami and Y. Kakutani, This Bulletin, **30**, 21 (1957).

2) C. F. Burmaster, *J. Biol. Chem.*, **164**, 233 (1946).

Experimental

Apparatus.—The chromatographic tube used was of the size 10 mm. in diameter and 150 mm. in length, provided with an inner joint connection with a sealed-in fritted glass disk and a stop-cock.

Spectrophotometric measurements were carried out with Shimazu Model DF-II with a filter No. 634. All measurements were taken within the range of its maximum sensitivity, 0.1-0.3 extinction.

Samples and Reagents.—The solutions for analysis of the samples, α-1, α-2 and β-3 as indicated in Table I, were prepared so that each ml. contained approximately 20 μg. of phosphorus. Assay of the solutions was carried out by taking one-half of this quantity.

The solutions of the following reagents were prepared according to the specifications given by Burmaster; anhydrous sodium sulfite (reagent grade of Wako Pure Chemicals Co.), ammonium molybdate (the first grade of Daito Chemical Co.), stannous chloride (special grade of Yashima Chemical Co.), and sodium periodate (Marukawa Chemical Co.).

Bromothymol blue, 0.1% solution, was used for detection of the zone of the glycerophosphoric acids.

Adsorbent.—One part by weight of alumina for chromatography (200 mesh, Yashima Chemical Co.) and nine parts by weight of cellulose powder (No. 50 of Toyo-filter paper Co.) were mixed thoroughly with a sufficient quantity of the mixed solvent, methanol-ammonia (60 : 5), and the mixture allowed to mercerate for ten hours. During the last two hours the mixture was stirred vigorously with a magnetic stirrer. About one gram of the slurry was poured, all at once, into the chromatographic tube and after the adsorbent had settled, the column was packed firmly with an additional quantity of the solvent, about 100 ml., by weighting at the top and applying suction at the base of the column to give 24-26 mm. in length.

Chromatographic Technique.—When about one ml. of the solvent was remaining over the surface of the column, a suspension of 2 mg. of the sample or the mixed sample containing one mg. each of the isomers in 5 ml. of the solvent mixture was applied and adsorption of the solute was allowed to take place for about one hour, with the stop-cock being left open and without application of suction. When a few mm. of the solvent were remaining over the surface of the column, a furthere amount of the solvent was added. Exposure of the column to air at this point should be strictly avoided, otherwise the adsorption of the solute is so strong that the zone will not move. The rate of flow was maintained at one ml. per min. by applying suction. The percolate was collected in a 100 ml. fraction up to a total volume of 1 l. The presence of the solute, the α-glycerophosphate, was found in the fraction collected between 850 and 950 ml. of the percolate. By applying the indicator, we have observed that the glycerophosphate advanced down the column in a clean-cut narrow zone.

Preparation of Solutions for Analysis.—A 100 ml. fraction containing the α-glycerophosphate was evaporated almost to dryness on a water bath at a low temperature, below 45°C, a small amount of distilled water added to the residue, any insoluble material found removed by filtration, and rinsed several times with fresh water to insure quantitative recovery of the phosphate. The filtrate and washings were combined and made up to 6 ml. in an accurately graduated tube. An aliquot of 3 ml. was used for analysis of α-glycerophosphoric acid and 1.5 ml. each for the β-isomer and inorganic phosphate.

The β-isomer was recovered in the following manner: First, the zone of the adsorbed β-isomer was located, after about 1 l. of the percolate had been collected, by passing a solution of a few drops of bromothymol blue indicator in the solvent and by drying the column somewhat with application of vacuum. An excessive drying should be avoided, or the detection of the zone would not be possible. A distinct yellow zone was found within 5 mm. from the surface of the column, the rest being colored blue green. Therefore, after extruding the somewhat wet column from the tube, a section was cut 5 mm. from the upper end of the adsorbent. It was extracted three times with a 5 ml. portion of a weak alkaline solution, pH 8, and any insoluble material removed by centrifugation. The supernant liquid obtained was evaporated to a small volume and made up to 6 ml. with distilled water. An aliquot of 3 ml. was used for analysis of the α- and 1.5 ml. each for the β-isomer and inorganic phosphorus.

Results and Discussion

By applying 2 mg. of the pure sample of barium α-glycerophosphate or sodium β-glycerophosphate to a column consisting of a mixture of alumina and cellulose (1 : 9) 25 mm. in length and by developing with methanol-ammonia (60 : 5) as a solvent, 85% of the former was recovered in the 100 ml. fraction collected between 850 and 950 ml. of the percolate and 35% of the latter in the extract of a section cut 5 mm. from the column surface, as shown in Table II. When a mixture of the sodium salts of the two isomers was applied, 53–56% of the α and 20–30% of the β were recovered. No inorganic phosphorus was detected in all these samples recovered and also no β-glycerophosphoric acid was found to be present in the fraction containing the α-isomer or the α in the extract containing the β-isomer, as shown in Table II.

We have also succeeded in separating the isomers by applying a 5 mg. load on the column of the same length but its retention volume was found to be less

TABLE I

ANALYSES OF GLYCEROPHOSPHATE SAMPLES

Sample No.	Diln. factor	Extinction			P, μg. found		Total P μg. found**		Total P, μg. calcd.	Purity %	
		Total	α	β*	α	β	α	β		α	β
α—1	2	0.108	0.108	0.000	4.1	0.0	8.2	0.0	10	82	00
	〃	0.203	0.203	0.000	4.3	0.0	8.6	0.0	10	86	00
	〃	0.202	0.202	0.000	4.25	0.0	8.5	0.0	10	85	00
α—2	〃	0.226	0.169	0.057	3.75	1.3	7.5	2.6	10	75	26
	〃	0.213	0.169	0.044	3.75	1.0	7.5	2.0	10	75	20
	〃	0.223	0.174	0.049	3.85	1.1	7.7	2.2	10	77	22
β—3	〃	0.230	0.000	0.230	0.0	4.8	0.0	9.6	10	00	96
	〃	0.230	0.000	0.230	0.0	4.8	0.0	9.6	10	00	96
	〃	0.228	0.000	0.228	0.0	4.75	0.0	9.5	10	00	95

* Obtained by subtracting extinction of α from that of total.

** Obtained by multiplying P, μg. found directly from the extinction by the dilution factor, 2.

In all these samples no inorganic phosphorous was detected.

α-1, Barium α-glycerophosphate[3]; α-2, Disodium α-glycerophosphate. $5.5H_2O$ (Wako Pure Chemicals Co.); β-3, Disodium β-glycerophosphate. $5.5H_2O$ (Yashima Chemical Co.).

TABLE II

ANALYSES OF GLYCEROPHOSPHATES OBTAINED BY CHROMATOGRAPHIC SEPARATION

Sample No.	Diln. factor	Extinction			P found μg.		Total P found, μg.		Total P in Sample, μg.		Recovery %	
		Total	α	β	α	β	α	β	α	β	α	β
α—1	14	0.234	0.234	0.000	10.35	0.00	144.9	00.0	171.7	00.0	84	00
β—3	6	0.216	0.000	0.216	0.00	9.6	0.0	57.6	0.0	163.0		35
Mixt. of												
α—2	8	0.103	0.103	0.000	4.2	0.0	33.6	0.0	63.4	20.3	53	
β—2	4	0.124	0.000	0.124	0.0	5.09	0.0	20.4		102.0		20
Mixt. of												
α—2	4	0.109	0.109	0.000	8.9	0.0	35.6	0.0	63.4	20.3	56	
β—3	4	0.188	0.000	0.188	0.0	7.6	0.0	30.5		102.0		30

A 2 mg. sample of the sodium salt was used for the individual run; one mg. each was used for the mixed sample. The α-sample was collected in a 100 cc. fraction taken between 850–950 ml. of the percolate: the β-sample was extracted from the adsorbent cut 5 mm. from the surface of the column. No inorganic phosphorus was detected in all these samples.

than 50 ml. and the recovery of the α less than 20%, the major portion being found in the first 100 ml. This indicates that a 5 mg. load is close to the saturation point for the capacity of the amount of the adsorbent employed. We have also attempted to increase the capacity of the column by increasing the column length but encountered some difficulty in obtaining a uniformly packed column, due to difference in density of the two components of the adsorbent used.

These results show, therefore, that a mixture of a milligram each of the sodium salts of α and β-glycerophosphoric acids can be resolved completely on the column chromatographic system of this nature and provide a conclusive evidence for our previous observation that no hydrolysis or migration of the phosphoryl group occurs during the course of the chromatography.

Faculty of Science of Living
Osaka City University, Osaka

3) C. Urakami and Y. Kakutani, *Repts. Sci. Living, Osaka City Univ., Series D*, No. 1, 3 (1953).

Primary Process in Photochemical Decomposition of AH_N-Type Molecules

By Jiro HIGUCHI

(Received December 6, 1956)

1. Introduction

Photochemical reactions have in general been discussed in the classification of the primary process and the succeeding secondary process. The latter process is concerned in the reaction of free radicals, and is essentially a problem of chemical kinetics. On the other hand, the detailed study of the primary process requires the knowledge concerned with the electronic structures of the molecules and the free radicals produced. Above all, the full comprehension of the nature of each orbital is necessary to discuss the properties of these electronic states, and particularly of the potential energy surfaces, which are closely connected with the primary process. Unfortunately, such a knowledge has scarcely ever been obtained from experiments, except for a few simple molecules, due to the difficulty of the spectroscopic analysis for polyatomic molecules and for free radicals. Accordingly, the theoretical investigation is of great significance for such problems. Another theoretically important known fact is the adiabatic correlation rule, which has been developed by Wigner and Witmer[1], by Mulliken[2] and by Shuler[3]. The rule must be taken into consideration for the polyatomic system, although occasionally it is not so effective for intermediates of low symmetry, because there are few restrictions on the correlations of the states between reactants and products. Other theoretical considerations may be of minor importance for qualitative discussions. However, it goes without saying that the experimental facts play the conclusive part of the present discussion.

In the present paper, the primary process of photochemical decomposition in the first absorption region will be taken up for AH_N-type (A denotes atoms like C, N, O and others; and $N=4,3,2$) molecules from the viewpoint of the molecular orbital theory. The experimental investigations of these reactions have long been done by many authors[4], and the electronic spectra of these molecules have also been observed[4-6]. On the other hand, the theoretical investigations of some of these electronic structures have recently been done with fruitful results by several authors[7-11]. Accordingly, these reactions may be said to be one of the most suitable examples in studying the photochemical primary process.

2. General Consideration

Electronic Structure.—Before discussing the primary process, it is convenient to explain briefly the common electronic properties of the AH_N molecules and the free AH_{N-1} radicals. For the ground state, the electron configuration of an AH_N molecule can in general be given by $K(\phi_1)^2(\phi_2)^2(\phi_3)^2(\phi_4)^2$, in which K is the inner-shell of the molecule, nearly the same as that of the A atom, and ϕ_i's are the molecular orbitals mainly built from the valence-shell electrons of the constituent atoms in the LCAO-MO approximation. The sufficies of these MOs are chosen in the order of increasing energy. The lowest vacant orbital is ϕ_5 with the total symmetry A_1 and the structure of the first excited state is $K(\phi_1)^2(\phi_2)^2(\phi_3)^2(\phi_4)(\phi_5)$. The ϕ_5 orbital has been considered to be of a considerable $(n+1)s$ orbital character of the A atom, n being the principal quantum number of the valence-shell electron.

1) E. Wigner and E. E. Witmer. *Z. Physik*, **51**, 859 (1928).
2) R. S. Mulliken, *Phys. Rev.*, **43**, 279 (1933).
3) K. E. Shuler, *J. Chem. Phys.*, **21**, 624 (1953).
4) For example, see G. K. Rollefson and M. Burton, "Photochemistry and the Mechanism of Chemical Reactions," Prentice-Hall, Inc. New York (1939), and W. A. Noyes, Jr. and P. A. Leighton, "The Photochemistry of Gases," Reinhold Publishing Corporation, New York (1941).
5) H. Sponer, "Molekülspektren und ihre Anwendung auf chemische Probleme," Verlag Julius Springer, Berlin (1935), I. Tabellen, p. 97.
6) H. Sponer and E. Teller, *Revs. Modern Phys.*, **13**, 75 (1941).
7) A. D. Walsh, *J. Chem. Soc.*, **1953**, 2260.
8) A. D. Walsh, ibid., 2296.
9) R. S. Mulliken, *J. Am. Chem. Soc.*, **77**, 887 (1955).
10) F O. Ellison and H. Shull, *J. Chem. Phys.*, **23**, 2348 (1955).
11) J. Higuchi, *J. Chem. Phys.*, **24**, 535 (1956).

TABLE I

MOLECULAR ORBITALS OF AH_N MOLECULES AND THEIR BONDING POWER

	T_d (AH_4)			D_{3h} (AH_3)	
ϕ_1	$1a_1$	Strong-bonding	ϕ_1	$1a_1'$	Strong-bonding
ϕ_2, ϕ_3, ϕ_4	$1t_2$	Strong-bonding	ϕ_2, ϕ_3	$1e'$	Strong-bonding
ϕ_5	$2a_1$	Non-bonding	ϕ_4	$1a_2''$	Non-bonding
ϕ_r	ra_1	Rather strong-antibonding	ϕ_5	$2a_1'$	Non-bonding
			ϕ_r	ra_1'	Rather strong-antibonding
	C_{3v} (AH_3)			C_{2v} (AH_2)	
ϕ_1	$1a_1$	Strong-bonding	ϕ_1	$1a_1$	Strong-bonding
ϕ_2, ϕ_3	$1e$	Strong-bonding	ϕ_2	$1b_2$	Strong-bonding
ϕ_4	$2a_1$	Weak-bonding	ϕ_3	$2a_1$	Weak-bonding
ϕ_5	$3a_1$	Non-bonding	ϕ_4	$1b_1$	Non-bonding
ϕ_r	ra_1	Strong-antibonding	ϕ_5	$3a_1$	Non-bonding
			ϕ_r	ra_1	Strong-antibonding
	$D_{\infty h}$ (AH_2)			$C_{\infty v}$ (AH)	
ϕ_1	$1\sigma_g$	Strong-bonding	ϕ_1	1σ	Strong-bonding
ϕ_2	$1\sigma_u$	Strong-bonding	ϕ_2	2σ	Weak-bonding
ϕ_3, ϕ_4	$1\pi_u$	Non-bonding	ϕ_3, ϕ_4	1π	Non-bonding
ϕ_5	$2\sigma_g$	Non-bonding	ϕ_5	3σ	Non-bonding
ϕ_r	$r\sigma_g$	Rather strong-antibonding	ϕ_r	$r\sigma$	Strong-antibonding

On the other hand, the LCAO-MO calculation of the AH_N molecule gives the strong-antibonding a_1 orbital ϕ_r, which may correspond to the ϕ_5 orbital, by taking the ns and np of the A atom and the 1s's of the H atoms into account. As discussed by Mulliken[12], however, the strong-antibonding orbital ϕ_r is not so good an approximation of the ϕ_5 orbital as compared with the $(n+1)s$ orbital of the A atom. It is noted that one higher strong-antibonding orbital is also expected instead of the above antibonding orbital, even if the $(n+1)s$ orbital is taken into account, because of the fairly large overlap between the $(n+1)s$ orbital of the A atom and the 1s orbital of the H atom. In that case, a more satisfactory approximation of the ϕ_5 orbital will be obtained with the better repulsive orbital ϕ_r. In the present paper, however, the ϕ_i ($i \leqq 4$) and ϕ_r orbitals will be considered as linear combinations of ns, np orbitals of A atom and 1s's of H atoms, and the properties on the ϕ_5 orbital will be discussed in taking the interaction with the ϕ_r orbital into account[13]. In such an argument, the repulsive state with configuration $K(\phi_1)^2(\phi_2)^2(\phi_3)^2(\phi_4)(\phi_r)$ may be a rather high location near the equilibrium structure. In a similar way, the electronic structures of the ground and the first excited state of a free AH_{N-1} radical can be represented by respectively $K'(\phi_1')^2(\phi_2')^2(\phi_3')^2(\phi_4')$ and $K'(\phi_1')^2(\phi_2')^2(\phi_3')(\phi_4')^2$ or $K'(\phi_1')^2(\phi_2')^2(\phi_3')^2(\phi_5')$, in which the dashes are given in order to distinguish that it is a free radical.

Actually, the stable structures of the AH_4, AH_3 and AH_2 molecules discussed here are respectively tetrahedral, pyramidal and isosceles triangle, the symmetry of which are T_d, C_{3v} and C_{2v} respectively. By taking the order of the increasing energy, the MOs ϕ_i's for each symmetry and the common bonding power near the equilibrium form can be listed as given in Table I. As can be seen from there, the bonding power of the ϕ_5 orbital of AH_N molecules can generally be shown as non-bonding and the difference is not great. But that of the ϕ_4 is somewhat different one to the other, and decreases with decreasing number of hydrogen atoms. This is one reason why the nature of the first excited state cannot be determined simply.

Potential Energy Surface.—Considering the property of ϕ_5 orbital, the first excited state $K(\phi_1)^2(\phi_2)^2(\phi_3)^2(\phi_4)(\phi_5)$ has rather less bonding property than the ground state, since the bonding power of the ϕ_4 orbital is at least not as weak as

12) R. S. Mulliken, *J. Chem. Phys.*, **3**, 517 (1935).

13) The forms of the ϕ_i ($i \leqq 4$) orbitals are scarcely changed at all by including the $(n+1)s$ orbital of A atom and the higher orbitals (J. Higuchi, unpublished work).

compared with the ϕ_5 orbital. In the approximation of single configuration, therefore, this state is not repulsive and may reach the excited doublet state $K'(\phi_1')^2(\phi_2')^2(\phi_3')(\phi_4')(\phi_5')$, or $K'(\phi_1)^2(\phi_2')^2(\phi_3')^2(\phi_5')$, of the free AH_{N-1} radical and the $1s\ ^2S$ state of the H atom by increasing one of the AH internuclear distances. The above doublet state of the AH_{N-1} radical, however, is in a rather high location as compared with the ground state $K(\phi_1')^2(\phi_2')^2(\phi_3')^2(\phi_4')$, since the ϕ_5' orbital has also a considerable $(n+1)s$ orbital character. In such a single configurational approximation, therefore, the fact that the first excited state of the AH_N molecule leads to decomposition cannot be explained.

The energy of the repulsive orbital ϕ_r is, however, rapidly lowered with increasing one of the AH internuclear distances because of the decrease of the overlap integrals, and so the ϕ_r orbital becomes the fifth orbital on the energetic ground. In the present paper, however, for convenience the sufficies i's are not changed at larger AH internuclear distances. Accordingly, some repulsive state $K(\phi_1)^2(\phi_2)^2(\phi_3)^2(\phi_4)(\phi_r)$ exists, which may reach the ground state $K'(\phi_1')^2(\phi_2')^2(\phi_3')^2(\phi_4')$, or the first excited state $K'(\phi_1')^2(\phi_2')^2(\phi_3')^2(\phi_4')(\phi_r')$, of the AH_{N-1} radical. However, this repulsive state has the same symmetry as that of the first excited state $K(\phi_1)^2(\phi_2)^2(\phi_3)^2(\phi_4)(\phi_5)$, and the former potential energy surface crosses that of the latter one near a somewhat larger AH internuclear distance in the single configurational approximation. In view of these facts, it is possible that the AH_N molecule decomposes to give the free AH_{N-1} radical and the H atom beyond the crossing curve between the above-mentioned potential energy surfaces.

Primary Process.—In general, no electronic spectrum of the AH_N molecule exists up to comparatively short wave-lengths, occasionaly until the Schumann region[1-6]. The first absorption spectrum of the AH_N molecule occurs as a continuum or as diffuse bands and is presumed to occur because of the transition from the ϕ_4 orbital to the ϕ_5 orbital. By absorbing the light of this region, the molecules are generally excited to the above-mentioned first excited singlet state, which is the lowest member of the Rydberg series of the molecule. The excited molecule dissociates to the ground, or the first excited, state of AH_{N-1} radical and the ground state $1s\ ^2S$ of H atom due to some of the AH stretching vibrations, beyond the crossing point between the first and the repulsive excited states. In this case, the shape of the potential energy surface of the first excited state differs from one molecule to the other, and so the condition of the photochemical decomposition is not always quite the same. However, it may be noted that the following rules are valuable to discuss the types of photochemical decomposition in the first absorption region.

(1) The first absorption spectrum is continuous, if the highest occupied orbital ϕ_4 is considerably strong-bonding.

(2) In the case of the highest occupied orbital ϕ_4 being not so strong-bonding, the type of the first absorption spectrum is determind from the antibonding property of the first excited state due to the interaction between the lowest vacant orbital ϕ_5 and the strong-antibonding orbital ϕ_r. In this case, (2a) the spectrum may be diffuse, if the ϕ_r orbital is not so strong-antibonding; (2b) the spectrum may be continuous, if the ϕ_r orbital is considerably strong-antibonding.

The reason for this can be explained as follows: in the case of (1) the AH equilibrium bond distance in the first excited state is fairly lengthened, and so the crossing may take place near the equilibrium internuclear distance of this state. Since the first and the repulsive state have the same symmetry, the actual potential energy curve to this decomposing direction may not have a maximum point. Accordingly, the decomposition in the first excited state takes place very easily by some of the AH stretching vibrations and the first absorption spectrum occurs as a continuum. In the case of (2a), however, the equilibrium internuclear distance in the first excited state is not so large that the crossing may take place at a somewhat larger AH internuclear distance than the equilibrium one. Accordingly, the actual potential energy curve to this decomposing direction may have a maximum point and the first absorption spectrum occurs as diffuse.

These rules, however, are also not useful to determine the state of the decomposed free AH_{N-1} radical, when its many states are lower than the first excited state of the AH_N molecule. In this case, certainly the adiabatic correlation rule occasionally plays some important role, but generally is not useful because of the lowering of symmetry for the intermediate. For the determination of the states of

products, therefore, it may be safe to investigate each molecule, at least to make a distinction of the molecule according to its symmetry, as will be discussed in the following chapters.

3. Primary Process in Photochemical Decomposition of AH_4 Molecules

The photolysis of the AH_4 molecule, such as CH_4, SiH_4, GeH_4, etc., has been investigated by several authors, but the works except for the CH_4 molecule are very few[13]. The first absorption of the molecules occurs as continuum below about 1600 Å, but no bands have been observed[1,5]. The primary process in photochemical decomposition by this absorption has been considered as follows:

$$AH_4 + h\nu \longrightarrow AH_3 + H,$$

although the other process has also been considered in shorter wave-lengths[1].

Electronic Structure.—The AH_4 molecule has tetrahedral symmetry T_d and the electron configuration of the ground state $^1A_1$ is $K(1a_1)^2(1t_2)^6$, and that of the first excited states $^{1,3}T_2$ is $K(1a_1)^2(1t_2)^5(2a_1)$. The $1a_1$ and the $1t_2$ orbitals are strong-bonding, while the $2a_1$ orbital is nearly non-bonding and has $(n+1)s$-like property of the A atom. Accordingly, the equilibrium bond distance of the $^{1,3}T_2$ states may be lengthened as compared with that of the ground state $^1A_1$, because of the excitation from the strong-bonding orbital $1t_2$ to the nearly non-bonding orbital $2a_1$. As discussed in the previous chapter, however, the molecule has a higher anti-bonding orbital ra_1, and so the repulsive $^3T_2$ state $K(1a_1)^2(1t_2)^5(ra_1)$ is also expected.

On the other hand, the AH_3 radical may be low-pyramidal with symmetry C_{3v} (or may occasionally be planar with symmetry D_{3h}). The electron configuration of the ground state $^2A_1$ (or $^2A_2''$) is $K(1a_1)^2(1e)^4(2a_1)$ (or $K(1a_1')^2(1e')^4(1a_2'')$), and the $1a_1$ (or $1a_1'$) and the $1e$ (or $1e'$) orbitals are strong-bonding, while the $2a_1$ (or $1a_2''$) orbital is weak-bonding (or non-bonding). The excited states of the AH_3 radical also exist, for example, ^2E $K(1a_1)^2(1e)^3(2a_1)^2$ (or $^2E'$ $K(1a_1')^2(1e')^3(1a_2'')^2$) and $^2A_1$ $K(1a_1)^2(1e)^4(3a_1)$ (or $^2A_1'$ $K(1a_1')^2(1e')^4(2a_1')$), but they are rather high as compared with the first excited state of the corresponding AH_4 molecules as shown in Fig. 1. Accordingly, they are not responsible for this reaction and need not be discussed in detail.

TABLE II
CORRELATION BETWEEN REPRESENTATIONS OF GROUPS $T_d-C_{3v}-D_{3h}$

T_d	C_{3v}	D_{3h}
A_1	A_1	A_1', A_2''
A_2	A_2	A_2', A_1''
E	E	E', E''
T_1	A_2, E	A_2', A_1'', E', E''
T_2	A_1, E	A_1', A_2'', E', E''

Potential Energy Surface.—The correlation between representations of groups $T_d-C_{3v}-D_{3h}$ is given in Table II. By increasing one of the AH internuclear distances, the first excited states $^{1,3}T_2$ of the AH_4 molecule with symmetry T_d reaches the $^2A_1$ state $K(1a_1)^2(1e)^4(3a_1)$ (or $^2A_1'$ $K(1a_1')^2(1e')^4(2a_1')$) of the AH_3 radical with symmetry C_{3v} (or D_{3h}) and the ^2S state of the H atom, passing through the $^{1,3}A_1$ state $K(1a_1)^2(1e)^4(2a_1)(3a_1)$ of the intermediate AH_4 with symmety C_{3v}, in the approximation of single configuration. But the repulsive excited state $^3T_2$ of the AH_4 molecule reaches the ground state $^2A_1$ (or $^2A_2''$) of the AH_3 radical and the ^2S state of the H atom[14]. The first and the repulsive excited states of the AH_4 molecule, however, have the same symmetry T_2 and so their interaction is not so weak. Furthermore, the equilibrium bond distance of the first excited state is fairly

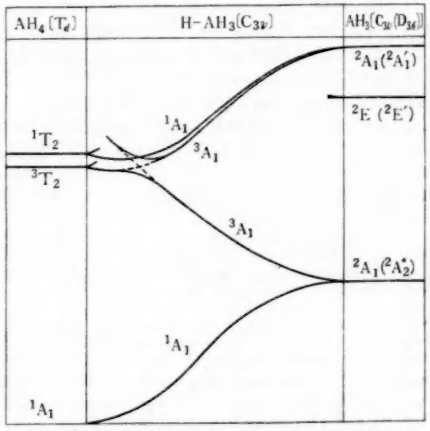

Fig. 1. Potential energy curves for photochemical decomposition of AH_4 molecule. The relative energy scale of the right and the left part was chosen to fit the CH_4 molecule and the CH_3 radical.

14) The instability of the $^{1,3}T_2$ states can also be supposed from the Jahn-Teller effect.

large, and the variation of energy by changing the AH internuclear distance may be small in this region. Accordingly, the actual potential energy curve of the first excited state $^3T_2$ to the $^2A_1$ state of the AH_3 radical may not have a maximum point as shown in Fig. 1[15]. As the result of this, the first absorption spectrum of the AH_3 molecule occurs as a continuum (case (1) of the rule in Chapter 2).

Primary Process.—In the AH_3 molecule, the influence of vibration is not important because the first excited states $^{1,3}T_2$ electronically correlate to the $^2A_1$ (or $^2A_2''$) state of the AH_3 radical and the ^2S state of the H atom[16]. It may, therefore, be most convenient to explain the mechanism from the electronic and energetic viewpoints. That is, the AH_3 molecule absorbing the wave-length of about 1600 Å is excited to the first $^1T_2$ state[17]. The excited molecule dissociates to the $^2A_1$ (or $^2A_2''$) state of the free AH_3 radical and the 1*s* ^2S state of the H atom due to the singlet-triplet transition and to some of the AH stretching vibration, passing through the intermediate with symmetry C_{3v} as shown in Fig. 1. In the meanwhile, the bond angle of ∠HAH′ may gradually be increased by the action of the AH bending vibration. The electronic property of the highest singly occupied orbital also changes from $(n+1)s$-like nearly non-bonding to strong-antibonding beyond the above-mentioned crossing point. The process passing through the other structures of the intermediates can also be considered. That is, it may be probable that one of the H atoms is slightly displaced from the trigonal axis in the excited state. Certainly, the process passing through this intermediate is not contradictory to the adiabatic correlation rule, and the potential energy curve and the electronic property in such a possible process are generally similar to those in the above-mentioned case. Accordingly, such processes are not discussed here in detail.

4. Primary Process in Photochemical Decomposition of AH_3 Molecules[18]

The photolysis of the NH_3 molecule has long been investigated by many authors, and that of the PH_3, AsH_3 and SbH_3 molecules has also been studied by several authors[4]. The first absorption spectrum of the NH_3 and the PH_3 molecules begins at about 2300 Å as diffuse bands, but that of the AsH_3 and the SbH_3 molecules appears to be continuous below about 2400 Å[4,5]. The primary process in the photochemical decomposition by this absorption has generally been considered to be predissociation:

$$AH_3 + h\nu \longrightarrow AH_3^* \longrightarrow AH_2 + H.$$

Electronic Structure.—The AH_3 molecule has pyramidal symmetry C_{3v} and the electron configuration of the ground state $^1A_1$ (or $^1A_1'$ for the symmetry D_{3h}) is $K(1a_1)^2(1e)^4(2a_1)^2$ (or $K(1a_1')^2(1e')^4(1a_2'')^2$). The $1a_1$ (or $1a_1'$) and the $1e$ (or $1e'$) orbitals are strong-bonding, while the $2a_1$ (or $1a_2''$) orbital is weak-bonding (or non-bonding) and its bonding power increases with decreasing bond angle of ∠HAH′. In the ground state of the PH_3, AsH_3 and SbH_3 molecules, the equilibrium bond angles decrease owing to the increase of the *nd*-orbital character of A atom[9,19], and the bonding power of the $2a_1$ orbital increases. As the results of this, the potential barrier of inversion increases with increasing the molecular weight of the AH_3 molecule[20].

The lowest vacant orbital $3a_1$ (or $2a_1'$) is nearly non-bonding and has $(n+1)s$-like property of the A atom, while the ra_1 (or ra_1') is strong-antibonding and the antibonding power increases with decreasing the bond angle ∠HAH′[21]. In the first excited states $^{1,3}A_1$ $K(1a_1)^2(1e)^4(2a_1)(3a_1)$ (or $^{1,3}A_2''$ $K(1a_1')^2(1e')^4(1a_2'')(2a_1')$), the equilibrium AH bond distance is somewhat lengthened and the equilibrium bond

15) In this case, the first excited singlet state $^1T_2$ does not reach the ground state $^2A_1$ of AH_3 from the atomic orbital consideration in the infinite internuclear separation between the AH_3 and the H.

16) The AH_4 molecule with symmetry T_d has nine fundamental vibrations: one with species a_1, one doubly degenerate frequencies with species e and two triply degenerate ones with species t_2. For the electronically excited $^{1,3}T_2$ states, therefore, the corresponding vibronic states to one of the AH stretching vibrations are $^{1,3}T_2\times A_1 = {}^{ev1,3}T_2$ and $^{1,3}T_2\times T_2 = {}^{ev1,3}A_1+{}^{ev1,3}E+{}^{ev1,3}T_1+{}^{ev1,3}T_2$ (In the present paper, only the species symbols for the vibronic states are prefixed by a left superscript ^{ev} to avoid confusion to the electronic states.) Accordingly, all the species come into question and therefore the vibronic correlation rule is not especially important to determine this primary process.

17) The possibility of the excitation to the first triplet state also exists, but may be fairly small as compared with that to the first excited singlet state.

18) Preliminary report on the NH_3 molecule was given in *Proc. Japan Acad.*, **32**, 276 (1956).

19) This decrease is also due to the considerably larger sizes of atoms, P, As and Sb, than the N atom (See, Ref. 9).

20) A. Gilchrist and L. E. Sutton, *J. Phys. Chem.*, **56**, 319 (1952).

21) This is due to the increase of *s-p* hybridization in the ϕ_r orbital, the coefficients of which have opposite signs to those of the 1*s*'s of H atoms. (See, Ref. (11)).

angle $\angle HAH'$ increases as compared with that of the ground state, since the one electron excitation from the weak-bonding $2a_1$ orbital decreases the power of bonding and also of pyramidalization. In fact, the first excited state of the NH_3 molecule is planar[11] and that of the other molecules are also expected to have a fairly large equilibrium bond angle.

On the other hand, the AH_2 radical is an isosceles triangle with symmetry C_{2v}. The ground state is the $^2B_1$ $K(1a_1)^2(1b_2)^2(2a_1)^2(1b_1)$ and the first excited state is the $^2A_1$ $K(1a_1)^2(1b_2)^2(2a_1)(1b_1)^2$. The energy separation between these states is not so large, for example, less than 2 eV for the NH_2 radical[22]. The $1a_1$ and the $1b_2$ orbitals are strong-bonding and the $2a_1$ orbital is weak-bonding but the $1b_1$ orbital is non-bonding, The higher excited states of the radical also exist, but they are high location as compared with the first excited states $^{1,3}A_1$ (or $^{1,3}A_2''$) of the corresponding AH_3 molecule. Accordingly, they are not responsible for this reaction and need not be discussed in detail.

Potential Energy Surface.—To discuss the potential energy surfaces, it is convenient to make a distinction between the process passing through the planar intermediate and the others, since the most stable structure of the first excited states are planar and the correlation between the planar molecules is characteristic. Accordingly, the correlations between representations of groups in Table III are separately given for $C_{3v}-D_{3h}-C_{2v}$ and $C_{3v}-C_s-C_{2v}$.

TABLE III

CORRELATION BETWEEN REPRESENTATIONS OF GROUPS $C_{3v}-D_{3h}-C_{2v}$ AND $C_{3v}-C_s-C_{2v}$

C_{3v}	D_{3h}	C_{2v}
A_1	A_1'	A_1
	A_2''	B_1
A_2	A_2'	B_2
	A_1''	A_2
E	E'	A_1, B_2
	E''	A_2, B_1
C_{3v}	C_s	C_{2v}
A_1	A'	A_1, B_1
A_2	A''	A_2, B_2
E	A', A''	A_1, A_2, B_1, B_2

For the planar AH_3 molecule with symmetry D_{3h}, the first excited states decompose to AH_2+H passing through the intermediate AH_3 molecule with symmetry C_{2v}. As can be seen from Table III, the ground state $^1A_1'$ $K(1a_1')^2(1e')^4(1a_2'')^2$, the first excited states $^{1,3}A_2''$ $K(1a_1')^2(1e')^4(1a_2'')(2a_1')$ and the repulsive excited states $^{1,3}A_2''$ $K(1a_1'')^2(1e')^4(1a_2'')(ra_1')$ of AH_3 with symmetry D_{3h} correspond to respectively the ground states $^1A_1$ $K(1a_1)^2(1b_2)^2(2a_1)^2(1b_1)^2$, the first excited states $^{1,3}B_1$ $K(1a_1)^2(1b_2)^2(2a_1)^2(1b_1)(3a_1)$ and the repulsive excited states $^{1,3}B_1$ $K(1a_1)^2(1b_2)^2(2a_1)^2(1b_1)(ra_1)$ of AH_3 with symmetry C_{2v}. As shown in Fig. 2, on stretching one AH bond distance, the ground state $^1A_1'$ becomes gradually unstable, and dissociates to the $^2A_1$ state of the AH_2 radical. Similarly, the first excited states $^{1,3}A_2''$ are also elevated and reach the second $^2B_1$ (or $^4B_1$) state $K(1a_1)^2(1b_2)^2(2a_1)(1b_1)(3a_1)$ of the AH_2 radical. On the other hand, the repulsive excited states $^{1,3}A_2''$ are continuously lowered with increasing one AH bond distance and dissociate to the ground state $^2B_1$. It is, however, noted that in the first excited states the difference of the equilibrium bond distance from the ground state is not much great, since the ϕ_4 orbital is the non-bonding $1a_2''$ and the antibonding property due to the interaction between the $2a_1'$ and the ra_1' orbital is rather weak because of no p-character in these orbitals. This makes possible the large deviation between the internuclear separation of the first excited state in equilibrium and that of the corresponding crossing point, and also makes possible the fairly large energy difference between these points. Accordingly, a maximum point exists in each actual potential energy curve of the first $^{1,3}B_1$ states as shown in Fig. 2, and the first absorption spectrum appears as diffuse in this process (case (2a) of the rule in Chapter 2, for example,

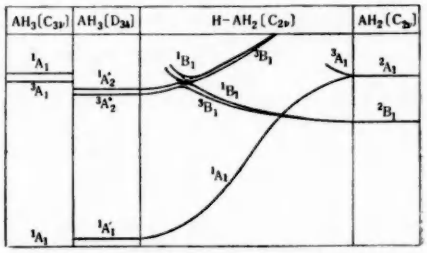

Fig. 2. Potential energy curves for photochemical decomposition of AH_3 molecule passing through the planar intermediate. The relative energy scale of the right and the left part was chosen to fit the NH_3 molecule and the NH_2 radical.

22) G. Herzberg and D. A. Ramsay, *Discussions Fraday Soc.*, No. 14, 11 (1952).

NH_3). At a fairly larger AH internuclear distance, the crossing between the $^{1,3}B_1$ states and the $^1A_1$ state also takes place, but their interactions need not be taken into consideration so greatly, because their symmetries are not the same.

For pyramidal AH_3 molecule with symmetry C_{3v}, the molecule dissociates to AH_2+H passing through the intermediate AH_3 with symmetry C_s. Analogous relations also exist in this case as shown in Fig. 3. The first excited states $^{1,3}A_1$, however, may be somewhat stabilized with the small increase of one AH bond distance, since the $2a_1$ orbital is weak-bonding. Furthermore, the bonding power of the $2a_1$ orbital and the antibonding power of the ra_1 orbital increases with decreasing the bond angle of $\angle$HAH', so that the stabilization by increasing one AH bond distance also increases[10]. Accordingly, the potential barrier in the crossing point of the first excited state $^3A'$ may be lowered and finally the potential energy curve may not have a maximum point at a bond angle smaller than a certain value. This tendency becomes strong with increasing molecular weight of the AH_3 molecule due to the stabilization of the $2a_1$ orbital under the influence of the *nd*-orbital character of the A atom in the molecule, and the first absorption spectrum appears as continuous (case (2b) of the rule in Chapter 2). Another difference from the planar molecule is the non-crossing between the ground state $^1A'$, which correlates with the $^1A_1$ state of C_{2v}, and the first excited singlet state $^1A'$, which correlates with the $^1B_1$ state of C_{2v}. Their symmetries are the same except for the symmetry C_{2v}, so that their interaction increases with decreasing the bond angle $\angle$HAH'. Consequently, the potential energy curve of the first excited singlet state $^1A_1$ of AH_3 reaches the $^2A_1$ state of AH_2. The first excited triplet state $^3A_1$, however, reaches the $^2B_1$ state of AH_2 passing through the intermediate with symmetry C_s, because of the difference in the spin multiplicities.

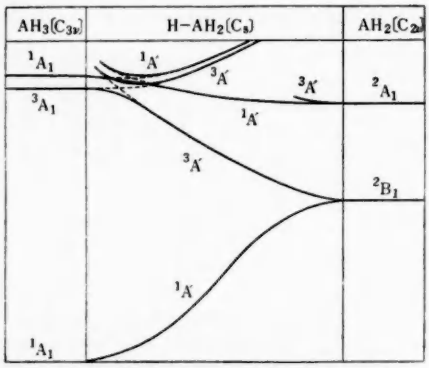

Fig. 3. Potential energy curves for photochemical decompostion of AH_3 molecule passing through the non-planar intermediate.

Primary Process.—In the primary process in photochemical decomposition, the AH_3 molecule in the ground state $^1A_1$ (or $^1A_1'$) absorbs the wave-length of about 2200 Å, and is excited to the first excited singlet state $^1A_1$. In the first excited states $^{1,3}A_1$, the planar molecule with symmetry D_3 is in general most stable, so that the probability of taking this shape is very large for light AH_3 molecules.

Few of the excited molecules return to the ground state and most of them decompose to the free AH_2 radical and the H atom due to some of the AH stretching vibrations. The AH_3 molecule with symmetry C_{3v} (or D_{3h}) has four fundamental vibrations: two with species a_1 and two doubly degenerate frequencies with species e (or one with species a_1', one with species a_2'' and two doubly degenerate frequencies with species e'). Accordingly, the mode of the AH stretching vibration has species a_1 (or a_1') or preferably e (or e'), and so the corresponding vibronic state, which arises from the excitation of such a vibrational mode, is $^1A_1\times A_1={}^{ev1}A_1$ (or $^1A_2''\times A_1'={}^{ev1}A_2''$) or preferably $^1A_1\times A_1={}^{ev1}E$ (or $^1A_2''\times E'={}^{ev1}E''$).

When the planar molecule with symmetry D_{3h} has been realized, this electronically excited state correlates with the ${}^{ev1}B_1$ state or the ${}^{ev1}B_1$ and ${}^{ev1}A_2$ states of the intermediate AH_3 molecule with symmetry C_{2v}. On the other hand, the free AH_2 radical with symmetry C_{2v} has three fundamental vibrations: two with species a_1 and one with species b_2. Therefore, the corresponding vibronic states are $^2B_1\times A_1={}^{ev2}B_1$ and $^2B_1\times B_2={}^{ev2}A_2$ to the electronic $^2B_1$ state and are $^2A_1\times A_1={}^{ev2}A_1$ and $^2A_1\times B_2={}^{ev2}B_2$ to the electronic $^2A_1$ state. Besides this, the electronic state of the H atom in question is $1s\ ^2S$. This means that in this case the restriction between these electronic states is not changed by the influence of vibration. For the excited AH_3 molecule with symmetry D_{3h}, therefore, the decomposition takes place passing through the potential energy curve shown in Fig. 2, and the products are the $^2B_1$ state of AH_2 and the ^2S state of H, but

are not the $^2A_1$ state of AH_2 and the ^2S state of H. In the meanwhile, the bond angle of $\angle HAH'$ may be changed by the action of the AH bending vibration from 120° to a somewhat small angle, for example 103° for NH_2[23]. On the other hand, the possibility of the process passing through the triplet state may generally be very small because of the inhibition by the spin correlation rule.

Especially for the heavy AH_3 molecules, the planar first excited state is not necessarily realized and the decomposition may take place passing through the intermediate with symmetry C_s, because the equilibrium bond angle of these molecules is nearly 90° in the ground state. In this case, the influence of vibration may not be so important, since both the first excited states $^{1,3}A_1$ of AH_3 are possible to correlate electronically to both the $^2B_1$ and $^2A_1$ states of AH_2[24]. Consequently, in the case of the decomposition passing through the intermediate with symmetry C_s, the state of product AH_2 cannot be determined from the adiabatic correlation rule. It can, however, be said that the probability of the product being $^2B_1$ state may decrease with decreasing the bond angle of the AH_3 molecule. It is also noted that the process passing through the singlet-triplet transition mainly reaches the $^2B_1$ state of AH_2 from the viewpoint of potential energy surface and is of importance for heavy AH_3 molecules because of the rather strong spin-orbit coupling.

5. Primary Process in Photochemical Decomposition of AH_2 Molecules

The photolysis of the AH_2 molecules, such as H_2O, H_2S, etc., has been investigated by several authors. The first absorption of H_2O and H_2S occurs as a continuum below 1780 Å and 2600Å, respectively[4,5]. The primary process of photochemical decomposition in this absorption has been considered as follows:

$$AH_2 + h\nu \longrightarrow AH + H.$$

Electronic Structure.—The AH_2 molecule is an isosceles triangle with symmetry C_{2v}. The electron configuration of the ground state $^1A_1$ is $K(1a_1)^2(1b_2)^2(2a_1)^2(1b_1)^2$, and that of the first excited states $^{1,3}B_1$ is $K(1a_1)^2(1b_2)^2(2a_1)^2(1b_1)(3a_1)$. The $1a_1$ and $1b_2$ orbitals are strong-bonding, while the $2a_1$ is weak-bonding and its bonding power increases with decreasing bond angle of $\angle HAH'$. The highest occupied orbital $1b_1$ is non-bonding and the lowest vacant orbital $3a_1$ is also nearly non-bonding and has $(n+1)s$-like property of the A atom. The vacant orbital ra_1 is strong-antibonding and its antibonding power increases with decreasing bond angle of $\angle HAH'$[21] and also with increasing ordinal number of Periodic Group of the central atom A, because of the increase of p-character[25].

On the other hand, the AH radical is a linear form with symmetry $C_{\infty v}$. The electron configuration of the ground state $^2\Pi$ is $K(1\sigma)^2(2\sigma)^2(1\pi)^3$, in which the 1σ orbital is strong-bonding and the 2σ orbital is weak-bonding while the 1π orbital is non-bonding. The excited states of the AH radical also exist, for example $^2\Sigma^+$ $K(1\sigma)^2(2\sigma)(1\pi)^4$ and $^2\Sigma^+$, $^{2,4}\Sigma^-$ and $^2\Delta$ $K(1\sigma)^2(2\sigma)^2(1\pi)^2(3\sigma)$, but they are rather high as compared with the first excited states of the corresponding AH_2 molecule. Accordingly, they are not responsible for this reaction and are not discussed here in detail.

Table IV

Correlations between representations of groups $C_{2v}-C_s-C_{\infty v}$ and $C_{2v}-D_{\infty h}-C_{\infty v}$

C_{2v}	C_s	$C_{\infty v}$
A_1, B_2	A'	Σ^+, Π, Δ,……
A_2, B_1	A''	Σ^-, Π, Δ,……

C_{2v}	$D_{\infty h}$	$C_{\infty v}$
A_1	Σ_g^+, Π_u, Δ_g,……	Σ^+, Π, Δ,……
A_2	Σ_u^-, Π_g, Δ_u,……	Σ^-, Π, Δ,……
B_1	Σ_g^-, Π_u, Δ_g,……	Σ^-, Π, Δ,……
B_2	Σ_u^+, Π_g, Δ_u,……	Σ^+, Π, Δ,……

Potential Energy Surface.—The AH_2 molecule with symmetry C_{2v} (or $D_{\infty h}$) dissociates to AH+H passing through the intermediate with symmetry C_s (or $C_{\infty v}$). Then, Table IV gives the correlations between representations of groups $C_{2v}-C_s-C_{\infty v}$ and $C_{2v}-D_{\infty h}-C_{\infty v}$. The ground state $^1A_1$, the first excited states $^{1,3}B_1$ and the repulsive excited states $^{1,3}B_1$ of the AH_2 with symmetry C_{2v} correspond to respectively the ground state $^1A'$, the first excited states $^{1,3}A''$ and the repulsive excited

23) D. A. Ramsay, *J. Chem. Phys.*, **25**, 188 (1956).

24) In this case, the $^{ev1,3}A_1$ state, or the $^{ev1,3}E$ states, which correlate with the first excited states $^{1,3}A_1$, correlates with the $^{ev1,3}A'$ states, or the $^{ev1,3}A'$ and $^{ev1,3}A''$ states, of the intermediate AH_3 molecule with symmetry C_s. Accordingly, all the species come into question and therefore the vibronic correlation rule is not especially important to determine this primary process.

25) This is the result of the increase of the ionization energy difference between the ns and the np orbital of the A atom.

states $^{1,3}A''$ of the AH_2 with symmetry C_s. By increasing one of the AH internuclear distances, the first excited states $^{1,3}B_1$ reach the $^{2,4}\Pi$ states $K(1\sigma)^2(2\sigma)(1\pi)^3(3\sigma)$ of the AH radical and the 1s ^2S state of the H atom in the approximation of single configuration, while the ground state $^1A_1$ and the repulsive excited states $^{1,3}B_1$ reach the ground state $^2\Pi$ $K(1\sigma)^2(2\sigma)^2(1\pi)^3$ of the AH radical and the 1s ^2S state of the H atom. Accordingly, the crossings between the first and the repulsive excited states take place. But the ra_1 orbital is very strong-antibonding, so that the antibonding property of the first excited states due to the interaction between the $3a_1$ and the ra_1 orbital is not so weak, and the elevation of the potential energy curves of these states to the crossing points may be small. As the result of this, the actual potential energy curves may not have a maximum point as shown in Fig. 4, and the first absorption spectrum of the molecule appears as continuous (case (2b) of the rule in Chapter 2)[26]. It is noted that such an argument is generally valid when the linear first excited states are realized.

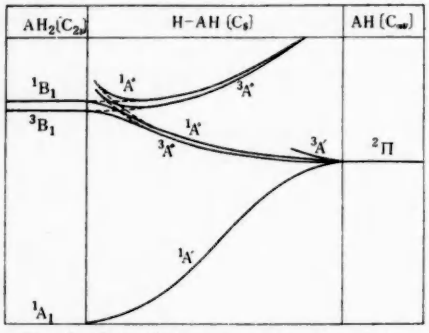

Fig. 4. Potential energy curves for photochemical decomposition of AH_2 molecule. The relative energy scale of the right and the left part was chosen to fit the H_2O molecule and the OH radical.

Primary Process.—In the AH_2 molecule, the influence of vibration is not so important, because all the decomposition to the $^2\Pi$ state of AH are electronically allowed[27]. Accordingly, the primary process in the photochemical decomposition of the AH_2 molecule can be explained as follows: the AH_2 molecule absorbs a rather short wave-length (for example, about 1800 Å for H_2O and about 2600 Å for H_2S) and is excited to the first excited state $^1B_1$[17]. The excited molecule dissociates to the $^2\Pi$ state of the free AH radical and the 1s ^2S state of the H atom due to some of the AH stretching vibration, passing through the intermediate with symmetry C_s. In this case, the realization of the linear intermediate with symmetry $C_{\infty v}$ may also be possible, since the equilibrium bond angle $\angle$HAH' in the first excited states may be expected to be fairly large as compared with the ground state. Meanwhile, the electronic property of the highest singly occupied orbital changes from $(n+1)s$-like non-bonding to strong-antibonding beyond the above-mentioned crossing. The process passing through the singlet-triplet transition can also be considered, but the products are the same as in the above case and the possibility may be small from the viewpoint of spin conservation. The conclusion in the present discussion is consistent with the experimental result that the fluorescence of the OH radical has never been observed in the direct photolysis of the H_2O molecule[28].

6. Some Remarks

The discussions in the present paper are rather similar to those of Mulliken[29] and of Walsh[7,8]. The purpose of these papers, however, was the explanation of spectra of the AH_N molecules and others and not of the primary process in photochemical decomposition, so that the discussion of potential energy surface were hardly done at all. Moreover, in the former, the available data at that time were rather few so that the discussion are not necessarily complete at present. In the latter, the $(n+1)s$-like orbital ϕ_5 and the antibonding orbital ϕ_r were separately treated, so that the explanations are not only ambiguous but involve some error. Accordingly, the present paper may be said to be the first one relevant to the primary process in photochemical decomposition in the approximation of the molecular orbital.

26) The difference of the potential energy surface between the cases of diffuse and continuous bands may be expected to be small by taking into consideration of the results of the free CH_3 and CD_3 radcials (G. Herzberg and J. Shoosmith, *Can. J. Phys.*, **34**, 523 (1956)).

27) The AH_2 molecule with symmetry C_{2v} has three fundamental vibrations: two with species a_1 and one with species b_2. For the first and repulsive excited states $^{1,3}B_1$, therefore, the corresponding vibronic states are $^{1,3}B_1\times A_1=^{e\nu 1,3}B_1$ and $^{1,3}B_1\times B_2=^{e\nu 1,3}A_2$. As can be seen from Table IV, they evidently correlate to the $^2\Pi$ state of the AH radical, since the AH has only one stretching vibration σ.

28) L. O. Brown and N. Miller, *Trans. Faraday Soc.*, **51**, 1623 (1955).

29) R. S. Mulliken, *J. Chem. Phys.*, **3**, 506 (1935).

In the present consideration, the vacant orbitals were treated as nearly non-bonding $(n+1)s$-like and strong-antibonding. In the precise discussion, however, this consideration is not always sufficient to the present purpose, and the mixing of the $(n+1)s$ and higher orbitals, or more strictly the effect of configuration interaction, must explicitly be included. In that case, the crossing between the potential energy curves with the same symmetry and the same spin multiplicity need not be taken into consideration and more satisfactory results will be expected. For example, the potential energy curve of the first excited singlet state of NH_3 will be obtained so as to give an explanation of the predissociation without the crossing. However, it may be said that the present consideration based on the approximation of single configuration is also convenient to a schematic understanding of the reactions.

The author wishes to thank Professor S. Shida for his helpful advice and kind discussion. He also wishes to thank Mr. Y. Mori for his valuable suggestion and instructive discussion. This research is supported in part by the grant in aid for the miscellaneous scientific researches of the Ministry of Education.

Laboratory of Physical Chemistry
Tokyo Institute of Technology
Ookayama, Meguro-ku, Tokyo

An Electron Diffraction Investigation of the Molecular Structure of 1,4-Dichlorobutyne. I. Determination of Bond Distances and Angles*

By Kôzo·Kuchitsu

(Received January 7, 1957)

1. Introduction

Thermodynamic measurements have shown that the C–C≡C–C axis in dimethylacetylene has no appreciable restriction on the internal rotation of the two end groups around this axis[1–3]. One is thus led to an expectation that the hindering barriers for substituted dimethylacetylene molecules would be much lower than that for the corresponding ethane derivatives, because the distance of the groups in the former is much longer than that in the latter. This has been confirmed by the measurement of the dipole moment of 1,4-dichloro-2-butyne, $ClCH_2–C≡C–CH_2Cl$[4,5].

This molecule seems to stimulate an electron diffraction investigation, because a heavy chlorine atom with a relatively large scattering power is included in each rotating group, so that the diffraction pattern will give us some information of the potential barrier; in addition, there have been reported very few electron-diffraction studies on the internal rotation of the molecules whose potential barriers are relatively low[6].

It is of particular importance to determine the C–Cl bond distances of this molecule. Pauling and his coworkers[7] found, by using visual electron diffraction data, that the C–Cl bond distance in propargyl chloride, H–C≡C–CH_2Cl, is 1.82± 0.02Å. This result is very striking, for it is well known that the carbon-chlorine bond distances in most chlorinated hydrocarbon molecules[8] are about 1.77Å ("normal" C–Cl bond distance), or shorter

* Presented at the Eighth Annual Meeting of the Chemical Society of Japan, April, 1955.

1) B. L. Crawford, Jr. and W. W. Rice, *J. Chem. Phys.*, **7**, 437 (1939).

2) G. B. Kistiakowsky and W. W. Rice, ibid., **8**, 618 (1940).

3) D. W. Osborne, C. S. Garner and D. M. Yost, ibid., **8**, 131 (1940).

4) Y. Morino, I. Miyagawa, T. Chiba and T. Shimozawa, This Bulletin, **30**, 222 (1957).

5) Y. Morino, I. Miyagawa and A. Wada, *J. Chem. Phys.*, **20**, 1976 (1952).

6) For example Si_2Cl_6. (K. Yamasaki, et al., *J. Chem. Soc. Japan.* **69**, 104 (1948); D. A. Swick and I. L. Karle, *J. Chem. Phys.*, **23**, 1499 (1955)). See also Ref. 24.

7) L. Pauling, W. Gordy and J. H. Saylor, *J. Am. Chem. Soc.*, **64**, 1753 (1942).

8) P. W. Allen and L. E. Sutton, *Acta Cryst.*, **3**, 46 (1950).

(e. g., 1.72Å in C_2Cl_4)[9], and we have seldom found molecules whose C–Cl bond distances are longer than 1.80Å[10,11]. If this abnormal increase is based on a special property of $-C\equiv C-CH_2Cl$ group, then it may be of interest to decide whether the C–Cl bond in $ClCH_2-C\equiv C-CH_2Cl$ molecule is longer than the "normal" distance or not. Furthermore, various data on $C\equiv C-C$ system[12–14] show that the C–C bond distance adjacent to a triple bond is about 1.46Å, much shorter than its normal value, and is nearly constant. Therefore, it is also desirable to determine the C–C bond distance accurately and to compare it with the known results.

The subject of this article is the determination of the bond distances and angles of this molecule by the electron diffraction method with a view to apply this structural information as basic data for the study of internal rotation in this molecule, which will be discussed in the following article[15].

2. Experimental[16]

The electron diffraction instrument used in this investigation which incorporates a rotating sector was designed by Morino, Kimura and Iwasaki[17]. The apparatus is essentially similar to that constructed by Ino[18].

Diffraction photographs were obtained on Fuji Process Hard Plates with an r^2-sector, which was placed 23.7 mm. from the photographic plate and was rotated rapidly during exposure. A camera length was either 11.82 cm. or 27.91 cm., to cover the angular range of 15 to 90, and 5 to 27 in q units, respectively. The accelerating voltage of the electron source was regulated to within 0.1 percent., and the electron beam was focused on the photographic plate to a point about 0.1 mm. in diameter. The wavelength of the electron was determined to be 0.0565Å by measuring the transmission patterns of gold foil.

1, 4-Dichloro-2-butyne was prepared by T. Shimozawa of our laboratory from 2-butyne-1, 4-diol and thionyl chloride[19], the boiling point being 62–64°C at 18 mmHg. The sample was introduced into the electron beam through a fine nozzle by heating to about 40°C[20]. The nozzle was surrounded by a liquid air trap to prevent the sample from diffusing through the camera. A set of two photographs were taken with consecutive exposures of 1/2 and 1 min. which were later used for density-intensity calibration[21]. The patterns were scanned by a Riken B-type recording microphotometer to measure the optical density as a function of the radius[22]. The photographic plates were rotated rapidly about the center of the diffraction pattern while being scanned by the microphotometer.

Optical densities were converted in to relative intensities by Karle's procedure[21]. The scattering intensity curve obtained with a short camera length was corrected to eliminate a small amount of extraneous scattering. A smooth background line was drawn through the intensity curve multiplied by q(L=11.82 cm.) or $q^{1/2}$(L=27.91 cm.), and the molecular intensity curve $M(q)$ was obtained by dividing the total intensity I_T by the background intensity I_B: $M(q)=(I_T-I_B)/I_B$. Three sets of photographs were taken at the short camera length and two sets at the long camera length and their respective averages were taken. For comparison, a set of photographs of carbon tetrachloride taken in the same condition was analyzed by the same procedure (Section 3 B).

The molecular intensity curves obtained with the long camera length were found to agree with each other to about 0.1 percent. in a relative intensity scale; in addition, it was found possible to connect these curves smoothly with the molecular intensity curves obtained with the short camera length. However, since the molecular intensity for this molecule is small compared with that for carbon tetrachloride (less than 40 percent), considerably larger experimental errors were involved in the photographs taken with the short camera length, particularly in larger scattering angles. Although it is difficult to estimate various sources of experimental errors individually, a rough measure of their total limit may be given by the discrepancy among the three molecular intensity curves shown in Fig. 1.

The corrections for such effects as the beam size, the sample size, and double scattering were not taken into account, because they have little effect on the determination of bond distances,

9) I. L. Karle and J. Karle, *J. Chem. Phys.*, **20**, 63 (1952).

10) H. J. M. Bowen, A. Gilchrist and L. E. Sutton (*Trans. Faraday Soc.*, **51**, 1341 (1955)) reported the C-Cl bond distance in CH_2=CH-CH_2Cl to be 1.82$_5$±0.025Å.

11) P. W. Allen and L. E. Sutton (*Trans. Faraday Soc.*, **47**, 236 (1951)) also reported the C-Cl bond distance in CH_3COCl to be 1.82±0.02Å. Note, however, that their conclusion was based on the data extended to a rather small scattering angle, and by our recent reinvestigation, it was found to be 1.77±0.02Å. (Y. Morino, et al., *J. Chem. Soc. Japan*, **75**, 647 (1954)).

12) See for example S. H. Bauer and P. Andersen, *Ann. Rev. Phys. Chem.*, **4**, 233 (1953).

13) G. Herzberg and B. P. Stoicheff, *Nature*, **175**, 79 (1955).

14) Recent X-ray study on solid dimethylacethylene $H_3C-C\equiv C-CH_3$ has given the following result: C≡C= 1.21$_1$Å and C-C=1.45$_7$Å. (E. Pignataro and B. Post, *Acta Cryst.*, **8**, 672 (1955)).

15) K. Kuchitsu, This Bulletin, **30**, 399 (1957).

16) Y. Morino and K. Kuchitsu, *J. Chem. Phys.*, (to be published).

17) Y. Morino, M. Kimura and M. Iwasaki, The Sixth Annual Meeting of the Chemical Society of Japan, April 1953.

18) T. Ino, *J. Phys. Soc. Japan*, **8**, 92 (1953).

19) A. W. Johnson, *J. Chem. Soc.*, **1946**, 1009.

20) The shape of this nozzle is similar to that described by M. Kimura and M. Aoki, This Bulletin, **26**, 429 (1953),

21) J. Karle and I. L. Karle, *J. Chem. Phys.*, **18**, 957, 963 (1950).

22) The microphotometric procedure was carried out by using an apparatus at Nagoya University, collaborated by Mr. H. Morimoto and Mr. S. Shibata.

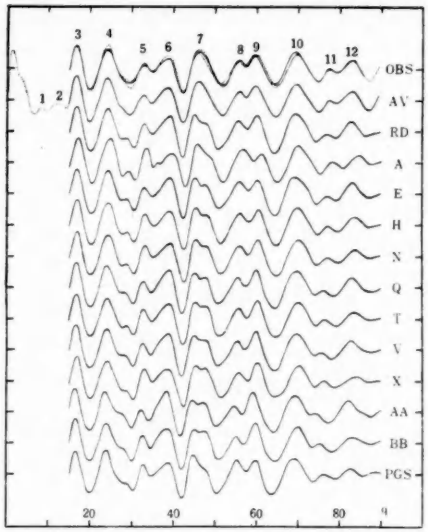

Fig. 1. Observed and calculated molecular scattering intensity curves $qM(q)$ for 1,4-dichlorobutyne.
OBS: three observed intensity curves obtained from independent experiments; AV: the averaged intensity curve, supplemented by a reasonable theoretical intensity curve in the inner region (the dotted curve). The other curves are calculated on the basis of the models indicated in the parameter chart (Fig. 5) (except the models RD and PGS, whose parameters are given in the text).

although they are quite important in the precise investigation of the mean square amplitudes[21,23].

3. Analysis

A. Procedure.—The modified radial distribution (RD) curves[24] were calculated from the molecular intensity curve according to the equation[25]

$$f(r)=\sum_{q=1}^{90} qM(q)\exp(-aq^2)\sin(\pi qr/10), \quad (1)$$

where $M(q)$ is the molecular scattering intensity, the value of a (0.000284) is chosen to make the integrand of Eq. (1) converge rapidly, and $q=(40/\lambda)\sin(\theta/2)$, where θ is the angle of scattering and λ is the wavelength of the electron beam.

The theoretical intensity curves were calculated using the equation[25,26]

$$qM_c(q)=\sum_{i>j}(c_{ij}/r_{ij})\exp(-b_{ij}q^2)\times\sin(\pi qr_{ij}/10), \quad (2)$$

where r_{ij} denotes the interatomic distance between the i-th and the j-th atoms, b_{ij} its temperature factor, and

$$c_{ij}=2Z_iZ_j/\{\sum_i Z_i(Z_i+1)\}, \quad (3)$$

except in the analysis of the small angle region[15], where

$$c_{ij}=2(Z_i-f_i)(Z_j-f_j)/\{\sum_i(Z_i-f_i)^2+S_i\}, \quad (4)$$

was used[27]; Z_i is the atomic number (for hydrogen, an effective value 1.25 was used in place of unity), and f_i and S_i are the elastic and inelastic atomic scattering factors, respectively[28]. These summations were performed by use of punched cards and a Remington Rand Type-285 Model-2 tabulating machine[29,25].

B. Carbon Tetrachloride.—The photographs of carbon tetrachloride were analyzed in the first place, because this molecule has been frequently used as a reference molecule for the determination of atomic distances. A theoretical intensity curve was computed based on the assumption that the C–Cl distance was 1.766Å, and that the mean amplitudes[30] of the C–Cl and the Cl–Cl distance were 0.054 Å and 0.069 Å, respectively[31]. A comparison of this curve with the observed molecular intensity curve shows a good agreement as illustrated in Fig. 2. The average $q_{\text{calcd.}}/q_{\text{obs.}}$ ratio for twenty-one maxima and minima is 1.000 ± 0.002, and the average fluctuation in the $I_{\text{obs.}}/I_{\text{calcd.}}$ ratio for these maxima and minima is 5.8 percent.

The C–Cl distance obtained from this analysis, $1.76_6\pm0.01$Å, coincides with the

23) R. B. Harvey, F. A. Keidel and S. H. Bauer, *J. Appl. Phys.*, **21**, 860 (1950).
24) Y. Morino and E. Hirota, *J. Chem. Phys.*, (to be published).
25) P. A. Shaffer, Jr., V. Schomaker and L. Pauling, *J. Chem. Phys.*, **14**, 648, 659 (1946).
26) M. E. Jones and V. Schomaker, *J. Chem. Phys.*, **19**, 511 (1951).
27) The use of Eq. (3) instead of Eq. (4) causes only a small decrease (about 11 percent at $q=17$, 4 percent at $q=20$, and less than 3 percent at $q>25$) in the peak intensity of a theoretical intensity curve.
28) The f_i and S_i values used here were taken from the table in the following textbook: A. H. Compton and S. K. Allison, "X-Rays in Theory and Experiment", 2nd. Ed., D. Van Nostrand Co., New York, (1936) p. 780. These f_i values are essentially the same as the data published recently; for example, H. Viervoll and O. Ögrim, *Acta Cryst.*, **2**, 277 (1949).
29) Y. Morino and K. Kuchitsu *X-Rays*, **8**, 37 (1954).
30) For simplicity, the term "root mean-square amplitude" will be hereafter referred to as "mean amplitude".
31) Y. Morino et al., *J. Chem. Phys.*, **21**, 1927 (1953).

TABLE I

THE RESULT OF THE ANALYSIS OF THE RADIAL DISTRIBUTION CURVE[a]

		C_1-Cl	C_2-Cl	C_3-Cl	C_4-Cl	$Cl-H$	$Cl-C_2$	$Cl-C_3$
Distance	obs.	1.79_5	2.69	3.71_5	5.08_5	2.38	1.47_7	2.69
	calcd.[b]	—	2.69	3.71	5.07	2.39	—	2.69
Mean Amplitude	obs.	0.055	0.077	0.080	0.123	0.086	0.054	0.051_a
	estd.[c]	0.054	0.073	0.080	0.090	0.114	0.047	0.051
Peak Area	obs.	197.9	223.3	171.2	219.7	53.8	67.8	77.6
	calcd.	204.0	204.0	204.0	204.0	85.0	72.0	72.0
		$C\equiv C$	C_1-C_4	C_1-H	C_2-H	C_3-H	C_4-H	$H-H$
Distance	obs.	1.21_3	4.07	1.10_8	2.10	3.18	4.63	1.80_8
	calcd.	—	4.17	—	2.11	3.23	4.65	1.80
Mean Amplitude	obs.	0.061	0.092	0.077_8	0.092	—	0.092	0.120_3
	estd.	0.036	0.060	0.077	0.120	0.120	0.120	0.120
Peak Area	obs.	39.2	63.1	28.3	34.7	17.7	42.8	3.0_8
	calcd.	36.0	36.0	30.0	30.0	30.0	30.0	3.1

a) Equilibrium distances and mean amplitudes are in Å unit. The subscript a denotes that the values listed were assumed in this analysis.
b) The calculated equilibrium distances are based on the four directly-bonded distances obtained from this analysis and the C-C-Cl angle of 110.5°.
c) Estimated values (see Ref. 34).

TABLE II

COMPARISON OF EXPERIMENTAL AND THEORETICAL INTENSITY CURVES[a]

Peak		Peak Position			Peak Height		
Max.	Min.	q_o	q_c	q_c/q_o	I_o	I_c	I_o/I_c
	1	6.7	6.7	1.000	−0.696	−0.829	0.840
1		8.3	8.3	1.000	−0.440	−0.524	0.840
	2	10.0	10.0	1.000	−0.687	−0.860	0.799
2		12.4	12.4	1.000	−0.367	−0.360	1.019
	3	14.0	13.9	0.993	−0.495	−0.671	0.738
3		16.7	16.7	1.000	1.140	1.393	0.818
	4	19.9	20.1	1.010	−1.018	−1.083	0.940
4		24.2	24.2	1.000	1.038	1.262	0.823
	5	29.7	30.4	(1.023)	−0.698	−0.924	0.755
5		33.0	33.0	1.000	0.222	0.405	0.548
	6	34.8	34.8	1.000	−0.140	−0.162	0.864
6		38.8	38.9	1.003	0.559	0.877	0.637
	7	42.3	42.1	0.995	−1.061	−1.470	0.722
7		45.9	45.2	(0.985)	0.780	0.952	0.819
	8	51.7	50.8	0.983	−0.720	−1.000	0.720
8		55.7	55.6	0.998	0.418	0.619	0.675
	9	57.4	57.7	1.005	0.150	0.143	(1.049)
9		59.6	60.0	1.007	0.682	0.914	0.746
	10	64.5	64.3	0.997	−0.761	−1.238	0.615
10		69.6	69.4	0.997	0.761	0.986	0.772
	11	75.0	74.4	(0.992)	−0.525	−0.545	(0.963)
11		77.3	76.7	(0.992)	0.016	−0.167	(—)
	12	79.1	79.0	(0.999)	−0.160	−0.360	(0.444)
12		82.9	82.8	0.999	0.422	0.600	0.703
	13	86.8	86.4	(0.997)	−0.482	−0.240	(2.008)
Average[b]				1.000			0.744
Average Deviation				0.004			0.078

a) The theoretical intensity curve is based on the results of the RD analysis. The observed data listed above the line (min. 1∼3) are the data obtained from the long camera-length photographs, and their ratios are not included in the average.
b) The ratios enclosed in parentheses are not included in the average either (see Ref. 42).

TABLE III

DISTANCES OBTAINED FROM $q_{calcd.}/q_{obs.}$ VALUES[a]

Acceptable Models	Average $q_{calcd.}/q_{obs.}$	Average deviation	∠C-C-Cl	C−Cl	C−C	C≡C	C−H
J	1.006	0.006	110°	1.80_0	1.47_8	1.21_7	1.10_6
K	1.003	0.005	110°	1.79_6	1.48_5	1.21_4	1.10_5
O	1.004	0.004	111°	1.79_8	1.46_8	1.21_5	1.10_5
P	1.003	0.005	111°	1.79_6	1.47_5	1.21_4	1.10_3
T	1.004	0.005	112°	1.79_6	1.45_5	1.21_4	1.10_4
U	1.001	0.004	112°	1.79_2	1.46_1	1.21_1	1.10_1
Most probable value			111°	1.79_6	1.47_0	1.21_4	1.10_4

a) The distances are in Å unit.

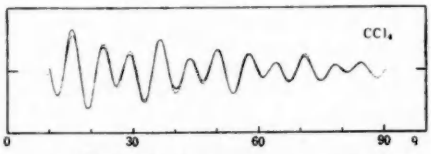

Fig. 2. Molecular intensity curves $qM(q)$ for carbon tetrachloride.
The solid and the dotted curves denote the observed and the calculated intensity curves in a relative scale, respectively.

similar sector-microphotometer data obtained by Karle and Karle[32] (1.770±0.01Å) and by Bartell and Brockway[33] (1.766 ±0.003Å).

C. Radial Distribution Curve.—In the calculation of the RD curve by Eq. (1) a molecular scattering curve which was computed from an assumed model (structural parameters and internal rotation) was attached to the experimental curve in the region $q=0\sim15$. A few steps of successive approximations were made in order to get a reasonable background-line which would satisfy Karle's criteria[21] as closely as possible ($q>15$), and also to make the assumed structural parameters self-consistent with the final RD curve.

In the above calculation various possible conditions of internal rotation were assumed; for instance, free rotation, a cosine-type barrier of 1 kcal./mole, and the rigid trans configuration. The RD curves show considerable difference between each other in the region $r>4.5$ Å, as shown in Fig. 3, particularly in the region of the H···Cl and Cl···Cl bond distances (5.4–6.4Å), which are dependent on the internal rotation. Therefore we cannot arrive at any confirmative conclusion about internal rotation from this RD curve alone. In order to investigate the internal rotation, it is necessary to examine the experimental molecular scattering curve in the region $q\lesssim15$.

On the other hand, these RD curves are found to be quite identical in the region

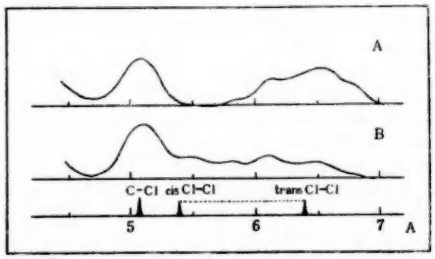

Fig. 3. A portion of a typical radial distribution curve.
(A) Rigid trans model, and (B) free rotation were assumed in the calculation of the theoretical intensity curves ($q=0-15$) which were attached to the same experimental curve. The distances under the curves indicate their approximate positions.

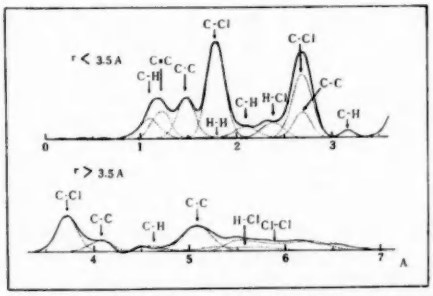

Fig. 4. A typical radial distribution curve for 1,4-dichloro-2-butyne (the solid line). Free internal rotation was assumed. The dotted line indicates the individual peak for each interatomic distance.

32) I. L. Karle and J. Karle, *J. Chem. Phys.*, **17**, 1052 (1949).
33) L. S. Bartell and L. O. Brockway, ibid., **23**, 1854 (1955).

$r \lesssim 4.5$ Å; therefore, by analyzing this region, structural parameters including the mean amplitudes of vibration can be determined without any knowledge of internal rotation. The RD curve, based on the assumption of free rotation, was analyzed in detail as follows. (Fig. 4).

The first peak of the RD curve ($r \lesssim 2.0$Å) was decomposed from the right-hand side successively into the contributions from the C–Cl and C–C distances, leaving a composite peak including the C≡C and C–H distances. To obtain the C≡C distance, the equilibrium distance and the mean amplitude of the C–H bond were assumed to be 1.10 Å and 0.077 Å[34], respectively, since these distances are close together, and it is difficult to separate them unambiguously.

In order to decompose the second large peak ($r \sim 2.7$ Å) into those of the $Cl-C_3$ and C_3-Cl distances, the sum of the C_1-C_2 and C≡C distances which had been obtained from the analysis of the first peak was used for the C_1-C_3 distance, and 0.051 Å was assumed for its mean amplitude[34].

The third peak ($r \sim 3.7$ Å) is due to the C_3-C_4 distance overlapped by the contribution of the C_1-C_4 distance on the right-hand side, and the fourth peak is due to the C_4-Cl distance. These peaks and other smaller peaks were analyzed in the same manner.

The area under the peak multiplied by the equilibrium distance should be proportional to the corresponding c_{ij} value[21]. The areas obtained from the above analysis are in fairly good agreement with the expected values, yet there is a discrepancy of ±15 percent., which indicates that a small amount of "ghost" included in the RD curve changes the shapes of small peaks (particularly in the region $r > 3.5$Å). The most part of this ghost is probably due to the errors in the observed intensity curve. Hence, in order to estimate the uncertainty, RD curves were calculated and analyzed from various experimental intensity curves which differ within the limits of experimental error. In spite of the slight difference in the areas (about 3% for C–Cl peaks, and 10% for C–C peaks) and in the mean amplitudes (about 10% for larger peaks) among various RD curves, the centers of the larger peaks remain practically constant. The possible range of the positions of these main peaks are as follows:

C≡C: 1.20–1.22 Å; C–C: 1.46–1.48 Å;
C–Cl: 1.79–1.80 Å; Cl–H: 2.36–2.38 Å;
C_1-C_3: 2.67–2.70 Å; C_2–Cl: 2.68–2.70 Å;
C_3–Cl: 3.70–3.74 Å.

A typical result of the RD analysis is given in Table I. The distances listed on the second row are calculated from the model with the directly bonded distances listed in the same table, a C–C–Cl angle of 110.5°, and C–C–H and H–C–H angles of 109.5°. The mean amplitudes listed on the third row are the values directly obtained from the Gaussian-type RD peaks, without the correction for second-order effects[21,22], such as a sample size, double scattering, and the failure of Born approximation[35,36].

D. Theoretical Intensity Curves. — A theoretical intensity curve was computed using the values obtained from the RD curve (C–H 1.10 Å, C≡C 1.21 Å, C–C 1.475 Å, C–Cl 1.795 Å, and ∠C–C–Cl

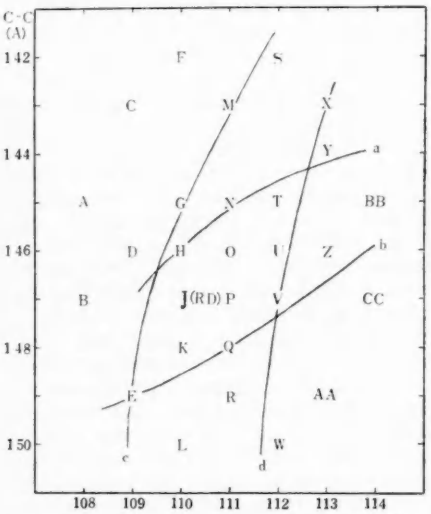

C–Cl=1.79 Å (C≡C=1.21 Å, C–H=1.10 Å, ∠C–C–H=∠H–C–H=109.5)

Fig. 5. Parameter chart for 1,4-dichloro-2-butyne.
The positions of the letters indicate the parameters of the models for which intensity curves in Fig. 1 were computed (except RD, which does not exactly correspond to the parameters of the model RD). The lines a, b, c and d indicate the border-line of the acceptable region for certain particular features.

34) The mean amplitudes listed in the fourth row of Table I are either calculated approximately using the force constants of dimethylacetylene (B. L. Crawford, Jr., *J. Chem. Phys.*, **7**, 555 (1939)), or estimated from the Table V and VI of the Reference 31.

110.5°); these values roughly correspond to the point "RD" in Fig. 5. The $q_{calcd.}/q_{obs.}$ ratio for the maxima and minima is 1.000 ±0.004 (Table II),[37] and the average fluctuation in the $I_{obs.}/I_{calcd.}$ ratio for these maxima and minima is about 10 percent.

In order to determine the range of uncertainty in various parameters, a number of intensity curves were computed based on assumed models. Since it is not feasible to exhaust the seven independent structural parameters and the mean amplitudes, the C≡C and C–H bond distances[38] and the C–C–H and H–C–H angles[39] were kept constant at 1.21 Å, 1.10 Å, and 109.5°, respectively, only the ratio C–C/C–Cl and the angle C–C–Cl being varied systematically. The parameter chart is given in Fig. 5. Estimated mean amplitudes[34] given in Table I were used throughout. Free internal rotation was assumed, and the theoretical intensity curves computed at each rotational angle at 10° intervals were summed up; mean amplitudes of the H–Cl and Cl–Cl distances were assumed to be 0.120 Å and 0.080 Å, respectively at all rotational angles, and the contribution from the H–H distances was ignored. When a high potential barrier is assumed, the resulting intensity curve shows features which completely disagree with the observed curve even in the region $q>15$ so that such a model is definitely excluded. This disagreement is most prominent in the extreme case that the barrier is infinite (i.e., any one of *trans-*, *gauche-* and *cis*-form, similar in configuration to those of 1,2-dichloroethane[40], or one of their possible mixtures). However, when a sufficiently low barrier ($V\lesssim 1$ kcal./mole) is assumed, the variation in the barrier from zero causes little change in the features of the theoretical intensity curve, which are thus in fairly good agreement with the observed curve. As a result, the assumption of free internal rotation, in accordance with the result of the following paper[15], may be reasonable in determining the structural parameter limit.

Some of the computed curves are reproduced in Fig. 1. The computed curves have the following features which are sensitive to small changes in some parameters[41]: the relative height of maxima 5 and 6, and that of maxima 8 and 9. The curves in the parameter chart illustrated in Fig. 5 denote the limit where a particular qualitative feature in the computed curves becomes sufficiently different from the experimental curve to be considered unacceptable.

No model above the line a (A, B, C, D, F, G, M, S and X) is acceptable because the fifth maximum is higher than, or almost the same height as the sixth maximum; model H, N and Y are estimated to be on the borderline. Each model below the line b (L, R, W, AA and CC) has too high and sharp sixth maximum, E and Q being estimated to be on the borderline. The line c excludes the models A, B, C, D and F because the eighth maximum has too high and broad features in each of them. The line d excludes the models Y, Z, AA, BB and CC because the ninth maximum is too high. Acceptable models, which are in the region enclosed

35) Recently, J. A. Ibers and J. A. Hoerni (*Acta Cryst.*, **7**, 405 (1954)) calculated a scattering phase shift η, in the form applicable to any atom under any voltage not too different from 40 KeV. The percentage apparent increase in the mean amplitudes of C-Cl, H-Cl and C-H distances due to this effect was calculated by use of their tables to be about 10 %, 7 % and 1 %, respectively, the first one being in exact agreement with the corresponding value estimated be Bartell and Brockway (Ref. 36b)).

36) a) R. Glauber and V. Schomaker, *Phys. Rev.*, **89**, 667 (1953).
b) L. S. Bartell and L. O. Brockway, *Nature*, **171**, 978 (1953).

37) The ratios for some maxima and minima are not included in the average. See Ref. 42.

38) The C≡C bond distance was found to be 1.207 Å is methylacetylene (L. F. Thomas, E. I. Sheppard and J. Sheridan, *Trans. Faraday Soc.*, **51**, 619 (1955)), and as pointed out by Herzberg and Stoicheff (Ref.13) and many other authors, C≡C bond distance remains remarkably constant in various molecules independent of the atoms linked to this system through a single bond. The result of the above RD analysis is also consistent with this fact. Thus, it will be reasonable in this case to fix the C≡C bond distance at 1.21Å. See also Ref. 12

39) Recent measurement of line shapes of nuclear magnetic resonace absorption led to an H-H distance of 1.71±0.02Å in the CH_2Cl-group of 1,2-dichloroethane (H. S. Gutowsky, et al., *J. Chem. Phys.*, **17**, 972 (1949)). These authors pointed out that the H-C-H angle of this group is significantly smaller than the tetrahedral angle if the C-H distance of 1.10Å or 1.09Å is assumed. Since no corresponding data have yet been found in 1,4-dichlorobutyne, and since the contributions of hydrogen terms to the total intensity curve are relatively small, tetrahedral angles were assumed for both H-C-H and C-C-H angles throughout this investigation.

40) S. Mizushima, "Structure of Molecules and Internal Rotation", Academic Press Inc., New York, (1954), p. 8.

41) Although the drawing of the background line is not unique, the relative heights of adjacent maxima are little changed by the redrawing of the background line, only if the line is smooth and roughly fulfills karle's criteria. As illustrated in Fig. 1, absolute heights of the maxima 5, 6, 8 and 9 change among the measurements of different photographs; nevertheless, the relative ratios of the peaks 5 to 6, and 8 to 9 remain nearly constant. For this reason, these ratios are regarded as the essential features of the experimental intensity and are used as the criteria for the following analysis.

by these four lines, are J, K, O, P, T and U[42].

The area of this "acceptable region" cannot be further reduced by taking other features into account such as the relative depths of minima, because small differences in these features are not significant enough to exclude any of these acceptable models.

The average $q_{calcd.}/q_{obs.}$ values for these acceptable models and the C–Cl and C–C distances determined from these averages are listed in Table III; they all agree satisfactorily with the RD results. The final choice of parameters with their estimated limits of uncertainty (including the error in the determination of q scale, which is estimated to be less than 0.4 percent) are as follows:

C–Cl: $1.79_6 \pm 0.01_5$ Å,
C≡C: 1.21_4 Å (not varied),
C–C: $1.47_0 \pm 0.02_5$ Å,
(C–H: 1.10_4 Å, assumed),
∠C–C–Cl: 111°±2°
(∠C–C–H = ∠H–C–H: 109.5°, assumed).

The C–Cl distance in this molecule is somewhat shorter than that of propargyl chloride (1.82±0.02 Å) found by Pauling et al.[7]. The theoretical intensity curve, based on the model in which all parameters were set equal to the values of propargyl chloride determined by these authors (C–Cl: 1.82 Å, C–C: 1.48 Å, C≡C: 1.20 Å, and ∠C–C–Cl: 111°), is shown as the curve PGS in Fig. 1. It shows a qualitative difficulty in the maximum 8, and its $q_{calcd.}/q_{obs.}$ average is less than unity (0.994±0.006).

4. Discussion

The C≡C and C–C distances obtained above agree, within the limit of experimental uncertainty, with those of similar molecules studied both by spectroscopy and by electron and X-ray diffraction[12–14]. It is a remarkable fact that the C–C distances in various molecules (1.46–1.47 Å) are much shorter than the normal C–C single-bond distance (ca. 1.54 Å), and that they are almost independent of the atoms or groups linked to the carbon atoms.

The C–C–Cl angle (111°±2°) is nearly the same as that in 1,2-dichloroethane (110°23′)[43] and in ethyl chloride (110°30′)[44], while the C–Cl distance ($1.79_6 \pm 0.01_5$ Å) seems to be a little longer than that in the latter molecules (1.78±0.01 Å, and 1.7770 Å, respectively). The increase in the C–Cl bond distance in this molecule compared with that in carbon tetrachloride ($1.76_6 \pm 0.01$ Å) will be real, because these data were obtained at the same condition and by the same procedure. The lengthening of the C–Cl bond is still more pronounced in propargyl chloride which was investigated by Pauling and his coworkers (1.82±0.02 Å)[7], but it is not yet clear whether there is any actual difference between the C-Cl bonds in 1,4-dichloro-2-butyne and in propargyl chloride.

Pauling and his coworkers attributed the lengthening of the C–X bond in propargyl halides to the contribution of the resonance structure (II):

(I) $H-C\equiv C-CH_2-X$,

(II) $H-\overset{+}{C}=C=CH_2 \quad X^-$.

If this were actually the case, large contribution of the similar resonance structures (III) and (IV):

(III) $Cl-H_2C-\overset{+}{C}=C=CH_2Cl^-$,

(IV) $Cl^- \; H_2C=C=\overset{+}{C}-CH_2Cl$,

would also be expected in 1,4-dichloro-2-butyne, whereas a recent measurement[45] of the dipole moments of propargyl chloride, bromide, and 1,4-dichloro-2-butyne has shown that these molecules have

42) These acceptable curves still have a slight disagreement with the experimental curve: namely, (a) the existence of the shoulders of minimum 5 and maximum 7, and (b) the feature near maximum 11. The discrepancy (b) cannot be taken so seriously because precise measurement of this region could not be made in this experiment. The discrepancy (a), however, should be noted, because it is not clear whether the main origin is in the experimental error or in the assumption of the computation.

Although the structural parameters of the acceptable models are consistent with the RD results, and the assumptions of temperature factors and of free internal rotation seems to be reasonable as stated above, there still remains some possibility that we may find a more satisfactory model by changing some of the parameters.

If, on the other hand, this discrepancy comes from the error in the experimental procedure, in other words, if these shoulders do exist, and were not resolved in this experiment, it corresponds to an error of the order of the width of the microphotometer trace (ca. 0.2 mm.). Although this is apparently larger than that of our usual measurement, existence of comparable error in these regions is suggested by the fact that the largest discrepancies among the three observed curves are found in these regions (Fig. 1). On the visual interpretation of the original diffraction pattern, no such shoulders can be clearly observed; but, of course, this visual estimation should not be conclusive.

For this reason, the $q_{calcd.}/q_{obs.}$ values of max. 7, 11, and min. 5, 11, 12 and 13 are not included in calculating their averages and average deviations.

43) J. Ainsworth and J. Karle, *J. Chem. Phys.*, **20**, 425 (1952).

44) R. S. Wagner and B. P. Dailey, ibid., **25**, 1355 (1955).

45) T. Chiba, T. Simozawa, I. Miyagawa and Y. Morino, This Bulletin, **30**, 223 (1957).

smaller C–X bond dipole moments than the normal C–X bond moments, in apparent contradiction to the above expectation. Consequently, it seems difficult to explain the lengthening of the C–Cl bond on the basis of these resonance structures.

Summary

The structure of 1,4-dichloro-2-butyne was investigated by means of the sector-microphotometer method of electron diffraction. The following values were obtained: C≡C: 1.21$_4$ Å, C–C: 1.47$_0$±0.02$_5$ Å, C–Cl: 1.79$_6$±0.01$_5$ Å, and ∠C-C-Cl: 111°±2°. The C–Cl distance was found to be longer than that in carbon tetrachloride, 1.76$_6$±0.01 Å.

The author wishes to express his gratiude to Professor Y. Morino, for his kind guidance and encouragement throughout the course of this work, to Professor R. Uyeda, Nagoya University, for his valuable advice for the construction of the sector apparatus, to Mr. H. Morimoto and Mr. S. Shibata, Nagoya University, for their kind help in the measurement of microphotometric tracing, and to Mr. R. Tsunoda and Mr. Y. Suzuki, Division of Health and Welfare Statistics, Welfare Minister's Secretariat, for the use of Punched Card Machine. The expenses of the work were defrayed from the Scientific Research Encouragement Grant of the Ministry of Education to which the author's thanks are also due.

Department of Chemistry
Faculty of Science
The University of Tokyo, Hongo, Tokyo

*An Electron Diffraction Investigation of the Molecular Structure of 1,4-Dichlorobutyne. II. A Study of Internal Rotation by Use of Halos in Small Angle Region**

By Kôzo Kuchitsu

(Received January 7, 1957)

1. Introduction

The internal rotation of two methyl groups in dimethylacetylene has been investigated by several authors. The measurements of heat capacity[1,2], and the third-law entropy[3] offered a proof of practically complete absence of hindrance to the rotation of these methyl groups (less than 500 cal./mole)[2]. The analysis of the rotational structure of the perpendicular-type infrared bands[4,5] led to the conclusion that the assumption of unrestricted internal rotation is consistent with their observed data, thus giving independent support to the results of the thermal measurements.

As for the substituted dimethylacetylene[6], the complex microwave spectrum[7] of CH_3—C≡C—CF_3 was explained satisfactorily on the basis of a zero, or very low potential barrier when centrifugal distortion effects were taken into account[8], and $ClCH_2$—C≡C—CH_2Cl molecule was shown, by means of temperature dependence of the dipole moment in the vapor state[9], to have a barrier of less than 0.1 kcal./mole, while in carbon tetrachloride and benzene solutions[10] the barrier was estimated to

* Presented at the Eighth Annual Meeting of the Chemical Society of Japan, April, 1955.

1) B. L. Crawford, Jr. and W. W. Rice, *J. Chem. Phys.*, **7**, 437 (1939).

2) G. B. Kistiakowsky and W. W. Rice, ibid., **8**, 618 (1940).

3) D. W. Osborne, C. S. Garner and D. M. Yost, ibid., **8**, 131 (1940).

4) D. R. J. Boyd, H. W. Thompson and R. L. Williams, *Disc. Faraday Soc.*, **9**, 154 (1950).

5) J. M. Mills and H. W. Thompson, *Proc. Roy. Soc.*, **A226**, 306 (1954).

6) A recent investigation of the vibrational spectrum of CF_3-C≡C-CF_3 by Miller and Bauman (*J. Chem. Phys.*, **22**, 1544 (1954)) has shown that this molecule follows D_{3d} selection rules, so that it is in either staggered configuration or free rotation. (R. P. Bauman, *J. Chem. Phys.*, **24**, 13 (1956)). However, no definite decision has yet been given.

7) B. Bak, L. Hansen and J. Rastrup-Andersen, *J. Chem. Phys.*, **21**, 1612 (1953).

8) D. R. Lide and D. Kivelson, ibid., **23**, 2191 (1955).

9) Y. Morino, I. Miyagawa, T. Chiba and T. Shimozawa, This Bulletin, **30**, 222 (1957).

10) Y. Morino, I. Miyagawa and A. Wada, *J. Chem. Phys.*, **20**, 1976 (1952).

be 0.75±0.20 kcal./mole. It is the main purpose of this article to apply the sector-microphotometer method of electron diffraction to the study of the internal rotation of 1,4-dichloro-2-butyne, using the structural data obtained in the preceding article[11], and to confirm the results of dipole moment measurement. This method will provide one of the effective means of determining the potential barrier of such a molecule, because a heavy chlorine atom is included in each of the rotating groups so that the diffraction pattern will show essential dependence on the internal rotation of these groups.

2. Experimental and Results

In order to study the internal rotation of this molecule, it is necessary to examine small-angle halos ($q \lesssim 15$). The theoretical intensity curves remain almost unchanged in this range when slightly different frame parameters (distances, angles, and mean amplitudes) are assumed, so that the essential features of the curves are determined by the assumption of the potential barrier alone. In the outer q region, on the other hand, the contribution from the Cl—Cl and H—Cl distances which change with the internal rotation damps rapidly, and in addition even a slight change of the frame parameters might cause a significant effect to the intensity curve enough to obscure the difference caused by the change of the potential barrier. Thus the photographs taken at the long camera length of about 27.9cm. ($q=5\sim27$) can be used as a means of estimating the potential barrier. The detail of the experimental procedure and numerical computation are given in the preceding article[11]. However, the usual technique of drawing the background line cannot be applied in this region. Karle's criterion of the non-negative Gaussian RD peaks[12a] is not applicable because the influence of f-factors upon the molecular intensity curve is not negligible in this region; nor can the background line be drawn through the zero-points of a reasonable theoretical curve[12b,13,14], because there is no zero-point from $q=5$ to 15. Consequently, we have to use some alternative standard for obtaining a reasonable background line. In this study a procedure similar to, but somewhat different from that of Bregman and Bauer[14] was used.

Assuming various types of potential barrier $V(\phi)$, theoretical intensity curves $M_c(q, V)$ were calculated from Eqs. (2) and (4) of Paper (I)[15]; the frame parameters were fixed at the values obtained in Paper (I), since the influence of their uncertainty was found to be negligible. To each M_c-curve the corresponding "background function" $I_b(q, V)$ was computed by the following formula:

$$I_b(q, V) = q^{1/2} I_o(q) / \{1 + 0.84 M_c(q, V)\} \qquad (1)$$

where $I_o(q)$ is the observed total scattering intensity, which was multiplied by $q^{1/2}$ to accentuate the oscillations in the region $q=8\sim15$. The absolute molecular intensity M_c was multiplied[16] by 0.84 to make it fit the experimental curve in the region $q=16.7$ to 20.0.

If the diffraction experiment were ideally performed and the assumed model were strictly correct, the I_b-function should have no sudden fluctuation of the frequency of the order of molecular intensity[17]; in general, the corresponding I_b-function will approach to a smooth curve as the assumed model becomes better. Thus the extent of its fluctuation from a smooth curve can be used as a criterion for choosing reasonable models, provided that the corrections for a non-ideal experiment are properly taken into account.

For simplicity, only the first term of the potential function

$$V(\phi) = \frac{1}{2}V_1(1-\cos\phi) + \frac{1}{2}V_2(1-\cos 2\phi) + \frac{1}{2}V_3(1-\cos 3\phi) + \cdots\cdots, \qquad (2)$$

is considered first; the variable ϕ is the angle of rotation from the *trans* position. When free internal rotation ($V_1=0$) is assumed, the corresponding I_b-curve contains little fluctuation (Fig. 1A), which shows that this model is satisfactory. When the rigid *trans* structure ($V_1=\infty$) is assumed, the corresponding I_b-curve has much greater fluctuations, indicating that this model is definitely unacceptable (Fig. 2A). In a similar fashion, the I_b-curve based on the assumption that $V_1=1$ kcal./mole is also unsatisfactory because it still has some fluctuations (Fig. 3A). This implies that, so far as the cosine-type barrier is assumed, free internal rotation is the

11) K. Kuchitsu, This Bulletin, **30**, 391(1957)(hereafter referred to as paper (I)).

12a) J. Karle and I. L. Karle, *J. Chem. Phys.*, **18**, 957, 963 (1950).

12b) I. L. Karle and J. Karle, ibid., **17**, 1052 (1949).

13) J. M. Hastings and S. H. Bauer, ibid., **18**, 13(1950).

14) J. Bregman and S. H. Bauer, *J. Am. Chem. Soc.*, **77**, 1955 (1955).

15) The following formula was used:

$$qM_c(q,V) = \{\sum_{\phi}\sum_{i>j}(c_{ij}/r_{ij})\exp(-b_{ij}q^2) \times \sin(\pi q r_{ij}(\phi)/10)\exp(-V(\phi)/RT)\Delta\phi\}/\{\sum_{\phi}\exp(-V(\phi)/RT)\},$$

where $\Delta\phi$ is 10° and b_{ij} is a constant.

16) The ratio of the observed molecular intensity to the theoretical one is always less than unity, since the background is raised by multiple and extraneous scattering. Even if the factor 0.84 is changed slightly, the conclusion given below is not altered essentially.

17) An ideal background line (atomic and inelastic scattering) is known to be a smooth function of q. Multiple scattering will also cause an essentially smooth background (Ref. (12a)); and extraneous scattering was found, by measuring a photograph taken without sample, to have no sudden change in intensity. Other possible sources of sudden change, such as grain irregularities, small particles of dusts on the plate, accidental error in the photometry procedure,etc., may be eliminated by rotating the plate while scanning, and by averaging among sets of plates. The smoothness of the background line is discussed more extensively in the authors' recent study on *n*-propyl chloride, (Y. Morino and K. Kuchitsu, *J. Chem. Phys.*, to be published). See also Ref. (11) of Karle's paper (Ref. (12b)).

most favorable model, V_1 being apparently less than 1 kcal./mole, although further quantitative estimation of its upper limit is difficult.

An alternative examination of the potential barrier is a comparison of the molecular intensity curve $qM_o(q)$, which is obtained by drawing a smooth background in such a way as to reproduce the theoretical intensity curve qM_c as closely as possible, in the resulting qM_o-curve. The model

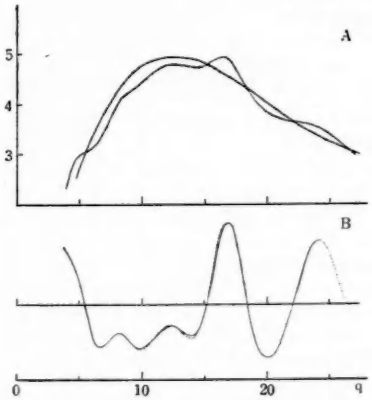

Fig. 1. (A) The observed intensity curve multiplied by $q^{1/2}$ obtained from the long camera-length photographs, and the I_b-curve for free internal rotation. (B) The qM_o-curve (solid line) which was obtained by drawing a smooth background line in such a way as to reproduce the theoretical intensity curve qM_c (dotted line) for free internal rotation as closely as possible.

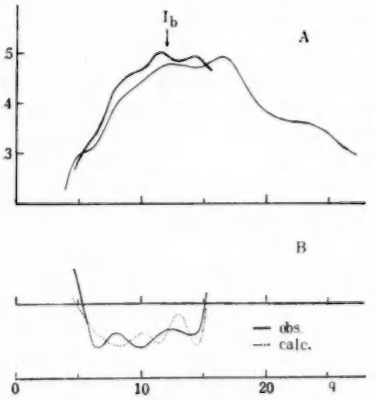

Fig. 2. (A) The I_b-curve for the rigid-*trans* model; the curve shows fluctuations with the frequencies of the order of molecular intensity. (B) The qM_c-curve (solid line) and the qM_c-curve (dotted line) for the rigid-*trans* model.

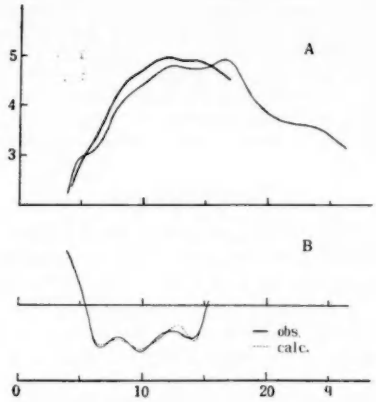

Fig. 3. (A) The I_b-curve for the model $V_1=1$ kcal./mole. (B) The qM_o-curve (solid line) and the qM_c-curve (dotted line) for the model $V_1=1$ kcal./mole.

$V_1=\infty$ is completely unsatisfactory because these curves disagree with each other (Fig. 2B); the qM_c-curve for the model $V_1=1$ kcal./mole shows features near $q=8$ and 12.5 which cannot be reproduced in the qM_o-curve (Fig. 3B). However, the qM_c-curve based on the model $V_1=0$ is reproduced satisfactorily by the corresponding qM_o-curve. (Fig. 1B). A factor σ defined by the following equation may be used as a numerical measure of the overall inconsistency between the qM_c- and qM_o-curves:

$$\sigma=\sum_q\{qM_o(q)-cqM_c(q)\}^2, \qquad (3)$$

where the summation is taken over the integral q values from 5 to 14, and c is a numerical factor adjusted to minimize the σ-value. Table I shows that the lower the barrier, the less σ-value may be obtained, which again favors practically free internal rotation.

TABLE I

THE σ FACTORS OF THE THEORETICAL CURVES CALCULATED BY ASSUMING VARIOUS TYPES OF POTENTIAL BARRIERS

Assumption	$V=0$	$V=1$ kcal.	$V=\infty$
V_1 term only	0.0070	0.0173	0.2165
V_2 term only	0.0070	0.0261	0.1016
V_3 term only	0.0070	0.0082	0.0163

The σ value among the two observed curves is about 0.0002.

Similar procedure can be applied for a potential function of any shape. If, for example, the potential function is assumed to have only the second term (the *trans* and the *cis* positions being the lowest ones), a high potential barrier is found to be impossible, and the σ-factor has the lowest value when V_2 is zero; so too is this the case when only the third term (the *trans* and the *gauche* positions being the stable ones)

is assumed, although the fact is less prominent than in the above cases (Table I). The actual potential barrier will naturally be neither of these extreme cases but a certain combination of these terms; nevertheless, it can be inferred from the above result that the internal rotation is practically unrestricted; in other words, the barrier higher than 1 kcal./mole is improbable.

3. Discussion

It is to be noted, in the first place, that the electron diffraction study, particularly the analysis of small angle halos, provides one method of investigating internal rotation. By the measurement of dipole moment, only the V_1-term can be determined[18]; on the contrary, more than one coefficient of the potential function (2) can be estimated, at least in principle, by the electron diffraction method if sufficiently accurate scattering data are available, although its precise evaluation is limited because of the difficulty in drawing a correct background line and in estimating experimental errors.

The analysis of 1,4-dichloro-2-butyne described above indicates that free internal rotation is in good agreement with the electron diffraction data, whereas a high potential barrier is inconsistent. This conclusion is consistent with that obtained from the dipole moment measurement of this molecule in the gaseous state; Morino and his collaborators[9] observed finite and constant values of the dipole moment, 2.08–2.09 D, in the temperature range of 90–160°C., from which they concluded that the V_1-coefficient of the potential function (2) is less than 0.1 kcal./mole.

It is well known that the potential barriers in ethane derivatives, such as 1,2-dichloroethane, are several kcal./mole[19]. The barrier in 1,4-dichloro-2-butyne is therefore much lower. This difference in barrier height arises mainly from the fact that the distance of the two rotating groups is longer in the latter molecule. In fact, the steric repulsion between the two C—Cl bond moments is shown to be only about 0.5 kcal./mole by a simple calculation[10].

18) I. Miyagawa, *J. Chem. Soc. Japan*, **75**, 970 (1954).

19) S. Mizushima, "Structure of Molecules and Internal Rotation", Academic Press Inc., New York (1954).

Summary

The internal rotation of 1,4-dichloro-2-butyne was investigated by the sector-microphotometer method of electron diffraction, examining the region of smaller scattering angles ($q \lesssim 15$); photographs taken at a long camera length were analyzed using a criterion that the "background function" should have no sudden fluctuation. Free internal rotation is in good agreement with the observed scattering data, and a high potential barrier is inconsistent.

The author wishes to express his gratitude to Professor Y. Morino for his kind guidance and encouragement througout the course of this work. The expenses of the work were defrayd from the Scientific Research Encouragement Grant of the Ministry of Education, to which the author's thanks are also due.

Department of Chemistry, Faculty of Science, Tokyo University, Hongo, Tokyo

Infrared Spectra of Organic Ammonium Compounds

By Koji NAKANISHI, Toshio GOTO and Mamoru OHASHI

(Received January 7, 1957)

In connection with the structural elucidation of the natural product, roseonine[1] and roseothricin[2], the infrared spectra of about one hundred authentic amines have been compared with the spectra of their hydrochlorides[3] (potassium bromide disk). Representative results are shown in Table I, Figs. 1–4, and are summarised in Table II.

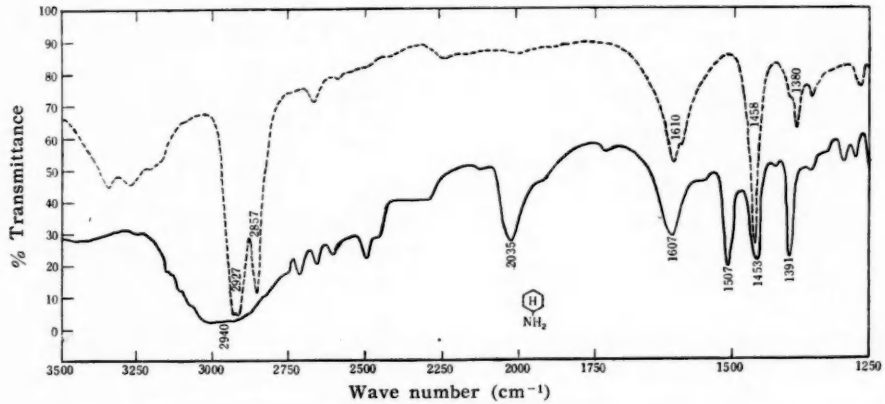

Fig. 1. Primary amine
Cyclohexylamine (No. 8, 8a): ---- free, —— hydrochloride

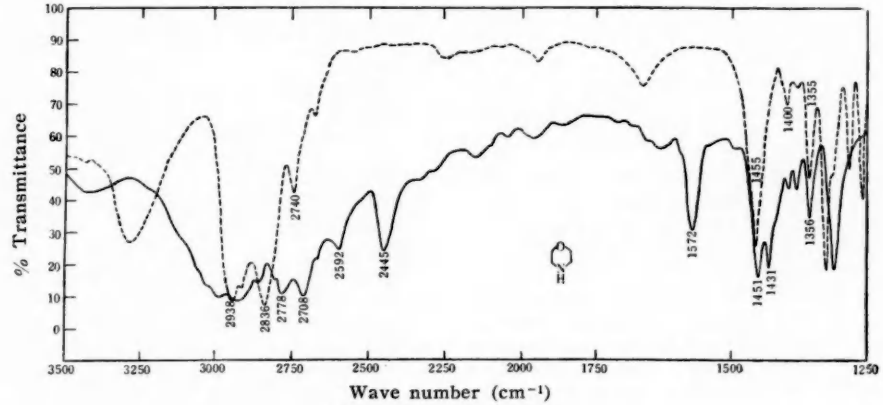

Fig. 2. Secondary amine
Morpholine (No. 18, 18a): ---- free, —— hydrochloride

1) K. Nakanishi, T. Ito, M. Ohashi, I. Morimoto and Y. Hirata, This Bulletin, **27**, 539 (1954).
K. Nakanishi, T. Ito and Y. Hirata, *J. Am. Chem. Soc.*, **76**, 2845 (1954); K. Nakanishi and M. Ohashi, This Bulletin, (in press).
2) T. Goto, Y. Hirata, S. Hosoya and N. Komatsu, ibid., **30**, 304 (1957).
3) For summaries of existing data on the ammonium group see L. J. Bellamy, "The Infrared Spectra of Complex Molecules," Methuen (1954), p. 202, and R. N. Jones and C. Sandorfy in "Chemical Applications of Spectroscopy," Interscience (1956), p. 514, 520.

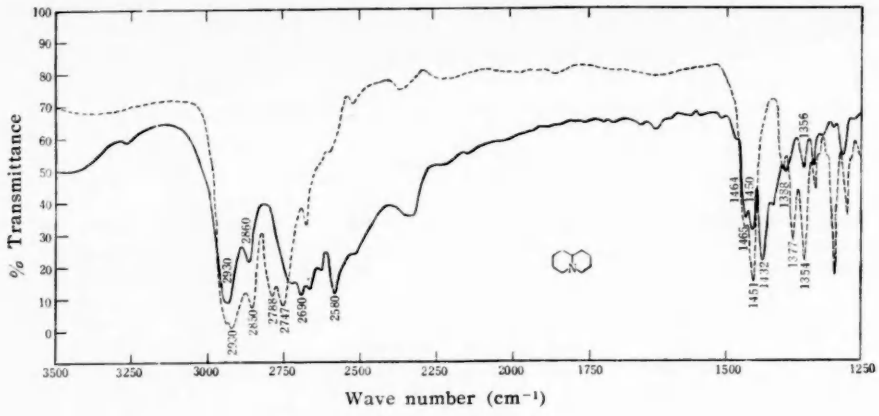

Fig. 3. Tertiary amine
Quinolizidine (No. 31, 31a): ---- free, —— hydrochloride

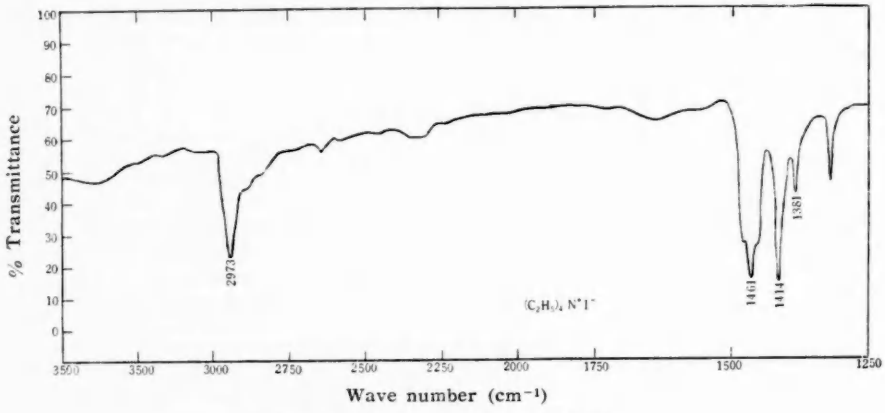

Fig. 4. Quaternary ammonium salt
Tetraethylammonium iodide (No. 50)

Thus primary, secondary, and tertiary amine hydrochlorides, and quaternary ammonium salts can be differentiated fairly accurately from the results of Table II. The characteristic shape and position of the prominent group of absorptions lying at the highest frequency usually suffice to identify primary and tertiary amine hydrochlorides. The corresponding absorption of secondary amine hydrochlorides is less characteristic and in this case absorption in the 1600–1550 cm^{-1} region also has to be taken into account. Open or cyclic azomethines containing the grouping $\rangle C{=}N-$ were not included in the studies. Hydrochlorides of these compounds possess one to several absorptions in the region of 2200–1800 cm^{-1} ("immonium band") in addition to the ammonium band at 2500–2300 cm^{-1}; furthermore the C=N stretching band is shifted 30–40 cm^{-1} toward higher frequency upon attachment of a proton to the nitrogen[4]. Incidentally the region of the ammonium band of azomethine hydrochlorides is roughly similar to that of tertiary amines and seem also to be easily differentiated from normal C—H stretching absorptions (see figures in reference 4). The α, β- and the β, γ-unsaturated tertiary amines and their salts[5] are not included in the present paper, either

4) a. B. Witkop, *Experientia*, **10**, 420 (1954).
b. *idem.*, *J. Am. Chem. Soc.*, **76**, 5597 (1954).
5) N. J. Leonard and V. W. Gash, ibid., **76**, 2681 (1954).

TABLE I

INFRARED ABSORPTION OF AMINES AND AMINE HYDROCHLORIDES

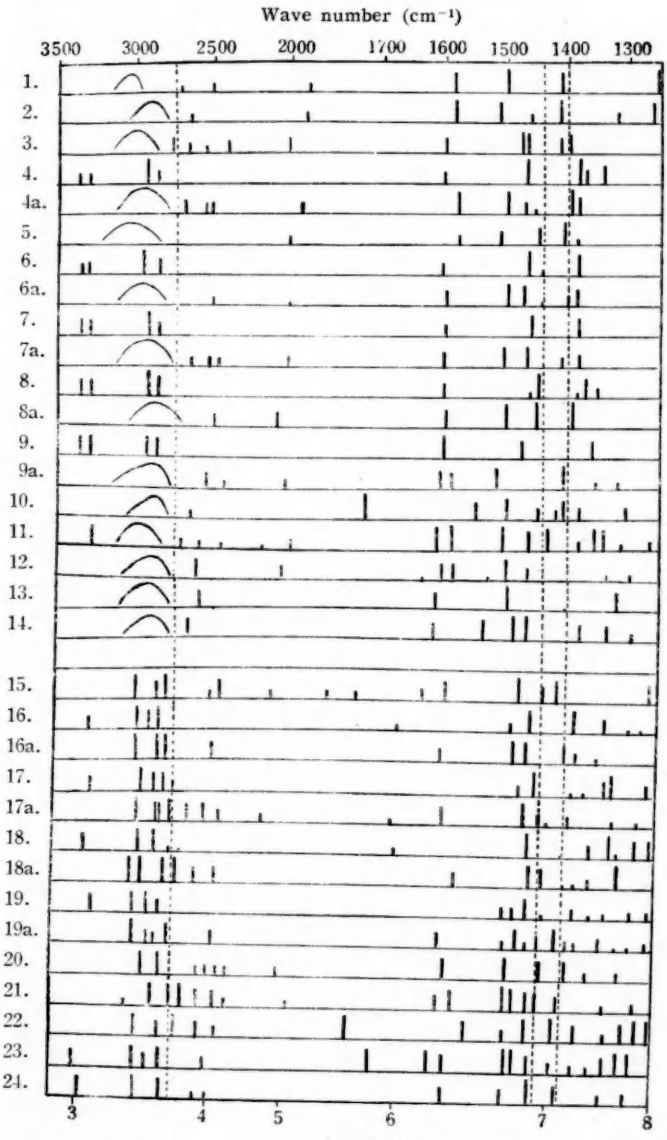

1. Methylamine HCl
   S. ♯6369
2. $CF_3CH_2NH_2 \cdot HCl$
   S. ♯7339
3. Ethylamine HCl
4. Isopropylamine
4a. Isopropylamine HCl
5. *n*-Propylamine HCl
6. *n*-Butylamine
6a. *n*-Butylamine HCl
7. *n*-Hexylamine
7a. *n*-Hexylamine HCl
8. Cyclohexylamine
8a. Cyclohexylamine HCl
9. Ethylenediamine
   S. ♯5319
9a. Ethylenediamine HCl
   S. ♯8183
10. Ethyl glycinate HCl
    S. ♯6702
11. Indolethylamine HCl
12. Aniline HCl
13. Benzidine 2HCl
    S. ♯6621
14. 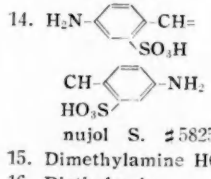
    nujol S. ♯5825
15. Dimethylamine HCl
16. Diethylamine
16a. Diethylamine HCl
17. Piperidine
17a. Piperidine HCl
18. Morpholine
18a. Morpholine HCl
19. *dl*-Ephedrine
19a. *dl*-Ephedrine HCl
20. 2-Me-piperidine HCl
    S. ♯8774
21. N-Benzylaniline HCl
    S. ♯8620
22. 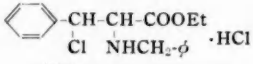
    S. ♯7911
23. 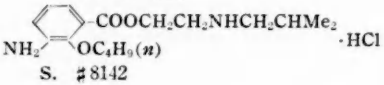
    S. ♯8142
24. 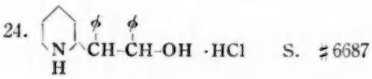
    S. ♯6687

TABLE I (continued)

25. Trimethylamine HCl
S. #6377
26. Triethylamine
26a. Triethylamine HCl
27. N-Ethylpiperidine
CCl_4 soln.
27a. N-Ethylpiperidine HI
28. N-Ethylmorpholine HI
29. Dimethylhexylamine HCl
30. Diethylhexylamine HCl
31a. ·HCl
31.
32. Dimethylbenzylamine HCl
33. Dimethylaniline HCl
34. Diethylaniline HCl
35. 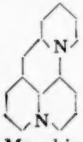 ·2HCl
36. Morphine HCl
37. Ethylmorphine
37a. Ethylmorphine HCl
38. Strychnine
38a. Strychnine HCl
39. 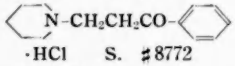
·HCl S. #8772
40. 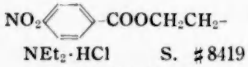
NEt_2·HCl S. #8419
41. 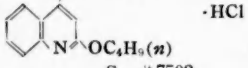
·HCl
S. #7502
42. 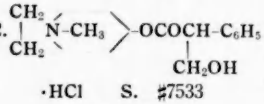
·HCl S. #7533
43. 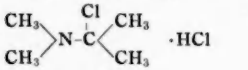
·HCl
S. #7388
44. 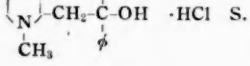
·HCl S. #6688
45. 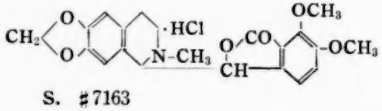
S. #7163

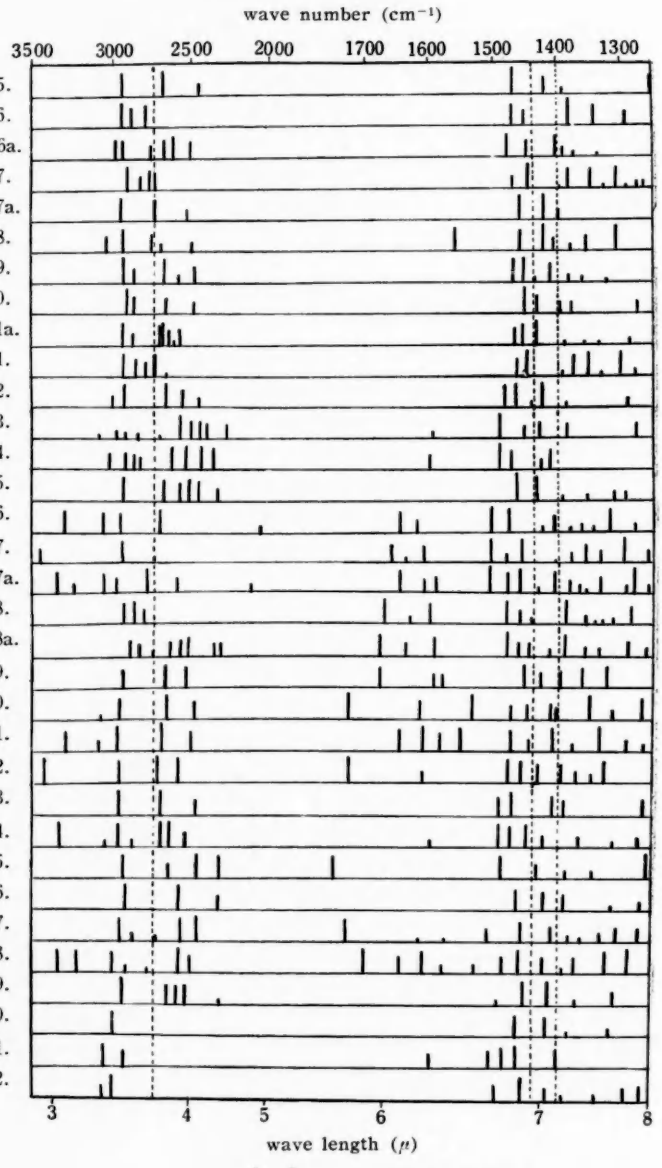

46. 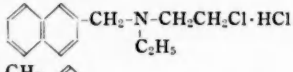 S. #7444
47. 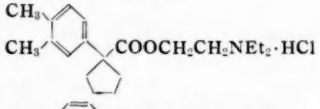
48. 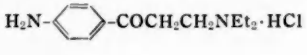

49. 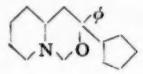 ·HCl S. #6678

50. $(C_2H_5)_4N^+ I^-$

51. 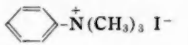 S. #7333

52. 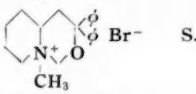 S. #6679

Dotted line at 2750 cm^{-1} marks approximate differentiating line between amines and hydrochlorides.
Dotted line covering the region 1440–1400 cm^{-1} shows the range of the $—CH_2—N^+—$ band. All data were obtained with KBr disks except when specified. Data taken from the Sadtler Catalog (S. P. Sadtler and Son, Inc., 2100 Arch St., Philadelphia 3, Pa., U. S. A.) are marked with S followed by the number of the spectrum card.

TABLE II

CHARACTERISTIC ABSORPTIONS OF AMINE SALTS

Figures in parentheses show number of samples examined, samples which conformed to the generalisation (+), and samples of which differentiation by means of infrared spectroscopy was somewhat dubious (±), respectively.

Primary amine-HCl (19, +17, ±2)

3200–2800: s and br, overlaps with C—H stretching bands.
2800–2400: several weak bands.
2100–1900: w, absent in some cases.
1610–1550 : m, obscured in aromatic compounds by the 1600, 1580, and
1510–1480 1500 bands; the second band is usually the stronger.

Secondary amine-HCl (18, +16, ±2)

2800–2400: s or m, several bands; the overlap with the C—H stretching band is midway between that of primary and tertiary amine hydrochlorides.
2100–1900: w, absent in some cases.
1600–1550: m, obscured in aromatic compounds by the 1600, 1580, and 1500 bands.

Tertiary amine-HCl (51, +46, ±5)

2750–2300: s, several bands; may be clearly differentiated from C—H stretching bands.

The intensity of the NH^+ bending band is too weak to be of any practical value.

Quaternary ammonium salt (4 samples) showed no absorption in the regions specified.

The shift to lower frequencies of the NH stretching band of tertiary amine hydrochlorides has been attributed to a strong hydrogen bond of the type $N^+—H\cdots Cl$[6]; in connection with this, it has been found that the tetraphenyl borates of mono-, di-, and tri-methylamine, in which the hydrogen bond $N^+—H\cdots(C_6H_5)_4B^-$ is sterically hindered, all absorb around 3100 cm^{-1}[7].

A peculiarity, observed in the spectra of many free secondary and tertiary amines, was the appearance of a set of medium to strong bands around 2800–2700 cm^{-1}, i. e., on the lower frequency side of the C—H stretching band*. For example, these are apparent in the spectra of diethylamine (Table I, No. 16), triethylamine (No. 26), piperidine (No. 17), quinolizidine (No. 31), N-dimethylbenzylamine etc. These bands, however, do not interfere with the characterization of amine types, since they disappear upon conversion into the hydrochloride. The same relation seems also to hold for solution spectra; compare the spectra of nicotine and nicotine monohydrochloride (carbon tetrachloride solution) in Fig. 1B of reference 4a, and it is seen that the band at 2809 cm^{-1} in the former compound is absent in the latter.

It has also been noted that a methylene group adjacent to an ammonium nitrogen absorbed in the region 1440–1400 cm^{-1} instead of the normal range around 1470 cm^{-1} (Fig. 5). This is a sort of behavior similar to the well-known displacement to lower frequencies of the bands of methylene and methyl groups alpha to a carbonyl group[8]. Provided that direct comparisons of spectra of amines with their respective hydrochlorides are possible, or that absorption in the 1440–1400 cm^{-1} region by other groups may safely be disregarded, the band would enable one to characterize

6) R. C. Lord and R. E. Merrifield, *J. Chem. Phys.*, **21**, 166 (1953).

7) Personal communication from Dr. K. Nakamoto, Osaka University. See also, *Kagaku-no-Ryoiki*, Extra Number, **23**, 84 (1956).

* Three communications dealing with these bands have recently been published. However, the origin is as yet not clear.
E. Wenkert, D. K. Roychaudhuri, *J. Am. Chem. Soc.*, **78**, 6417 (1965); **79** 1519 (1957).
S. Oseko, *J. Pharm. Soc. Japan*, **77**, 118 (1957).

8) S. A. Francis, *J. Chem. Phys.*, **19**, 942 (1951).
R. N. Jones and A. R. H. Cole, *J. Am. Chem. Soc.*, **74**, 5648 (1952).
R. N. Jones, A. R. H. Cole and B. Nolin, ibid., 5662.

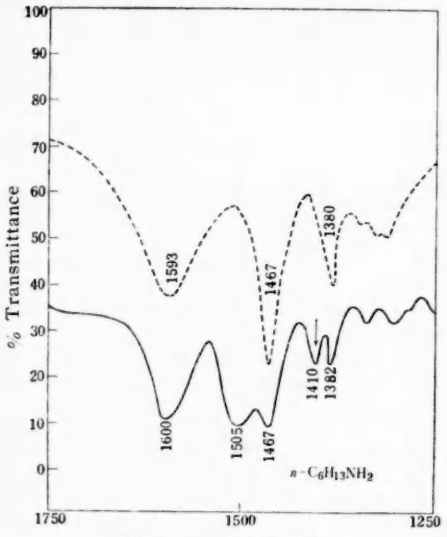

Fig. 5. $-CH_2-N^+-$ band
n-Hexylamine: ---- free, —— hydrochloride

the grouping $-CH_2-N^+-$. Thus the spectra of isopropylamine hydrochloride and cyclohexylamine hydrochloride (Fig. 1) which lack the adjacent methylene group show no (additional) band in this region. Amongst 74 ammonium salts devoid of groupings which could absorb around 1420 cm^{-1}, e. g., —COOH, —OH, $-CONH_2$, $-COOCH_3$, $-CH_2CO-$, 62 gave positive results, 5 gave somewhat dubious results, and 7 gave negative results. With amines containing the above-mentioned groups, characterization of the $-CH_2N-$ group was equally possible in most cases by comparing the spectra of the free amine and its hydrochloride.

Infrared Absorption Measurements.—The spectra were recorded on a Hilger H 800 double beam instrument equipped with sodium chloride optics; whenever necessary the region 1300–1750 cm^{-1} was measured with a calcium fluoride prism. Potassium bromide disks were used, and the die and handpress were those supplied by the Hilger and Watts Co. Analytical grade potassium bromide was ground to pass a 200 mesh sieve and dried at 150°C for 24 hours. The samples (ca. 1 mg.) were ground evenly with 300 mg. of this potassium bromide for 5 min.

The authors wish to express their gratitude to Professor Yoshimasa Hirata for his guidance and interest in this research, to Drs. Junji Koizumi, Nihon Shinyaku Co., Shigeo Oseko, Dainihon Pharmaceutical Co., Akira Fujino and Masao Yamaguchi, Osaka City University, for the gifts of valuable amines, and to Dr. Hideo Kamio, Takeda Pharmaceutical Co. for giving them access to the Sadtler Catalog. They are also grateful for a grant from the Ministry of Education for the purchase of the spectrophotometer.

Chemical Institute, Nagoya University
Chikusa, Nagoya

Ionization Potentials of Some Organic Molecules. IV. Troponoid Compounds

By Keniti HIGASI, Tetsuo NOZOE and Itiro OMURA

(Received January 16, 1957)

A considerable amount of knowledge has been accumulated concerning the physical properties of troponoid compounds. Dipole moments, electron diffraction, X-ray analysis on crystals, near-ultra violet absorption, infrared absorption, Raman effect, magnetic susceptibilities, molecular refraction and the heats of formation have been investigated. Broadly speaking these results have been found to lead to consistent conclusions[1,2].

The object of the present paper is to supply ionization potential data of some troponoid compounds. As is well-known, the energy required to remove one of the most loosely bound electrons is given by

1) P. L. Pauson, *Chem. Revs.*, **55**, 9 (1955); T. Nozoe, "Progr. Chem. Org. Nat. Prod," Bd. XIII, Springer-Verlag, Wien (1956), p. 232.
2) For a review of these studies in Japan, see M. Kubo, Y. Kurita and M. Kimura, *Monogr. Res. Inst. Appl. Elec.*, **4**, 1 (1954).

the first ionization potential of the molecule. From this energy value, an important clue is obtained to the electronic state of a molecule.

Experimental Materials

Tropolone[1]: m. p. 50–51°C.

Tropone[1]: b. p. 84–85°C/6 mmHg, d_4^{25} 1.0825, n_D^{27} 1.6020.

2-Aminotropone[1]: m. p. 106–107°C.

Cyclohexanone:—this substance was kindly provided by Professor K. Kozima, Tokyo Institute of Technology—b. p. 52°C/24 mmHg.

Experimental Method and Result

The measurements of first appearance potentials were carried out in a Hagstrum type mass-spectrometer which was constructed by the present writers[3]. Comparatively weak ion currents were observed when the troponoid compounds were treated. In order to overcome the difficulty arising from this, special attention was paid to the space-charge effects[4] in the ionization chamber and also to the sensibility of the detector of ions.

The determination of the appearance potentials has been made by a modified method of critical slope as in a previous work[3]. Besides this the linear extrapolation method was employed for the sake of comparison. Ionization efficiency curves for tropolone and tropone are shown in Fig. 1.

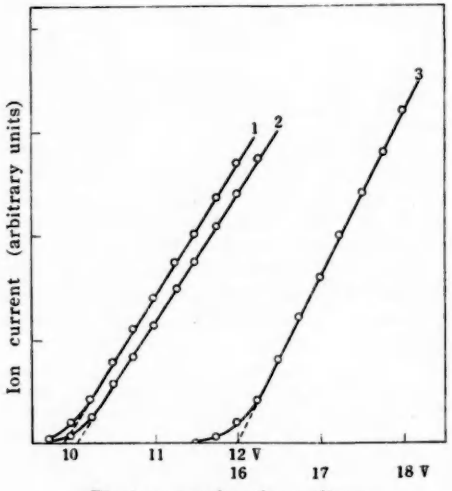

Fig. 1. Relative ionization efficiency curves for troponoids. 1 tropone; 2 tropolone; 3 argon.

The evaluation of the potential was made using the spectroscopic value for argon 15.76eV. Table I records the results thus obtained. No data for comparison exist in the literature.

TABLE I
FIRST IONIZATION POTENTIALS, eV.

Substance	Critical slope	Linear extrapolation
Tropone	9.68±0.02	9.69±0.02
Tropolone	9.86±0.02	9.83±0.02
2-Aminotropone	9.43±0.02	9.50±0.02
Cyclohexanone	9.91±0.05	9.83±0.05

Discussion

It has been concluded through the studies on dipole moment[5] and other properties[1] that the double bond of the carbonyl group

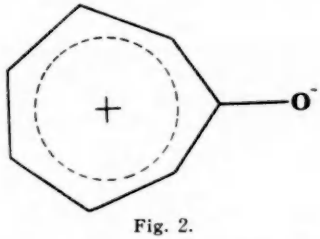

Fig. 2.

in tropone is exceptionally ionic, so that polar structure (Fig. 2) makes a large contribution to the normal state of the molecule. Concerning the structure of tropolone, it is believed that a strong hydrogen bond is formed between the two oxygen atoms of the molecule[1,5–7].

Are the above conclusions consistent with the observed ionization potentials? The answer will be affirmative, if this assumption be true: that, as in other carbonyl molecules[8–10] the first ionization energies of tropone and tropolone are largely determined by the nonbonding electrons at the O-atom of the carbonyl group.

Regarding tropone it is to be noted that both the critical slope and the linear extrapolation method gave lower ionization potential values than a related ketone, cyclohexanone by the amount 0.14–0.23 eV. The dipole moment of tropone 4.17 D[5] is

3) I. Omura, K. Higasi and H. Baba, This Bulletin, **29**, 501 (1955).
4) J. Marriott and J. D. Craggs, "Applied Mass Spectrometry," London (1954), p. 173.
5) Y. Kurita, S. Seto, T. Nozoe and M. Kubo, This Bulletin, **26**, 272 (1953).
6) K. Kuratani, M. Tsuboi and T. Simanouchi, ibid., **25**, 250 (1952).
7) S. Imanishi and M. Ito, ibid., **28**, 75 (1955).
8) C. A. Coulson, "Valence," Oxford (1952), p. 186
9) K. Higasi, I. Omura and H. Baba, *Nature*. **178**, 652 (1956).
10) I. Omura, K. Higasi and H. Baba, This Bulletin, **29**, 504 (1955).

the largest of the ketones, while cyclohexanone has a normal value of 2.75 D. Both of these facts may be interpreted as indicating that extra electric charge flows from the seven-membered ring into the oxygen. Consequently the effective electronegativity of the O-atom in tropone becomes smaller than in cyclohexanone, the ionization potential of tropone being thus decreased.

Further, by use of the same assumption the apparent rise in the potential of tropolone may be explained. Suppose that a strong hydrogen bond is formed between the two oxygen atoms in tropolone, that is, the non-bonding electrons of the oxygen atom of the carbonyl group become bound by the field of a proton. The energy for removing a loosely bound electron in tropolone will then become larger than in tropone.

The situation is more complicated in 2-aminotropone. It may be argued that only a weak hydrogen bond exists in the case of aminotropone[6]. Perhaps a decrease in ionization energy may result from this. But the observed decrease is more pronounced than is to be expected. It may be pointed out that the value 9.43 eV. for 2-aminotropone is near to that of methyl amine 9.41 eV. Generally aliphatic amines have lower potential values than corresponding ketones[10,11] e. g., ethyl amine 9.23 eV., *n*-propyl amine 9.17 eV., acetone 9.89 eV., methyl ethyl ketone 9.76 eV., etc. Therefore it may be reasonable to suppose that the most weakly bound electron in aminotropone is no longer situated at the O-atom. If it be localized at all, it will rather be near the N-atom of the NH_2 group.

Next, attention should be directed to the existence of pi-electrons in the seven-membered ring. Possibly these pi-electrons of the aromatic unsaturated carbon ring may be removed more easily than non-bonding electrons in the carbonyl group. But no reliable discussion can be presented on this possibility in the present stage of knowledge on this point.

Lastly a few words must be added concerning the difficulty of this sort of study. First, there are uncertainties in the interpretation of the ionization energy. For instance, against the explanation offered for tropone one may argue with good reason[8] that the measured ionization energy is very much higher than expected from the extremely ionic character of the carbonyl bond. Further one may point out that acetamide has a high ionization energy 10.39 eV.[10], so that the most loosely bound electron may not be localized at the N-atom of the molecule. In general it is questionable whether or not one can safely consider that the electron responsible for the first ionization is any one of the non-bonding electrons at a certain atom or that the ionization is due to pi-electrons of the conjugated system. Perhaps an *ad hoc* interpretation may be partly justified at the present stage, when few successful trials are known to explain the observed ionization potentials quantitatively even for the pi-electron systems containing no heteroatoms where molecular orbital calculations are relatively easy.

Second, some unknown source of error still exists in the measured potential values[12]. In the first report[3] of this series the writers tried to justify the use of argon as the standard gas and also the application of the critical slope method. The result of the examination was found satisfactory for eleven compounds. But one is not certain whether they are valid for any and every sort of molecule.

Summary

First ionization potentials are obtained for the four substances: tropolone (a) 9.86, (b) 9.83; tropone (a) 9.68, (b) 9.69; 2-aminotropone (a) 9.43, (b) 9.50; cyclohexanone (a) 9.91, (b) 9.83 (units being eV.). Classification symbols, (a) and (b), denote that the measurement was made either by the method of critical slope or by the linear extrpolation method. These results are consistent with the conclusions from other physical data under certain conditions.

The writers' thanks are due to Asst. Prof. H. Baba for valuable suggestions.

Research Institute of Applied Electricity Hokkaide University, Sapporo and Faculty of Science, Tohoku University, Sendai

11) J. D. Morrison and A. J. D, Nicholson, *J. Chem. Phys.*, **20**, 1021 (1952).

12) See for instance, A. J. B. Robertson, "Mass Spectrometry," Methuen (1954), pp. 34-55. See also the subsequent paper of the writers.

Dielectric Studies on Colloidal Solutions. III. The Mobilities of Micelles of Long-chain Amine Hydrohalides

By Michio SHIRAI and Bun-ichi TAMAMUSHI

(Received January 16, 1957)

In the previous paper of this series[1], the transference numbers of long-chain amine hydrochlorides were determined, and the fraction of small counter ions bound to a micelle and the mobility of a micelle were computed therefrom. In this paper, we shall present the direct measurement of the electrophoretic mobilities of the micelles of long-chain amine hydrohalides, and the relation between these mobilities and transference numbers or high-frequency effects will be discussed.

Experimental

Procedure.—The measurement of electrophoretic mobility was carried out by means of the tracer electrophoresis method designed by Mysels and his collaborators[2]. The cell used is shown in Fig. 1. Silver wire is used as the

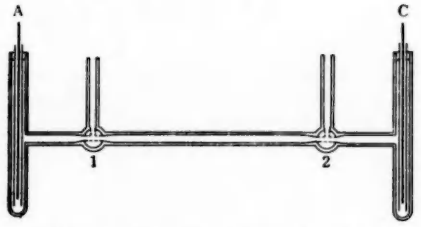

Fig. 1. The electrophoresis cell.

anode A, and silver wire coated with silver halides is used as the cathode C. These electrodes are unpolarizable. The central horizontal tube limited by three-way stopcocks 1 and 2 is filled with the solution of colloidal electrolytes tagged with orange OT, and the adjoining tubes on both sides are filled with an untagged solution. The apparatus is immersed in a thermostat. The electric current flowing through the cell is supplied by a constant current regulator. The electrophoretic mobility u is expressed by the following formula:[2]

$$u=\frac{\lambda}{it}\frac{(Co-C)v}{Co} \qquad (1)$$

where λ is the specific conductivity of the solution (mho/cm), i the current flowing through the cell (amp.), t the duration of the experiment (sec.), Co the concentration of the tracer in the initial solution, C the average concentration of the trace rafter letting the current flow, and v the volume of the tube between stopcocks 1 and 2.

The conductivity of the solution was measured with the impedance bridge of Yokogawa & Co., and the concentration of the tracer with the spectrophotometer of Hitachi & Co.

Materials.—The preparation of dodecyl-, tetradecyl-, and hexadecylamine hydrochloride has been described in the previous paper[1]. Dodecylamine hydrobromide was prepared from dodecylamine (Armour & Co., U.S.A.) by the addition of hydrobromic acid to its ethanol solution and distillation with benzene to remove the water introduced by the addition of the acid. Dodecylamine hydroiodide was prepared from dodecylamine in the same way as above by adding hydroiodic acid. All these products were recrystallized from ethanol.

Orange OT was purified from a commercial sample by solution in acetone and precipitation with water, followed by recrystallization from ethanol-benzene.

Results and Discussion

The experimental results are shown in Table I and Fig. 2. As is shown in Fig. 2, the mobility of a micelle decreases with

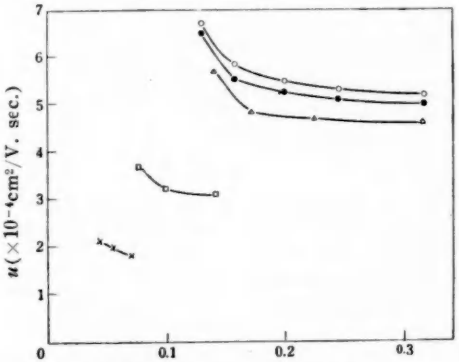

Fig. 2. The electrophoretic mobility.
○, dodecylamine hydrochloride;
●, — hydrobromide;
△, — hydroiodide;
□, tetradecylamine hydrochloride;
×, hexadecylamine hydrochloride.

1) M. Shirai and B. Tamamushi, This Bulletin, **29**, 733 (1956).
2) H. W. Hoyer, K. J. Mysels and D. Stigter, *J. Phys. Chem.*, **58**, 385 (1954).

TABLE I
ELECTROPHORETIC MOBILITY AT 30°C

Substance	Concn. (mole/l.)	λ ($\times 10^{-3}$mho/cm.)	it (coul.)	$\frac{C_0-C}{C_0}$	u ($\times 10^{-4}$cm^2/v.sec.)
Dodecylamine hydrochloride	0.017	1.60	3.30	0.365	6.7
	0.025	1.88	5.28	0.430	5.8
	0.04	2.24	8.64	0.559	5.5
	0.06	2.76	6.20	0.313	5.3
	0.1	4.00	6.30	0.216	5.2
Dodecylamine hydrobromide	0.017	1.46	2.24	0.262	6.5
	0.025	1.75	3.85	0.320	5.5
	0.04	2.08	4.62	0.310	5.3
	0.06	2.64	4.49	0.228	5.1
	0.1	3.60	7.11	0.260	5.0
Dodecylamine hydroiodide	0.02	1.12	1.86	0.249	5.7
	0.03	1.34	2.67	0.252	4.8
	0.05	1.65	2.40	0.180	4.7
	0.1	2.52	7.05	0.339	4.6
Tetradecylamine hydrochloride	0.006	0.558	1.08	0.187	3.7
	0.01	0.681	1.27	0.158	3.2
	0.02	0.970	1.37	0.115	3.1
Hexadecylamine hydrochloride	0.002	0.174	0.507	0.162	2.1
	0.003	0.192	0.648	0.169	1.9
	0.005	0.202	0.648	0.152	1.8

TABLE II
THE FRACTION OF BOUND IONS AND THE ζ-POTENTIAL

Substance	Concn. (mole/l.)	θ from mobility	θ from transference number	ζ-Potential (mV.)
Dodecylamine hydrochloride	0.017	0.37	0.42	119
	0.025	0.46	0.46	103
	0.04	0.59	0.56	98
	0.06	0.66	0.63	94
	0.1	0.70	0.66	92
Dodecylamine hydrobromide	0.017	0.44	—	115
	0.025	0.51	—	98
	0.04	0.62	—	94
	0.06	0.68	—	91
	0.1	0.73	—	89
Dodecylamine hydroiodide	0.02	0.60	—	101
	0.03	0.66	—	85
	0.05	0.75	—	83
	0.1	0.81	—	82
Tetradecylamine hydrochloride	0.006	0.22	—	65
	0.01	0.41	0.38	57
	0.02	0.58	0.60	55
Hexadecylamine hydrochloride	0.002	0.17	0.20	37
	0.003	0.38	0.46	34
	0.005	0.60	0.67	32

increasing concentration, the slope of the curve being considerably steep. This result is probably mainly due to the electrostatic interaction between large ionic micelles and small counter ions, as was discussed previously[3].

If we make some assumptions on the conductivity behavior of these salts, the fraction of counter ions bound to micelles can be calculated from the observed electrophoretic mobility. Those assumptions are: (1) The mobility of a free counter ion is not altered with increasing concentration, and is equal to that of a counter ion at infinite dilution; (2) beyond the critical micelle concentration there are no molecules of long-chain salts existing as single ones. Under these assumptions, if we denote the equivalent conductivity of total ions and free anions by Λ and Λ_-^0, respectively, the relation between the fraction of bound ions θ and the electrophoretic mobility u will be expressed as follows:

$$\frac{\Lambda-(1-\theta)\Lambda_-^0}{1-\theta}=Fu \qquad (2)$$

where F is Faraday's constant. The solution of this equation for θ gives,

$$\theta=1-\frac{\Lambda}{\Lambda_-^0+Fu} \qquad (3)$$

On account of the second assumption, equation (2) is not valid near the critical micelle concentration. Table II shows the values of θ thus obtained, together with those computed from the transference numbers for dodecyl-, tetradecyl-, and hexadecyl- amine hydrochlorides. The difference between these two series of values may arise from the assumptions (1) and (2) above settled.

For dodecylamine hydrochloride, hydrobromide, and hydroiodide, the values of electrophoretic mobility are nearly the same, but the value for dodecylamine hydrochloride is slightly greater than that for dodecylamine hydrobromide and the latter is greater than that for dodecylamine hydroiodide. And as to the fraction of bound ions θ indicated in Table II, there is the following order: dodecylamine hydrochloride < dodecylamine hydrobromide < dodecylamine hydroiodide. On the other hand, for the critical micelle concentration the reverse order has been demonstrated, namely[4]: dodecylamine hydrochloride>dodecylamine hydrobromide>dodecylamine hydroiodide. This shows that there is a close relation between the tendency towards association of counter ions and the critical micelle concentration, that is, the stronger the tendency towards association of counter ions, the smaller the critical micelle concentration.

The electrophoretic mobility u is related to the so-called ζ-potential, that is, the electrokinetic potential of micelle ions. However, in order to calculate the ζ-potential the knowledge concerning the thickness of the double layer, $1/\kappa$, and the radius of the micelle, a, is necessary. Considering that the relaxation effect is abnormally large in the range of concentration at which the measurement was a carried out, we assume $\kappa a \gg 1$. In such case, the relation between u and the ζ-potential has been given by Henry[5], which is shown as follows:

$$u=\varepsilon\zeta/6\pi\eta, \qquad (4)$$

where η and ε denote the viscosity and the dielectric constant of the solvent, respectively. The values of ζ-potential computed from the value of u by this formula are shown in Table II. Henry's formula is valid if the relaxation effect is negligible, but in our case the relaxation effect is so great that the real ζ-potential is considerably greater than that indicated in Table II. Several formulas involving the relaxation effect have been proposed by Overbeek[6] and Booth[7], but to micelle ions which have abnormally high valency, these formulas are not valid, the theoretical solution of this problem being probably very difficult. But, if we can determine the high-frequency effect over a very wide range of frequency, more exact values of the ζ-potential will be obtained.

Summary

The electrophoretic mobilities of dodecylamine hydrochloride, hydrobromide and hydroiodide, as well as tetradecylamine and hexadecylamine hydrochlorides have been measured. They decrease with increasing concentration as is expected from the electrostatic point-of-view of the micelle structure.

3) M. Shirai and B. Tamamushi, This Bulletin, **28**, 545 (1955).
4) M. Shirai, *Sci. Pap. Coll. Gen. Educ., Univ. Tokyo.* **VI**, 29 (1956).
5) D. C. Henry, *Proc. Roy. Soc.* (*London*), **A133**, 106 (1931).
6) J. Th. G. Overbeek, *Kolt. Beih.*, **54**, 316 (1943).
7) F. Booth, *Proc. Roy. Soc.* (*London*), **A203**, 514 (1950).

The fractions of counter ions bound to micelles are computed from the electrophoretic mobilities obtained. These values are found consistent with the result obtained by the transference number measurement.

The ζ-potentials of micelle ions are calculated from the electrophoretic mobilities by Henry's formula. They must be, however, less than the real values, if we take into account the expected high-frequency effects.

Chemistry Dept., College of General Education, and Institute of Science and Technology
The University of Tokyo, Meguro, Tokyo

Study on the Electric Conductivity of Sodium Silicate Aqueous Solution. II

By Hiroshi UKIHASHI

(Received August 10, 1956)

Introduction

Few data have been reported on the dependence of the electric conductivity of sodium silicate solution on temperature. In the present paper are given the electric conductivities measured at 5°, 15°, 25°, 35°, 45° and 60°C of sodium silicate solution of silica-alkali molar ratio ranging from 1 to 3.95 over a wide range of concentration.

From the results, temperature coefficients of the specific conductivity were computed and compared with those of simple strong electrolyte solutions. The equivalent conductivity was derived in the same way as reported in the preceding paper[1]. For the dilute solutions the applicability of Walden's rule, i.e., the independency of the product of equivalent conductivity and solvent viscosity on temperature was examined, and the ionic radius of silicate ion was estimated therefrom. Theoretical treatment of the equivalent conductivity for the 3.95 molar ratio solution was extended to those at other temperatures than 25°C, and it was confirmed that they could be explained theoretically at each temperature with the same assumption as previously described.

Meanwhile, hydroxyl ion concentration was checked at these temperatures for the sodium silicate solutions of three kinds of molar ratio to examine its contribution to their conductivities.

The independence of the conductivity on the viscosity of solution in the higher concentration range was emphasized, and this problem will be discussed in the succeeding paper.

Experimental

Materials. — The sodium silicate solutions were prepared by the same method as described previously[1]. The silica-alkali molar ratio of the solutions herein used were 1.00, 1.55, 2.13, 3.19, and 3.95.

Apparatus and Measurements.—Apparatus for the conductivity measurement was the same as previously reported. The six cells were used, the constants of which were 0.4850, 0.6568, 1.242, 1.380, 16.86 and 18.75. The measurements were made at a series of increasing temperatures from 5° to 60°C, without replacing the solution, except in the case where variation in conductivity with temperature was so much as to require the use of different cell constant. For a dilute solution having possibility of change in conductivity with time, the measurement at each temperature was made 30 minutes after preparation. However, the conductivity change with time was small as compared with the accuracy of this experiment, at most within ±0.5% during the first one hour after preparation. For each molar ratio solution density was measured at these temperatures over a wide range of concentration, using 25 cc. pycnometer. These values were needed for expressing concentration as normality.

Besides, pH was measured for three kinds of sodium silicate solution of molar ratio 1.00, 2.13, and 3.95, at temperatures 5°, 15°, 25°, 35 and 45°C. Beckman Model H-2 *p*H-Meter was used with Beckman type E glass electrode especially designed for the measurements in highly alkaline solution. It is questioned, however, whether the silicate solution does not give any detrimental effect on the glass electrode. To ascertain the reliability of the observed data *p*H values obtained

1) H. Ukihashi. This Bulletin, **29**, 537 (1956).

2) R. W. Harman. *J. Phys. Chem.*, **30**, 1100 (1926).

at 25°C were compared with those obtained by Harman[2] with hydrogen electrode, and those measured by Küntzel et al.[3]. They were approximately in accord with each other within ±0.1, whereas no comparison was available for the values obtained at other temperatures than 25°C[4,5]. For pH measurement, a sample solution was put in 100 cc. polyethylene beaker and covered with vinyl plate with two holes for insertion of electrodes. The meter was frequently standardized with borax and soda buffer solution at each temperature.

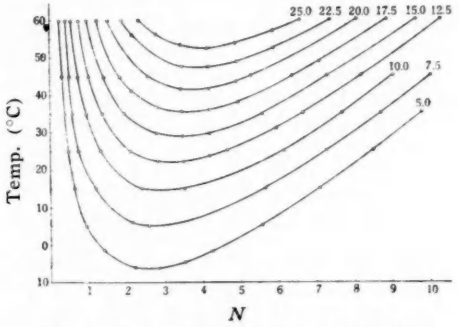

Fig. 1. Iso-conductivity curve of sodium metasilicate solution (numerals for each curve denote $\lambda \times 10^2$)

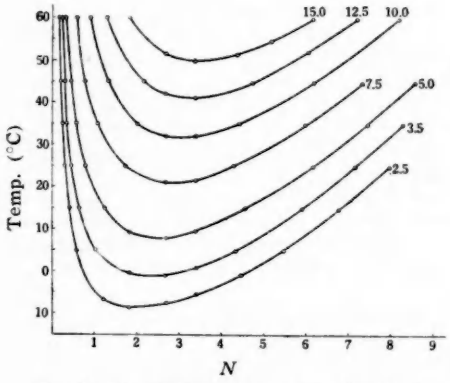

Fig. 2. Iso-conductivity curve of sodium silicate solution of molar ratio 1.55 (numerals for each curve denote $\lambda \times 10^2$)

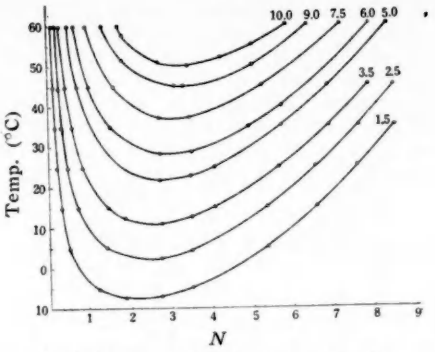

Fig. 3 Iso-conductivity curve of sodium silicate solution of molar ratio 2.13 (numerals for each curve denote $\lambda \times 10^2$)

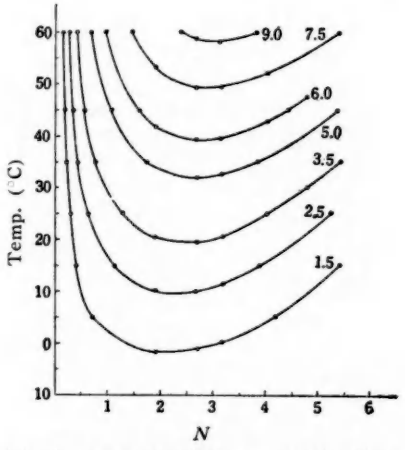

Fig. 4. Iso-conductivity curve of sodium silicate solution of molar ratio 3.19 (numerals for each curve denote $\lambda \times 10^2$)

Results and Discussion

In Fig. 1–5 contour maps are given, which express the specific conductivity as a function of temperature and concentration. Here points on each line have the same conductivity. These curves were drawn as follows. Points on temperature absissas of 5°, 15°, 25°, 35°, 45° and 60° were taken from the data on the curves expressing the relation between specific conductivity and concentration at respective temperatures. Other data were obtained by the inter- and extrapolation of the relation curves between conductivity and temperature at various concentrations.

3) L. E. Küntzel, J. W. Hensley and L. R. Bacon, *Ind. Eng. Chem.*, **35**, 1286 (1943).

4) Schuffelen and Hulst[6], who measured the pH of some concentrated water glass, stated that glass electrode did not produce a satisfactory result, while Sb electrode did. On the other hand, Küntzel et al. measured the pH of dilute sodium silicate solution with both hydrogen and glass electrode, and found the differences between two values to be very small at room temperature but to increase as temperature increases. The pH values obtained by Schuffelen and Hulst are 0.3—0.5 smaller than those obtained by other workers cited herein.

5) Complete data of pH hereby measured will be reported in *Reports of the Research Laboratory, Asahi Glass Co.*

6) A. C. Schuffelen and L. J. N. van der Hulst, *C. A.* **36**, 3583, 5580 (1942).

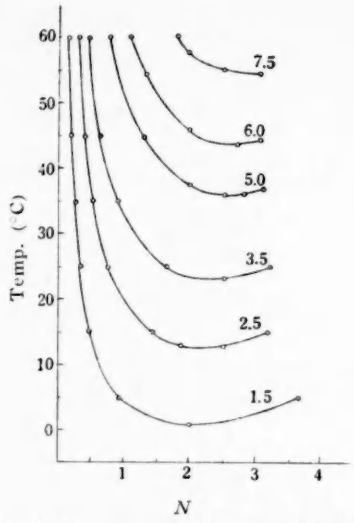

Fig. 5. Iso-conductivity curve of sodium silicate solutions of molar ratio 3.95 (numerals for each curve denote $\lambda \times 10^2$)

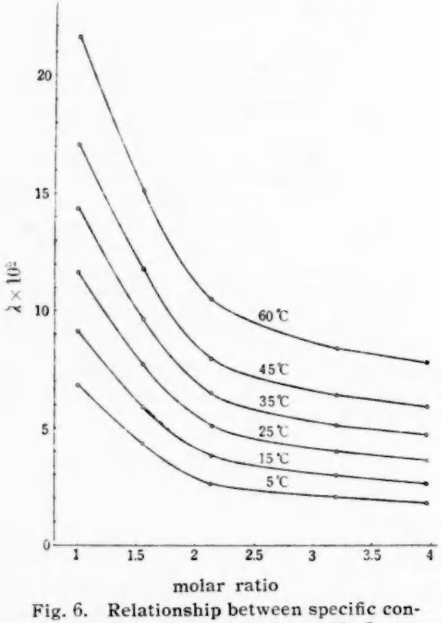

Fig. 6. Relationship between specific conductivity and molar ratio at Na_2O wt. % 5.00.

Here the concentration is indicated by normality of sodium ion content. As seen in these figures the change in specific conductivity with temperature increases as concentration increases in view of wide temperature range, but at a fixed temperature it has the maximum at a moderate concentration, where maximum specific conductivity is attained. As for the concentration dependence of specific conductivity, it increases as temperature rises up, and at a fixed temperature it becomes the minimum around a moderate concentration where specific conductivity shows the maximum. This concentration moves upwards with temperature increase. Fig. 6 shows the relationship between conductivity and molar ratio of sodium silicate solution at a fixed concentration. It is seen that decrease in conductivity with molar ratio gets more remarkable as temperature goes up, and yet all the curves have an obvious bend around molar ratio 2. In Fig. 7 the concentration showing maximum conductivity is plotted against the molar ratio of the solution. In this case no bend seems to appear. This fact should be expected, because the change in conductivity with molar ratio is due primarily to the difference of hydrolysis percentage in the solutions, while the concentration giving maximum specific conductivity may be attributed to the degree of compactness of the solute molecule in the solution and dependent on the molecular volume of sodium silicate molecule in respective molar ratio solution. If the latter is admitted, intermolecular distance at that concentration may have a linear relation with cubic root of molecular weight. This was the case as seen in Fig. 8, where two curves were drawn for both 5°C and 60°C. Here molecular weight was assumed as such

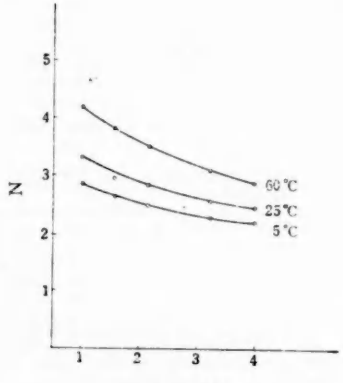

Fig. 7. Change of concentration showing maximum specific conductivity with molar ratio of sodium silicate solutions.

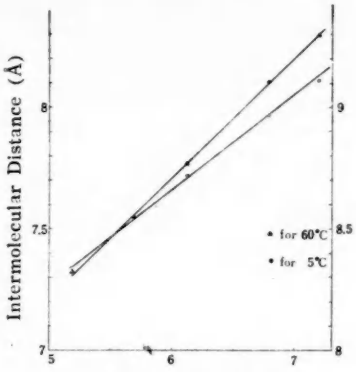

Fig. 8. Relationship between intermolecular distance at concentration showing maximum specific conductivity and cubic root of molecular weight of various sodium silicates.

expressed by the conventional formula.

The temperature coefficient of specific conductivity, as expressed by a and b in the following equation were calculated by the least square method and tabulated in Table 1.

$$\lambda=\lambda_0+aT+bT^2$$

λ_0 is the specific conductivity at 0°C. The table indicates that the first order temperature coefficient has the maximum values in a moderate concentration, while the second order temperature coefficient continues to increase with concentration. This means that the higher the temperature, the larger the temperature coefficient of the more concentrated solution becomes. In Fig. 9 $d\lambda/dT$ at 25°C was plotted against concentration of various sodium silicate solutions together with those of simple strong electrolyte solutions, the latter being quoted from "Landolt und Börnstein Tabellen" with adequate unit conversion.

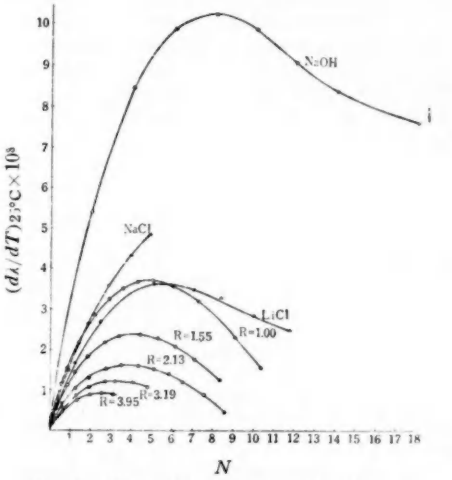

Fig. 9. The change of temperature coefficient of specific conductivity.

TABLE I

TEMPERATURE COEFFICIENT OF SPECIFIC CONDUCTIVITY OF VARIOUS MOLAR RATIO SODIUM SILICATE SOLUTIONS

Na_2O wt% / Molar Ratio		1.00	2.50	5.00	7.50	9.00	10.50	12.00	16.00
1.00	$\lambda_0\times10^2$	1.96	3.93	5.78	6.20	5.93	5.31	4.50	2.03
	a $\times10^4$	6.36	13.10	20.25	25.21	26.01	25.73	23.82	13.32
	b $\times10^6$	1.74	4.36	9.18	14.53	18.29	22.19	26.77	37.35
									(15.00)
1.55	$\lambda_0\times10^2$	1.35	2.60	3.57	3.55	3.21	2.60	1.97	0.84
	a $\times10^4$	4.79	9.31	14.43	16.28	16.03	14.90	12.54	5.05
	b $\times10^6$	1.63	4.14	7.82	12.15	15.06	17.78	20.56	25.25
2.13	$\lambda_0\times10^2$	0.874	1.59	2.16	2.15	1.89	1.49	1.03	0.332
	a $\times10^4$	3.50	6.77	9.98	11.10	10.72	9.06	6.94	4.72
	b $\times10^6$	1.69	3.52	6.25	9.08	11.06	13.40	15.25	17.53
							(10.13)		
3.20	$\lambda_0\times10^2$	0.739	1.30	1.64	1.47	1.15	0.861		
	a $\times10^4$	2.95	5.71	8.23	8.34	7.14	5.58		
	b $\times10^6$	1.49	2.90	5.08	7.89	9.70	11.03		
					(6.47)				
3.95	$\lambda_0\times10^2$	0.688	1.16	1.41	1.36				
	a $\times10^4$	2.93	5.78	7.86	8.03				
	b $\times10^6$	1.19	2.34	4.64	5.83				

The figure shows that the temperature coefficient of specific conductivity of sodium silicate solution is rather small as compared with simple strong electrolyte solutions, and the decrease in temperature coefficient with concentration in the higher concentration range is more marked than that of those solutions. This might lead to a suggestion that the temperature coefficient of mobility of silicate ion is small and its trend of making a kind of configuration in the solution is greater than that with simple strong electrolyte.

The equivalent conductivity Λ at various temperatures were plotted against the square root of concentration. Fig. 10, 11 and 12 show those obtained for the silicate solutions of molar ratio 1, 2.13 and 3.95.

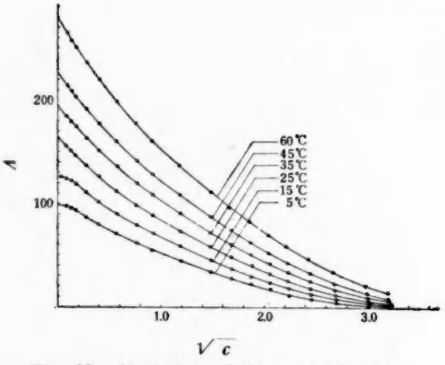

Fig. 10. Variation of the equivalent conductivity of sodium metasilicate solution with square root of concentration at various temperatures.

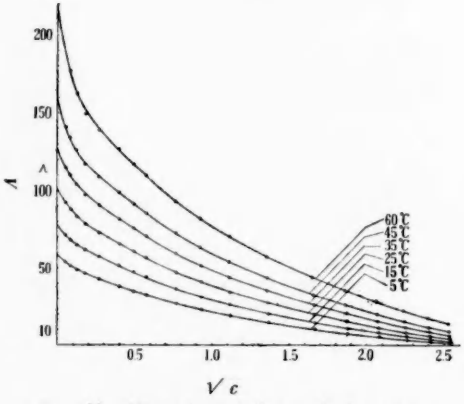

Fig. 11. Variation of the equivalent conductivity of molar ratio 2.13 sodium silicate solution with square root of concentration at various temperatures.

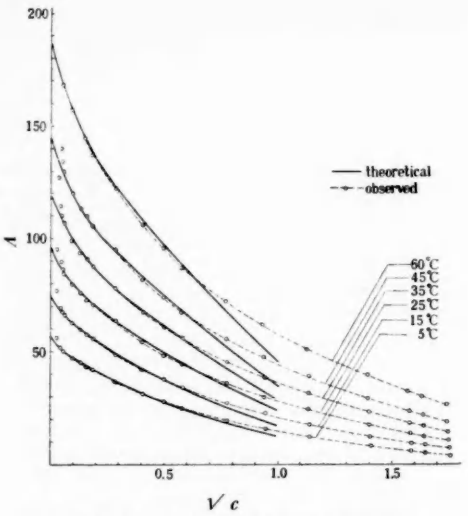

Fig. 12. Comparison of the equivalent conductivity of molar ratio 3.95 sodium silicate solution with those calculated from the theoretical equation at various temperatures.

The limiting equivalent conductivity Λ_0 was estimated by the extrapolation of curves to infinite dilute concentration. They are tabulated in Table II, together

TABLE II

LIMITING EQUIVALENT CONDUCTIVITY AND ITS PRODUCT WITH VISCOSITY OF SOLVENT

M.R.	1.00		2.13		3.95	
Temp.	Λ_0	$\Lambda_0\eta_0$	Λ_0	$\Lambda_0\eta_0$	Λ_0	$\Lambda_0\eta_0$
5°C	98	149	59	90	56	85
15°C	128	145	79	90	74	84.4
25°C	165	148	102	91.5	96	85.8
35°C	194	140	128	92.5	119	85.9
45°C	227	136	158	94.6	144	86.2
60°C	282	132	210	98.5	186	87.2

with the product of Λ_0 and solvent viscosity η_0. In Fig. 13 $\Lambda\eta$, including $\Lambda_0\eta_0$, are plotted against temperature for dilute solutions of these three kinds of molar ratio. It is seen that while Walden's rule is fully applicable to the 3.95 molar ratio solution, $\Lambda\eta$ for metasilicate solution decreases markedly with increase in temperature, and that for the 2.13 molar ratio solution increases slightly with it. These facts may be explained by considering the contribution of OH^- ion in the solutions to the equivalent conductivity.

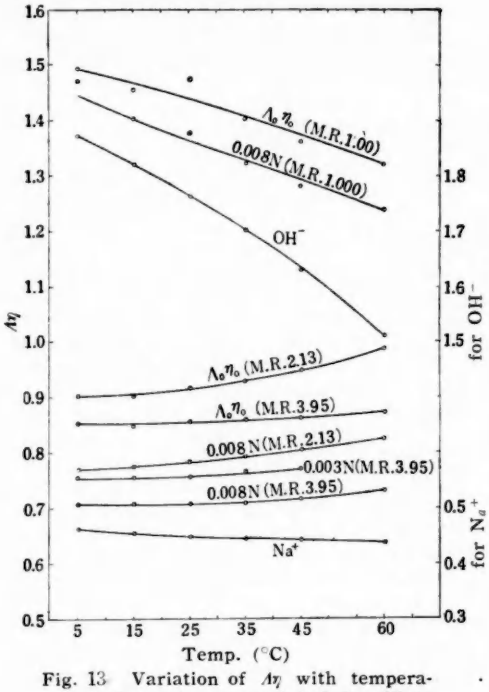

Fig. 13 Variation of $\Lambda\eta$ with temperature for extreme, and infinite dilute sodium silicate solutions and for Na^+ and OH^- ion at infinite dilution

In order to examine this, OH^- ion concentration at various temperatures was calculated from *p*H values, and hydrolysis percentages were derived from them[7]. They were 23, 26, 28, 26 and 26% at 5°, 15°, 25°, 35° and 45°C for 0.008 N metasilicate solution, 1.4, 2.8, 3.2, 3.9 and 4.2% at above respective temperatures for the 2.13 molar ratio solution. For the 3.95 molar ratio solution they were negligibly small, i. e. varies only from 0.7% to 1.9% at 0.008 N between 5° and 45°C. Thus it is well understood that for the metasilicate solution, the decreasing tendency with temperature of $\Lambda_0\eta_0$ of OH^- ion, which is shown also in Fig. 13 along with that of Na^+ ion, appears to give a prominent effect on its $\Lambda\eta$ while the constancy of $\Lambda\eta$ of the 3.95 molar ratio solution is well satisfied. For the 2.13 molar ratio solution Λ increase with temperature is affected by the change in OH^- ion concentration with temperature, so that $\Lambda\eta$ becomes larger than in the case where the composition of the solution holds constant.

$\Lambda_0\eta_0$ for an ion is related to the ionic radius r as shown by the equation $r=0.820|z|/\Lambda_0\eta_0$ where r is expressed by Ångstrom and $|z|$ denotes the charge valency. Since this relation was derived from Stokes' law $r=1/(6\pi\eta u)$, where ionic mobility u is related to the limiting equivalent conductivity by $6.47\times10^6\Lambda_0/|z|$, it is applicable only to the ion of symmetrical shape. Therefore, though this treatment may be merely a rough approximation, it would be of some value to estimate the radius of silicate ion by this equation. Λ_0 of silicate ion in the solution of molar ratio 1.00, 2.13 and 3.95 were computed from their limiting equivalent conductivity as follows,

$$\Lambda_{0(\text{sil.})}=(\Lambda_0-\Lambda_{0(Na^+)}-C_{OH}\Lambda_{0(OH^-)})/C_{\text{sil.}}$$

where C_{OH} and $C_{\text{sil.}}$ are OH^- ion and silicate ion concentration at infinite dilution. It seems difficult, however, to get the hydrolysis percentage at infinite dilution by the extrapolation of a curve plotted against concentration, and further more, unstable *p*H values observed in this dilute region do not enable one to get hydrolysis percentage. Meanwhile, the limiting equivalent conductivity was obtained by extrapolation of curve by neglecting the abruptly increased value observed in this extreme dilution. Thus replacement of the hydrolysis percentage at 0.008 N for that at infinite dilution will be tentatively justified. The concentration of silicate ion at infinite dilution was assumed to be $(1-X)$ N, where X denoted degree of hydrolysis. As a result, r=4.0 Å was obtained for both 2.13 and 3.95 molar ratio solutions, and r=2.24 Å for metasilicate solution. However, it is recognized that the Stokes' law radius is known to require the correction if applied for the smaller radius than 5 Å, due to the deviation of numerical constant from 6π. After the above-mentioned radii were multiplied by the correction factor[8] they become 4.56 Å and 3.63 Å. These values, despite a result of rather drastic estimation and resultant failure to distinguish between the radii of silicate ions in the 2.13 and 3.95 molar ratio solutions, their order seems quite reasonable as compared with data regarding the size of sodium silicate molecule

7) Because of lack of extreme accuracy in the measurement hereby used, pH value ±0.1 would be within the error. This led to a considerable inconsistency of data of hydrolysis percentage especially for the solution having high OH^- ion concentration, such as sodium silicate solution.

8) This correction factor was cited from, R. A. Robinson and R. H. Stokes, "Electrolyte Solutions," Butterworths Scientific Publications, London (1955), p. 119.

reported elsewhere.

In the preceding paper the change in equivalent conductivity with concentration has been computed for the 3.95 molar ratio solution at 25°C, on the basis of Falkenhagen's equation,

$$\Lambda=\left(\Lambda_0-\frac{41.25(|z_1|+|z_2|)\sqrt{I}}{\eta(\varepsilon T)^{1/2}(1+\kappa a)}\right)\times\left(1-\frac{2.801\times10^6|z_1z_2|q}{(\varepsilon T)^{3/2}(1+\sqrt{q})}\cdot\frac{e^{\kappa a(1-\sqrt{q})}-1}{\kappa a(1-\sqrt{q})}\cdot\frac{\sqrt{I}}{(1+\kappa a)}\right)$$

$$\kappa=\left(\frac{8\pi Ne^2}{1000\varepsilon kT}\right)^{1/2}\sqrt{I}$$

where notation is the same as used before.

This computation was extended for the equivalent conductivities measured at other temperatures, 7 Å for the mean ionic diameter a being used as in the previous treatment. The results were corrected for the solution viscosity and plotted in Fig. 12. The accordance of observed values with those theoretically computed is quite satisfactory as far as the concentration 0.8–0.9 N is reached. This consistent agreement at any temperature of theoretical and observed data shows that the change with temperature of equivalent conductivity—square root of concentration curve is explained only in terms of temperature change and consequent change of dielectric constant and viscosity of solvent, and that the change of composition of solution need not be considered; this change may occur, if any, on the part of silicate ion or molecule therein, because pH measurements indicated that OH^- ion concentration did not vary appreciably over the temperature range measured. Also it is recognized that the assumption, which has been set upon computing equivalent conductivity at 25°C on the basis of Falkenhagen's equation, was proved sufficient at any other temperature for the explanation of them.

Above the concentration 0.8–0.9 N, the theoretical values fall increasingly below the observed one. This was caused by the fact that the viscosity increase outgrew more and more the conductivity decrease, as concentration increased. On the other hand it has been already noticed that at the concentration where specific conductivity became maximum the viscosity of the solution varied strikingly according to the molar ratio of the solution and it appeared to have little effect on the specific conductivity at this concentration range. These facts suggest that the higher the concentration, the larger difference between the mechanisms of conductance and viscosity may appear. The correlation of conductivity and viscosity of the sodium silicate solution would be a very interesting subject, further study of which may throw some light upon the investigation of the structure of the concentrated solution. It will be dealt with in the succeeding paper.

The author would like to express his sincere thanks to Dr. T. Yawataya for his kind encouragement throughout this work.

Research Laboratory Asahi Glass Co. Ltd. No. 2 Benten-cho Tsurumi-ku, Yokohama

Relation between the Contents of Radon and Radium B in Several Radioactive Mineral Springs

By Shunji UMEMOTO

(Received June 11, 1956)

Introduction

The relation between the contents of radon and its decay products was first studied by K. Kimura, K. Kuroda and Y. Yokoyama[1] at Masutomi Mineral Springs. Further studies were made by Y. Yokoyama[2] at Ikeda and Misasa Springs. Their results are summerised as follows.

(1) The contents of radium A, radium B and radium C are smaller than expected from their equilibrium states with radon.

(2) The greater the radon content, the greater is the extent to which the equilibrium states between radon and its decay products decreased.

(3) In a sealed vessel the equilibrium between radon and radium A is achieved within 20 min. after the issue, and that between radon and radium B and radium C within 3 hours.

(4) In a mineral spring, the contents (expressed in Curie) of Rn, RaA, RaB and RaC decrease in this sequence.

(5) The relationship between the contents of Rn and RaA, RaB and RaC can be accounted for when it is assumed that the latter three are produced within 2 to 45 min. before the issue from Rn free from its decay products.

S. Umemoto[3] reported, however, that RaB can be present more than the equilibrium amount to the Rn, on a continuous measurement of their contents in "Hisuino-yu" of Misasa Hot Springs. T. Ishimori and I. Hatae[4] measured the contents of Ra, Rn, RaA, RaB, RaC, RaF, ThX, Tn, ThB and ThC in Ikeda Mineral Springs and discussed the relation between the contents of Rn and RaB, showing that RaB can be present more than the equilibrium amount to the Rn*. K. Kimura, K. Nagashima, N. Ikeda and Ka. Kimura[5] also studied the contents of RaB and Rn in the mineral springs of Naegi district, Gifu Prefecture, and found that the RaB content is merely several fractions of the equilibrium amount to the Rn. S. Umemoto[6] continuously measured the contents of Rn and RaB for a year at Misasa Hot Springs. When the content of RaB was compared with that of Rn 20 min. after the issue, the ratio RaB/Rn became greater with increase in the rate of flow, with a few exceptions. It was also made clear that the ratio RaB/Rn decreases when the rate remarkably increases. In special cases, the ratio RaB/Rn is greater than unity but decreases in autumn when water is removed from the surrounding rice field.

The present author intended to determine the content of RaB and other relating components immediately after the issue in order to disclose the relationship between the contents of Rn and RaB. The measurements were made at Hamamura (Kachimi) Hot Springs, Misasa Hot Springs and Sekigane Hot Springs, Tottori Prefecture.

Location and Methods for Experiments

These three Springs are situated in the middle of Tottori Prefecture and are found in a granite zone. Hamamura Hot Springs (I) are among sand hills along the sea side. Misasa Hot Springs (II) are found along the valley of the river Misasa. Sekigane Hot Springs (III) are found along a mountain torrent which flows into the river Ogamo (Fig. 1). Water temperature, rate of flow and the contents of chloride, sulfate, radon and radium B were measured once a month for a year at one spring in I, five springs in II and one in III. Their names are as follows:

1) K. Kimura, K. Kuroda and Y. Yokoyama, *J. Chem. Soc. Japan* (*Pure Chem. Sect.*), **69**, 34 (1948).
2) Y. Yokoyama, ibid., **70**, 399 (1949).
3) S. Umemoto, This Bulletin, **26**, 160 (1953).
4) T. Ishimori and I. Hatae, Read before the symposium on geochemistry of the Chemical Society of Japan, Sapporo, July, 1952,; Read before the seventh annual meeting of the Chemical Society of Japan, Tokyo, April, 1954.

* Yokoyama's report mentioned above also shows that RaB is contained more than the equivalent amount to the Rn in Ikeda Spring No.2; (he considered that this is due to escape of Rn) hence it appears certain that the amount of RaB is more than that expected from the Rn content.
5) K. Kimura, K. Nagashima, N. Ikeda and Ka. Kimura, *Radioisotopes*, **4**, 31 (1955).
6) S. Umemoto, *J. Chem. Soc. Japan* (*Pure Chem. Sect.*), **75**, 352 (1954).

TABLE I

OBSERVATIONAL RESULTS IN I

Time of sampling	Weather	Temperature °C	Rate of flow l./min.	Water temperature °C	Cl^- mg./l.	Rn Mache	Rn 10^{-10} c./l.	RaB	RaB/Rn	SO_4^{2-} mg./l.
1954, 26/V a. m. 11.40	Cloudy Fine later	20.5	18.38	69.7	290.6	20.0	72.8	14.6	0.200	392.1
25/VI a. m. 11.40	Cloudy	20.2	17.21	69.7	289.6	19.5	70.9	9.08	0.128	396.1
6/VII a. m. 11.15	Fine	30.5	19.10	69.7	289.6	20.8	75.7	18.2	0.240	437.6
26/VIII a. m. 11.17	Cloudy	32.8	22.17	69.6	290.6	21.9	79.7	16.6	0.208	465.1
27/IX a. m. 11.40	〃	22.0	21.49	69.7	285.1	21.4	77.9	19.5	0.250	426.1
13/X a. m. 11.07	〃	13.8	17.12	69.7	287.6	20.1	73.2	27.5	0.376	409.1
17/XI a. m. 11.11	Rainy	9.3	17.73	70.0	281.6	19.8	72.1	15.3	0.212	416.4
16/XII a. m. 11.22	Fine	4.4	19.32	70.0	286.6	23.2	84.4	25.8	0.306	460.2
1955, 14/I a. m. 11.14	Cloudy	5.0	20.06	70.0	288.1	19.7	71.7	20.8	0.290	452.6
15/II a. m. 11.09	Fine	5.4	16.24	70.0	297.0	20.7	75.3	28.1	0.373	456.2
14/III a. m. 10.54	Cloudy	6.0	17.45	70.0	294.0	19.3	70.2	12.5	0.178	449.8
27/IV a. m. 11.17	Fine	14.0	21.72	69.9	293.5	21.5	78.3	26.8	0.342	436.5

TABLE II

OBSERVATIONAL RESULTS IN II-1

Time of sampling	Weather	Temperature °C	Rate of flow l./min.	Water temperature °C	Cl^- mg./l.	Rn Mache	Rn 10^{-10} c./l.	RaB	RaB/Rn
1953, 1/VI a. m. 11.00	Cloudy	24.0	2.860	63.2	414.7	33.3	121	14.9	0.123
23/VI a. m. 9.10	Cloudy Rainy later	25.8	3.973	66.4	411.7	22.0	80.1	15.7	0.196
6/VII a. m. 10.18	Cloudy	28.6	4.610	66.6	390.2	26.6	96.8	26.4	0.273
11/VIII a. m. 10.20	〃	30.4	2.538	69.6	605.4	21.0	76.4	23.6	0.309
1/IX a. m. 10.05	Rainy Cloudy later	27.0	2.403	69.8	401.7	20.1	73.1	18.1	0.248
22/IX a. m. 10.10	Fine Cloudy later	22.1	2.750	69.3	400.2	18.5	67.3	18.2	0.271
13/X a. m. 10.07	Cloudy Fine later	19.0	1.710	68.2	396.2	10.7	38.9	14.5	0.373
9/XI a. m. 10.16	Fine	16.6	1.893	67.6	395.2	14.8	53.9	18.0	0.334
14/XII a. m. 10.10	〃	7.2	2.476	68.0	405.7	11.1	40.4	12.9	0.319
1954, 11/I a. m. 10.35	Rainy	7.8	2.645	67.0	400.7	14.4	52.4	13.5	0.258
15/II a. m. 10.40	Cloudy	6.0	2.091	66.2	400.2	13.2	48.0	15.1	0.314
15/III a. m. 10.22	〃	5.0	1.993	66.5	402.7	14.5	52.8	16.6	0.314
20/IV a. m. 10.32	〃	13.0	1.585	65.8	377.2	10.7	38.9	7.5	0.192
20/V a. m. 10.15	〃	21.6	1.673	67.3	399.2	13.8	50.2	12.1	0.240

TABLE III

OBSERVATIONAL RESULTS IN II-2

Time of sampling	Weather	Temperature C°	Rate of flow l./min.	Water temperature °C	Cl^- mg./l.	Rn Mache	Rn 10^{-10} c./l.	RaB	RaB/Rn
1953, 16/X a. m. 10.06	Cloudy	16.6	0.731	58.0	613.9	13.5	49.1	39.0	0.794
13/XI a. m. 10.06	〃	11.0	1.022	59.0	629.8	13.8	50.2	29.4	0.586
17/XII a. m. 10.04	〃	12.0	0.696	57.3	655.6	14.1	51.3	40.8	0.795
1954, 16/I a. m. 10.14	〃	7.2	0.745	58.3	663.3	16.5	60.1	41.0	0.682
25/II a. m. 10.30	Fine Cloudy later	7.0	1.060	58.0	657.8	15.7	57.1	36.0	0.630
18/III a. m. 10.10	Cloudy	8.5	1.063	59.3	650.8	19.0	69.2	42.1	0.608
23/IV a. m. 10.29	Fine	16.7	1.053	59.4	655.3	15.0	54.6	38.9	0.713
19/V a. m. 10.12	Cloudy	21.6	1.030	59.5	660.3	15.7	57.1	36.9	0.646
22/VI a. m. 9.54	〃	19.0	1.500	61.0	661.8	16.7	60.8	13.8	0.227
23/VII a. m. 10.01	Fine	28.5	1.260	60.4	620.2	17.1	62.2	32.8	0.527
23/VIII a. m. 10.06	〃	31.2	1.000	61.0	591.2	19.9	72.4	22.9	0.316
21/IX a. m. 9.50	〃	25.0	1.250	59.0	611.7	17.5	63.7	17.0	0.268

TABLE IV

OBSERVATIONAL RESULTS IN II-3

Time of sampling	Weather	Temperature C°	Rate of flow l./min.	Water temperature °C	Cl^- mg./l.	Rn Mache	Rn 10^{-10} c./l.	RaB	RaB/Rn
1953, 4/VI a. m. 10.10	Cloudy	22.8	5.06	41.6	505.6	268	976	248	0.254
24/VI a. m. 9.50	Fine Cloudy later	27.1	11.28	44.4	354.2	357	1300	884	0.680
8/VII a. m. 10.15	Cloudy Rainy later	28.0	11.59	44.0	355.2	372	1350	1060	0.788
12/VIII a. m. 10.23	Fine	31.3	9.82	41.3	188.1	473	1720	2100	1.22
2/IX a. m. 10.40	Fine Cloudy later	29.0	8.78	40.0	182.1	471	1710	1120	0.655
28/IX a. m. 10.13	Fine	21.2	7.42	39.2	216.6	449	1630	311	0.191
14/X a. m. 10.14	〃	17.2	2.87	39.4	375.1	414	1510	1450	0.960
10/XI a. m. 10.20	Cloudy Rainy later	14.7	2.68	40.0	505.2	483	1760	2650	1.503
15/XII a. m. 10.15	Cloudy	8.0	3.60	41.7	460.7	440	1600	1700	1.064
1954, 13/I a. m. 10.41	Rainy	5.0	4.91	42.0	495.2	311	1132	1260	1.114
24/II a. m. 10.15	Fine	6.3	6.95	43.0	392.2	619	2250	1660	0.739
16/III a. m. 10.15	Cloudy	7.2	5.90	42.4	340.1	610	2220	2850	1.285
21/IV a. m. 10.10	Fine	13.5	3.89	42.2	471.7	496	1805	2096	1.161
18/V a. m. 9.29	〃	20.9	3.88	42.6	492.2	393	1430	1270	0.886
24/VI a. m. 10.00	Cloudy	19.6	8.35	44.0	369.1	471	1714	864	0.504
25/VII a. m. 9.55	Fine	29.0	7.73	42.7	240.1	420	1530	1580	1.035
24/VIII a. m. 10.20	〃	30.0	6.50	42.4	283.6	568	2070	2047	0.989
22/IX a. m. 9.50	〃	25.0	4.06	41.3	272.6	379	1380	903	0.654

TABLE V

OBSERVATIONAL RESULTS IN II-4

Time of sampling	Weather	Temperature C°	Rate of flow l./min.	Water temperature °C	Cl⁻ mg./l.	Rn Mache	Rn 10^{-10} c./l.	RaB	RaB/Rn
1954, 24/V a. m. 10.09	Cloudy Rainy later	20.5	2.927	46.7	580.6	244	888	674	0.759
23/VI a. m. 10.00	Rainy	19.7	4.010	46.3	505.7	266	968	1066	1.101
26/VII a. m. 9.49	Cloudy	29.0	3.000	50.0	635.5	237	863	803	0.930
25/VIII a. m. 10.08	Fine	30.8	3.150	50.0	603.8	240	873	947	1.085
24/IX a. m. 10.07	Cloudy	25.4	2.992	49.0	496.7	228	828	801	0.967
14/X a. m. 11.01	Fine Cloudy later	14.0	3.339	47.0	560.2	236	859	729	0.849
16/XI a. m. 10.30	Cloudy Fine later	13.0	3.140	46.0	522.7	227	826	686	0.830
14/XII a. m. 10.08	Rainy	5.2	2.964	43.0	522.7	245	892	901	1.01
1955, 24/I a. m. 10.33	Fine	5.0	3.258	39.2	545.2	231	841	717	0.852
14/II a. m. 10.48	Fine Cloudy later	3.6	2.719	40.9	615.2	213	775	721	0.930
11/III a. m. 10.30	Fine	8.3	0.810	43.2	634.2	218	793	495	0.624
29/IV a. m. 10.06	Cloudy	14.0	1.230	45.3	609.1	243	885	717	0.810

TABLE VI

OBSERVATIONAL RESULTS IN II-5

Time of sampling	Weather	Temperature C°	Rate of flow l./min.	Water temperature °C	Cl⁻ mg./l.	Rn Mache	Rn 10^{-10} c./l.	RaB	RaB/Rn
1953, 13/VI a. m. 10.11	Fine	22.3	2.600	57.3	268.7	21.5	78.3	18.1	0.231
25/VI a. m. 9.50	Cloudy	28.0	2.892	57.7	286.2	22.9	83.4	22.2	0.266
9/VII a. m. 10.20	〃	25.5	3.130	58.0	273.5	22.0	80.0	21.9	0.274
13/VIII a. m. 10.15	Fine Cloudy later	31.0	2.644	57.6	280.2	21.4	77.9	21.4	0.275
3/IX a. m. 10.15	Cloudy	26.3	2.756	57.7	279.2	21.9	79.7	38.1	0.478
29/IX a. m. 10.15	Rainy	20.7	2.898	57.8	270.6	21.4	77.9	24.2	0.311
15/X a. m. 10.07	Fine	17.0	2.345	57.2	260.1	19.7	71.7	28.5	0.398
12/XI a. m. 11.25	Cloudy	10.3	3.759	57.6	275.9	20.2	73.5	38.7	0.527
16/XII a. m. 10.18	Fine	6.2	2.505	57.3	255.6	20.7	75.3	30.8	0.409
1954, 14/I a. m. 10.35	Rainy	7.0	2.904	57.6	257.6	21.8	79.4	29.5	0.371
16/II a. m. 10.31	〃	5.0	3.017	57.9	256.1	21.2	77.2	31.9	0.413
17/III a. m. 10.22	Cloudy Fine later	8.4	3.307	58.0	251.6	22.0	80.1	32.1	0.401
22/IV a. m. 10.13	Cloudy	13.5	3.149	58.0	232.6	20.7	75.3	35.1	0.466
17/V a. m. 10.05	Cloudy Fine later	17.0	3.178	58.0	214.1	19.7	71.7	14.7	0.201

TABLE VII

OBSERVATIONAL RESULTS IN III

Time of sampling	Weather	Temperature °C	Rate of flow l./min.	Water temperature °C	Cl^- mg./l.	Rn Mache	Rn 10^{-10} c./l.	RaB	RaB/Rn	SO_4^{2-} mg./l.
1954, 27/VIII a. m. 10.10	Fine	31.5	11.62	46.0	101.5	36.2	132	65.1	0.493	84.7
28/IX a. m. 10.05	Rainy	—	11.44	46.2	104.0	37.5	137	70.0	0.511	81.5
12/X a. m. 10.28	Cloudy	12.5	11.48	46.1	102.0	32.1	117	64.4	0.550	80.5
18/XI a. m. 10.29	Fine	12.0	11.44	46.5	108.5	33.2	121	57.2	0.473	83.6
15/XII a. m. 10.05	〃	4.5	10.61	46.4	108.5	31.9	116	64.5	0.556	87.2
1955, 12/I a. m. 10.43	Fine Cloudy later	2.0	11.76	46.0	106.0	31.6	115	65.3	0.568	95.4
17/II a. m. 10.04	Cloudy	—	11.49	46.0	110.5	32.6	119	67.2	0.565	94.8
15/III a. m. 10.02	Fine	7.3	11.91	46.0	109.7	32.1	117	36.0	0.308	95.6
26/IV a. m. 10.20	〃	13.5	11.91	45.7	110.5	26.9	97.9	36.1	0.369	91.9
19/V a. m. 10.25	〃	22.3	11.35	46.0	106.7	36.7	133.5	70.2	0.526	91.9
21/VI a. m. 10.18	〃	27.5	11.45	47.0	106.2	35.0	127.4	72.2	0.567	90.9
21/VII a. m. 10.07	〃	31.0	11.00	47.0	107.5	38.2	139	83.4	0.600	92.0

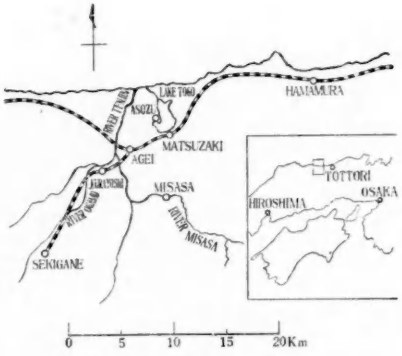

Fig. 1. Locality map

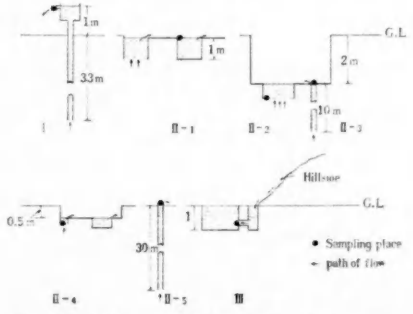

Fig. 2. Schematically states of springs

I	Hamamura (Kachimi)	The Institute for Live Stock.
II-1	Misasa	Bun-aburaya.
II-2	Misasa	Hisui-no-yu (orifice).
II-3	Misasa	Hisui-no-yu (bathtub).
II-4	Misasa	Gunze-shinsenryo.
II-5	Misasa	Tanaka-no-yu.
III	Sekigane	Torikai-ryokan.

The present states of these spings are schematically shown in Fig. 2. Chloride was determined by Mohr's method, sulfate by the barium chromate method and Rn with I. M. fontactoscope. RaB was measured by the dithyzone extraction method[7] immediately after the sampling. The same water was equally treated after three hours and the result was taken as standard*. Measurements were made by Lauritzen electroscope. Results are shown in Table I to VII.

Discussion

Concerning the daily change in the content of various elements, some springs (I, II-2, II-5 and III) show very little fluctuation with time. Others show marked

7) S. Umemoto, *Japan Analyst*, **2**, 201 (1953).

* It is possible that RaB is adsorbed on the glass surface while kept for 3 hours. When the surface is washed with nitric acid (1:9) or acetic acid (1:9) for 3 min. after the mineral water is decanted off after 3 hours' storage, only 1 to 5 percent. of the initial activity of the original RaB is found in the extract. This value can not be regarded to be significant for the following discussion.

change in the content to different extents. (II-3 very marked; II-1, II-4 less so) This fact depends on the following factors:

(1) the depth of the well (i. e. the depth of sampling)

When water is collected at a depth of 10 m. or more, the fluctuation in the content is generally small.

(2) the location of the well.

The fluctuation is more marked when the spring is among other springs comprising water of different salt content. When the salt content of other springs in the neiborhood is similar, only a very slight fluctuation is observed with time. Springs which show marked fluctuation in the contents are about 3 m. deep on the northern beach of the river Misasa, where springs of various salt contents are found. The latter shows a marked difference between the content of the component of one compared with another, but the ratio of the components is rather similar. It is, therefore, predicted that the difference is due to the different extent to which ordinary ground water is mixed with an identical hot water which originates in a same source[8]. This also accounts for the observation that flactuation is greater for a shallower spring.

Nothing conclusive can be stated from the present data about the annual change in the content.

On the examination of the diagrams temp.–Cl, Rn–Cl, RaB–Cl, Rn–RaB and rate of flow–ratio RaB/Rn, only a few correlations are found. The correlation coefficients for rate of flow–ratio RaB/Rn in II-4, II-2 and III are respectively 0.661, −0.789 and −0.627. (Fig. 3-5) (All these coefficients are significant stochastically)

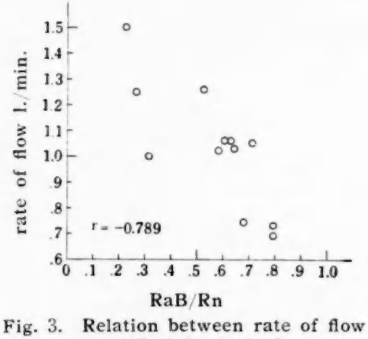

Fig. 3. Relation between rate of flow and RaB/Rn in II-2

8) S. Umemoto, *J. Chem Soc. Japan (Pure Chem. Sect.)*, **74**, 94 (1954).

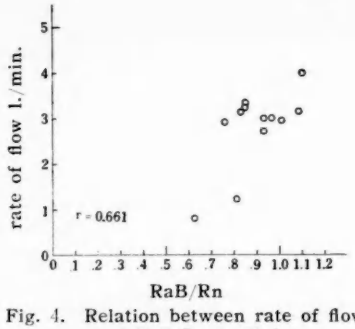

Fig. 4. Relation between rate of flow and RaB/Rn in II-4

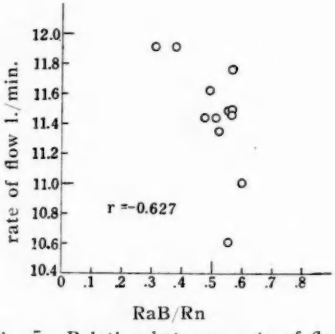

Fig. 5. Relation between rate of flow and RaB/Rn in III

The fact that the latter two have negative values of correlation coefficient provides support to the view of Kimura, Kuroda and Yokoyama about the relationship of the content of Rn and that of its decay products. They claim that radium B in the mineral spring is produced only from Rn which was supplied free from its decay products, the chemical behavior of both species being similar until they reach the surface. Since the contents of chemical constituents in II-2 and III remain almost unchanged with time, it could be reasonably assumed that a radioactive substance is supplied and springs out in a definite manner.

The correlation coefficient between the rate of flow and the ratio of RaB to Rn is positive for II-4; an inversed relationship to the above mentioned case can be predicted. Their assumption appears not to be valid in this case. Since the ratio RaB to Rn is sometimes greater than unity, there must be cases when the RaB is supplied not by the Rn only or when a part of the Rn escapes. The depth at which the mineral water of both II-4 and II-3 (sometimes both having the ratio

greater than unity) is taken, is less than 3 m. and both show very strong overall activity. Strongly radioactive springs are also found in their neighborhood as well as radioactive ground water[9]. They all come from shallow wells less than 3 m. in depth. It is thus possible that Rn and RaB are supplied to the mineral water near the surface or Rn escapes preferentially near the surface, resulting in unusual contents of both species as mentioned above. Another example of a mineral spring that has a greater value than unity for the ratio RaB to Rn, is provided in Ikeda Mineral Springs in Shimane Prefecture. The correlation between the rate of flow and the ratio RaB/Rn in II-4 appears to arise from a still uncertain regularity including the state of supply of both species.

No significant correlation between the rate of flow and the ratio RaB/Rn was observed in other springs. Considering the variation of the main constituents, the ratio in II-3 seems to be liable to fluctuation of influence near the surface, and also those in II-1; nothing regular can be expected for either of them. For I and II-5, the fluctuation in main constituents is less, but it is considered that the contents of minor constituents are not sufficient to fulfill the necessary assumption for Kimura et al's consideration. From the fact that more than the half of the examples are not in accord with their comments, not many mineral springs appear to satisfy the conditions suggested by them. It does not imply, however, that their examples have been rather exceptional. Their second statement appears not to be true for the present example; i. e. the extent to which the RaB content is decreased from the equilibrium amount to the Rn does not increase with increasing Rn content.

9) T. Sugihara, *Repts. Balneol. Lab. Okayama Univ.*, **9**, 37 (1953).

Conclusion

The above observed mineral springs are classified into three groups regarding the correlation between the rate of flow and the ratio RaB/Rn: (1) negatively correlating, (2) positively correlating and (3) without significant correlation. In the first group Rn appears to be free from its decay products at the point of its supply and it is the source of all other radioactive species in the mineral water, all of them showing a chemical behavior similar to one another. For the second group no appropriate explanation has been available as yet. For the third group, it could be assumed that the source, path of supply and the chemical behavior after the supply of Rn are too complicated or that these are disturbed by secondary phenomena near the surface. It appears as if the third group comprises most of mineral springs.

Balneological Laboratory
Okayama University
Misasa Hot Springs
Tottori Prefecture

SHORT COMMUNICATIONS

Nuclear Magnetic Resonance of Polyvinyl-alcohol (Transition Temperature)

By Kōji TANAKA, Kyōzō YAMAGATA, Masako YOSHIDA and Minoru ODAJIMA

(Received December 18, 1956)

In our previous communication[1], the results of the measurements of the nuclear magnetic resonance absorption of protons in polyvinyl alcohol (P. V. A.) fibers from 10°C to 170°C were reported. After that, the measurements were done for the samples of P. V. A. powder and film from −50°C to 200°C. The P. V. A. powder was purified and fractionated. The P.V.A. film was cast from about 2.5% aqueous solution of P. V. A. on a glass plate placed horizontally in an air-thermostat at 50°C and dried at 50°C and 10^{-5} mmHg for several days.

The apparatus used is the same as mentioned before, except that the cryostat[2] was used to cool the sample to below 20°C. The field intensity was about 3000 gauss.

The width between the points of the maximum slope of the adsorption curve is shown in Fig. 1 as the function of temperature. Below 20°C the widths are almost constant with the value of about 12 gauss, but in the range from 20°C to 50°C, the width decreases gradually with temperature and remains unchanged from

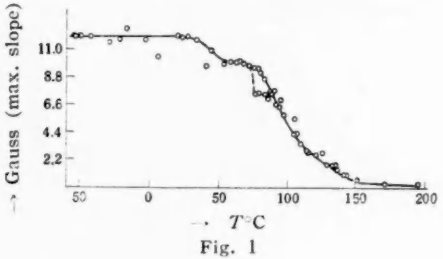

Fig. 1

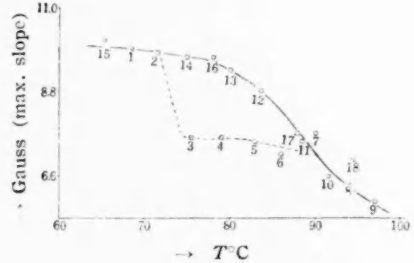

Fig. 2

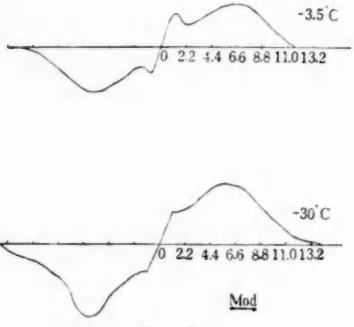

Fig. 3

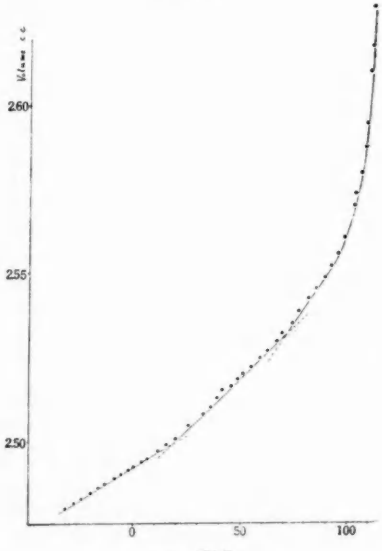

Fig. 4

1) Kōji Tanaka, Kyōzō Yamagata and Shigeyoshi Kittaka, This Bulletin, **29**, 843 (1956).
2) H. G. Gutowsky, L. H. Meyer and R. E. McClure, *Rev. Sci. Instr.* **24**, 644 (1953).

50°C to 70°C, then it decreases again in the range between 70°C and 120°C. With respect to this transition at around 70°C, an irreversible hysteresis is observed for the sample with smaller degree of crystallinity which has not been thermally pretreated. The results are shown in Fig. 2 where the numbers in the figure denote the order of the treatments of the sample. For the sample, which is thermally pretreated, this hysteresis is not observed and the decreasing of the line width occurs along the upper curve of the hysteresis curve in the figure.

The derivative curves of proton resonance at −3.5°C and −30°C are shown in Fig. 3 and at −50°C the central component is still observed though it is very weak.

In order to compare the results obtained by nuclear magnetic resonance method with those by dilatometric method, volume-temperature curve of P. V. A. film was obtained and its result is shown in Fig. 4.

It is interesting to note that the transition temperatures of about 15°C and 70°C[3] obtained by the dilatometric method coincide with the starting temperatures of the transition obtained by the nuclear magnetic resonance method.

The authors wish to exress their appreciation to Prof. Masatami Takeda for his kind advice and encouragement.

Tokyo College of Science,
Shinjuku-ku, Tokyo

3) Y. Yano. *J. Chem. Soc. Japan*, **73**, 708 (1952).

Diamagnetic Susceptibilities of Azo-derivatives of 2-Naphthol

By Yoshio MATSUNAGA

(Received February 28, 1957)

In the previous paper[1], the procedure to estimate the molar susceptibilities of the azophenol and the quinonehydrazone forms of hydroxyazobenzene was presented. We applied it to twenty compounds and concluded that they are all in the azophenol form in the solid state. Continuing this study, we measured the diamagnetic susceptibilities of eight azo-derivatives of 2-naphthol. All specimens were purified finally by sublimation in vacuo. As shown in the Table, we found that the structure of these compounds depends on the nature and the position of the substituents.

It must be noted that our calculated values for the azophenol and the quinonehydrazone forms given by the procedure similar to that described in the previous paper, are in serious disagreement with those given by Pascal[4] and Pacault[5]. As an example, our value for the azophenol form of 1-phenylazo-2-naphthol -146.7×10^{-6} is appreciably smaller than -154×10^{-6} given by the French workers, and the value for the quinonehydrazone form -135.8×10^{-6} estimated by use of the observed value for quinone monoxime is remarkably larger than -124.8×10^{-6} given by Pascal and -130.8×10^{-6} by Pacault. However, the experimental results seem to support our estimations. The observed values of the molar susceptibility of 1-phenylazo-2-naphthol and its *o*-methyl-, *m*-nitro- and *p*-nitro-derivatives are in accordance with the calculated values for the quinonehyrazone form (I), but *p*-methyl-, *o*-methoxy-, *o*-chloro- and *p*-chloroderivatives are found to exist in the azophenol form (II) in the solid state.

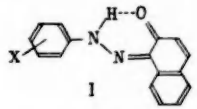

I

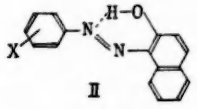

II

The effect of substituents on the equilibria between these two tautomeric forms in various solutions was examined by Burawoy and his collaborators[6]. According to their conclusion, the concentration of the quinonehydrazone tautomers increases in the order of substituents, *p*-Me $<$H$\sim$*p*-Cl$<$*o*-Me$<$*o*-Cl$<$*m*-$NO_2$$<$*o*-MeO$<$*p*-$NO_2$. In contrast to the above series, our results suggest that MeO, Me and Cl substituted both in the ortho- and para-positions favor the azophenol form, and methyl group in the ortho-position is not so effective as that in the para-position.

1) Y. Matsunaga, This Bulletin, **29**, 308 (1956).
2) Y. Matsunaga, ibid., **29**, 969 (1956).
3) P. Pascal, *Bull. soc. chim. France*, **9**, 177 (1911).
4) P. Pascal, *Ann. chim. phys.* **25**, 289 (1912).
5) A. Pacault and J. Chauvelier, *Bull. soc. chim. France*, **17**, 367 (1950).
6) A. Burawoy, A. G. Salem, and A. R. Thompson, *J. Chem. Soc.*, **1952**, 4793.

TABLE

DIAMAGNETIC SUSCEPTIBILITIES OF AZO-DERIVATIVES OF 2-NAPHTHOL

Substance	Suscept. ($-\chi \cdot 10^6$)	Molar Suscept. ($-\chi_M \cdot 10^6$) Obs.	Calc. (I)	Calc. (II)	Lit.
β-Naphthoquinone-1-oxime	—	—	—	—	83.9[2]
2-Naphthol	—	—	—	—	97.0[3]
1-Phenylazo-2-naphthol	0.554	137.6	135.8	146.7	140.7[4], 135.5[5]
1-*o*-Tolylazo-2-naphthol	0.567	148.7	146.4	157.3	—
1-*p*-Tolylazo-2-naphthol	0.601	157.6	146.4	157.3	—
1-*o*-Methoxyphenylazo-2-naphthol	0.588	163.6	152.2	164.1	—
1-*o*-Chlorophenylazo-2-naphthol	0.570	161.0	150.6	161.5	—
1-*p*-Chlorophenylazo-2-naphthol	0.571	161.4	150.6	161.5	—
1-*m*-Nitrophenylazo-2-naphthol	0.484	142.0	142.4	153.3	—
1-*p*-Nitrophenylazo-2-naphthol	0.483	141.7	142.4	153.3	—

In the solid state, the effect of substituents appears to be not necessarily similar to that observed by Burawoy on the tautomeric equilibria in the dissolved state.

The author wishes to express his hearty thanks to Professor H. Akamatu for his kind direction.

Department of Chemistry
Faculty of Science
The University of Tokyo
Hongo, Tokyo

Natural Furan Derivatives. Part I. The Synthesis of Perillaketone

By Teruo MATSUURA

(Received March 4, 1957)

Perillaketone was isolated from the leaves of the Manchurian *Perilla frutescens Brit.* and was given the structural formula (I) by Goto[1]. Sebe also isolated perillaketone from the Formosan Perilla frutescens form viridis Kudo and independently gave the same formula (I) to it[2]. For the purpose of the confirmation of its structure, the present synthesis of β-furyl isoamyl ketone has been furnished.

The reaction of the acid chloride of 3-furoic acid with diisoamyl cadmium gave the desired β-furyl isoamyl ketone, which was purified with the Girard reagent P. The pure ketone has the similar physical constants to natural perillaketone, as are shown in Table I, and it gives the oxime, m. p. 65–67°, and the 2,4-dinitro-phenylhydrazone, m. p. 149–150°. The latter derivative was identical with the 2,4-dinitro-phenylhydrazone of the natural substance in the infrared spectrum and the mixed melting point. From the above results, it is established that perillaketone is β-furyl isoamyl ketone.

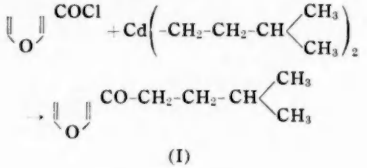

(I)

Experimental

3-Furoyl chloride[3] 3-Furoic acid (25.0 g.) and thionyl chloride (50 cc.) were heated in benzene (160 cc.) for 9 hours. The solvent and an excess of thionyl chloride were evaporated and the residual liquid was distilled *in vacuo*. The acid chloride (16.2 g.) was obtained as a colorless liquid, b. p. 73–76°/46 mm.

β-Furyl isoamyl ketone (Perillaketone) To the Grignard solution, prepared from isoamyl bromide (30 g.), magnesium (4.9 g.) and absolute ether (80 cc.), dried cadmium chloride (19 g.) was added in portions under ice-cooling and the mixture was refluxed until a negative Gilman-Schulz test was given. Ether was evaporated and benzene (100 cc.) was added. A solution of 3-furoyl chloride (16.2 g.) in benzene (50 cc.) was rapidly added to the above cadmium diisoamyl solution at room temperature. The mixture was refluxed for 20 minutes and was decomposed with diluted hydrochloric acid under ice-cooling. The benzene layer was separated, washed with bicarbonate solution, dried and evaporated. Distillation of the residual liquid (17.0 g.) gave the crude ketone as a pale yellow liquid (8.5 g.); b. p. 73–75°/3 mm. and n_D^{27} 1.4685.

The crude product was treated with the Gigrard reagent P in the usual method. Distillation of the ketonic part gave the pure ketone as a color-

1) R. Goto, *J. Pharm. Soc. Japan*, **57**, 77 (1937).
2) Y. Sebe, *J. Chem. Soc. Japan*, **64**, 1130 (1943).
3) H. Gilman, R. Burtner, *J. Am. Chem Soc.*, **55**, 2903 (1933).

TABLE I

		B. P.	n_D	d	Oxime (m. p.)	2,4-Dinitrophenyl-hydrazone (m. p.)
β-Furyl isoamyl ketone		72—73°/3 mm	n_D^{17} 1.4741	d_4^{24} 0.9924	65—66°	149—150°
Perillaketone	Goto[1]	196°	n_D^{20} 1.4781	d_{15}^{15} 0.9920	67°	—
	Sebe[2]	95—97°/7 mm	n_D^{17} 1.4759	d_4^{17} 0.9897	66—67°	152—153°

less liquid; b. p. 72–73°/3 mm., n_D^{17} 1.4741 and d_4^{24} 0.9924. The substance gives a negative test with the Ehrlich reagent and shows a pale yellow color with acetic anhydride and sulfuric acid. The ketone is sensitive to oxygen and on standing becomes a reddish orange color.

IR-absorptions: 3.18, 3.42, 3.50, 6.00, 6.41, 6.63, 6.82, 7.20, 7.30–7.34, 7.78, 8.10, 8.32, 8.66, 9.25, 9.50, 9.77, 10.02, 10.78, 11.45, 12.30, 12.90 and 13.48 μ.

Oxime of β-furyl isoamyl ketone The ketone (2.1 g.), hydroxylamine hydrochloride (1.3 g.) and sodium acetate (2.5 g.) were treated in the usual method in diluted alcohol. The oily product (1.9 g.) solidified on standing in the ice-chest. The oxime crystallized from petroleum ether in colorless needles, m. p. 65–66°. Anal. Found: C, 66.52; H, 8.41; N, 8.03%. Calcd. for $C_{10}H_{15}NO_2$: C, 66.27; H, 8.34; N, 7.73%.

2,4-Dinitro-phenylhydrazone of β-furyl isoamyl ketone The ketone (0.3 g.) and 2,4-dinitro-phenylhydrazine (0.4 g.) precipitated reddish orange needles in the presence of sulfuric acid in alcohol. Recrystallizations of the needles gave the pure 2,4-dinitro-phenylhydrazone, m. p. 149–150°, which showed no depression on admixture with 2,4-dinitro-phenylhydrazone, m. p. 151–152°, of natural perillaketone. Anal. Found: C, 55.48; H, 5.20; N, 16.08%. Calcd. for $C_{16}H_{18}N_4O_5$: C, 55.48; H, 5.24; N, 16.18%.

The author is greatly indebted to Dr. Yeigai Sebe at Kumamoto University and Dr. Yodo Rin at National Taiwan University for a gift of the authentic sample.

Institute of Polytechnics
Osaka City University
Minamiogimachi, Kitaku, Osaka

Catalytic Hydrogenation in Vapor Phase Using Urushibara Nickel as Catalyst

By Kazuo HATA, Ken-ichi WATANABE and Shiro SATO

(Received November 20, 1956)

Urushibara nickel (U-Ni in abbreviation), a new catalyst made from nickel choride and zinc dust, has been reported to show excellent behavior in the catalytic reduction of many organic compounds[1-5].

In this paper, we introduce a new idea applying this catalyts to vapor phase hydrogenation. The procedure of the vapor phase hydrogenation with U-Ni as catalyst is not so troublesome as that with other catalysts, and efficient reduction was observed except in special cases. U-Ni-A, which was used in these experiments, was prepared by treating precipitated nickel with acetic acid as previously reported[4].

Nitrobenzene was reduced to aniline, styrene and acetophenone to ethylbenzene respectively, and benzonitrile to primary and secondary amines together with some toluene. However, benzene could not be reduced by this method. The conditions of the reaction and products are shown in Table I.

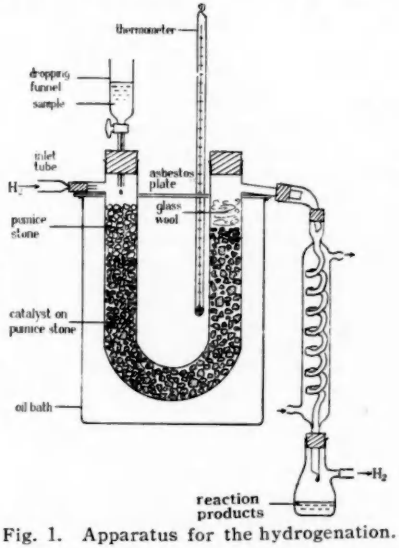

Fig. 1. Apparatus for the hydrogenation.

1) Y. Urushibara, This Bulletin, **25**, 280 (1952).
2) S. Nishimura, *J. Chem. Soc. Japan (Pure Chem. Sect.)*, **77**, 340 (1956).
3) Y. Urushibara and S. Nishimura, This Bulletin, **27**, 480 (1954).
4) Y. Urushibara, S. Nishimura and H. Uehara, ibid., **28**, 446 (1955).
5) K. Hata, K. Watanabe, S. Taira, T. Higase, I. Motoyama and T. Tamura, *J. Chem. Soc. Japan (Pure Chem. Sect.)*, **77**, 1405 (1956); T. Higase, S. Taira and K. Hata, ibid., **78**, 186 (1957).

TABLE I

VAPOR PHASE HYDROGENATION USING U-Ni-A AS CATALYST

Compound	Weight of Sample (g.)	Nickel (g.)	Temp. (°C)	Time (hr.)	Flow Velocity of Sample (g./min.)	Weight of Product (g.)	Product and Yield (%)
Nirobenzene	10	4	220	3	0.08	9.7	Aniline (81)
Benzene	10	4	180	4	0.06	9.0	(Benzene recovered)
Styrene	10.4	4	165	3	0.08	9.3	Ethylbenzene (88)
Acetophenone	9.9	4	200	$3^1/_2$	0.06	9.1	Ethylbenzene (90)
Benzonitrile	8.0	4	250	3	0.07	6.5	Toluene (14)
							Benzylamine (29)
							Dibenzylamine (41)
							Ammonia (50)

The hydrogenating apparatus used in these experiments is shown in Fig. 1. A hard glass U-tube, 3 cm. in diameter and about 50 cm. in total length, was used as a reaction tube. Small grains of pumice stone were put in the U-tube to fill about three quarters of its content. Freshly prepared U-Ni-A catalyst was washed with alcohol, and was poured on the pumice stone in the U-tube together with a small quantity of alcohol. The catalyst settled over the surface of the pumice stone when treated by this method. Then, other pieces of pumice stone were added to fill up the U-tube, and the tube was set in an oil bath after the greater part of the alcohol was decanted away. A small dropping funnel to introduce the liquid sample was fitted on the top of the U-tube over the hydrogen inlet tube. A condenser and a receiver were connected with the other branch of the U-tube. The reaction tube was heated and hydrogen was passed through the tube to expel the vapor of alcohol. Now the receiver was changed to catch the reaction products, and the temperature of the bath was suitably controlled for the hydrogenation. The liquid sample was then slowly dropped into the U-tube. The liquid was vaporized on the upper grains of pumice stone and was hydrogenated on the nickel catalyst, the reaction products being distilled into the receiver.

Each sample was hydrogenated under the suitable temperature with a large excess of hydrogen. After all the sample had been supplied, more hydrogen was passed through for 30–60 minutes to expel the hydrogenation products throughly. After the reaction was over, each product in the receiver was fractionally distilled, and then identified by preparing an appropriate solid derivative.

From these experiments, it was proved to be very convenient to use U-Ni in the vapor phase catalytic hydrogenation. For the preparation of the catalyst, it is not necessary to reduce the nickel compound at high temperature such as by Sabatier's method; all procedures are simple and quick, and the yields of the hydrogenation products are pretty good.

Different results from the hydrogenation with Sabatier's reduced nickel were obtained in the hydrogenation of benzene and benzonitrile. Benzene nucleus could not be hydrogenated with U-Ni by any way, though Sabatier's reduced nickel converts benzene into cyclohexane[6]. Benzonitrile can be hydrogenated almost perfectly to toluene and ammonia with reduced nickel catalyst at 250°C[7], but with U-Ni, the formation of toluene was largely depressed alternatively yielding primary and secondary amines.

The further investigation on the activity of Urushibara nickel in vapor phase hydrogenation is now in progress.

Department of Chemistry, Faculty of Science, Tokyo Metropolitan University, Setagaya, Tokyo

6) P. Sabatier and J. B. Senderens, *Compt. rend.*, **132**, 210 (1901).
7) P. Sabatier and J. B. Senderens, *Compt. rend.*, **140**, 482 (1905): K. Hata, *Sci. Papers Inst. Phys. Chem. Research* (Tokyo), **23**, 224 (1944): M. Tanaka, K. Watanabe and K. Hata, *J. Chem. Soc. Japan* (*Pure Chem. Sect.*), **76**, 1392 (1955).